New insights along the gut-liver axis in cardiometabolic disease

Witjes, J.J.

Publication date
2023
Document Version
Final published version

New insights along the gut-liver axis in cardiometabolic disease

Julia Witjes

New insights along the gut-liver axis in cardiometabolic disease

Julia Witjes

New insights along the gut-liver axis in cardiometabolic disease

ISBN 978-94-6469-638-7

Cover design: Sander Oenema || studio-sander.nl
Lay-out: RON Graphic Power || www.ron.nu
Printed by: ProefschriftMaken || www.proefschriftmaken.nl

Financial support by the Dutch Heart Foundation for the publication of this thesis is gratefully acknowledged.

Additional financial support for printing this thesis was kindly provided by ChipSoft, Stichting tot Steun Promovendi Vasculaire Geneeskunde and the Amsterdam University Medical Center.

New insights along the gut-liver axis in cardiometabolic disease

ACADEMISCH PROEFSCHRIFT

ter verkrijging van de graad van doctor
aan de Universiteit van Amsterdam
op gezag van de Rector Magnificus
prof. dr. ir. P.P.C.C. Verbeek
ten overstaan van een door het College voor Promoties ingestelde
commissie, in het openbaar te verdedigen in de Agnietenkapel
op vrijdag 8 december 2023, te 13.00 uur

door Julia Joeke Witjes
geboren te
Amsterdam

PROMOTIECOMMISSIE

Promotores: prof. dr. M. Nieuwdorp, AMC-UvA
prof. dr. U.H.W. Beuers, AMC-UvA

Copromotores: dr. A.G. Holleboom, AMC-UvA
prof. dr. ir. A.J. Nederveen, AMC-UvA

Overige leden: prof. dr. M.J.M. Serlie, AMC-UvA
prof. dr. M.A. Benninga, AMC-UvA
dr. V.E.A. Gerdes, AMC-UvA
prof. dr. S.W.C. van Mil, Universiteit Utrecht
prof. dr. R. Shiri-Sverdlov, Universiteit Maastricht
dr. M.E. Tushuizen, LUMC

Faculteit der Geneeskunde

Table of contents

chapter 1

General introduction
and thesis outline

GENERAL INTRODUCTION

As a consequence of the global increase of obesity, the prevalence of related conditions such as insulin resistance, type 2 diabetes (T2D) and metabolic dysfunction associated steatotic liver disease (MASLD), formerly known as non-alcoholic fatty liver disease (NAFLD)[1] is increasing[2]. In fact, the worldwide prevalence of T2D is expected to rise to 33% of the adult population in 2050[3] and 60% of individuals with T2D are found to have MASLD[4]. The pathophysiology of these metabolic disorders is complex with a root cause in insulin resistance and including lifestyle and genetic factors, with altered gut microbiota composition as an emerging contributor[5].

Disturbances in the gut microbiome, i.e. the microbial community within the gastrointestinal tract, have been linked to the pathophysiology of metabolic diseases[6,7] such as the metabolic syndrome, T2D and MASLD, with a decreased abundance of microbes involved in the conversion of dietary fiber to butyrate and other short-chain fatty acids in T2D[8] and an increased abundance of Proteobacteria in MASLD[9]. Moreover, the endogenous production of ethanol by microbes in individuals with steatosis is found to be a potential contributor to the development of MASLD[10]. Furthermore, the human gut microbiome is playing an increasingly important role in the search for both preventive and treatment strategies for these diseases. These findings formed the basis for the development of strategies to manipulate the gut microbiota composition, such as dietary interventions, probiotics and fecal microbiota transplantation (FMT), in order to prove causality and ultimately prevent or cure a specific disease.

MASLD, including the more advanced and progressive stage steatohepatitis (MASH, formerly known as NASH), is a liver disease which often co-occurs with obesity and T2D. About 25% of all adults worldwide exhibit steatosis[11], whereas 5-6% has MASH[12]. MASLD is defined as hepatic fat accumulation (hepatic steatosis) in the absence of excessive alcohol consumption and represents a spectrum of liver disease, ranging from simple steatosis to MASH and fibrosis[13]. The transition from simple steatosis to MASH and especially the subsequent development of liver fibrosis is associated with an increased risk of liver-related complications such as cirrhosis, hepatocellular carcinoma and hepatic decompensation and liver-related and all-cause mortality, as well as incident atherosclerotic cardiovascular disease[14,15].

Currently, liver biopsy remains the diagnostic reference standard for MASLD, as it can distinguish simple steatosis from MASH and establish the degree of inflammation and fibrosis[16]. Yet it is an invasive, potentially painful and labor-intensive procedure with a small risk of complications. Together, these disadvantages make a liver biopsy a suboptimal diagnostic method for screening and monitoring of MASLD in clinical practice. Therefore, noninvasive diagnostic methods for disease screening,

diagnosis or monitoring disease progression have been developed, with the ultimate goal to reduce the need for future liver biopsies in MASLD.

The aim of the present thesis was first to target the gut microbiome for the development of therapeutic strategies in metabolic disease, specifically by studying the effect of probiotic treatment in metabolic syndrome and T2D individuals on insulin resistance as well as the effect of multiple FMTs on individuals with histologically characterized MASLD. Secondly, we aimed to identify and validate noninvasive diagnostic methods for disease staging of MASLD.

THESIS OUTLINE

This thesis consists of two parts. Part I focusses on the potential role of the gut microbiome in treating metabolic diseases, whereas in part II we focus specifically on MASLD, the treatment of this condition by altering the gut microbiota composition and assessing possible non-invasive diagnostic methods.

PART I – THE GUT MICROBIOME AS A THERAPEUTIC TARGET IN CARDIOMETABOLIC DISORDERS

This part starts with a review on the interplay between the gut microbiota composition and the development of insulin resistance and cardiovascular disease (CVD) as well as how these findings are being pursued to develop novel diagnostic and therapeutic targeting options for metabolic disorders (**chapter 2**). By supplying missing bacterial strains or their produced metabolites, intestinal microbiota composition might be beneficially altered and thus prevent the development of cardiometabolic disorders. Previous studies have shown that transplantation of lean healthy microbiota in individuals with insulin resistance significantly increased insulin sensitivity and found an increased abundance of butyrate-producing bacteria in the gut[18,19], specifically of the butyrate-producer *Anaerobutyricum soehngenii* (previously known as *Eubacterium hallii)*. **Chapter 3** describes a randomized placebo-controlled cross-over study in individuals with the metabolic syndrome in which we showed that a single duodenal infusion of *A. soehngenii* improved peripheral glycemic control, specifically by stimulating intestinal GLP-1 production. As *A. soehngenii* has the capacity to produce butyrate from lactate and acetate in an acidic environment as found in the small intestine[20], it is interesting to note that individuals with T2D treated with metformin have increased levels of lactate in their feces[21]. Since *A. soehngenii* uses intestinally produced lactate to produce the SCFA butyrate, which is known to exert beneficial effects on glucose metabolism, these findings prompted us to study

the effect of a 2 weeks oral *A. soehngenii* treatment in individuals with T2D treated with metformin on their glycemic control (**chapter 4**).

PART II - DEVELOPMENT OF MICROBIOTA-BASED THERAPEUTICS AND NONINVASIVE DIAGNOSTICS IN MASLD

This part of the thesis focuses on MASLD, which has become the most common cause of chronic liver dysfunction worldwide[4]. In **chapter 5** we review the gut microbiome and gut microbial-derived metabolite signatures associated with the development and disease progression of MASLD, focusing on which microbial signatures are specific to liver injury versus those common to other metabolic diseases. To dissect causality of intestinal microbiota in MASLD, in **chapter 6** we performed a single-center, double-blind, randomized controlled proof-of-principle pilot study comparing the effect of three 8-weekly lean vegan donor FMT versus autologous FMT on the severity of MASLD, using liver biopsies in individuals with hepatic steatosis on ultrasound. In **chapter 7** we move from treatment to diagnostics in MASLD. As a liver biopsy, the diagnostic reference standard for MASLD, has apparent disadvantages noninvasive diagnostic methods are urgently required in disease stratification and monitoring in MASLD. Here we examine the diagnostic performance of multiparametric MRI for the assessment of disease severity along the MASLD disease spectrum with comparison to histological scores.

REFERENCES

1. Rinella, M. E. *et al.* A multi-society Delphi consensus statement on new fatty liver disease nomenclature. *J. Hepatol.* (2023). doi:10.1016/j.jhep.2023.06.003
2. NCD Risk Factor Collaboration (NCD-RisC). Worldwide trends in body-mass index, underweight, overweight, and obesity from 1975 to 2016: a pooled analysis of 2416 population-based measurement studies in 128·9 million children, adolescents, and adults. *Lancet (London, England)* **390**, 2627–2642 (2017).
3. Boyle, J. P., Thompson, T. J., Gregg, E. W., Barker, L. E. & Williamson, D. F. Projection of the year 2050 burden of diabetes in the US adult population: Dynamic modeling of incidence, mortality, and prediabetes prevalence. *Popul. Health Metr.* **8**, 29 (2010).
4. Younossi, Z. *et al.* Global Perspectives on Nonalcoholic Fatty Liver Disease and Nonalcoholic Steatohepatitis. *Hepatology* **69**, 2672–2682 (2019).
5. Aron-Wisnewsky, J., Warmbrunn, M., Nieuwdorp, M. & Clément, K. Nonalcoholic Fatty Liver Disease: Modulating Gut Microbiota to Improve Severity? *Gastroenterology* (2020). doi:10.1053/j.gastro.2020.01.049
6. Ridaura, V. K. *et al.* Gut microbiota from twins discordant for obesity modulate metabolism in mice. *Science* **341**, 1241214 (2013).
7. Pedersen, H. K. *et al.* Human gut microbes impact host serum metabolome and insulin sensitivity. *Nature* **535**, 376–381 (2016).
8. Karlsson, F. H. *et al.* Gut metagenome in European women with normal, impaired and diabetic glucose control. *Nature* **498**, 99–103 (2013).
9. Hoyles, L. *et al.* Molecular phenomics and metagenomics of hepatic steatosis in non-diabetic obese women. *Nat. Med.* **24**, 1070–1080 (2018).
10. Meijnikman, A. S. *et al.* Microbiome-derived ethanol in nonalcoholic fatty liver disease. *Nat. Med.* **28**, 2100–2106 (2022).
11. Fazel, Y., Koenig, A. B., Sayiner, M., Goodman, Z. D. & Younossi, Z. M. Epidemiology and natural history of non-alcoholic fatty liver disease. *Metabolism.* **65**, 1017–1025 (2016).
12. Diehl, A. M. & Day, C. Cause, Pathogenesis, and Treatment of Nonalcoholic Steatohepatitis. *N. Engl. J. Med.* **377**, 2063–2072 (2017).
13. Hardy, T., Oakley, F., Anstee, Q. M. & Day, C. P. Nonalcoholic Fatty Liver Disease: Pathogenesis and Disease Spectrum. *Annu. Rev. Pathol. Mech. Dis.* **11**, 451–496 (2016).
14. Dulai, P. S. *et al.* Increased risk of mortality by fibrosis stage in nonalcoholic fatty liver disease: Systematic review and meta-analysis. *Hepatology* **65**, 1557–1565 (2017).
15. Taylor, R. S. *et al.* Association Between Fibrosis Stage and Outcomes of Patients With Nonalcoholic Fatty Liver Disease: A Systematic Review and Meta-Analysis. *Gastroenterology* **158**, 1611–1625.e12 (2020).
16. Marchesini, G. *et al.* EASL–EASD–EASO Clinical Practice Guidelines for the management of non-alcoholic fatty liver disease. *J. Hepatol.* **64**, 1388–1402 (2016).
17. Vrieze, A. *et al.* Transfer of intestinal microbiota from lean donors increases insulin sensitivity in individuals with metabolic syndrome. *Gastroenterology* **143**, 913–916.e7 (2012).
18. Kootte, R. S. *et al.* Improvement of Insulin Sensitivity after Lean Donor Feces in Metabolic Syndrome Is Driven by Baseline Intestinal Microbiota Composition. *Cell Metab.* **26**, 611–619.e6 (2017).
19. Vrieze, A. *et al.* Transfer of Intestinal Microbiota From Lean Donors Increases Insulin Sensitivity in Individuals With Metabolic Syndrome. *Gastroenterology* **143**, 913–916.e7 (2012).
20. Duncan, S. H., Louis, P. & Flint, H. J. Lactate-Utilizing Bacteria, Isolated from Human Feces, That Produce Butyrate as a Major Fermentation Product. *Appl. Environ. Microbiol.* **70**, 5810–5817 (2004).
21. Wu, H. *et al.* Metformin alters the gut microbiome of individuals with treatment-naive type 2 diabetes, contributing to the therapeutic effects of the drug. *Nat. Med.* **23**, 850–858 (2017).

Part one

The gut microbiome as a therapeutic target in cardiometabolic disorders

chapter 2

About the gut microbiome as a pharmacological target in atherosclerosis

Julia J. Witjes
Daniel H. van Raalte
Max Nieuwdorp

European Journal of Pharmacology,
Volume 763, Part A, 15 September 2015, Pages 75–78

ABSTRACT

The contribution of intestinal bacterial strains (gut microbiota) in the development of cardiometabolic disease is increasingly recognized as potential diagnostic and pharmacological target. Changes in the intestinal bacterial composition and subsequent altered diversity has been associated with presence of chronic low-grade inflammation of mesenteric visceral adipose tissue, a known feature of malign obesity which can eventually lead to insulin resistance and type 2 diabetes mellitus. However, causality still needs to be proven. In this regard, both fecal transplantation studies as well as multiethnic prospective cohorts can help to identify the causally involved driving intestinal bacterial strains in human cardiometabolism. Ultimately, it is expected that novel diagnostic markers as well as therapeutics (pharmabiotics and vaccine strategies) can be developed.

INTRODUCTION

Type 2 diabetes mellitus (T2D) and cardiovascular disease (CVD) are growing epidemics in the Western world, and there is an urgent need to further dissect the underlying pathophysiological mechanisms (Hossain et al., 2007). Although genetic and environmental factors are generally known to contribute to the development of insulin resistance a key effect in CVD and T2D, the gutmicrobiota only recently gained interest in the pathophysiology of cardiometabolic complications (Tilg et al., 2009). The human fecal intestinal microbiome exists of about 4000–6000 bacterial species, with the majority of them being anaerobic (Turnbaugh et al., 2007). Intestinal microbiota is found to remain relatively stable over time from the childhood till elderly age (Mueller et al., 2006, Tsai and Coyle, 2009). Moreover, although the composition of intestinal microbiota seems to be mainly driven by dietary composition as well as medication (antibiotic) use, endogenous factors such as genetics are also thought to impact intestinal microbiota homeostasis (Cotillard et al., 2013). In this paper, we will thus review the current knowledge on the interplay between intestinal microbiota composition and development of insulin resistance and CVD as well as how these findings may provide us with novel diagnostic and therapeutic targets for cardiometabolic disease.

The intestinal microbiota in obesity and insulin resistance

The prevalence of obesity and T2D continues to rise to 1 out of 3 adult subjects being diagnosed with T2D in 2050 (Boyle et al., 2010). The pathophysiology of these metabolic disorders is complex, involving both environmental (dietary) and genetic factors affecting altered intestinal microbiota composition (Wu et al., 2011, David et al., 2014, Goodrich et al., 2014). It is thought that the intestinal microbiota regulate metabolism indirectly via their metabolites including short chain fatty acids (SCFA) like acetate, propionate and butyrate (Gao et al., 2009) or directly (via bacterial wall compounds such as endotoxin regulating innate immunity and chronic inflammatory tone) (Cani et al., 2007). Moreover, microRNA components of (dead) bacteria (Swaminathan et al., 2012) as well as bacterial products such as butyrate (Chang et al., 2014) affect macrophage function and subsequent inflammatory tone. The latter might be of specific interest, as it has been suggested that in specific metabolic states like insulin resistance, macrophage function is differentially regulated with an altered response against specific (intestinal) bacterial strains (Saeed et al., 2014, Cheng et al., 2014). This training includes altered function of macrophages resulting either polarization or depolarization resulting in improved or decreased function based on differences in macrophage histone methylation driven by bacteria or their metabolites. As glycolysis is the rate limiting step in training of monocyte–

macrophages, it might thus be very well possible that intestinal microbiota composition influences innate immune response in insulin resistance and vice versa.

In line, the intestinal microbiota and their SCFA product butyrate, propionate and acetate might also play a direct role in controlling energy homeostasis by affecting hepatic gluconeogenesis and (de novo) lipogenesis (Gao et al., 2009, Tilg, 2010). Research performed in conventional and germ-free mice both fed a normal chow diet and a high-fat diet showed the involvement of gut microbiota in the development of obesity, as the germ-free mice remained significantly leaner than the conventional raised mice, despite a significantly higher food intake (Bäckhed et al., 2004). Consequently, an enrichment of genes involved in the degradation of carbohydrates, revealed by metagenomic sequencing of the cecum microbiome was found (Turnbaugh et al., 2006). Furthermore, colonization of germ-free mice with cecum-derived microbiota of conventional mice demonstrated a significant increase in total body fat content without changes in the caloric intake (Bäckhed et al., 2007).

In this regard, it is well known that in order to prevent pathogens from settling in the intestine, intestinal bacteria produce SCFA, peroxidases, proteases and bacteriocins with indigestible dietary carbohydrates as substrate (Tremaroli and Bäckhed, 2012). Indigestible carbohydrates are fermented into SCFA by intestinal microbes in order to produce energy. Based on stable isotope fluxes it is estimated that SCFA turnover accounts for approximately 7% of total resting energy expenditure with an calculated productionrate of 8 g per day in the human intestine (Pouteau et al., 2003). These produced SCFA may serve as an energy source for the intestinal epithelium and the liver, as they are absorbed and transported mainly via the portal vein. Reduced intestinal levels of SCFA with a subsequent increase in indigestible carbohydrate excretion in the feces were found in germ-free raised mice, demonstrating a crucial role of intestinal bacteria in the production of these SCFAs (Maslowski et al., 2009). Interestingly, intestinal epithelial MyD88 (which is a downstream target of the toll-like receptor (TLR) functions as a sensor by which host metabolism is regulated by energy expenditure and SCFA (Everard et al., 2014). It is therefore tempting to speculate that intestinal SCFA produced by specific bacterial strains fine-tune whole body metabolism either by directly regulating hepatic gluconeogenesis but also by affecting intestinal glucose production, a process that only has recently gained attention (De Vadder et al., 2014).

Recent studies in humans indeed found a decreased amount of SCFA butyrate-producing bacterial strains (Clostridiales) as well as an increase in the amount of gram negative proteobacteria (Escherichia coli) in subjects with insulin resistance and T2D of both Chinese and Caucasian descent (Qin et al., 2012, Karlsson et al., 2013). Together, these data suggest a potential pathophysiological mechanism

and support the role of butyrate-producing bacteria as metabolism regulators. As lysis of Gram-negative bacteria in the intestine of both mice and humans leads to the production of lipopolysaccharides (LPS), which subsequently triggers pro-inflammatory cytokines and results in insulin resistance (Everard et al., 2014) the reduction in SCFA producing bacteria might facilitate bacterial translocation due to impaired intestinal barrier function leading into low-grade endotoxaemia.

Low-grade abdominal adipose tissue inflammation, diet and gutmicrobiota composition

Chronic mesenteric visceral adipose tissue inflammation and the production of pro-inflammatory cytokines subsequently occur in the majority of obese subjects and eventually lead to insulin resistance and T2D (Smith et al., 2012). Several lines of evidence point to a direct relation between the intestinal microbiota composition and adipose tissue inflammation, as the infiltration of macrophages in adipose tissue directly correlated with pro-inflammatory gene expression in adipocytes (Apovian et al., 2008, Wentworth et al., 2010). In this respect, bacterial translocation and endotoxins are thought to be instrumental in this process recognized by the host macrophages TLRs (Le Chatelier et al., 2013, Kong et al., 2013)., whereas SCFAs mediate protective immunity via G-coupled protein receptors (GPR) 41 and 43 on intestinal epithelial cells (Kim et al., 2013). Indeed, chronic LPS exposure in mice showed to lead to the activation of the innate inflammatory pathway, causing hepatic insulin resistance, hepatic steatosis, adipose tissue macrophages infiltration, dyslipidemia, fasting hyperglycemia, hyperinsulinemia and eventually obesity (Cani et al., 2007). The question however remains whether intestinal microbiota composition is a cause or consequence in the development of insulin resistance and obesity (Qin et al., 2012, Karlsson et al., 2013). Using both lean donor fecal transplantation and antibiotic intervention studies, we have demonstrated that intestinal microbes indeed regulate whole body metabolism (Vrieze, 2012, Vrieze et al., 2014). The underlying mechanism of action is thought to consist of replacement of pathological microbes by beneficial commensals including an increase in SCFA butyrate-producing bacteria. Further studies are underway to show reproducibility and more in-depth studying of the pathophysiological mechanisms including adipose tissue and macrovascular inflammation.

Gut microbiota and cardiovascular disease

A chronic inflammatory state, caused by altered intestinal microbiota derived endotoxaemia, has been suggested to contribute to obesity as well as to atherosclerosis (Sanz et al., 2010). Recent studies in both mice and rabbits showed an accelerated cholesterol-induced development of atherosclerosis after repetitive

injections of endotoxins (Westerterp et al., 2007; Caesar et al., 2010; Lehr et al., 2001). However, treatment with systemic antibiotics in humans in the only prospective randomized controlled trial done so far showed no reduction in cardiovascular event rates, possibly due specific eradication of gram positive strains by azithromycin thus not affecting gram negative (LPS containing) intestinal bacteria (Grayston et al., 2005). Another possible pathway in which intestinal microbiota are thought to contribute to the pathogenesis of CVD is by the production of a pro-atherogenic compound, named trimethylamine-N-oxide (TMAO), which is produced by the degradation of dietary trimethylamines, like free choline, phosphatidylcholine and carnitine (Wang et al., 2011; Tang et al., 2013; Koeth et al., 2013). The overflow of TMAO in the systemic circulation can trigger macrophages to accumulate cholesterol and resulting in foam cells in atherosclerotic lesions (Bennett et al., 2013). In line, identical associations of TMAO with heart failure have also been described (Tang, 2014), whereas causality was proven using fecal transplantations in mice (Gregory et al., 2015). However, it should be noted that the relationship proposed between dietary carnitine and atherosclerotic CVD pathogenesis refers to a process that takes decades to develop and which appears at least in part to exert its pro-atherogenic effect via alterations in cholesterol and sterol metabolism such as involved in the reverse cholesterol transport (Wang et al., 2012). Thus, TMAO might be a good example of a new gutmicrobiota metabolite that is involved in development of CVD but that needs to be further investigation to dissect the therapeutic value in the prevention of CVD.

The gut microbiota as diagnostic and therapeutic target

Overall, the intestinal microbiota seems to play a role in the development of cardiometabolic disorders, however the magnitude of its effect remains to be established. There are several scientific ways to further study causality and magnitude of effect of the intestinal microbiota. One can think in this regard of prospective collection of fecal samples in otherwise healthy subjects, of whom a substantial amount will convert from obesity to metabolic syndrome, a project that is currently studied in the HELIUS study (Stronks et al., 2013). From a more therapeutic angle, one may think of replenishing missing intestinal bacterial strains to efficiently process dietary compounds such as protein and carbohydrates, which are known to affect postprandial glycemic profiles in insulin resistant subjects (Belinova et al., 2014). On the other hand, in line with murine studies, supplementation of intestinal metabolites such as butyrate (Schwiertz et al., 2010) might beneficially influence metabolism to reverse insulin resistance and increase energy expenditure, a study which is currently ongoing at our department. Finally, a way to prevent intestinal bacterial pathogen overgrowth and subsequent intestinal bacterial translocation might be targeted using classical vaccination strategies to boost (trained) immunity against involved gutmicrobiota strains in cardiometabolis (Spaulding et al., 2012).

Conclusion

Using targeted vaccination against intestinal microbiota or by supplying missing bacterial strains or their produced metabolites might enable us to beneficially alter intestinal microbiota composition and thus to prevent the development of cardiometabolic disease. In order to find diagnostic and therapeutic targeting options in metabolic disorders, understanding of the optimal intestinal microbiota composition and the key bacterial species involved is essential. Further research in humans is thus needed to confirm the causality of intestinal microbial strains in cardiometabolism found, but even more important, experimental findings on correlations between microbial communities and specific cardiometabolic phenotypes should be corroborated by more detailed mechanistic investigations, and ideally, therapeutic intervention studies in humans.

REFERENCES

Apovian CM, et al. Adipose macrophage infiltration is associated with insulin resistance and vascular endothelial dysfunction in obese subjects. 2008 Arterioscler. Thromb. Vasc. Biol, 28(9), 1654-9.

Bäckhed F, et al. The gut microbiota as an environmental factor that regulates fat storage. 2004 Proc. Natl. Acad. Sci. U. S. A. , 101(44), 15718-23.

Bäckhed F, et al Mechanisms underlying the resistance to diet-induced obesity in germ-free mice. 2007 Proc. Natl. Acad. Sci. U. S. A. , 104(3), 979-84.

Belinova L et al. Differential acute postprandial effects of processed meat and isocaloric vegan meals on the gastrointestinal hormone response in subjects suffering from type 2 diabetes and healthy controls: a randomized crossover study 2014. PLoS One, 9(9), e107561.

Bennett BJ et al. Trimethylamine-N-oxide, a metabolite associated with atherosclerosis, exhibits complex genetic and dietary regulation. 2013 Cell Metab.17(1), 49-60.

Boyle JP, et al Projection of the year 2050 burden of diabetes in the US adult population: dynamic modeling of incidence, mortality, and prediabetes prevalence. 2010 Popul Health Metr. 8:29.

Caesar R et a. Effects of gut microbiota on obesity and atherosclerosis via modulation of inflammation and lipid metabolism, 2010, J. Intern. Med. 268(4), 320-8.

Cani PD, et al. Selective increases of bifidobacteria in gut microflora improve high-fat-diet-induced diabetes in mice through a mechanism associated with endotoxaemia. 2007 Diabetologia, 50(11), 2374-83

Chang PV, et al. The microbial metabolite butyrate regulates intestinal macrophage function via histone deacetylase inhibition. 2014 Proc Natl Acad Sci U S A. 111(6), 2247-52.

Cheng SC, et a;. mTOR- and HIF-1α-mediated aerobic glycolysis as metabolic basis for trained immunity. 2014 Science. 345(6204), 1250684.

Cotillard A, et al 2013. Dietary intervention impact on gut microbial gene richness. Nature.500(7464); 585-8

David LA, et al. Diet rapidly and reproducibly alters the human gut microbiome 2014. Nature ;505(7484), 559-63.

De Vadder F, et al Microbiota-generated metabolites promote metabolic benefits via gut-brain neural circuits. 2014 Cell, 156(1-2), 84-96.

Everard A, et al Intestinal epithelial MyD88 is a sensor switching host metabolism towards obesity according to nutritional status. 2014 Nat Commun (5), 5648.

Gao Z, et al. Butyrate improves insulin sensitivity and increases energy expenditure in mice. 2009, Diabetes.;58(7), 1509-17

Goodrich JK et al. Human genetics shape the gut microbiome. 2014 Cell 159(4), 789-99.

Grayston JT et al. Azithromycin for the secondary prevention of coronary events, 2005,. N. Engl. J. Med. 352(16), 1637-45.

Gregory JC et al. Transmission of Atherosclerosis Susceptibility with Gut Microbial Transplantation 2014. J Biol Chem, [Epub ahead of print]

Hossain P, et al. Obesity and diabetes in the developing world--a growing challenge 2007. N. Engl. J. Med. 356(3), 213-5.

Karlsson FH, et al. Gut metagenome in European women with normal, impaired and diabetic glucose control. 2013 Nature, 498(7452), 99-103

Kim MH, et al. Short-chain fatty acids activate GPR41 and GPR43 on intestinal epithelial cells to promote inflammatory responses in mice. Gastroenterology 2013, 145(2), 396-406.

Koeth RA, et al. Intestinal microbiota metabolism of L-carnitine, a nutrient in red meat, promotes atherosclerosis. 2013 Nat. Med. 19(5), 576-85.

Kong LC, et al. Gut microbiota after gastric bypass in human obesity: increased richness and associations of bacterial genera with adipose tissue genes. 2013 Am J Clin Nutr, 98(1), 16-24. Le Chatelier E, et al. Richness of human gut microbiome correlates with metabolic markers, 2013. Nature, 500(7464), 541-6.

Lehr HA, et al. Immunopathogenesis of atherosclerosis: endotoxin accelerates atherosclerosis in rabbits on hypercholesterolemic diet, 2001 Circulation, 104(8), 914-20.

Maslowski KM, et al. Regulation of inflammatory responses by gut microbiota and chemoattractant receptor GPR43. 2009 Nature, 461(7268), 1282-6.

Mueller S, et al. 2006 Differences in fecal microbiota in different European study populations in relation to age, gender, and country: a cross-sectional study. *Appl.* Environ. Microbiol. 72(2), 1027-33.

Pouteau E et al. Production rates and metabolism of short-chain fatty acids in the colon and whole body using stable isotopes. 2003 Proc Nutr Soc., 62(1), 87-93.

Qin J, et al. A metagenome-wide association study of gut microbiota in type 2 diabetes. 2012; *Nature* 490 (7418), 55-60.

Saeed S, et al . Epigenetic programming of monocyte-to-macrophage differentiation and trained innate immunity. 2014 Science, 345(6204), 1251086.

Sanz Y, et al Gut microbiota in obesity and metabolic disorders 2010. Proc. Nutr. Soc. 2010, 69(3), 434-41.

Smith JD, et al. Visceral adipose tissue indicates the severity of cardiometabolic risk in patients with and without type 2 diabetes: results from the INSPIRE ME IAA study 2012 . J. Clin. Endocrinol. Meta*b.*97(5), 1517-25.

Spaulding AR, et al.Immunity to Staphylococcus aureus secreted proteins protects rabbits from serious illnesses. 2012 Vaccine, 30(34), 5099-109

Stronks K et al. Unravelling the impact of ethnicity on health in Europe: the HELIUS study, 2013 BMC Public Health. 13, 402.

Swaminathan G, et al. A role for microRNA-155 modulation in the effects of Toll-like receptor 3 stimulation in macrophages. 2012 PLoS Pathog. , 8(9), e1002937

Schwiertz A et al. Microbiota and SCFA in lean and overweight healthy subjects. 2010 Obesity, 18(1), 190-5.

Tang WHW et al. Intestinal microbial metabolism of phosphatidylcholine and cardiovascular risk. 2013 N. Engl. J. Med, 368(17), 1575-84.

Tang WH, et al .Prognostic value of elevated levels of intestinal microbe-generated metabolite trimethylamine-N-oxide in patients with heart failure: refining the gut hypothesis. 2014 J Am Coll Cardiol. 64(18), 1908-14.

Tsai F, Coyle WJ. The microbiome and obesity: is obesity linked to our gut flora? 2009 Curr. Gastroenterol. Rep. 11(4), 307-13.

Tilg H, et al. Obesity and the microbiota 2009. Gastroenterology 136(5), 1476-83.

Tilg H. 2010 Obesity, metabolic syndrome, and microbiota: multiple interactions. *J.* Clin. Gastroenterol. 44, S16-8.

Tremaroli V, Bäckhed F. Functional interactions between the gut microbiota and host metabolism. Nature 2012;489(7415):242-9. doi:10.1038/nature11552.

Turnbaugh PJ, et al. An obesity-associated gut microbiome with increased capacity for energy harvest. 2006 Nature 444(7122), 1027-31.

Turnbaugh PJ, et al. The human microbiome project. Nature 2007;449(7164), 804-10.

Vrieze A, et al. . Transfer of intestinal microbiota from lean donors increases insulin sensitivity in individuals with metabolic syndrome. 2012 Gastroenterology. 2012, 143(4), 913-6.

Vrieze A, et al. Impact of oral vancomycin on gut microbiota, bile acid metabolism, and insulin sensitivity. 2014 J Hepatol. , 60(4), 824-31.

Wang Z et al. Gut flora metabolism of phosphatidylcholine promotes cardiovascular disease, 2011. Nature , 472(7341), 57-63.

Wentworth JM, , et al. Pro-inflammatory CD11c+CD206+ adipose tissue macrophages are associated with insulin resistance in human obesity. 2010 *Diabetes*, 59(7), 1648-56.

Westerterp M et al. Apolipoprotein C-I is crucially involved in lipopolysaccharide-induced atherosclerosis development in apolipoprotein E-knockout mice 2007. Circulation, 116(19), 2173-81.

Wang D et al. Gut microbiota metabolism of anthocyanin promotes reverse cholesterol transport in mice via repressing miRNA-10b 2012. Circ. Res. , 111(8), 967-81.

Wu GD, et al. Linking long-term dietary patterns with gut microbial enterotypes. 2011 Science ;334(6052), 105-8.

chapter 3

Duodenal Anaerobutyricum soehngenii infusion stimulates GLP-1 production, ameliorates glycaemic control and beneficially shapes the duodenal transcriptome in metabolic syndrome subjects: a randomised double-blind placebo-controlled cross-over study

Annefleur M. Koopen, Julia J. Witjes, Koen Wortelboer, Soumia Majait, Andrei Prodan, Evgeni Levin, Hilde Herrema, Maaike Winkelmeijer, Steven Aalvink, Jacques J. Bergman, Stephan R. Havik, Bolette Hartmann, Johannes H. Levels, Per-Olof Bergh, Jamie van Son, Manon Balvers, Diogo N. Mendes Bastos , Erik S. Stroes, Albert K. Groen, Marcus Henricsson, Ellis M. Kemper, Jens J. Holst, Christopher M. Strauch, Stanley L. Hazen, Fredrik Bäckhed, Willem M. De Vos, Max Nieuwdorp, Elena Rampanelli

Gut,
Published Online First: 25 October 2021.
doi: 10.1136/gutjnl-2020-323297

ABSTRACT

Objective: Although gut dysbiosis is increasingly recognized as a pathophysiological component of metabolic syndrome (MetS), the role and mode of action of specific gut microbes in metabolic health remain elusive. Previously, we identified the commensal butyrogenic *Anaerobutyricum soehngenii* to be associated with improved insulin sensitivity in MetS subjects. In this proof-of-concept study, we investigated the potential therapeutic effects of *A. soehngenii* L2-7 on systemic metabolic responses and duodenal transcriptome profiles in MetS individuals.

Design: In this randomized double-blind placebo-controlled cross-over study, 12 MetS male subjects received duodenal infusions of *A. soehngenii*/placebo and underwent duodenal biopsies, mixed meal tests (6 hours post-infusion), and 24-hour continuous glucose monitoring.

Results: *A. soehngenii*-treatment provoked a markedly increased postprandial excursion of the insulinotropic hormone glucagon-like peptide 1 (GLP-1), and an elevation of plasma secondary bile acids, which positively associated with GLP-1 levels. Moreover, *A. soehngenii*-treatment robustly shaped the duodenal expression of 73 genes, with the highest fold-induction in the expression of regenerating islet-protein 1B (*REG1B*)-encoding gene. Strikingly, duodenal *REG1B* expression positively correlated with GLP-1 levels and negatively correlated with peripheral glucose variability, which was significantly diminished in the 24 hours following *A. soehngenii* intake. Mechanistically, Reg1B expression is induced upon sensing butyrate or bacterial peptidoglycan. Importantly, *A. soehngenii* duodenal administration was safe and well-tolerated.

Conclusions: A single-dose of *A. soehngenii* improves peripheral glycemic control within 24 hours, it specifically stimulates intestinal GLP-1 production and *REG1B* expression. Further studies are needed to delineate the specific pathways involved in REG1B induction and function in insulin sensitivity.

INTRODUCTION

Along with lifestyle, diet and visceral obesity, the gut microbiota constitutes an important modulator of metabolic heath[1] . Accumulating evidence has now established that intestinal microbiota-diet-host interactions shape host metabolic homeostasis[2–4]; particularly, an unbalanced gut microbiome is increasingly recognized as an important risk factor for metabolic disorders, such as obesity, insulin resistance and type 2 diabetes (T2D)[3–5]. In the pursuit of novel therapeutic insight for the rising cardiometabolic disease burden, the development of culture-independent approaches using high-throughput sequencing has tremendously advanced our knowledge of the microbial signatures of obesity and T2D[6]. General traits of obesogenic microbiota include a decline in fecal microbial community diversity, constriction of species richness and deprivation in short-chain fatty acids (SCFA)-producing microbes[7,8]. Nonetheless, the exact mechanisms by which specific bacterial strains regulate metabolic functions and influence the pathophysiology of metabolic disorders in humans are still poorly understood.

In an attempt to move from association to causality, we previously conducted repetitive fecal microbiota transplantations (FMTs) in humans to gain insights into the microbiome-derived effects on glucose and lipid metabolism. We proved that transfer of healthy microbiota from lean donors into metabolic syndrome patients improved their peripheral insulin sensitivity[3,9], and discovered that the latter was associated with increased relative abundance of *Anaerobutyricum* spp., including *Anaerobutyricum soehngenii*, in the small intestine (SI) following lean donor FMTs[3].

A. soehngenii (formerly classified *Eubacterium hallii)* strain L2-7 is an anaerobic Gram-positive, catalase-negative bacterium belonging to the *Lachnospiraceae* family of the phylum Firmicutes[10]. This strain is capable of converting sugars as well as lactate and acetate into the SCFA butyrate[11], which was shown to exert beneficial effects on glucose metabolism in obese mice and lean humans[12,13], thus underscoring a potential therapeutic benefit of intestinal *A. soehngenii*. We previously described the efficacy of oral *A. soehngenii* L2-7 supplementation in improving insulin resistance and energy expenditure in diabetic and obese db/db mice[14]. Moreover, in a phase I/II safety and dose-finding trial, we showed that 4-week daily oral *A. soehngenii* L2-7 intake is safe and well-tolerated and disclosed a positive correlation between fecal *A. soehngenii* L2-7 abundance and whole-body glucose rate of disposal[15]. However, a major disadvantage of oral administration of bacterial strains is the loss of viability due to contact with oxygen and stomach acid. Therefore, in the present study duodenal tube infusion was chosen to bypass this issue and, hence, maximize the therapeutic potential by delivering viable bacteria directly into the SI, the first anatomical site with a central role in glucosensing, regulation of peripheral insulin sensitivity/secretion and glucose homeostasis[16].

Table 1. Baseline characteristics at screening.

	SCREENING (N = 12)
MALE GENDER (%)	100
AGE (YEARS)	64 [56 – 67]
WAIST CIRCUMFERENCE (CM)	120 [115 – 127]
WEIGHT (KG)	113.6 [99.5 – 122.2]
BMI (KG/M2)	35.9 [32.3 – 37.9]
BLOOD PRESSURE: SYSTOLIC (MMHG)	146 [136 – 159]
BLOOD PRESSURE: DIASTOLIC (MMHG)	95 [86 – 98]
FASTING GLUCOSE (MMOL/L)	5.8 [5.5 – 6.4]
INSULIN (PMOL/L)	82 [66 – 116]
HOMA - IR	3.3 [2.3 – 4.0]
HBA1C (MMOL/MOL)	37 [36 – 38]
CHOLESTEROL: TOTAL (MMOL/L)	5.04 [4.87 – 6.47]
CHOLESTEROL: HDL (MMOL/L)	1.25 [1.03 – 1.37]
CHOLESTEROL: LDL (MMOL/L)	3.12 [2.90 – 4.02]
CHOLESTEROL: TRIGLYCERIDES (MMOL/L)	1.74 [1.27 – 2.30]
CREATININE (UMOL/L)	88 [81 -95]
AST (U/L)	26 [24 – 30]
ALT (U/L)	31 [23 – 37]
AP (U/L)	77 [63 – 92]
YGT (U/L)	35 [22 – 66]
CRP (MG/ML)	3.1 [1.7 – 5.6]
LEUKOCYTES (10^E9/L)	6.1 [5.3 – 6.9]

Figure 1. Study overview.

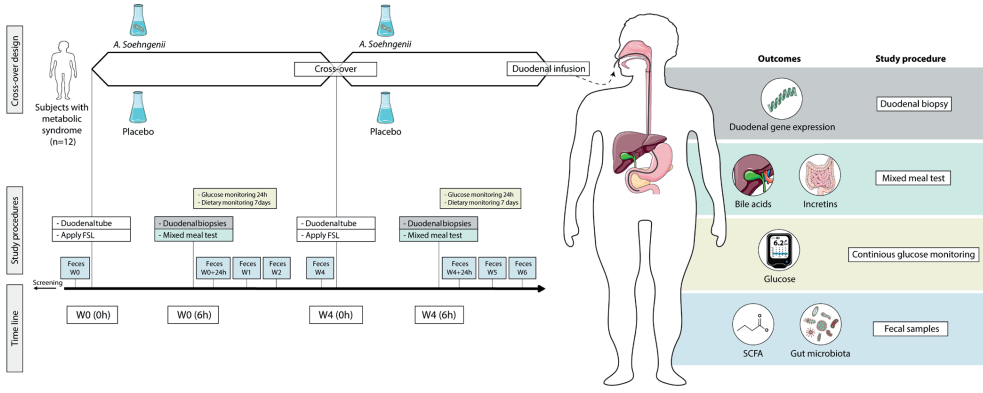

Schematic representation of the study design showing the time-points of interventions and of biological samplings: all 12 subjects received placebo (10%glycerol in PBS) or treatment (*A. soehngenii* L2-7) at week 0 or week 4 (time of intervention cross-over). *FSL:* FreeStyle Libre.

In this regard, within the intestinal milieu, SI enteroendocrine cells act as 'chemo sensors' of diet- and microbiota-derived metabolites, such as butyrate, and can regulate host glucose metabolism by secreting a variety of hormones, such as the incretin glucagon-like peptide-1 (GLP-1), which in turn enhances both insulin secretion and sensitivity[16–18]. However, the role of single bacterial strains on the human enteroendocrine system remains elusive.

We therefore performed a randomized double-blind placebo-controlled crossover trial to determine the localized and systemic effects of a single duodenal infusion of *A. soehngenii* L2-7 in male subjects with metabolic syndrome. Our primary objective was to characterize the immediate changes induced by *A. soehngenii* L2-7 in the SI transcriptomic profile (6 hours post-infusion). Secondary objectives consisted of investigating the effects of *A. soehngenii* L2-7 on circulating (post-prandial) incretins, fecal SCFA rates, as well as gut microbiota composition.

RESULTS

Baseline characteristics and safety parameters

We included 15 Caucasian treatment naïve males with metabolic syndrome. During the trial, 3 subjects were excluded (2 subjects refrained from participation after the screening due to personal reasons, 1 subject was excluded because of antibiotic use) and thus 12 subjects were left for primary endpoint analyses. Baseline characteristics are presented in **Table 1**. Participants were randomized to receive either 10% glycerol infusion (placebo, N=6) or 10^{11} cells of *A. soehngenii* L2-7 in 10% glycerol (treatment, N=6) as first intervention, and switch to treatment/placebo 4 weeks later (**Figure 1**). Both infusions were well tolerated and no (severe) adverse events occurred during the entire study. Safety laboratory parameters (inflammatory, kidney and liver parameters) were all stable during the study. Energy and macronutrient intake did not differ in the week after *A. soehngenii* L2-7 or placebo administration (**Table S1**). We also observed no differences in body weight, blood pressure, glucose, insulin, HOMA or cholesterol levels between placebo and *A. soehngenii* L2-7 treatments (**Table S1**).

All parameters were measured at fasted state. Values expressed as medians and interquartile ranges. BMI: body mass index; HOMA-IR: homeostatic model assessment of insulin resistance; HbA1c: glycated hemoglobin; HDL: high-density lipoprotein; LDL: low-density lipoprotein; AST: aspartate transaminase; ALT: alanine transaminase; AP: alkaline phosphatase; γGT: gamma-glutamyltransferase; CRP: c-reactive protein.

Figure 2. Microbiota composition and fecal SCFA.

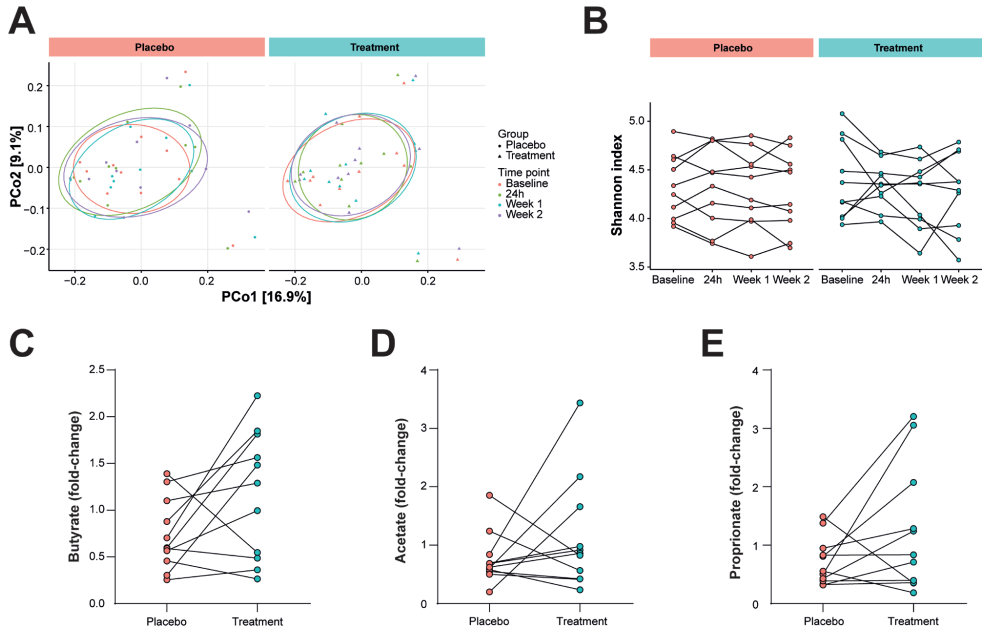

(**A**) Principal coordinates analysis (PCoA) plot on the unweighted UniFrac distances showing the clusters of 16S rRNA sequences. (**B**) Alpha diversity (Shannon index) in fecal microbiota composition in stool samples collected at baseline, 1 day, 1 week and 2 weeks after placebo/treatment intervention. (**C**) Fecal levels of butyrate, (**D**) acetate, and (**E**) propionate shown as fold-change of concentrations (nmol/mg dried feces weight) obtained 1 day after intervention versus baseline.

A single-dose of *A. soehngenii* L2-7 has no impact on microbiota richness/diversity nor fecal SCFA

To discern the impact of *A. soehngenii* L2-7 infusion on gut microbial communities, 16S rRNA gene amplicon sequencing was performed using fecal DNA extracted from stool samples collected at baseline, 1 day, 1 and 2 weeks after interventions. A single infusion of *A. soehngenii* L2-7 did not affect gut microbiota composition or alpha-diversity (Shannon index) either in the short- (24 hours) or long-term (2 weeks) after intervention (**Figure 2A, B**). Similarly, the abundance of *A. soehngenii* L2-7 in fecal samples, assessed by qPCR, was not durably altered over time (**Figure S1**). Notably, these data exclude microbiota-mediated carry-over effects at the time of cross-over (4 weeks post-first intervention). Duodenal *A. soehngenii* L2-7 levels were below minimal detection rates, indicating that administered *A. soehngenii* L2-7 is not colonizing the SI but rather transiting through the intestinal tract.

Given the capacity of *A. soehngenii* to produce butyrate (from sugars and lactate/acetate) and propionate (from 1,2-propanediol)[11,19,20], SCFAs (butyrate, acetate, propionate) were measured in fecal samples taken at baseline and 24 hours after duodenal infusion. Surprisingly, glycerol placebo intervention significantly

decreased the levels of butyrate and acetate (p=0.02, p=0.01, respectively), whereas fecal SCFA remained stable upon *A. soehngenii* L2-7 delivery (**Figure S2A-C**), possibly indicating that the vehicle glycerol-containing solution inhibits SCFA production. However, when comparing the intervention-induced changes in SCFA concentrations within the first 24 hours, no significant differences were found between placebo and treatment groups (**Figure 2C-E**). Nonetheless, fold-change values of butyrate tended to be higher following *A. soehngenii* L2-7 feeding (p=0.06, **Figure 2C**).

A. soehngenii L2-7 intake increases postprandial GLP-1 response and reduces the extent of glucose variability

To establish the immediate metabolic effects of *A. soehngenii* L2-7 intake, a standardized mixed meal test (MMT) was performed in all participants 6 hours post-interventions and the excursion of incretins, glucose, insulin and triglycerides was followed over 120 minutes. A significant increase in postprandial plasma GLP-1 levels was observed upon *A. soehngenii* L2-7 treatment (**Figure 3A**, B, p=0.021). In line, during the first 24 hours, glucose excursions, determined as median absolute deviations (MAD) of continuous glucose measurements by FreeStyle Libre technology, were significantly diminished after the *A. soehngenii* L2-7 intake compared to placebo infusion (**Figure 3C**, p=0.045). In contrast, postprandial circulating levels of gastric inhibitory polypeptide (GIP), glucose, insulin and triglycerides were comparable between both interventions (**Figure S3A-D**). Given the higher fecal butyrate levels 24 hours post-*A. soehngenii* infusion, we assessed the concentrations of plasma SCFA at the end of the MMT; however, no significant differences in butyrate, acetate or propionate levels were observed between placebo and treatment intervention-groups (**Figure S4A-C**).

Since the genome of *A. soehngenii* L2-7 strain includes genes encoding a bile acid (BA) sodium symporter (EHLA_2286) and BA hydrolases (EHLA_1602, EHLA_2245)[21,22], we investigated the effects of *A. soehngenii* L2-7 on secondary BA. Albeit borderline significant (p=0.06), *A. soehngenii* L2-7 infusion augmented the postprandial excursions of secondary BA (**Figure 3D**). Notably, the postprandial levels of the secondary BA taurodeoxycholic acid (TDCA), taurolithocholic acid (TLCA), and glycodeoxycholic acid (GDCA) positively correlated with the GLP-1 postprandial excursion rate; whereas iso-ursodeoxycholic acid (IsoUDCA) rates associated with GLP-1 concentrations at 6h post-infusion (**Figure 3E**).

In light of the positive effects of *A. soehngenii* L2-7 on GLP-1 and BA plasma concentrations, we subsequently questioned whether the observed systemic outcomes were linked to differential expression of the butyrate and BA receptors in SI.

Figure 3. GLP-1, glucose and bile acid metabolism.

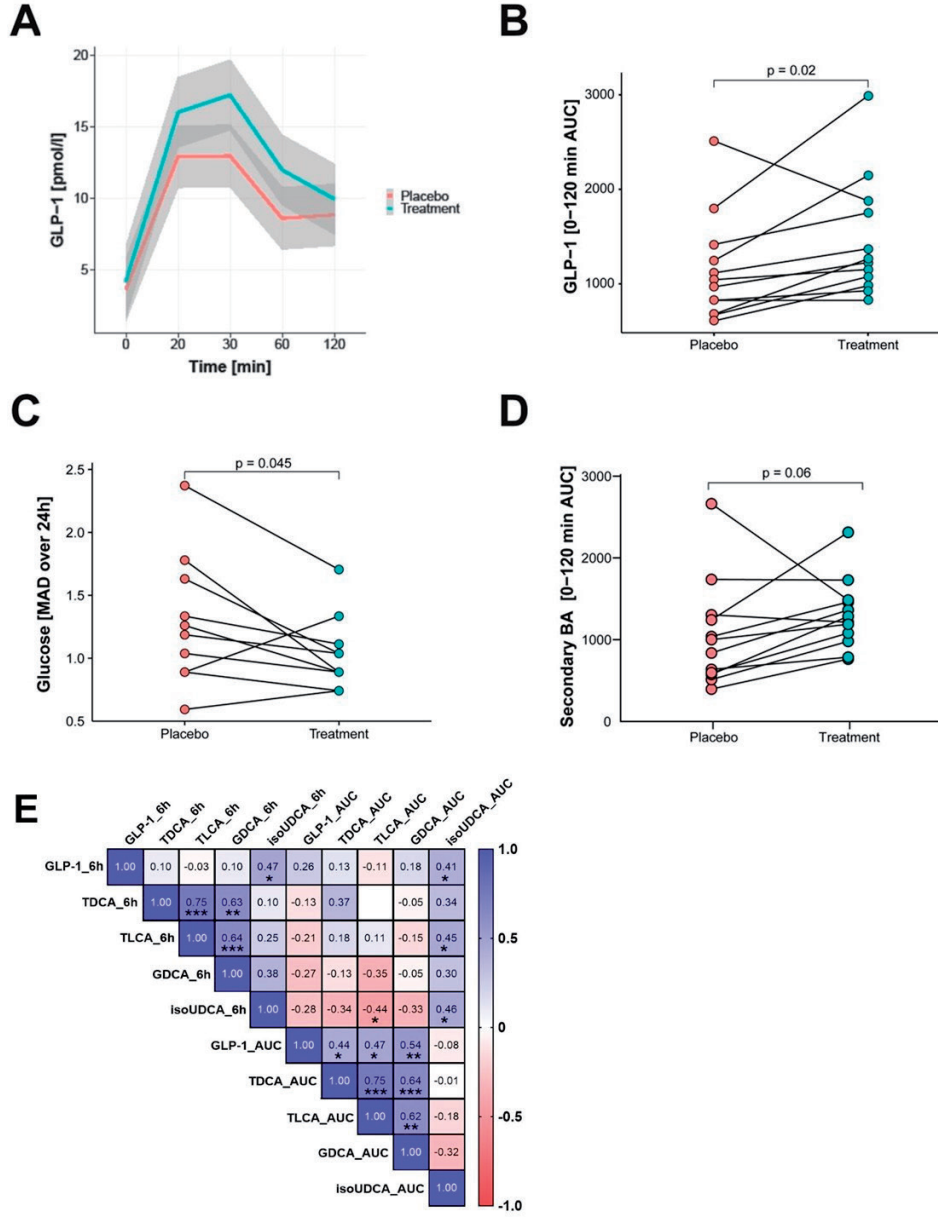

(**A**) Plasma GLP-1 levels (pmol/l) at 0, 20, 30, 120 minutes during mixed meal test (MMT). (**B**) Plasma GLP-1 levels during MMT as total area under the curve (AUC). (**C**) Median absolute deviation (MAD) of continuous glucose measurements (CGM) over the first 24 hours after placebo/treatment-intervention. (**D**) Total secondary bile acid plasma levels during MMT, shown as sum of areas under the curve (AUC) of TOMCA, TUDCA, TDCA, TUDCA, TLCA, GHDCA, GDCA, GUDCA, GLCA, OMCA, DCA, UDCA, LCA, HDCA, MuroCA, IsoUDCA. (**E**) Correlation heatmap showing the Spearman's rho rank correlation coefficients and statistically significant correlations (*=p-values ≤ 0.05, **=p-values ≤ 0.01, ***=p-values ≤ 0.001) between BA and GLP-1 levels 6 hours post-infusion (6h) or during the MMT (AUC).

Figure 4. Duodenal gene expression.

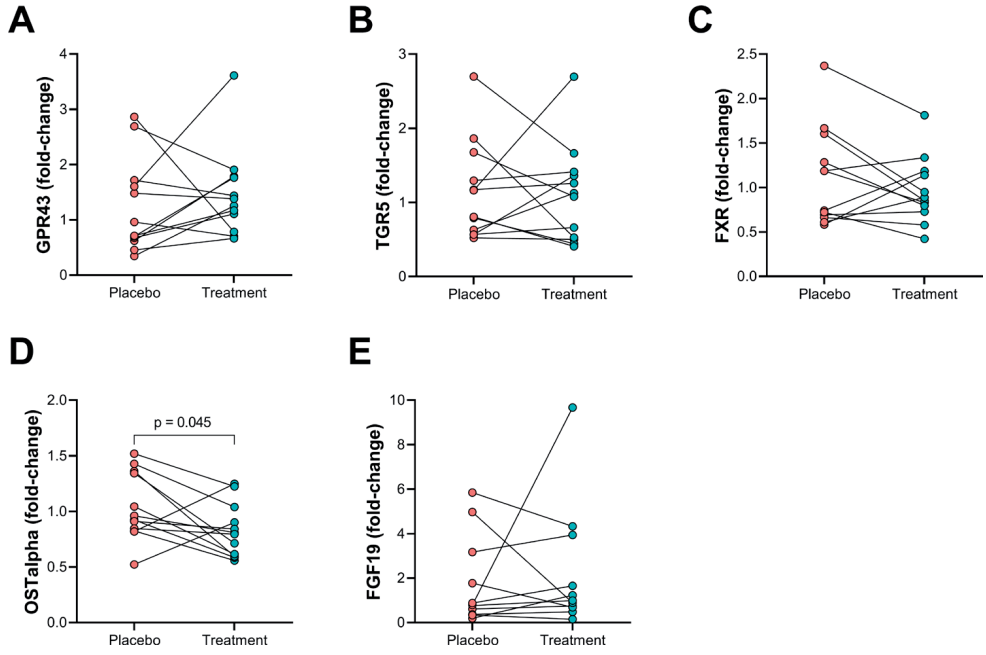

Gene expression measured by qPCR in duodenal biopsies of (**A**) *GPR43*, (**B**) *TGR5*, (**C**) *FXR*, (**D**) *OSTalpha*, and (**E**) *FGF19*. Data showing the relative gene expression (to placebo) using the 2^-(delta delta Ct) method.

Indeed, both butyrate and BA may act as GLP-1 secretagogues on intestinal L cells by binding the transmembrane receptors G protein-coupled receptor 43 (GPR43) and Takeda G protein-coupled receptor 5 (TGR5), respectively[23,24], whereas activation of the nuclear BA Farnesoid X receptor (FXR) inhibits GLP-1 secretion[25,26]. Gene expression of *GPR43*, *TGR5*, *FXR* and of the FXR-target genes *FGF19* and *OSTα*[27,28] was analyzed in duodenal biopsies taken at 6 hours post-infusion (**Figure 4A-E**). Gene expression of *GPR43*, *TGR5* and *FGF19* was comparable between placebo and treatment (median fold-change equal to 1.3, 1.1 and 0.9, respectively) (Figure 4A, B, E). Instead, upon *A. soehngenii* L2-7 intake, the transcript levels of *OSTα* were significantly decreased while *FXR* expression tended to be lower (median fold-change equal to 0.8 and 0.86, respectively) (**Figure 4C, D**), hinting to a reduced FXR activity.

A. soehngenii L2-7 significantly impacts duodenal gene expression with a remarkable upregulation of *REG1B* expression

To obtain an unbiased and in-depth snapshot of the intestinal transcriptome upon placebo/treatment-infusions, we employed RNA sequencing (RNAseq) technology using RNA isolated from duodenum biopsies. The RNAseq data set analysis shows

Figure 5. RNA sequencing (duodenal gene expression).

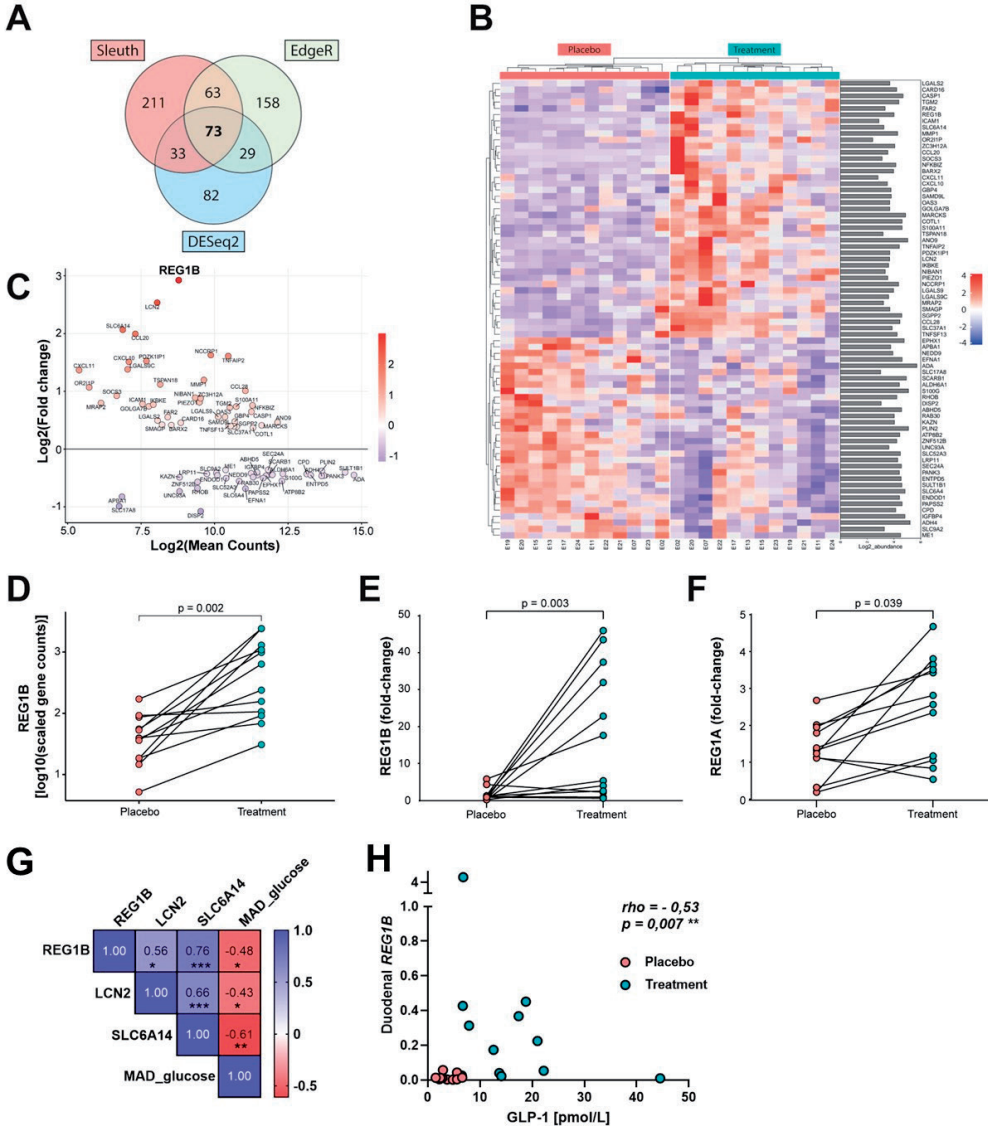

(**A**) RNA sequencing data sets analyzed by 3 digital gene expression (DGE) technologies: Sleuth, EdgeR and DESeq2 identified. Venn diagram showing the numbers of genes significantly up- or down-regulated in either one of the pipelines. (**B**) Heatmap of the 73 top differentially expressed (DE) genes between placebo and treatment, identified by all 3 DGE technologies. (**C**) MA (ratio intensity) plot visualizing the gene expression ratios (fold-changes treatment versus placebo, y axis) and the mean expression intensity (average RNAseq counts per gene, x axis) of DE genes. (**D**) RNAseq read counts of REG1B gene, duodenal expression. (**E**) Gene expression measured by qPCR in duodenal biopsies of REG1B and (**F**) REG1A, shown as fold-change versus placebo by 2^-(delta delta Ct) data analysis. (**G**) Correlation heatmap showing the Spearman's rho rank correlation coefficients and statistically significant correlations (*=p-values ≤ 0.05, **=p-values ≤ 0.01, ***=p-values ≤ 0.001) between duodenal gene expression of REG1B, LCN2, SLC6A14 and MAD (median absolute deviation of continuous glucose measurements over the first 24 hours after placebo/treatment-intervention. (**H**) Spearman's correlation between GLP-1 plasma concentrations 6 hours post-infusion and duodenal gene expression of REG1B (assessed by qPCR).

that a single-dose of *A. soehngenii* L2-7 is sufficient to substantially change the transcriptomic profile of duodenal mucosa as early as 6 hours after intake. Indeed, using the digital gene expression (DGE) analysis pipelines Sleuth, EdgeR and DESeq2, we found respectively 380, 323 and 217 genes significantly up- or down-regulated by *A. soehngenii* L2-7 intake (**Figure 5A**). Only the genes with significant adjusted p-values in all three statistical packages were retained, resulting in a total of 73 differentially expressed genes between placebo and treatment (**Figure 5B**). Among these genes, *REG1B*, *LCN2*, and *SLC6A14*, showed an upregulation above 2 log2(fold-change) after *A. soehngenii*-treatment, whereas *DISP2* was the most downregulated gene (-1 log2 (fold-change)) as compared to placebo. Overall, the most remarkable effect was the *A. soehngenii*-induced expression of *REG1B*, which encodes for the Regenerating Islet-Derived 1 Beta protein (**Figure 5C, D**). Originally discovered in pancreatic calculi, Reg family members 1-4 are small secreted proteins that have been reported to promote proliferation, b-cell mass expansion and exert antidiabetogenic activities[29–31]. We therefore further studied the gene and protein expression of Reg1B in SI biopsies upon placebo/treatment-interventions. By qPCR, we validated the RNAseq findings on *REG1B* expression and found that the expression of the closely related *REG1A* gene was also strongly upregulated in response to *A. soehngenii*-treatment (**Figure 5E,F, S5A**), whereas the transcript levels of *REG3A*, *REG3G* and *REG4* were not significantly upregulated upon *A. soehngenii* L2-7 infusion (**Figure S5B-D**). We next questioned whether the treatment-mediated intestinal alterations are linked to systemic responses. Strikingly, an inverse correlation was found between the duodenal expression of the most upregulated genes *REG1B*, *LCN2* and *SLC6A14* and systemic glucose variability (MAD), monitored continuously in the first 24 hours (**Figure 5G**). In addition, duodenal *REG1B* levels positively associated with the expression rates of *LCN2* and *SLC6A14*, and most importantly with the plasma concentrations of GLP1, underscoring systemic favourable effects of this single-bacterial strain intervention (**Figure 5G,H**).

Subsequently, we investigated the intestinal expression and localization of Reg1B and Reg1A proteins by westernblotting and immunohistochemistry (IHC) in small intestinal tissues. At protein level the mean expression of Reg1B and Reg1A within the duodenal mucosa trended toward higher expression after treatment, albeit not significant compared to placebo (**Figure 6A-C, S5E-G**). This inconsistency with gene expression rates is likely due to the fact that Reg proteins are secreted molecules. Immunostaining for Reg1B (performed with 2 different antibodies) showed a strong expression at the base of the crypts, where also stem cells and Paneth cells are located, and a milder staining throughout the villi and in the area delimited vacuolated cells (**Figure 6D, S5H**). Comparing the IHC staining for Reg1B and Reg1A, at the same

Figure 6. Reg1B expression in duodenum.

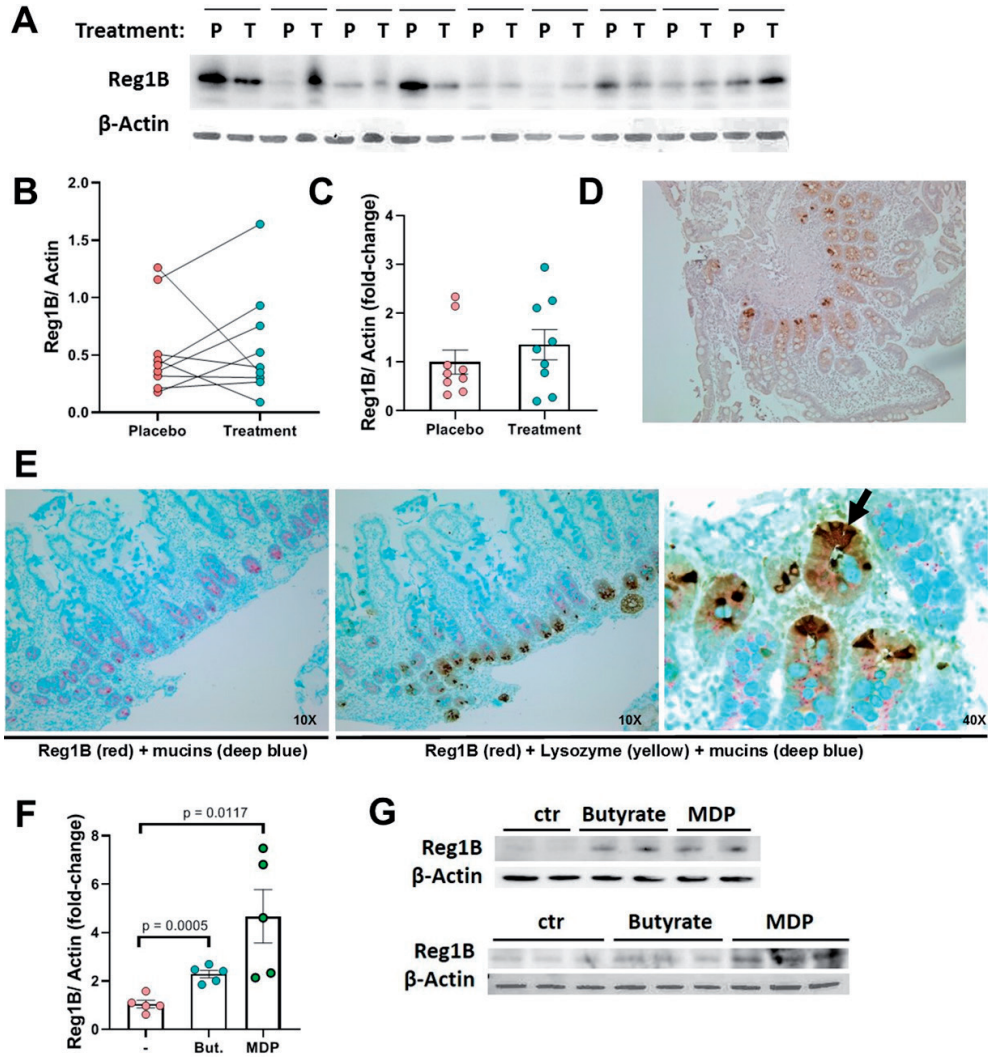

(**A**) Westernblot image of duodenal lysates blotted with antibodies against Reg1B and b-actin. (**B**) Quantification of Reg1B expression level in duodenal biopsies, Reg1B expression normalized to b-actin (loading control). (**C**) Reg1B protein expression shown as fold-change treatment versus placebo. (**D**) Immunohistochemical staining of Reg1B in duodenal biopsies. (**E**) Sequential immunostaining of duodenal biopsies for Reg1B (red), lysozyme (yellow, Paneth cells) and mucins (deep blue, Goblet cells). Images shown at 10X or 40X magnification, as indicated. Arrow indicating one of the Reg1B+Lysozyme co-localization point. (**F**) Quantification of Reg1B expression level in Caco-2 cells, Reg1B expression normalized to b-actin (loading control); Reg1B expression shown as fold-change treatment versus placebo. But.: Butyrate 1mM; MDP: muramyl dipeptide 1μg/ml. (**G**) Westernblot images of Caco-2 cell lysates blotted with antibodies against Reg1B and b-actin.

antibody concentrations, revealed that both proteins localize at the duodenal crypt bases, with Reg1B being more prominently expressed both in the crypt and villi compartments (Figure S5H). Since Reg1A and Reg1B belong to the same protein-family and are highly similar proteins of almost equal size, we excluded cross-reactivity of the antibodies utilized by using recombinant human (rh) Reg1B and Reg1A proteins in Westernblotting assays, as performed by Zheng *et al.*[32]. The antibodies directed against Reg1B did not recognize Reg1A and *vice versa* **(Figure S5I,K**).

To further unravel the nature of the cell-types expressing REG1B within crypt-villus units, we performed a triple-staining to visualize Reg1B (red), lysozyme (yellow, Paneth cell marker), and mucins (Alcian blue dye, Goblet cell marker) (**Figure 6E**). As for the single-staining, the Reg1B red staining is prominently found at the crypt base, co-localized with the immunostaining (brown) of lysozyme, and it is adjacent to blue dyed mucin-positive cells. Although further investigations are needed to understand the nature of these transcriptional changes, our findings indicate that Reg1B is expressed in intestinal villi, especially at the crypt-base and might be produced and secreted by Paneth cells in response to *A. soehngenii* L2-7 transit. In this regard, the low concentrations of plasma Reg1B, assessed 8 hours post-duodenal infusion (at the end of the MMT) (**Figure S5J**) suggest that Reg1B is mainly secreted into the (small) intestinal lumen, thereby acting in a paracrine manner on intestinal cells. To understand how *A. soehngenii* L2-7 may regulate Reg1B expression, we further exposed Caco-2 cells for 6 hours to either butyrate or muramyl dipeptide (MDP), the bioactive bacterial peptidoglycan motif, and found a marked upregulation of Reg1B upon both stimulations (**Figure 6F,G**). In line, direct exposure to heat-inactivated *A. soehngenii* L2-7 bacteria upregulates Reg1B expression (**Figure S5L**).

Importantly, no carry-over effects were observed between week 0 and week 4, independently of the intervention order, as shown in Figure S6 for baseline fecal levels of *A. soehngenii*, fecal butyrate, plasma GLP1 excursions and glucose MAD in the first 24 hours post-infusion (**Figure S6A-D**).

DISCUSSION

In this pioneer randomized cross-over phase 2 trial, we demonstrate the early and wide impact of a single duodenal infusion of *A. soehngenii* L2-7 on the duodenal transcriptomic profile and, moreover, we identify the metabolic parameters being influenced (for up to 24 hours) by a single-dose of live *A. soehngenii* L2-7 in treatment-naïve subjects with metabolic syndrome. Indeed, administration of *A. soehngenii* L2-7 (versus placebo) resulted in an altered small intestinal gene expression signature and, most prominently, in the upregulation of *REG1B*. Moreover,

A. soehngenii L2-7 infusion induced higher postprandial plasma bile salt and GLP-1 levels as well as lower glucose variability (MAD) within 24 hours after the infusion of *A. soehngenii* L2-7. Although further investigations are warranted, these data, combined with our previous studies[14,15], suggest that *A. soehngenii* L2-7 improves human glucose metabolism in human metabolic syndrome, likely by shaping BA metabolism and augmenting intestinal GLP-1 production.

We previously showed that, in subjects with metabolic syndrome, oral intake of *A. soehngenii* L2-7 for 4 weeks increased plasma primary and, particularly, secondary bile acids[15], which are known to be formed by commensal microbes, such as those belonging to the *Ruminococcaceae* and *Lachnospiraceae*[33,34]. Moreover, in db/db mice, 4-week oral *A. soehngenii* L2-7 treatment alleviated insulin resistance and modified bile salt metabolism in conjunction with augmenting the expression of genes involved in BA metabolism/transport in SI, including suppression of duodenal *Fxr* and *Ost-alpha* expression[14]. Remarkably, we here disclose that a single duodenal infusion of *A. soehngenii* L2-7 is sufficient to increase secondary BA, of which TDCA, TLCA, GDCA, and isoUDCA associate with increase GLP-1 levels. These findings are in line with previous studies showing that conjugated BA, including TDCA, TLCA, GDCA and UDCA, promote GLP-1 release by intestinal L cells[35–39]. Notably, the genome of *A. soehngenii* L2-7 harbors a bile acid sodium symporter gene (EHLA_2286) as well as two bile salt hydrolase (BSH)-encoding genes (locus tags EHLA_1602 and EHLA_2245)[21]. Besides, transcriptome analysis of a simplified microbiota community (harboring the *A. soehngenii* L2-7 strain) engrafted in murine guts confirmed that both bsh genes are functionally expressed in the intestinal tract[22]. These findings together with our observations of increased secondary BA upon *A. soehngenii* feeding (this study,[15]) point to an active role of this strain in the formation of secondary BA, which may act as GLP-1 secretagogues by binding the TGR5 receptor[24,40,41]. In addition, *A. soehngenii* L2-7 decreased the duodenal expression of the FXR-target *OSTalpha*[27], consistent with a de-activation of FXR signaling observed in *A. soehngenii* L2-7–treated ob/ob mice[14]. Notably, FXR suppresses GLP-1 secretion by enteroendocrine L cells, whereas its inhibition improves metabolic control[25,26,42]. Thus, the diminished FXR activation may also account for more GLP-1 availability and, according to the study of Ducastel *et al.*, more L cells' responsiveness to butyrate/GPR43 signaling[26]. Indeed, we observed a significant effect of *A. soehngenii* L2-7 infusion on postprandial levels of GLP-1, but not GIP, suggesting that this strain sensitizes L cells to secrete more GLP-1, likely in response to its own metabolites, such as butyrate and secondary (hydrophobic) BA. This hypothesis is supported by animal studies showing that gut microbiota has a rapid and pronounced effect on L cell and GLP-1 content, predominantly in the small intestine where there is direct contact between enteroendocrine cells and mucosal microbiota[16,43,44]. Moreover, *A. soehngenii* L2-7

is a known producer of the SCFA butyrate[11], which by binding its receptor GPR43 expressed on L cells stimulates GLP-1 secretion[23]. Overall, the *A. soehngenii* L2-7-mediated increase in plasma GLP-1, whether through butyrate/BA signaling and/or FXR inhibition, may justify the observed reduction in glucose MAD after bacteria intake. This improvement in glycemic variability may be the result of the insulin sensitizing effects of butyrate as well as GLP-1[12,17,18]. In addition, we cannot exclude that *A. soehngenii* L2-7 ameliorates the glycemic control through alternative (less obvious) mechanisms: e.g. by contributing to the generation of microbiota-derived neurotransmitters, in forms of proteins/peptides or gases, which can act locally on gut muscle relaxation or enteric neuron activation as well as distally on the brain influencing appetite, behavior and peripheral glucose homeostasis[45]. Furthermore, a recent study disclosed that the beneficial action of *Akkermansia muciniphila* on the systemic metabolic profile are accounted by a bacterial protein, named P9, of the peptidase S41A family that stimulates, *in vivo*, thermogenesis and GLP-1 secretion[46]. Curiously, *A. soehngenii* has the genetic capacity to express the peptidase S41 family, underscoring that multiple processes may dictate the observed metabolic benefits of *A. soehngenii,* beyond BA/butyrate production (e.g. *via* production of bioactive molecules or possibly *via* Reg1B induction).

Although the fold-change comparison of fecal butyrate rates showed that butyrate tended to be higher after *A. soehngenii*-treatment, herewith, we also found a negative effect of placebo infusion on butyrate and acetate concentrations; an effect most likely due to side-effects of glycerol on SCFA production, as earlier described[47]. Nonetheless, SCFA levels remained stable after *A. soehngenii* L2-7 administration suggesting that an increased SCFA production by *A. soehngenii* L2-7 counterbalances the reduction in SCFA caused by glycerol infusion and can hence better modulate intestinal GLP-1 production. In contrast to the changes seen in fecal butyrate, the plasma levels of butyrate were largely unaffected 8 hours after *A. soehngenii*-treatment. This might be due to the fact that microbially-produced butyrate is the primary energy source for colonocytes and hepatic lipid and glucose production[1] rendering more difficult to detect disparities in its circulating peripheral plasma levels. Notwithstanding, we cannot exclude that variations in circulating SCFA concentrations become evident at later time-point (e.g. 24 hours, as for the fecal SCFA levels).

Being at the interface with intestinal microbiota, duodenal mucosa cells underwent a robust transcriptional reprogramming upon encountering *A. soehngenii* L2-7. The most differentially expressed genes after bacteria administration encode for proteins involved in metabolite transport, cholesterol metabolism or cytokine signaling. Nevertheless, the 3 most upregulated genes *REG1B*, *LCN2* and *SLC6A14* were found to negatively correlate with glucose MAD rates, hinting to a protective

function in glycemic control. In line, rodent studies demonstrate that increased LCN2 expression promotes glucose tolerance, insulin sensitivity and controls appetite[48] whereas LCN2 deficiency worsens insulin resistance[49]. Similarly, SLC6A14 deficiency in high-fat diet-fed mice worsens adiposity and metabolic syndrome. Accordingly, the obesity-linked single-nucleotide polymorphism (SNP) in SLC6A14 has been shown to reduce SLC6A14 expression[50].

The most prominent changes were seen in the expression of *REG1B*, which along with *REG1A* was markedly upregulated after *A. soehngenii* L2-7 administration. They are both members of the regenerating islet-derives (REG) gene family, which was first discovered in pancreas, being expressed mainly by exocrine acinar cells and, upon cellular damage, in the islets of Langerhans[51]. Animal studies utilizing Reg knock-out, overexpression or administration of recombinant REG proteins showed that Reg proteins elicit mitogenic effects on b-cells and protection against diabetes[29,52,53]. However, genomic SNPs in the REG1B were not associated with T2D[54] suggesting that tissue specific expression is more relevant. Similarly to the pancreas, intestinal Reg protein expression has been linked to proliferation being enhanced in inflamed and neoplastic conditions[55–57]. By immunostaining we found that Reg1B and Reg1A are localized at the base of small-intestinal crypts with Reg1B being more prominently expressed by Paneth cells as compared to it expression (at a lower extent) in enterocytes; this corroborated by a previous study describing *REG1A*, *REG1B*, and *REG3* gene expression in Paneth cells[57]. Notably, Paneth cells guard $Lgr5^{+}$ stem cells in the crypt bases through production signaling and bactericidal molecules. Indeed, Paneth cells have been reported to directly sense indigenous microbes via Toll-like receptor engagement and, thus, limit mucosa penetration by commensals by secreting antimicrobial products, which include Reg3b and Reg3g proteins[58]. In line, we disclose that in enterocytes Reg1B expression is triggered by peptidoglycan and butyrate. Although further investigations are needed, we can argue that intestinal epithelial and Paneth cells sense the administered bacteria via GPR and innate immune receptors, resulting in the induction of *REG1* expression. The regenerating activities of Reg proteins on pancreatic cells seem to act in an auto/paracrine manner[51,53], hence it is likely that the duodenally secreted Reg1A/B act locally, possibly inducing progenitor or L cell hyperplasia. In support of a "local" effect of Reg1B on intestinal L cells, duodenal *REG1B* levels significantly associated with GLP-1 concentrations, and Reg1B concentrations were markedly lower in plasma samples than in duodenal tissues. Indeed, Reg1B was non-detectable in plasma samples of 6 patients 8 hours after placebo intake and in 2 samples following *A. soehngenii* L2-7 infusion. At protein levels, we did not find a significant difference in Reg1B/1A expression in duodenum between placebo- and treatment-interventions although increased in the latter. We therefore feel that this is likely due to their secretion into the intestinal lumen and hence loss of Reg proteins within the duodenal mucosa[59].

As expected and importantly for the cross-over nature of our study-design, the single duodenal bacteria infusion did not affect fecal microbiota composition and Shannon microbial diversity in a major manner, therefore excluding treatment-induced carry-over effects. Accordingly, the order of interventions did not impact the levels of fecal butyrate, postprandial GLP-1 responses nor the 24-hour glucose variability. Also, the lack of fluctuations in fecal *A. soehngenii* L2-7 abundancy over time was anticipated as it is unlikely that a single-dose of 10^{11} bacteria results in colonic colonization. Notwithstanding, these findings implicate that the herein reported effects of *A. soehngenii* are triggered solely by its transit throughout the gut and they would be greatly enhanced with a full bacteria engraftment of the SI/colon.

Limitations

Some limitations of this study need to be acknowledged. We administered the bacterial strain only once, as performed by Van Baarlen *et al.* [60] with a Lactobacillus strain; nonetheless multiple infusions could permit bacteria colonization of the gut and, consequently, elicit more prominent and lasting metabolic responses. Herein, by using a nosoduodenal infusion, we limited the deleterious effects of stomach acid and oxygen exposure on the viability of *A. soehngenii* L2-7, thus optimizing the clinical potential of *A. soehngenii*. Nevertheless, future studies will have to demonstrate whether multiple bacterial administrations *via* duodenal-tube infusions or enteric-coated capsules will result in more pronounced effects[61].

Conclusions

To our knowledge, this is the first study to administer a single strain of a strict anaerobe directly into the duodenum to maximally preserve viability bypassing the stomach. Single duodenal infusion of *A. soehngenii* L2-7 resulted in a significantly altered expression of small intestinal genes with the most prominent effect on *REG1B*, which was found to be associated with increased GLP-1 levels and improved peripheral glycemic control and to be strongly expressed at the base of the intestinal crypts within Paneth cells. Moreover, the infusion of *A. soehngenii* L2-7 rapidly triggers favorable changes in metabolic parameters: it significantly enhances post-prandial GLP-1 response (6 hours after intake) and ameliorates blood glucose variability (MAD, first 24 hours). Although *A. soehngenii*-derived bioactive metabolites and the incretin system may drive the improvement in glycemic control and the insulin sensitizing effects of this strain, further studies are warranted to elucidate the mechanisms underlying the beneficial effects of *A. soehngenii*.

MATERIAL AND METHODS

Patient recruitment and involvement

Twelve Caucasian male subjects (age 21 – 69 years) with a body mass index (BMI) between 30 and 43 kg/m^2 were recruited by local newspaper advertisements (period of recruitment and follow-up: December 2017-February 2019). In order to be included in the trial, all subjects had to be treatment-naïve and suffer from metabolic syndrome, determined by the presence of ≥ 3 criteria out of the 5 following criteria: fasting plasma glucose ≥ 5.6 mmol/l, triglycerides ≥ 1.7 mmol/l, waist-circumference ≥ 102 cm, high-density lipoprotein (HDL-) cholesterol ≤ 1.04 mmol/l and blood pressure ≥ 130/85 mmHg[62]. Also, HOMA (>2.5) was included as an extra screening marker of insulin resistance. Exclusion criteria included a history of cardiovascular event, cholecystectomy, overt untreated gastrointestinal disease or abnormal bowel habits, liver enzymes >2.5-fold higher than the upper limit of normal range, smoking, alcohol abuse and use of proton pump inhibitors or antibiotics in the past three months. Only males were included in the study to avoid confounding effects on insulin sensitivity due to changes in female hormone concentrations in (postmenopausal) women[63]. Study participants were requested not to alter their physical exercise and dietary patterns after inclusion. The study was approved by the local Institutional Review Board of the Amsterdam University Medical Center (Amsterdam UMC) in Amsterdam, the Netherlands, and conducted in accordance with the Declaration of Helsinki. Patients were not involved in the design and conduct of this research; although they were thoroughly informed about the procedures and goals of the study upon recruitment visits. All participants signed a written informed consent. The study was registered at the Dutch Trial Register (NL6630).

STUDY DESIGN

This was a randomized double-blind placebo-controlled cross-over phase 2 study. All subjects (N=12) received both treatment (10^{11} *A. soehngenii* L2-7 cells, dosage based on our previous study[15]) and placebo (10% glycerol-PBS), with a washout period of four weeks in between, as depicted in **Figure 1**. The order of administration was randomized in a 1:1 fashion, using computerized randomization, and double-blinded (to patients and doctor in charge). After overnight fasting, a duodenal tube was placed using the electromagnetic-guided (EM-guided) system Cortrak®. The treatment arm received 10 ml of 10:90 glycerol:PBS solution containing *A. soehngenii* L2-7 (NCBI taxonomy ID 105843)[10] at a concentration of 10^{10} cells/ml (total of 10^{11} cells) infused distally to the papilla of Vater; whereas the placebo arm underwent

the same intervention receiving only 10ml of vehicle solution (10% glycerol in PBS). Six hours later a gastro duodenoscopy was performed and duodenal biopsies were taken around the same location as the duodenal infusion and either stored in paraffin for histology or snap-frozen in liquid nitrogen and then stored at -80°C. After the gastro-duodenoscopy a two-hour mixed meal test was conducted as previously described[9]. Subjects received an intravenous catheter in a distal arm vein over which baseline blood samples were drawn, hereafter subjects immediately ingested a liquid meal solution (Nutridrink, Nutricia Advanced Medical Nutrition, Amsterdam, Netherlands) containing 600kcal (35% fat, 49% carbohydrates and 16% proteins) and for the subsequent two hours blood samples were drawn for postprandial glucose, insulin, triglyceride, GIP and GLP-1 excursions (measured by standard clinical diagnostic methods). Subjects received a continuous glucose monitor (CGM, FreeStyle Libre System, FSL, Abbott USA) for 24 hours. Finally, subjects were asked to keep an online nutritional diary to monitor food intake during these days after the intervention (https://mijn.voedingscentrum.nl/nl/eetmeter/) and collect fecal samples at several time-points (see **Figure 1**). Four weeks after the first visit the complete study cycle was repeated switching intervention arms for each patient.

Detailed method description is provided in Supplementary Material.

REFERENCES

1. Warmbrunn, M. V. *et al.* Gut microbiota: a promising target against cardiometabolic diseases. *Expert Rev. Endocrinol. Metab.* **15**, 13–27 (2020).
2. Ridaura, V. K. *et al.* Gut microbiota from twins discordant for obesity modulate metabolism in mice. *Science (80-.).* **341**, (2013).
3. Vrieze, A. *et al.* Transfer of intestinal microbiota from lean donors increases insulin sensitivity in individuals with metabolic syndrome. *Gastroenterology* **143**, (2012).
4. Kootte, R. S. *et al.* Improvement of Insulin Sensitivity after Lean Donor Feces in Metabolic Syndrome Is Driven by Baseline Intestinal Microbiota Composition. *Cell Metab.* **26**, 611–619. e6 (2017).
5. Pedersen, H. K. *et al.* Human gut microbes impact host serum metabolome and insulin sensitivity. *Nature* **535**, 376–381 (2016).
6. Thingholm, L. B. *et al.* Obese Individuals with and without Type 2 Diabetes Show Different Gut Microbial Functional Capacity and Composition. *Cell Host Microbe* **26**, 252-264.e10 (2019).
7. Karlsson, F. H. *et al.* Gut metagenome in European women with normal, impaired and diabetic glucose control. *Nature* **498**, 99–103 (2013).
8. Le Chatelier, E. *et al.* Richness of human gut microbiome correlates with metabolic markers. *Nature* **500**, 541–546 (2013).
9. Kootte, R. S. *et al.* Improvement of Insulin Sensitivity after Lean Donor Feces in Metabolic Syndrome Is Driven by Baseline Intestinal Microbiota Composition. *Cell Metab.* (2017). doi:10.1016/j.cmet.2017.09.008
10. Shetty, S. A. *et al.* Reclassification of eubacterium hallii as Anaerobutyricum hallii gen. nov., comb. nov., and description of Anaerobutyricum soehngenii sp. nov., a butyrate and propionate-producing bacterium from infant faeces. *Int. J. Syst. Evol. Microbiol.* **68**, 3741–3746 (2018).
11. Duncan, S. H., Louis, P. & Flint, H. J. Lactate-utilizing bacteria, isolated from human feces, that produce butyrate as a major fermentation product. *Appl. Environ. Microbiol.* **70**, 5810–7 (2004).
12. Gao, Z. *et al.* Butyrate improves insulin sensitivity and increases energy expenditure in mice. *Diabetes* **58**, 1509–1517 (2009).
13. Bouter, K. E. C. *et al.* Differential metabolic effects of oral butyrate treatment in lean versus metabolic syndrome subjects article. *Clin. Transl. Gastroenterol.* **9**, (2018).
14. Udayappan, S. *et al.* Oral treatment with Eubacterium hallii improves insulin sensitivity in db/db mice. *npj Biofilms Microbiomes* **2**, (2016).
15. Gilijamse, P. W. *et al.* Treatment with Anaerobutyricum soehngenii: a pilot study of safety and dose–response effects on glucose metabolism in human subjects with metabolic syndrome. *npj Biofilms Microbiomes* **6**, 1–10 (2020).
16. Greiner, T. U. & Bäckhed, F. Microbial regulation of GLP-1 and L-cell biology. *Mol. Metab.* **5**, 753–758 (2016).
17. Jiang, Y. *et al.* GLP-1 improves adipocyte insulin sensitivity following induction of endoplasmic reticulum stress. *Front. Pharmacol.* **9**, 1–10 (2018).
18. Guo, C. *et al.* Glucagon-like peptide 1 improves insulin resistance in vitro through anti-inflammation of macrophages. *Brazilian J. Med. Biol. Res.* **49**, 1–9 (2016).
19. Louis, P., Young, P., Holtrop, G. & Flint, H. J. Diversity of human colonic butyrate-producing bacteria revealed by analysis of the butyryl-CoA:acetate CoA-transferase gene. *Environ. Microbiol.* **12**, 304–314 (2010).
20. Engels, C., Ruscheweyh, H. J., Beerenwinkel, N., Lacroix, C. & Schwab, C. The common gut microbe Eubacterium hallii also contributes to intestinal propionate formation. *Front. Microbiol.* **7**, 1–12 (2016).

21. Shetty, S. A., Ritari, J., Paulin, L., Smidt, H. & De Vos, W. M. Complete Genome Sequence of Eubacterium hallii Strain L2-7. *Genome Announc.* **5**, 4–5 (2017).
22. Kovatcheva-Datchary, P. *et al.* Simplified Intestinal Microbiota to Study Microbe-Diet-Host Interactions in a Mouse Model. *Cell Rep.* **26**, 3772–3783.e6 (2019).
23. Tolhurst, G. *et al.* Short-chain fatty acids stimulate glucagon-like peptide-1 secretion via the G-protein-coupled receptor FFAR2. *Diabetes* **61**, 364–71 (2012).
24. Thomas, C. *et al.* TGR5-mediated bile acid sensing controls glucose homeostasis. *Cell Metab.* **10**, 167–77 (2009).
25. Trabelsi, M. S. *et al.* Farnesoid X receptor inhibits glucagon-like peptide-1 production by enteroendocrine L cells. *Nat. Commun.* **6**, 1–13 (2015).
26. Ducastel, S. *et al.* The nuclear receptor FXR inhibits Glucagon-Like Peptide-1 secretion in response to microbiota-derived Short-Chain Fatty Acids. *Sci. Rep.* **10**, 1–10 (2020).
27. Landrier, J. F., Eloranta, J. J., Vavricka, S. R. & Kullak-Ublick, G. A. The nuclear receptor for bile acids, FXR, transactivates human organic solute transporter-α and -β genes. *Am. J. Physiol. - Gastrointest. Liver Physiol.* **290**, 476–485 (2006).
28. Inagaki, T. *et al.* Fibroblast growth factor 15 functions as an enterohepatic signal to regulate bile acid homeostasis. *Cell Metab.* **2**, 217–225 (2005).
29. Unno, M. *et al.* Production and characterization of Reg knockout mice: Reduced proliferation of pancreatic β-cells in Reg knockout mice. *Diabetes* **51**, (2002).
30. Gross, D. J. *et al.* Amelioration of diabetes in nonobese diabetic mice with advanced disease by linomide-induced immunoregulation combined with Reg protein treatment. *Endocrinology* **139**, 2369–2374 (1998).
31. Cui, W. *et al.* Overexpression of Reg3α increases cell growth and the levels of cyclin D1 and CDK4 in insulinoma cells. *Growth Factors* **27**, 195–202 (2009).
32. Zheng , H. *et al.* Expression profile of the REG gene family in colorectal carcinoma. *J Histochem Cytochem.* **59**, 106-15 (2011).
33. Begley, M., Hill, C. & Gahan, C. G. M. Bile salt hydrolase activity in probiotics. *Appl. Environ. Microbiol.* **72**, 1729–1738 (2006).
34. Id, M. H. F., Id, S. O. F., Id, R. B. & Id, C. M. T. Bile salt hydrolases : Gatekeepers of bile acid metabolism and host-microbiome crosstalk in the gastrointestinal tract. *PLOS Pathog.* 1–6 (2019).
35. Brighton , C. A. *et al.* Bile Acids Trigger GLP-1 Release Predominantly by Accessing Basolaterally Located G Protein-Coupled Bile Acid Receptors. *Endocrinology.* **156**, 3961-70 (2015).
36. Kuhre, R. E. *et al.* Bile acids are important direct and indirect regulators of the secretion of appetite- and metabolism-regulating hormones from the gut and pancreas. *Mol Metab.* **11**, 84-95 (2018).
37. van Nierop, F. S. *et al.* Differential effects of a 40-hour fast and bile acid supplementation on human GLP-1 and FGF19 responses. *J Physiol Endocrinol Metab.* **317**, E494-E502 (2019).
38. Calderon, G. *et al.* Ileo-colonic delivery of conjugated bile acids improves glucose homeostasis via colonic GLP-1-producing enteroendocrine cells in human obesity and diabetes. *EBioMedicine.* **55**, 102759 (2020).
39. Murakami, M. *et al.* Incretin secretion stimulated by ursodeoxycholic acid in healthy subjects. *Springerplus.* **2**, 20 (2013).
40. Katsuma, S., Hirasawa, A. & Tsujimoto, G. Bile acids promote glucagon-like peptide-1 secretion through TGR5 in a murine enteroendocrine cell line STC-1. *Biochem. Biophys. Res. Commun.* **329**, 386–90 (2005).
41. Brighton, C. A. *et al.* Bile acids trigger GLP-1 release predominantly by accessing basolaterally located G protein-coupled bile acid receptors. *Endocrinology* **156**, 3961–3970 (2015).
42. Jiang, C. *et al.* Intestine-selective farnesoid X receptor inhibition improves obesity-related metabolic dysfunction. *Nat. Commun.* **6**, (2015).

43. Arora, T. *et al.* Microbial regulation of the L cell transcriptome. *Sci. Rep.* **8**, 1–9 (2018).
44. Cani, P. D., Hoste, S., Guiot, Y. & Delzenne, N. M. Dietary non-digestible carbohydrates promote L-cell differentiation in the proximal colon of rats. *Br. J. Nutr.* **98**, 32–37 (2007).
45. Knauf, C. *et al.* Targeting the Enteric Nervous System to Treat Metabolic Disorders? "Enterosynes" as Therapeutic Gut Factors. *Neuroendocrinology*. **110**, 139-146 (2020).
46. Yoon, H. S. *et al.* Akkermansia muciniphila secretes a glucagon-like peptide-1-inducing protein that improves glucose homeostasis and ameliorates metabolic disease in mice. *Nat Microbiol.* **6**, 563-573 (2021).
47. De Weirdt, R. *et al.* Human faecal microbiota display variable patterns of glycerol metabolism. *FEMS Microbiol. Ecol.* **74**, 601–611 (2010).
48. Mosialou, I. *et al.* MC4R-dependent suppression of appetite by bone-derived lipocalin 2. *Nature* **543**, 385–390 (2017).
49. Guo, H. *et al.* Lipocalin-2 deficiency impairs thermogenesis and potentiates diet-induced insulin resistance in mice. *Diabetes* **59**, 1376–1385 (2010).
50. Sivaprakasam, S. *et al.* SLC6A14 deficiency is linked to obesity, fatty liver, and metabolic syndrome but only under conditions of a high-fat diet. *Biochim Biophys Acta Mol Basis Dis*. **1867**, 166087 (2021).
51. Baeza, N. *et al.* Pancreatitis-associated protein (HIP/PAP) gene expression is upregulated in NOD mice pancreas and localized in exocrine tissue during diabetes. *Digestion* **64**, 233–239 (2001).
52. Takasawa, S. *et al.* Cyclin D1 activation through ATF-2 in Reg-induced pancreatic β-cell regeneration. *FEBS Lett.* **580**, 585–591 (2006).
53. Xiong, X. *et al.* Pancreatic islet-specific overexpression of Reg3β protein induced the expression of pro-islet genes and protected the mice against streptozotoc in induced diabetes mellitus. *Am. J. Physiol. - Endocrinol. Metab.* **300**, 669–680 (2011).
54. Banchuin, N. *et al.* No abnormalities of reg1α and reg1β gene associated with diabetes mellitus. *Diabetes Res. Clin. Pract.* **55**, 105–111 (2002).
55. Tsuchida, C. *et al.* Expression of REG family genes in human inflammatory bowel diseases and its regulation. *Biochem. Biophys. Reports* **12**, 198–205 (2017).
56. Zheng, H. C. *et al.* Expression profile of the REG gene family in colorectal carcinoma. *J. Histochem. Cytochem.* **59**, 106–115 (2011).
57. Van Beelen Granlund, A. *et al.* REG gene expression in inflamed and healthy colon mucosa explored by in situ hybridisation. *Cell Tissue Res.* **352**, 639–646 (2013).
58. Vaishnava, S., Behrendt, C. L., Ismail, A. S., Eckmann, L. & Hooper, L. V. Paneth cells directly sense gut commensals and maintain homeostasis at the intestinal host-microbial interface. *Proc. Natl. Acad. Sci.* **105**, 20858–20863 (2008).
59. Peterson, K. M. *et al.* REG1B as a predictor of childhood stunting in Bangladesh and Peru1-3. *Am. J. Clin. Nutr.* **97**, 1129–1133 (2013).
60. van Baarlen, P. *et al.* Differential NF- B pathways induction by Lactobacillus plantarum in the duodenum of healthy humans correlating with immune tolerance. *Proc. Natl. Acad. Sci.* **106**, 2371–2376 (2009).
61. Del Piano, M. *et al.* Evaluation of the intestinal colonization by microencapsulated probiotic bacteria in comparison with the same uncoated strains. *J. Clin. Gastroenterol.* **44**, 42–46 (2010).
62. Alberti, K. G. M. M., Zimmet, P. & Shaw, J. Metabolic syndrome - A new world-wide definition. A consensus statement from the International Diabetes Federation. *Diabet. Med.* **23**, 469–480 (2006).
63. Brown, M. D. *et al.* Insulin Sensitivity in Postmenopausal Women. *Diabetes Care* **23**, 1731–1736 (2000).

SUPPLEMENTAL MATERIAL AND METHODS

Culturing of *A. soehngenii*

The cells were obtained as described previously[1] by culturing *A. soehngenii L2-7* at 500-liter scale in a basic phosphate-bicarbonate salt medium containing 2% yeast extract, 0.4% soy peptone, and 2% sucrose, at pH 6.8 and 37C. Following autoclaving, filter-sterilized components were added, including cysteine (final concentration 0.05%) and a 1 ml per liter of a vitamin solution (containing per liter 10 mg biotin, 10 mg cobalamin, 30 mg para-aminobenzoic acid, 50 mg folic acid, and 150 mg pyridoxamine). *A. soehngenii* L2-7 cells were harvested by microfiltration, washed with PBS, and finally stored in PBS containing 10% glycerol at a concentration of 10^{10} cells/ml in 10 ml tubes at -80°C. *A. soehngenii* L2-7 was handled under strict anaerobic conditions which were maintained during all stages of the production of the concentrated cells: during growth, microfiltration, glycerol mixing, and filling of the tubes with a nitrogen atmosphere. The viability of *A. soehngenii* L2-7 in randomly selected tubes (stored at -80°C at the AMC Department of Clinical Pharmacy) was tested every 6 months during the study using most probable number (MPN) analysis in YCFA medium. MPN analyses were performed in duplicate in anoxic YCFA medium containing sucrose incubated at 37°C for 5 days[1]. Growth was scored by visual and microscopic inspection. Viability stayed constant at 10^{10} cells/ml during the time of the study.

Duodenal RNA sequencing and differential gene expression analysis

RNA for RNA sequencing analysis was isolated from duodenum biopsies, which were directly snap-frozen in liquid nitrogen after biopsy and stored at -80˚C until analysis, from all 12 included participants, using an RNA isolation protocol optimized for small tissue biopsies. In short, biopsies were mixed with 300 μl TriPure (Roche, Basel, Switzerland) and homogenized on ice using a sterile, RNAse free pestle. After short centrifugation, 60 μl of chloroform was added. Samples were then added to a Heavy Phase Lock gel tube (Quanta Bio, Beverly, USA) and centrifuged (15 min, 12.000 x g, 4˚C). The aqueous phase was transferred and mixed with 1 volume of 70% ethanol. The mixture was added to a RNeasy MinElute spin column (QIAgen, Tegelen, the Netherlands). RNA was washed according to manufacturer's protocol and eluted in 14 μl RNAse free water. RNA concentration was measured using the NanoDrop 1000 (Thermo Scientific, Landsmeer, the Netherlands). RIN scores were assessed on a Bioanalyzer 2100 using Eukaryote Total RNA Nano chips (Agilent Technologies, Santa Clara, USA). RNA was depleted from rRNA and sequenced on a HiSeq4000 (paired-end, 150 bp) by Genomescan BV, Amsterdam, The Netherlands.

RNA raw sequence quality was checked using FastQC (v0.11.9)[2] and quality trimmed and filtered using Trimmomatic (v0.38)[3]. The single, 50 bp reads were processed by removing the first 5 bases, applying a sliding-window quality trim 4 bp wide with a threshold of Q15, then removing all reads shorter than 36 bp after trimming. Quality checked and trimmed reads were subsequently pseudo aligned to the human transcriptome (GRCh38 release 97) using Kallisto (v0.46.0)[4]. The transcript-level counts from Kallisto output were used to perform differential gene expression analysis using 3 different R packages: sleuth (v0.30.0)[5], DESeq2 (v1.28.1)[6], and edgeR (v3.30.3)[7–10]. Count data was imported to DESeq2 and edgeR using the tximport package[11]. Transcript to gene mappings were obtained using the biomaRt package (v2.44.0)[12]. In all 3 workflows, likelihood ratio tests were applied using '~ Subject + Visit' as the full model design and '~ Subject' as the reduced model in order to detect genes that were differentially expressed after *A. soehngenii L2-7* infusion compared to after placebo infusion. All p-values were adjusted for multiple comparisons using the Benjamini-Hochberg method[13]. Significance thresholds were 0.05 for sleuth and edgeR and 0.10 for DESeq2. Only genes found to be differentially expressed by all 3 workflows were examined in downstream analyses.

Real Time quantitative polymerase chain reaction (RT-qPCR)

Total RNA was extracted from frozen duodenal biopsies from 12 patients as described above. Briefly, 1mg of RNA was converted to cDNA with iScript cDNA synthesis kit (BioRad, Veenendaal, The Netherlands). qPCR was performed on a ViiA7 PCR machine (Applied Biosystems, Bleiswijk, The Netherlands). using Sybr Green Fast (Bioline Meridian Bioscience, Cincinnati, Ohio, USA). Gene expression was normalized towards the housekeeping gene Actin, and relative gene expression was calculated with the "delta delta Ct" method and shown as 2^-delta delta Ct. Primer sequences are outlined in Supplementary Table 2; all primers were manufactured by Sigma-Aldrich (Zwijndrecht, The Netherlands).

Western blotting

Duodenal biopsies (from 8/9 patients) were lysated in RIPA buffer (Thermo Fisher Scientific, Breda, The Netherlands) containing protease and phosphatase inhibitors (cOmplete™ Protease inhibitor and PhosSTOP Phosphatase Inhibitor Cocktails, Sigma, Zwijndrecht, The Netherlands) using a ceramic beads homogenizer. For westernblotting of cell lysates, Caco-2 cells were incubated for 30 minutes 4˚C in RIPA buffer supplemented with protease and phosphatase inhibitors. BCA protein assay kit (Thermo Fisher) was used to determine protein concentrations.b-mercaptoethanol was added as reducing agent to all sample lysates, which were run on 4-12% polyacrylamide gels (BioRad, GE, Boston, USA) in MES running buffer.

Proteins were transferred to PVDF membranes (BioRad) and were blocked using 5% milk in TBS-T (Tris Buffered Saline – Tween-20). Membranes were incubated overnight a 4˚C with primary polyclonal rabbit antibodies anti-Reg1B (for Figure 6A/6G: 1:500, E-AB-52897, Elabscience, Houston, USA) and Actin (AB306371, Abcam, Cambridge, UK) or anti –Reg1A (for Figure S5G: 1:500, orb100720, Biorbyt, Cambridge, UK). Horseradish peroxidase (HRP)-conjugated secondary antibodies (R&D systems, Minneapolis, USA) were incubated for 1hour at room temperature. HRP activity was visualized with peroxidase substrate for enhanced chemiluminescence and imaged with ChemiDoc MP Imaging System (BioRad) using Image Lab software (BioRad). Densitometric quantification analysis was performed using the Image J software. All protein levels were normalized to the loading control (b-actin). Reg1B protein expression shown as ratio of densitometric quantification of Reg1B versus b-actin and as intraindividual fold-changes of treatment versus placebo (expression rates of placebo group normalized to mean to represent distribution in expression levels among subjects). In order to show lack of cross-reactivity of the antibodies anti-Reg1B and anti-Reg1A, recombinant Reg1A (Prospec) and Reg1B (Sino Biological) proteins were loaded on polyacrylamide gels and immunoblotted using antibodies anti-Reg1A (orb100720, Biorbyt) or Reg1B (E-AB-52897, Elabscience) (Figure S5I,K).

Immunohistochemical staining

Formalin-fixed paraffin-embedded (FFPE) duodenal 4 mm sections were utilized for immunohistochemical staining. Slides were deparaffinized in 100% Xylene and rehydrated in ethanol (100%, 96% and 70%) and H2O, following by block of endogenous peroxidase in 3% H2O2 methanol for 20 minutes and heat-induced epitope retrieval (HIER) in citrate buffer pH 6.0 at 98°C for 10 minutes in the Thermo Scientific PT Module. After incubation for 10 minutes with Ultravision protein block (Thermo Fisher Scientific, Breda, The Netherlands), FFPE sections were incubated with anti-Reg1B primary antibody (for Figure 6D,E: 1:100 dilution in TBS, MA5-29517, Invitrogen, Waltham, Massachusetts, USA) for 1 hour at room temperature (RT), following by incubation with the secondary antibodies BrightVision Poly-HRP-conjugates goat anti-rabbit IgG (undiluted) for 30 minutes. For assessing the expression and localization of Reg1B in duodenal tissue with different antibodies and to compare its expression to the one of Reg1A (Figure S5H), following 10-minutes HIER in citrate buffer, duodenal sections were incubated with primary antibodies against Reg1B (1:2000, E-AB-52897, Elabscience, Houston, USA) or against Reg1A (1:2000, orb100720, Biorbyt, Cambridge, UK). All single-stainings were visualized with 3,3'Diaminobenzidine (DAB) kit (Sigma Aldrich, Zwijndrecht, The Nederlands).

For the triple staining of REG1B, lysozyme and mucin were stained in sequential order using sequentially cut duodenal FFPE sections. Reg1B expression was

visualized by: 10-minute HIER in citrate buffer pH 6.0 at 98°C, 1-hour incubation at RT with anti-Reg1B rabbit IgG (Invitrogen, MA5-29517, 1:100 dilution in TBS), 30-minute incubation with BrightVision Poly-alkaline phosphatase (AP)-conjugated goat anti-rabbit IgG (undiluted) and staining development with Perma Red/AP kit (Diagnostic BioSystem, Pleasanton, California, USA). Lysozyme (as marker of Paneth cells) was stained following: 5-minute HIER in Tris-EDTA pH 9.0 buffer at 98°C, 30-minute incubation at RT with polyclonal rabbit anti-lysozyme (1:2000 dilution in TBS, Dako EC 3.2.1.17, Agilent Technologies, Santa Clara, California, USA), 30-minute incubation with BrightVision Poly-HRP-conjugated goat anti-rabbit IgG (1:2 dilution in TBS) and staining development with Perma Yellow/HRP kit (Diagnostic BioSystem). For the final detection of acidic mucins (to mark Goblet cells), FFPE double-stained slides were incubated with Alcian Blue solution (1% in 3% acetic acid, pH 2.5, Sigma Aldrich) for 5 minutes and eventually covered with coverslips using VectaMount mounting medium (Thermo Fisher Scientific, H-5000).

Cell culture and assay procedure

Caco-2 cells were cultured in Gibco Dulbecco's Modified Eagle Medium (DMEM) supplemented with 10% fetal bovine serum (FBS), 100 IU/ml penicillin, 100 IU/ml streptomycin, and 2mM glutamine (Thermo Fisher Scientific) in T75 flasks. The day prior to the stimulation assays, cells were seeded at $1x10^5$/well in a 12-well plates; after resting overnight, cells were exposed to 1mM butyrate or 1 μg/ml muramyl dipeptide (MDP) (both stock solutions diluted in water) for 6 hours. Afterwards cells were washed once in PBS and lysated in RIPA buffer. Reg1B concentrations were determined by ELISA (Cloud-Clone Corp., Uscn Life Science Kit Inc., Wuhan, China) accordingly to the manufacturer's instructions in Caco-2 cells exposed to increasing concentrations of *A. soehngenii* L2-7 cells (10^5/ml and 10^6/ml). Prior to use in cell culture, bacteria were heat-inactivated at 65°C for 20 minutes. BCA protein assay kit (Thermo Fisher) was used to assess protein concentrations.

Measurements of fecal SCFA and plasma SCFA, incretins, bile acids and Reg1B

Fecal SCFAs (butyrate, acetate, propionate) were measured in morning stool samples (N=11), directly frozen at -20°C after collection, using gas chromatography coupled to tandem mass spectrometry detection (GC-MS/MS) as described previously[14]. Briefly, approximately 20-100 mg of fecal samples were mixed with internal standards, added to glass vials and freeze dried. All samples were then acidified with HCl, and SCFAs were extracted with two rounds of diethyl ether extraction. The organic supernatant was collected, the derivatization agent N-tert-butyldimethylsilyl-N-methyltrifluoroacetamide (Sigma-Aldrich, Stockholm, Sweden) was added and samples were incubated at room temperature overnight. SCFAs were quantified with

a gas chromatograph (Agilent Technologies 7890A, Santa Clara, California, USA) coupled to a mass spectrometer (Agilent Technologies 5975C). Short chain fatty acid standards were attained from Sigma-Aldrich (Stockholm, Sweden).

Plasma SCFA (butyrate, acetate, propionate) were measured at Cleveland Clinic (OH, USA) in heparin plasma samples (N=12), directly frozen at -80-°C after collection, using gas chromatography coupled to TANDEM mass spectrometry (GC-MS/MS) as previously described[15]. Briefly, 30 μl aliquots of plasma were mixed with 50 μl 2-Butanol/Pyridine (3:2) and 5 μl containing the heavy labeled internal standards. Afterwards, the carboxylic acids were derivatized by mixing 50 μl supernatant with 10 μl isobutyl chloroformate, followed by vortexing and sonicating the mixture. After derivatization, 50 μl hexane were added and mixed; following centrifugation, the top hexane layer was removed for GC-MS/MS analysis and 1 μl was injected into GC column. The quantitation of butyric acid, acetic acid, and propionic acid was performed using isotope dilution GC-MS/MS and the absolute concentration of each SCFA was determined using calibrations curves measured for each analyte. Samples were analyzed on a Thermo TSQ-Evo triple quadrupole mass spectrometer interfaced with the Trace 1310 gas chromatograph (Thermo Fisher Scientific). Chromatographic separation was achieved by using an HP-5MS fused-silica capillary column (30 m × 0.250 mm × 0.25 μm; Agilent Technologies, Santa Clara, CA, USA) coated with 5% phenymethyl siloxane as previously described[15]. The mass spectrometer was used in MRM mode with the following parent to daughter ion transitions: m/z 61.0 → 43.0 for acetic acid, m/z 63.0 → 45.0 for [13C2]-acetic acid, m/z 61.0 → 43.0 m/z 71.0 → 41.0 for butyric acid, m/z 78.1 → 46.1 for D7-butyric acid, m/z 75.1 → 57.0 for propionic acid, m/z 77.1 → 59.0 for D2-propionic acid.

Plasma incretin levels of all 12 individuals were determined in postprandial (2-hour mixed meal test) samples as previously described[16]. Plasma concentrations of GIP (total) and GLP-1 (total) were measured by Holst group with ELISA (cat no. 10-1258-01 and 10-1278-01, Mercodia, Sweden). All quality controls provided by the manufacturer were within allowed limits. All samples from the same individual were measured in the same assay run.

Concentrations of the secondary bile acids tauro-omega-muricholic acid (TOMCA), tauroursodeoxycholic acid (TUDCA), taurodeoxycholic acid (TDCA), tauroursodeoxycholic acid (TUDCA), taurolithocholic acid (TLCA), glycohyodeoxycholic acid (GHDCA), glycodeoxycholic acid (GDCA), glycoursodeoxycholic acid (GUDCA), glycolithocholic acid (GLCA), omega-muricholic acid (OMCA), deoxycholic acid (DCA), ursodeoxycholic acid (UDCA), lithocholic acid (LCA), hyodeoxycholic acid (HDCA), murocholic acid (MuroCA), iso-ursodeoxycholic acid (IsoUDCA) were measured in plasma samples from all 12 participants by means of ultra-performance liquid chromatography-tandem mass

spectrometry (UPLCMS/MS), as previously performed[17]. Briefly, samples (50μl) were extracted with 10 volumes of methanol containing deuterated internal standards (d_4-TCA, d_4-GCA, d_4-GCDCA, d_4-GUDCA, d_4-GLCA, d_4-UDCA, d_4-CDCA, d_4-LCA; 50nM of each). After 10 minutes of vortex and 10 minutes of centrifugation at 20 000g, the supernatant was evaporated under a stream of nitrogen and reconstituted in 200μl methanol:water [1:1]. The samples were injected (5μl) and bile acids were separated on a C18 column (1.7μ, 2.1 x 100mm; Kinetex, Phenomenex, USA) using water with 7.5mM ammonium acetate and 0.019% formic acid (mobile phase A) and acetonitrile with 0.1% formic acid (mobile phase B). The chromatographic separation started with 1 minute isocratic separation at 20%B. The B-phase was then increased to 35% during 4 minutes. During the next 10 minutes the B-phase was increased to 100%. The B-phase was held at 100% for 3.5 minutes before returning to 20%. The total runtime was 20 minutes. Bile acids were detected using multiple reaction monitoring (MRM) in negative mode on a QTRAP 5500 mass spectrometer (Sciex, Concord, Canada) and quantification was made using external standard curves.

Concentrations of Reg1B in plasma samples and duodenal tissue lysates was assessed by ELISA (Cloud-Clone Corp., Uscn Life Science Kit Inc., Wuhan, China) accordingly to the manufacturer's instructions.

Strain-specific qPCR

The DNA concentrations were determined fluorometrically (Qubit dsDNA HS assay; Invitrogen) and adjusted to 1 ng/μl prior to use as the template in qPCR. Primers targeting 16S rRNA gene of *A. soehngenii* L2-7 EhalF (5'GCGTAGGTGGCAGTGCAA) and EhalR (5'GCACCGRAGCCTATACGG) (Ramirez et al. 2008) were used for quantification. Standard template DNA was prepared from the 16S rRNA gene of *A. soehngenii* L2-7 by amplification with primers 27F (5'-AGAGTTTGATCCTGGCTCAG-3') and 1492R (5'-GGTTACCTTGTTACGACTT-3'). Standard curves were prepared with nine standard concentrations of 100 to 10^8 gene copies/μl. PCRs were performed in triplicate with iQ SYBR Green Supermix (Bio-Rad) in a total volume of 10 μl with primers at 500 nM in 384-well plates sealed with optical sealing tape. Amplification was performed with an iCycler (Bio-Rad, USA) with the following protocol: one cycle of 95°C for 10 min; 40 cycles of 95°C for 15 s, 55°C for 20 s, and 72°C for 30 s each; one cycle of 95°C for 1 min, one cycle of 60°C for 1 min, and a stepwise increase of the temperature from 60 to 95°C (at 0.5°C per 5 s) to obtain melt curve data. Data were analysed using the Bio-Rad CFX Manager 3.0.

Fecal 16S rRNA gene amplicon sequencing and bioinformatics

DNA extraction from fecal samples from 11 patients was performed using the repeated bead beating protocol as previously described[18]. DNA was eluted in 50 μl of DNAse-

RNAse-free water and its concentration and quality were evaluated using NanoDrop 2000 spectrophotometry. Subsequently, DNA was diluted to reach a concentration of 20 ng/μl which served as template for PCR. The V5-V6 region of 16S ribosomal RNA (rRNA) gene was amplified in duplicate PCR reactions for each sample in a total reaction volume of 50 μl using a master mix containing 1 μl of a unique barcoded primer, 784F-n and 1064R-n (10 μM each per reaction), 1 μl dNTPs mixture, 0.5 μl Phusion Green Hot Start II High-Fidelity DNA Polymerase (2 U/μl; Thermo Scientific, Landsmeer, The Netherlands), 10 μl 5× Phusion Green HF Buffer, and 36.5 μl DNAse-RNAse-free water[19]. The amplification program included 30 seconds (s) of initial denaturation step at 98°C, followed by 25 cycles of denaturation at 98°C for 10 s, annealing at 42°C for 10 s, elongation at 72°C for 10 s, and a final extension step at 72°C for 7 minutes. The PCR product was visualized on 1% agarose gel (~280 bp) and purified with CleanPCR kit (CleanNA, Alphen aan den Rijn, The Netherlands). The concentration of the purified PCR product was measured with Qubit dsDNA BR Assay Kit (Invitrogen, California, USA) and 200 ng of microbial DNA from each sample were pooled for the creation of the final amplicon library which was sequenced (150 bp, paired-end) on the Illumina HiSeq 2500 platform (GATC Biotech, Constance, Germany).

Raw reads were demultiplexed using the Je software suite (v2.0)[20] allowing no mismatches in the barcodes. After removing the barcodes, linker and primers, reads were mapped against the human genome using bowtie2 (v2.4.1)[21] in order to remove human reads. Surviving microbial forward and reverse reads were pipelined separately using DADA2 (v1.12.1)[22]. Amplicon Sequence Variants (AVSs) inferred from the reverse reads were reverse-complemented and matched against ASVs inferred from the forwards reads. Only non-chimeric forward reads ASVs that matched reverse-complemented reverse reads ASVs were kept. ASV sample counts were inferred from the forward reads. ASV taxonomy was assigned using DADA2 and the SILVA (v132) database. The resulting ASV table and taxonomy assignments were integrated using the phyloseq R package (v1.28.0)[23]. ASVs sequences were aligned using MAFFT (v.7.427)[24] using the auto settings. A phylogenetic tree was constructed from the resulting multiple sequence alignment with FastTree (v.2.1.11 Double Precision)[25] using a generalized time-reversible model ('-gtr'). Biopsy samples were rarefied to 24947 counts per sample, while fecal samples were rarefied to 13229 counts per sample. The vegan R package (v2.5.6)[26] was used to calculate alpha-diversity metrics (Shannon index and ASV richness) and Bray-Curtis dissimilarities. Weighted-Unifrac distances were calculated using the phyloseq package.

Power calculation and statistical analyses

We based our power calculation on the study of Van Baarlen *et al.*[27], in which a striking difference in duodenal mucosal transcriptomic profiling was reported 6 hours after introduction of a single *Lactobacillus* bacterial strain. Based on 60% decrease in duodenal *Fxr* gene expression upon *A. soehngenii* L2-7 administration to db/db mice, compared to placebo[18], with one sample Chi^2 test, the sample size in each group needed to be 12 in order to have a group proportion of 0.5 and with a comparison proportion of 0.1. Mean absolute deviation of glucose (MAD), continuously measured using FreeStyle Libre technology, was calculated using the default 'mad' function from R stats package[28]. Wilcoxon signed rank tests and Mann-Whitney U-tests were used to compare within-group changes of related samples and to compare intervention groups. Student's t-test was used for analyzing differences in groups from *in vitro* experiments. Area under the curve (AUCs) for MMT measurement were calculated using the DescTools package (v0.99.36) [29,30]. Correlation plots were made using the corrplot package (v0.84) [31]. The mixOmics package (v6.12.1) [32] was used to perform multilevel PCA analyses. Principal Coordinate Analyses (PCoA) were performed using the ape package (v5.4)[33]. All other statistical analyses and visualizations were performed in R (v4.0.1)[34] using the tidyverse (v1.3.0)[35] and ggplot2 package (v3.3.1)[30]. P values <0.05 were considered statistically significant.

REFERENCES

1. Gilijamse, P. W. *et al.* Treatment with Anaerobutyricum soehngenii: a pilot study of safety and dose–response effects on glucose metabolism in human subjects with metabolic syndrome. *npj Biofilms Microbiomes* **6**, 1–10 (2020).
2. Andrews, S. FastQC: a quality control tool for high throughput sequence data. (2015).
3. Bolger, A. M., Lohse, M. & Usadel, B. Trimmomatic: a flexible trimmer for Illumina sequence data. *Bioinformatics* **30**, 2114–2120 (2014).
4. Bray, N. L., Pimentel, H., Melsted, P. & Pachter, L. Near-optimal probabilistic RNA-seq quantification. *Nat. Biotechnol.* **34**, 525–527 (2016).
5. Pimentel, H., Bray, N. L., Puente, S., Melsted, P. & Pachter, L. Differential analysis of RNA-seq incorporating quantification uncertainty. *Nat. Methods* **14**, 687–690 (2017).
6. Love, M. I., Huber, W. & Anders, S. Moderated estimation of fold change and dispersion for RNA-seq data with DESeq2. *Genome Biol.* **15**, 550 (2014).
7. Robinson, M. D., McCarthy, D. J. & Smyth, G. K. edgeR: a Bioconductor package for differential expression analysis of digital gene expression data. *Bioinformatics* **26**, 139–140 (2010).
8. Robinson, M., Mccarthy, D., Chen, Y., Lun, A. & Smyth, G. K. edgeR: differential expression analysis of digital gene expression data. (2012).
9. Fernandes, A. D. *et al.* Unifying the analysis of high-throughput sequencing datasets: characterizing RNA-seq, 16S rRNA gene sequencing and selective growth experiments by compositional data analysis. *Microbiome* **2**, 15 (2014).
10. McCarthy, D. J., Chen, Y. & Smyth, G. K. Differential expression analysis of multifactor RNA-Seq experiments with respect to biological variation. *Nucleic Acids Res.* **40**, 4288–4297 (2012).
11. Soneson, C., Love, M. I. & Robinson, M. D. Differential analyses for RNA-seq: transcript-level estimates improve gene-level inferences. *F1000Research* **4**, 1521 (2015).
12. Durinck, S., Spellman, P. T., Birney, E. & Huber, W. Mapping identifiers for the integration of genomic datasets with the R/Bioconductor package biomaRt. *Nat. Protoc.* **4**, 1184 (2009).
13. Benjamini, Y. & Hochberg, Y. Controlling the false discovery rate: a practical and powerful approach to multiple testing. *J. R. Stat. Soc. Ser. B* 289–300 (1995).
14. Wichmann, A. *et al.* Microbial modulation of energy availability in the colon regulates intestinal transit. *Cell Host Microbe* **14**, 582–590 (2013).
15. Arnon D Lieber, AD. et al. Loss of HDAC6 alters gut microbiota and worsens obesity. FASEB J 33(1), 1098-1109 (2019).
16. Kootte, R. S. *et al.* Improvement of Insulin Sensitivity after Lean Donor Feces in Metabolic Syndrome Is Driven by Baseline Intestinal Microbiota Composition. *Cell Metab.* (2017). doi:10.1016/j.cmet.2017.09.008
17. Tremaroli, V. *et al.* Roux-en-Y Gastric Bypass and Vertical Banded Gastroplasty Induce Long-Term Changes on the Human Gut Microbiome Contributing to Fat Mass Regulation. *Cell Metab.* **22**, 228–238 (2015).
18. Salonen, A. *et al.* Comparative analysis of fecal DNA extraction methods with phylogenetic microarray: Effective recovery of bacterial and archaeal DNA using mechanical cell lysis. *J. Microbiol. Methods* **81**, 127–134 (2010).
19. Ramiro-Garcia, J. *et al.* NG-Tax, a highly accurate and validated pipeline for analysis of 16S rRNA amplicons from complex biomes. *F1000Research* **5**, 1791 (2016).
20. Girardot, C., Scholtalbers, J., Sauer, S., Su, S.-Y. & Furlong, E. E. M. Je, a versatile suite to handle multiplexed NGS libraries with unique molecular identifiers. *BMC Bioinformatics* **17**, 419 (2016).
21. Langmead, B. & Salzberg, S. L. Fast gapped-read alignment with Bowtie 2. *Nat. Methods* **9**, 357 (2012).

22. Callahan, B. J. *et al.* DADA2: High-resolution sample inference from Illumina amplicon data. *Nat Meth* **13**, 581–583 (2016).
23. McMurdie, P. J. & Holmes, S. phyloseq: An R Package for Reproducible Interactive Analysis and Graphics of Microbiome Census Data. *PLoS One* **8**, e61217 (2013).
24. Katoh, K., Misawa, K., Kuma, K. & Miyata, T. MAFFT: a novel method for rapid multiple sequence alignment based on fast Fourier transform. *Nucleic Acids Res.* **30**, 3059–66 (2002).
25. Price, M. N., Dehal, P. S. & Arkin, A. P. FastTree 2 – Approximately maximum-likelihood trees for large alignments. *PLoS One* **5**, e9490 (2010).
26. Oksanen, J. *et al.* vegan: Community Ecology Package. (2017).
27. van Baarlen, P. *et al.* Differential NF- B pathways induction by Lactobacillus plantarum in the duodenum of healthy humans correlating with immune tolerance. *Proc. Natl. Acad. Sci.* **106**, 2371–2376 (2009).
28. Fokkert, M. J. *et al.* Performance of the freestyle libre flash glucose monitoring system in patients with type 1 and 2 diabetes mellitus. *BMJ Open Diabetes Res. Care* **5**, 1–8 (2017).
29. Signorell, A. DescTools: Tools for Descriptive Statistics. (2020).
30. Wickham, H. *ggplot2: Elegant Graphics for Data Analysis*. (Springer-Verlag New York, 2016).
31. Wei, T. & Simko, V. R package 'corrplot': visualization of a correlation matrix (version 0.84).'. *Retrived from https//github. com/taiyun/corrplot* (2017).
32. Cao, K.-A. Le, Rohart, F., Gonzalez, I. & Dejean, S. mixOmics: Omics Data Integration Project, package version 6.1.2 https://CRAN.R-project.org/package=mixOmics. (2017).
33. Paradis, E. & Schliep, K. ape 5.0: an environment for modern phylogenetics and evolutionary analyses in R. *Bioinformatics* **35**, 526–528 (2019).
34. R Core Team. R: A language and environment for statistical computing. R Foundation for Statistical Computing. (2016).
35. Wickham, H. *et al.* Welcome to the Tidyverse. *J. Open Source Softw.* **4**, 1686 (2019).

SUPPLEMENTAL FIGURES

Figure S1. Fecal *A. soehngenii* L2-7 levels.

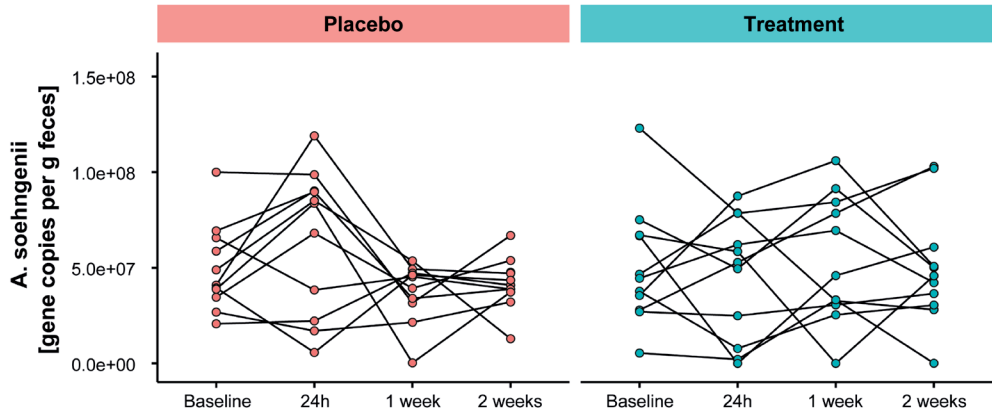

Fecal *A. soehngenii* L2-7 levels determined by qPCR at 0, 24 hours, 1 week, 2 weeks after placebo/treatment-interventions. Values indicate gene copies per gr of feces.

Figure S2. Fecal short-chain fatty acids.

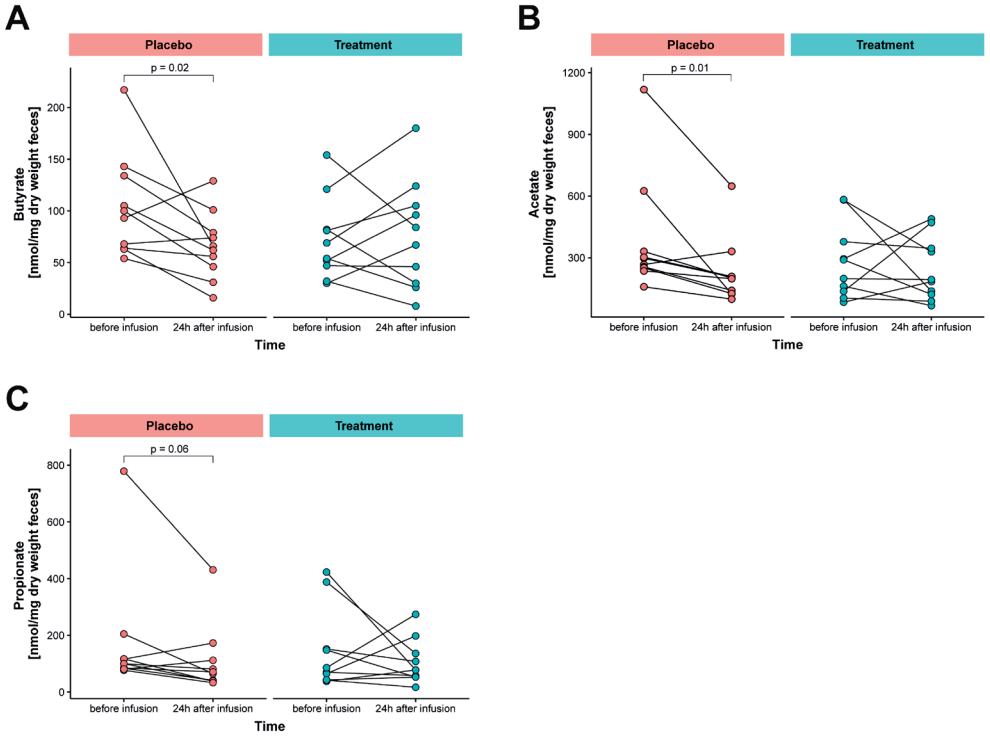

(A) Concentrations (nmol/mg dried feces weight) of butyrate, (**B**) acetate, and (**C**) propionate in morning stool samples obtained at baseline and 1 day after placebo/treatment-intervention.

Figure S3. Postprandial glucose and insulin.

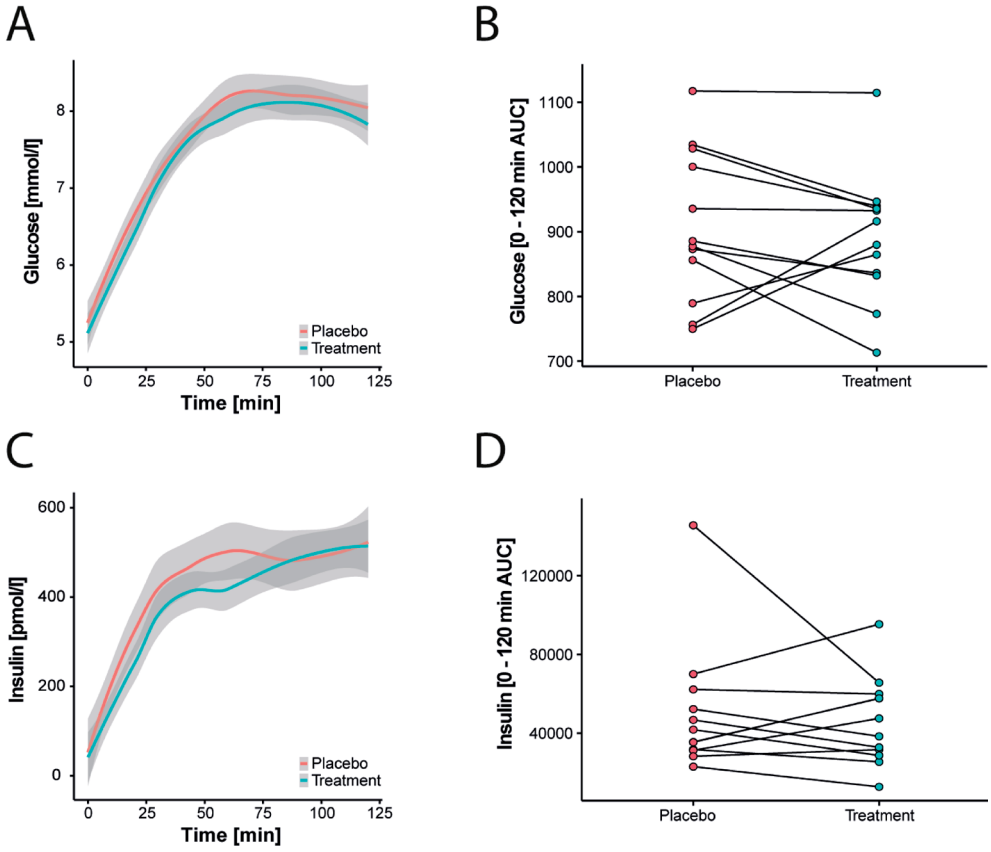

(**A**) Plasma glucose levels (mmol/l) at 0, 20, 30, 120 minutes during mixed meal test (MMT). (**B**) Plasma glucose levels during MMT as total area under the curve (AUC). (**C**) Plasma insulin levels (pmol/l) at 0, 20, 30, 120 minutes during MMT. (**D**) Plasma insulin levels during MMT as total area under the curve (AUC).

Figure S4. Plasma short-chain fatty acids.

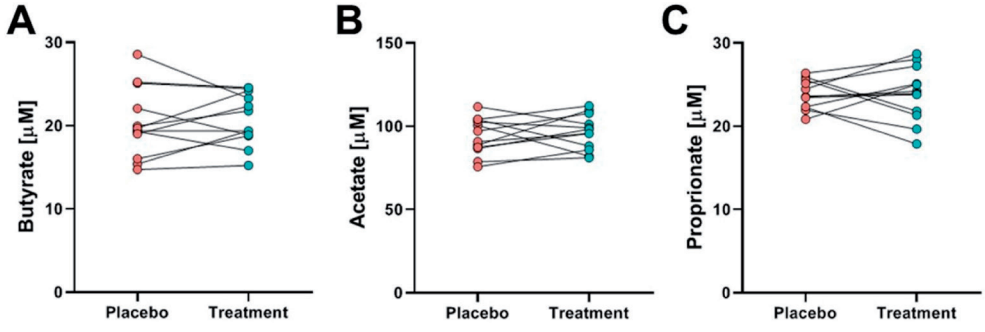

(A) Concentrations (μM) of butyrate, (**B**) acetate, and (**C**) propionate in plasma at 120 minutes of mixed meal test (MMT).

Figure S5. Duodenal expression of REG genes and Reg1A/1B proteins.

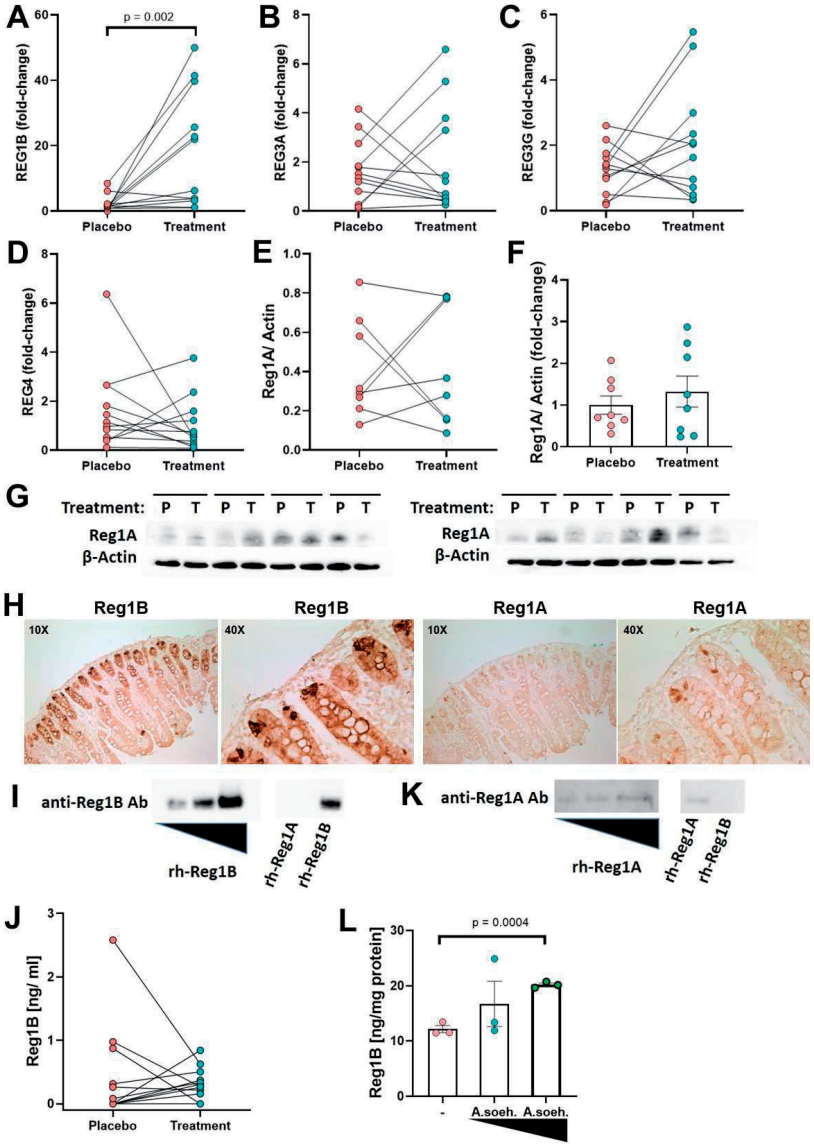

Gene expression measured by qPCR in duodenal biopsies at 6 hours post-intervention of (**A**) *REG1B* (different set of forward and reverse primers than in Figure 6B), (**B**) *REG3A*, (**C**) *REG3G*, and (**D**) *REG4*. (**A-D**) Data showing the relative gene expression (to placebo) using the 2^-(delta delta Ct) method. (**E**) Quantification of Reg1A expression levels in duodenal biopsies, Reg1A expression normalized to b-actin (loading control). (**F**) Reg1A expression shown as fold-change treatment versus placebo. (**G**) Westernblot images of duodenal lysates blotted with antibodies against Reg1A and b-actin. (**H**) Immunohistochemical staining of Reg1B (different antibodies used than in Figures 6D,6E) and Reg1A in duodenal biopsies. (**I,K**) Westernblot images showing the specificity of the antibodies against Reg1B and Reg1A; (**I**) Westernblotting for Reg1B: enhanced band intensity with increasing amount of loaded recombinant human (rh) Reg1B and absence of a band when rh Reg1A is loaded; ; (**K**) Westernblotting for Reg1A: stronger band intensity with increasing amount of loaded rh Reg1A and absence of a band when rh Reg1B is loaded. (**J**) Circulating levels (ng/ml) of Reg1B measured by ELISA in plasma samples taken at 8 hours post-intervention. (**L**) Reg1b expression by Caco-2 cells in response to exposure to increasing concentrations of heat-inactivated *A. soehngenii* L2-7 cells.

Figure S6. Assessment of carry-over affect between week 0 and week 4.

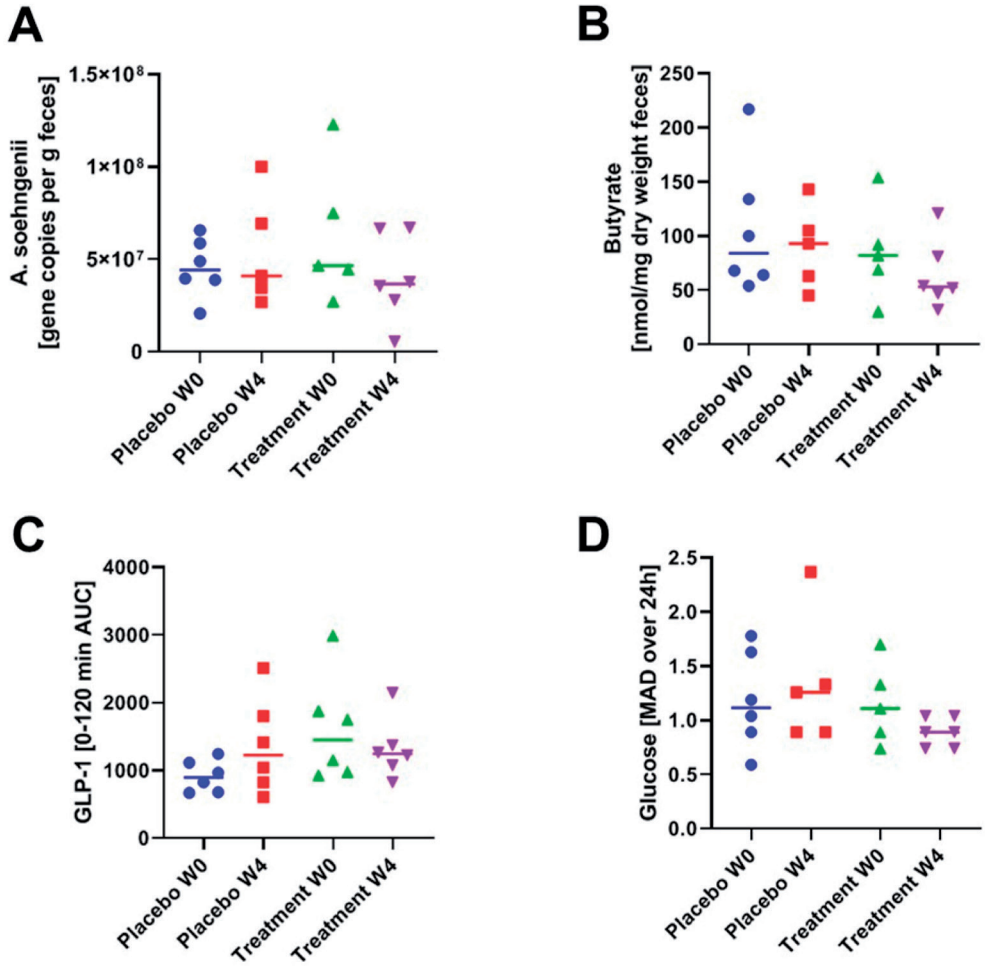

(**A**) Fecal *A. soehngenii* L2-7 levels determined by qPCR at baseline (week 0 and week 4); values indicate gene copies per gr of feces. (**B**) Concentrations (nmol/mg dried feces weight) of butyrate in morning stool samples obtained at baseline (week 0 and week 4). (**C**) Plasma GLP-1 levels during mixed meal test (MMT) shown as total area under the curve (AUC). (**D**) Median absolute deviation (MAD) of continuous glucose measurements (CGM) over the first 24 hours after placebo/treatment-intervention.

SUPPLEMENTAL TABLES

Table S1. Baseline characteristics and safety parameters at both study visits.

	PLACEBO	A. SOEHNGENII	P - VALUE
WEIGHT (KG)	110.1 [100.0 – 120.2]	110.4 [101.3 – 122.0]	0.812
BMI (KG/M2)	33.4 [32.2 – 38.]	33.7 [31.8 – 37.8]	0.859
BLOOD PRESSURE: SYSTOLIC (MMHG)	135 [129 – 147]	144 [131 – 156]	0.258
BLOOD PRESSURE: DIASTOLIC (MMHG)	89 [84 – 91)	91 [79 – 95)	0.917
FASTING GLUCOSE (MMOL/L)	5.3 [5.0 – 5.6]	5.1 [4.8 – 5.7]	0.430
INSULIN (PMOL/L)	65 [48 – 83]	56 [34 – 81]	0.099
HOMA - IR	2.3 [1.7 – 2.8]	1.9 [1.1 – 2.8]	0.158
HBA1C (MMOL/MOL)	37 [36 – 39]	37 [36 – 39]	0.942
CHOLESTEROL: TOTAL (MMOL/L)	5.29 [4.57 – 6.26]	5.13 [4.71 – 6.08]	0.255
CHOLESTEROL: HDL (MMOL/L)	1.17 [0.91 – 1.31]	1.13 [0.97 – 1.32]	0.929
CHOLESTEROL: LDL (MMOL/L)	3.05 [2.69 - 3.90]	3.21 [2.79 – 3.83]	0.638
CHOLESTEROL: TRIGLYCERIDES (MMOL/L)	1.65 [1.12 – 2.92]	1.66 [1.19 – 2.31]	0.433
CREATININE (UMOL/L)	87 [78 – 92]	84 [79 – 93]	0.342
AST (U/L)	25 [19 – 31]	26 [23 – 33]	0.109
ALT (U/L)	25 [21 – 36]	27 [22 – 35]	0.124
AP (U/L)	70 [62 – 85]	72 [60 -87]	0.783
YGT (U/L)	39 [26 – 52]	31 [26 – 49]	0.254
CRP (MG/ML)	2.8 [1.8 – 5.0]	3.0 [2.3 – 5.3]	0.477
LEUKOCYTES (10^E9/L)	6.2 [5.6 – 6.7]	6.5 [5.9 – 7.3]	0.130
CALORIC INTAKE (KCAL/DAY)	1843 [1607 – 2090]	1888 [1667 – 2041]	0.424
FAT INTAKE (G)	68 [57 – 75]	61 [56 – 81]	0.790
PROTEIN INTAKE (G)	76 [65 – 85]	77 [60 – 91]	0.333
CARBOHYDRATE INTAKE (G)	201 [162 – 233]	228 [173 – 254]	0.241
FIBER INTAKE (G)	18 [14 – 19]	19 [16 – 21]	0.339

Data expressed as medians and interquartile ranges. There were no differences after the *A. Soehngenii* L2-7 infusion compared to the placebo infusion. BMI: body mass index, HOMA-IR: homeostatic model assessment of insulin resistance, HbA1c: glycated hemoglobin, HDL: high-density lipoprotein, LDL: low-density lipoprotein; AST: aspartate transaminase, ALT: alanine transaminase, AP: alkaline phosphatase; ggt: gamma-glutamyltransferase; CRP: c-reactive protein.

Table S2.

Gene	Forward primer sequence	Reverse primer sequence
GPR43/FFAR2	TGCTACGAGAACTTCACCGAT	GGAGAGCATGATCCACACAAAAC
TGR5	CACTGTTGTCCCTCCTCTCC	ACACTGCTTTGGCTGCTTG
FXR	TACATGCGAAGAAAGTGTCAAGA	ACTGTCTTCATTCACGGTCTGAT
FGF19	CGGAGGAAGACTGTGCTTTCG	CTCGGATCGGTACACATTGTAG
OSTalpha	CTGGGCTCCATTGCCATCTT	CACGGCATAAAACGAGGTGAT
REG1B	GGTCCCTGGTCTCCTACAAG	TCCATTTCTTGAATCCTGAGCA
REG1A	GGTCCCTGGTCTCCTACAAG	CATTTCTGGAATCCTGTGCTTG
REG1B*	AGTAGTGGGTCCCTGGTCTC	TGAATCCTGAGCATGAAGTCA
REG3A	AGCTACTCATACGTCTGGATTGG	CACCTCAGAAATGCTGTGCTT
REG3G	GGTGAGGAGCATTAGTAACAGC	CCAGGGTTTAAGATGGTGGAGG
REG4	CTGCTCCTATTGCTGAGCTG	GGACTTGTGGTAAAACCATCCAG
ACTB	CCAACCGCGAGAAGATGA	CCAGAGGCGTACAGGGATAG

Primer sequences utilized in the analysis of duodenal gene expression. *: primers used in Figure S5A.

chapter 4

Oral treatment with Anaerobutyricum soehngenii augments glycemic control in male individuals with type 2 diabetes treated with metformin: a randomized double-blind placebo-controlled single center study

Julia J. Witjes*, Ilias Attaye*, Annefleur M. Koopen, Eduard W. J. van der Vossen, Diona Zwirs, Koen Wortelboer, Didier Collard, Elles Marleen Kemper, Maaike Winkelmeijer, Jens J. Holst, Stanley L. Hazen, Folkert Kuipers, Erik S.G. Stroes, Albert K. Groen, Willem M. de Vos, Max Nieuwdorp, Hilde Herrema

*Both authors contributed equally

Cell reports,
under review

SUMMARY

Objective: To investigate the effects of daily oral Anaerobutyricum soehngenii L2-7 supplementation for 14 days on postprandial glucose levels in individuals with type 2 diabetes (T2D) treated with metformin.

Research design and methods: Randomized, double-blind, placebo-controlled, single center trial in 25 white Dutch males with T2D on stable metformin monotherapy receiving either 14 days supplementation with A. soehngenii or placebo. Primary endpoint was the effect of A. soehngenii versus placebo on (postprandial) glucose excursions and variability as determined by continuous glucose monitoring. Secondary endpoints were changes in ambulatory 24h blood pressure; incretins; circulating metabolites and (postprandial) excursions of plasma short-chain fatty acids (SCFA) and bile acids upon a standardized meal.

Results: A.soehngenii supplementation on top of metformin treatment was well-tolerated and significantly improved glycemic variability (standard deviation (SD), $p = 0.034$; mean amplitude of glycemic excursion (MAGE) $p = 0.04$; mean of daily differences (MODD), $p = 0.031$) and increased the level of active cells in fecal samples ($p = 0.0066$). Mean arterial 24h blood pressure (MAP) decreased in the treatment group ($p = 0.04$). A. soehngenii supplementation did not induce significant changes in (postprandial) SCFA, fecal bile acids, incretin levels or anthropometric parameters.

Conclusions: Men with T2D on metformin monotherapy had significantly improved glycemic variability and MAP upon two-week supplementation with A. soehngenii compared to placebo-treated controls. Although (longitudinal) studies in larger, ethnic- and sex-diverse populations are needed, our data suggest that A. soehngenii can aid in improving glycemic control in metformin-treated individuals with T2D.
WHO International Dutch Clinical Trial Register: https://clinicaltrialregister.nl/nl/trial/28536; registration number NL7121

INTRODUCTION

The worldwide prevalence of type 2 diabetes (T2D) is expected to increase to 3% of the adult population by 2050 [1], highlighting the urgent need for novel insights into this pandemic disease. The pathophysiology of T2D is complex and includes both environmental (such as lifestyle and diet) and genetic factors, with altered gut microbiota composition and functional potential as possible disease modulators [2]. Over the past two decades, disturbances in the gut microbiota, both in animals and humans, have been linked to the pathophysiology of metabolic diseases such as obesity and T2D [3,4]. Obese (insulin-resistant) individuals have been shown to have lower levels of fecal short-chain fatty acid (SCFA)-producing bacteria [5]. SCFAs are metabolites produced from microbial fermentation of complex fibers, which have been widely implicated in conveying health benefits, such as insulin sensitivity, obesity, and blood pressure regulation, all of which are important elements in the pathophysiology of T2D[6–8]. Therapeutic modulation of gut microbiota could serve as an important parameter in both preventive and therapeutic strategies for T2D.

We have previously shown that transplantation of fecal microbiota from lean healthy subjects to insulin-resistant individuals significantly increases insulin sensitivity [9]. This coincided with an increased relative abundance of bacteria that produced butyrate, an abundant SCFA. Specifically, *Anaerobutyricum soehngenii* (previously known as *Eubacterium hallii)* [10] increased in the small intestine of treated subjects[10]. *A. soehngenii* is a well-characterized anaerobe that belongs to the phylum Firmicutes. It can produce butyrate from lactate and acetate in an acidic environment, as found in the small intestine [11,12]. In this regard, it is interesting to note that metformin-treated T2D individuals have increased levels of lactate in their feces [13]. Additionally, lactate levels are positively correlated with blood pressure [14]. As *A. soehngenii* uses intestinally produced lactate to produce butyrate, which is known to exert beneficial effects on glucose metabolism [11] and blood pressure [15], we hypothesized that adding *A. soehngenii* to metformin treatment in individuals with T2D may improve their cardiometabolic profile.

We previously showed that oral treatment with *A. soehngenii* improves insulin sensitivity and energy expenditure in obese and diabetic *db/db* mice [16]. In a pilot safety and dose-finding trial in humans, we found that daily oral *A. soehngenii* treatment was safe and well tolerated. Moreover, the relative abundance of the administered *A. soehngenii* was significantly associated with insulin sensitivity, with the highest dose resulting in significant blood pressure reduction [17]. Furthermore, in a randomized placebo-controlled crossover study in individuals with metabolic syndrome, we showed that a single duodenal infusion of *A. soehngenii* improved 24 hours peripheral glycemic control, possibly by modulating intestinal GLP-1 production and/or secondary bile acid levels [18].

These findings prompted us to study the effect of oral administration of *A. soehngenii* in combination with metformin on (postprandial) glucose excursions, as determined by a wearable flash glucose sensor in individuals with T2D. The secondary endpoints were changes in ambulatory blood pressure, GLP-1 production, circulating metabolites, and (postprandial) excursions of plasma SCFA and bile acids after a standardized meal.

METHODS AND MATERIALS

Study population

Twenty-six white Dutch males with T2D on metformin monotherapy were recruited through local newspaper advertisements. To be eligible to participate, all individuals had to be on a stable dose of metformin (*i.e.*, no changes in the last three months), two or three times daily 500 mg or twice daily 850 mg, with no other medication use. The exclusion criteria included smoking, moderate to heavy alcohol use (defined as >12 g/day), a history of cardiovascular events, cholecystectomy, overt untreated gastrointestinal disease or abnormal bowel habits, elevated liver enzymes >2.5 times the upper limit of the normal range, prolonged compromised immunity, and the use of antibiotics in the past three months. Only male individuals were included, because changes in female hormone concentrations in (postmenopausal) women have a disturbing effect on insulin sensitivity [19]. Participants were requested to maintain their usual physical exercise and dietary patterns during the study and to keep an online nutritional diary to monitor food intake (https://mijn.voedingscentrum.nl/nl/eetmeter/).

The study protocol was reviewed and approved by the local Institutional Review Board of the Amsterdam University Medical Center (Amsterdam UMC, Amsterdam, Netherlands) and conducted in accordance with the Declaration of Helsinki and CONSORT guidelines. The study was registered at the Dutch Clinical Trial Register (registration number NL7121), which is a primary registry included in the International Clinical Trial Registry Platform (ICTRP). All the participants provided written informed consent.

Study design

This was a randomized double-blind placebo-controlled single-center study. See **Suppl Figure 1** shows an overview of the study design. During the run-in phase, the participants continued their stable dosage of metformin, and their glucose levels were continuously measured using a disposable flash glucose sensor (FreeStyle Libre, FSL, Abbott, USA). Afterwards, participants were randomized to receive either

14 days of once-daily oral treatment with *A. soehngenii L2-7* or placebo. Participants in the treatment arm ingested daily one 10 ml vial of A. soehngenii in phosphate-buffered saline (PBS) with 10% glycerol, whereas participants in the placebo arm received 10 ml of PBS with 10% glycerol. We recently described the anaerobic production of *A. soehngenii* [20] in detail. The earlier Most Probable Number (MPN) analysis for quantifying live and anaerobic cells has been complemented with high-throughput determination based on flow cytometry according to ISO 19344 (ISO 2015)[21].

Based on the latter method, the daily dose was estimated to be 10^{10} active cells. The viability of *A. soehngenii L2-7* in randomly selected tubes (stored at -80°C at the AMC Department of Clinical Pharmacy, conforming to good clinical practice (GCP)) was regularly tested, while purity was assessed by testing the growth/presence of various pathogens/contaminants[20].

Participants underwent a two-hour mixed meal test, conducted as previously described [22], before and after the intervention, with baseline blood sampling from an intravenous catheter in a distal arm vein. Thereafter, participants immediately ingested a liquid meal solution (Nutridrink; Nutricia Advanced Medical Nutrition, Amsterdam, Netherlands) containing 600 kcal (35% fat, 49% carbohydrates, and 16% proteins), and for the next two hours blood samples were drawn to determine postprandial glucose, insulin, and GLP-1 excursions. Afterwards, the participants were equipped with a disposable flash glucose sensor (FreeStyle Libre, FSL, Abbott, USA), which was worn for 14 days before and 14 days during the intervention to continuously monitor (postprandial) glucose excursions. In addition, participants received a blood pressure monitor to measure ambulatory blood pressure for 24 h before and after treatment. Finally, feces were collected from all participants at baseline, week two and week four of the study. Compliance was determined by having participants return empty vials and keep track of daily intake of either the placebo or *A. soehngenii L2-7* via diaries.

Randomization and blinding

The study participants and all trial physicians were blinded to the treatment until the completion of the trial. The participants were randomized using a randomization list produced by the clinical pharmacy of the Amsterdam UMC.

Power calculation and statistical analyses

Based on previous studies [9,18] and the hypothesized peak difference in postprandial glucose excursion, we calculated that we needed 12 subjects per arm to detect a significant difference in this trial. This number was based on a significance level of 0.05 and 80% power, and was calculated using an online power calculation

(www.biomath.info/power). Delta changes before and after the intervention were calculated and appropriate (non) parametric tests were performed. All statistical analyses were performed using the open software program, R (version 4.2.1). FreeStyle Libre data were processed using the CGDA package [23]. Statistical significance was set at $P < 0.05$.

Biochemical, Microbiome and Metabolome analyses
Please see Online-Only Supplemental Material.

DATA AVAILABILITY
The datasets and R scripts used in this study are available from the corresponding author upon reasonable request.

RESULTS

We included twenty-six white Dutch males with T2D who were on stable metformin monotherapy. Before randomization, one participant was excluded because of acute prednisolone use; during the study, one subject had a malfunctioning FSL monitor, and we thus included another subject in order to meet the primary endpoint. A total of 25 individuals completed the trial. Data analysis revealed that one individual had extremely high concentrations of plasma bile acids and an exceptional compositional profile. We excluded this individual from the data analyses. Hence, data analyses were performed on 12 placebo-treated and 12 *A. soehngenii* treated individuals. Baseline body weight, dietary intake, and caloric content did not significantly differ between placebo-and *A. soehngenii*-treated individuals. At baseline, anthropometric and biochemical parameters were similar in both the groups (Supplementary **Table 1)**. Both treatments were well tolerated and no adverse events occurred during the study. The safety laboratory parameters (inflammatory markers and liver parameters) and anthropometric and biochemical parameters were similar in both groups after the intervention (**Table 1**).

***A. soehngenii* supplementation improves glycemic variability**
We previously showed that four weeks of oral supplementation and direct duodenal infusion of *A. soehngenii* in male individuals with metabolic syndrome, who are at increased risk of developing T2D, can affect glycemic control, incretin levels, and blood pressure[17,18]. Therefore, we first determined these parameters in metformin-treated T2D individuals orally supplemented with *A. soehngenii* for two weeks. Glucose metabolism was studied using mixed-meal testing (MMT), HOMA-IR, and

Table 1. Four weeks post-intervention characteristics of the EDM2 study.

	Placebo (n = 12)	Intervention (n = 12)	p-value
BMI (kg/m2)	27.11 (2.53)	27.46 (4.14)	0.81
Weight (kg)	86.53 (12.94)	91.18 (17.26)	0.46
Blood pressure: overall Systolic	91.70 (9.24)	99.33 (13.67)	0.15
Blood pressure: overall Diastolic	53.00 (7.32)	54.17 (7.84)	0.72
Blood pressure: overall MAP	69.20 (7.41)	70.67 (8.64)	0.68
Fasting glucose (mmol/L)	8.48 (1.99)	8.03 (0.76)	0.46
Insulin (pmol/L)	49.08 (34.26)	42.50 (12.74)	0.54
HbA1c (mmol/mol)	6.71 (0.60)	6.52 (0.57)	0.44
Total Cholesterol (mmol/L)	5.54 (0.69)	5.03 (0.90)	0.14
HDL (mmol/L)	1.30 (0.24)	1.36 (0.32)	0.65
LDL (mmol/L)	3.51 (0.61)	3.02 (0.65)	0.07
Triglycerides (mmol/L)	1.61 (0.69)	1.44 (0.77)	0.58
AST (U/L)	24.42 (5.87)	21.67 (3.08)	0.17
ALT (U/L)	27.42 (11.12)	24.17 (11.58)	0.49
AP (U/L)	73.08 (16.73)	69.25 (16.32)	0.58
yGT (U/L)	32.67 (25.40)	26.67 (22.48)	0.55
CRP (mg/mL)	2.01 (1.72)	1.69 (1.42)	0.63
Leucocytes (109/L)	5.97 (1.60)	6.33 (2.12)	0.64
Caloric intake (kcal/day)	1726.68 (418.11)	1749.10 (314.87)	0.89
Fat intake (g/day)	70.23 (30.11)	73.80 (18.62)	0.74
Carbohydrates intake (g/day)	159.15 (58.63)	151.32 (49.60)	0.74
Protein intake (g/day)	87.24 (31.63)	96.05 (26.60)	0.49
Fiber intake (g/day)	18.18 (6.82)	19.72 (5.81)	0.58

Data is expressed as mean ± standard deviation. BMI: body mass index, ALP: alkaline phosphatase, g-GT: gamma glutamyl transferase, ALT: alanine aminotransferase, AST aspartate aminotransferase, HDLc: high density lipoprotein cholesterol, LDLc: low density lipoprotein cholesterol, CRP: C-reactive protein.

continuous glucose monitoring. Glucose excursions after intake of a standardized mixed meal were similar after two weeks of supplementation with *A. soehngenii* or placebo compared to the baseline (**Figure1A-B).** Insulin excursions during MMT were unaltered by *A. soehngenii* or placebo supplementation compared to baseline (**Suppl Figure 2A-B)**. In contrast to our recent findings[18], *A. soehngenii* supplementation did not increase GLP1 levels during MMT compared to placebo supplementation (**Suppl Figure 2C-D**). In line with observations that glucose and insulin excursions were unaltered, HOMA-IR, as calculated from fasting insulin and glucose levels prior to MMT, remained statistically similar in both groups (**Suppl Figure 2E**).

In addition to an 'acute' challenge (MMT) to address glucose tolerance, we equipped subjects with a continuous glucose measuring device (FreeStyle Libre (FSL)) for 14 days during the run-in phase and then during the 14-day supplementation with *A. soehngenii* or placebo. FSL allows for continuous, long-term, ambulatory glucose measurements, and is increasingly considered a clinically relevant tool to

Figure 1. Effect of 14 days placebo **(A)** and *A. soehngenii* **(B)** supplementation on glucose levels following a 2-hour mixed-meal test (ns; data represented as mean± standard deviation). *A. soehngenii* supplementation significantly improved delta standard deviation (SD) **(C)**, mean amplitude of glycaemic excursions (MAGE) **(D)**, Mean of daily differences (MODD) **(E)** and mean amplitude of blood pressure (MAP) **(F).** p<0.05 was considered statistically significant, data represented as median± interquartile range in **C-F**.

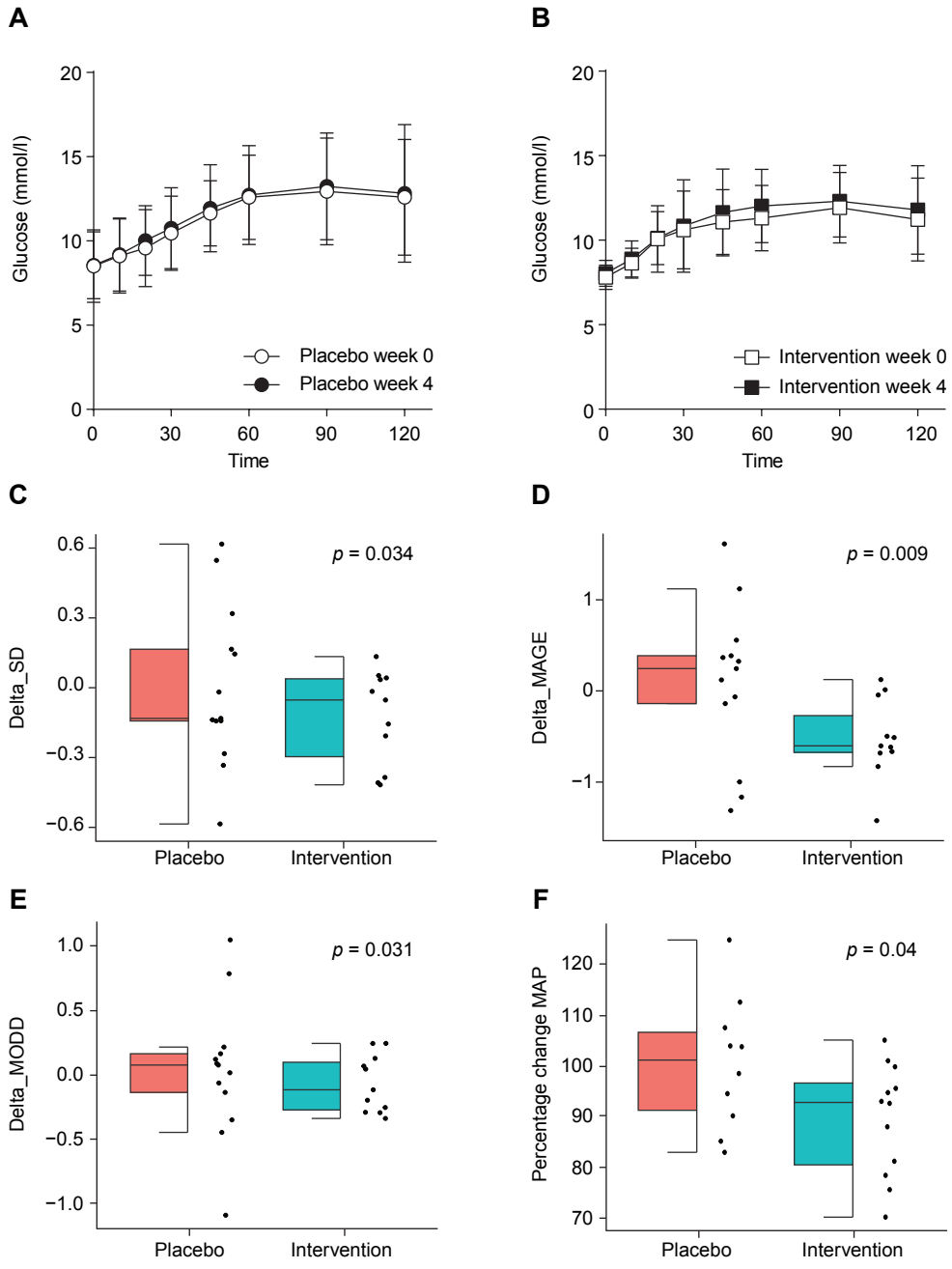

address glucose homeostasis in individuals with T2D or those at risk of developing T2D[24]. Interestingly, glycemic variability metrics such as standard deviation (SD), mean amplitude of glycemic excursion (MAGE), and mean of daily differences (MODD)) were significantly improved in the *A. soehngenii*-treated group compared to the control group. SD was reduced by 7.96% (p = 0.034), MAGE was reduced by 16.82% (p = 0.009), and MODD was reduced by 3.9% (p = 0.031) (**Figure 1C-E**).

Mean arterial blood pressure is reduced in individuals supplemented with *A. soehngenii*

SCFA have been associated with beneficial effects on blood pressure; we hypothesized that *A. soehngenii*, potentially via SCFA, would affect blood pressure in our study group. We therefore measured ambulatory blood pressure for 24 h before and after 2 weeks of *A. soehngenii* supplementation and found that mean arterial blood pressure (MAP) was reduced by 10.24% (p = 0.04), when looking at percentual change between placebo and intervention group, thereby correcting for potential baseline differences (**Figure 1F**). This effect is unlikely to be explained by alterations in SCFA levels, since these were unaltered in plasma under both fasting and stimulated (MMT) conditions (**Suppl Table 2**). However, it should be noted that SCFA concentrations in the plasma and feces often poorly reflect (local, small intestinal) SCFA production and metabolism[2].

In our previous safety and dose-response study using *A soehngenii* in individuals with metabolic syndrome, plasma bile acid levels were found to be altered[17]. In our current cohort, however, *A. soehngenii* supplementation did not affect (postprandial) plasma bile acid levels (**Figure 2A-D** and **Suppl Table 3).** Hence, we were unable to reproduce these findings in individuals with T2D on metformin, since fasting and stimulated (MMT) plasma bile acids were similar in individuals supplemented with *A. soehngenii* and placebo. Fecal bile acids were largely unaltered by *A. soehngenii* supplementation, with the exception of a trend (p=0.08) of increased levels of plasma GUDCA and significantly increased LCA in the intervention group (**Suppl Table 4**).

A. *soehngenii* abundance and replication activity

We performed shotgun metagenomics to determine whether *A. soehngenii* supplementation altered the gut microbiome composition and diversity. Alpha diversity (Shannon index) (**Figure 3A**) and beta diversity (Aitchison) (**Figure 3B**) were similar between *A. soehngenii* and placebo-treated groups. The relative abundance of *A. soehngenii* showed an increasing trend in the intervention group but was not significant (**Figure 3C**). This could be attributed to potential competition for the niche in the GI tract between our supplemented *A. soehngenii* L2-7 and the endogenous *A. soehngenii* which was already present in two subjects receiving the intervention

Figure 2. Effect of 14 days *A. soehngenii* supplementation on delta levels of plasma total bile acid (**A)**, primary bile acids (**B)**, secondary bile acids (**C)** and Glycoursodeoxycholic acid (GUDCA) (**D).** Data represented as median± interquartile range, and not significant (ns). A p<0.05 was considered statistically significant.

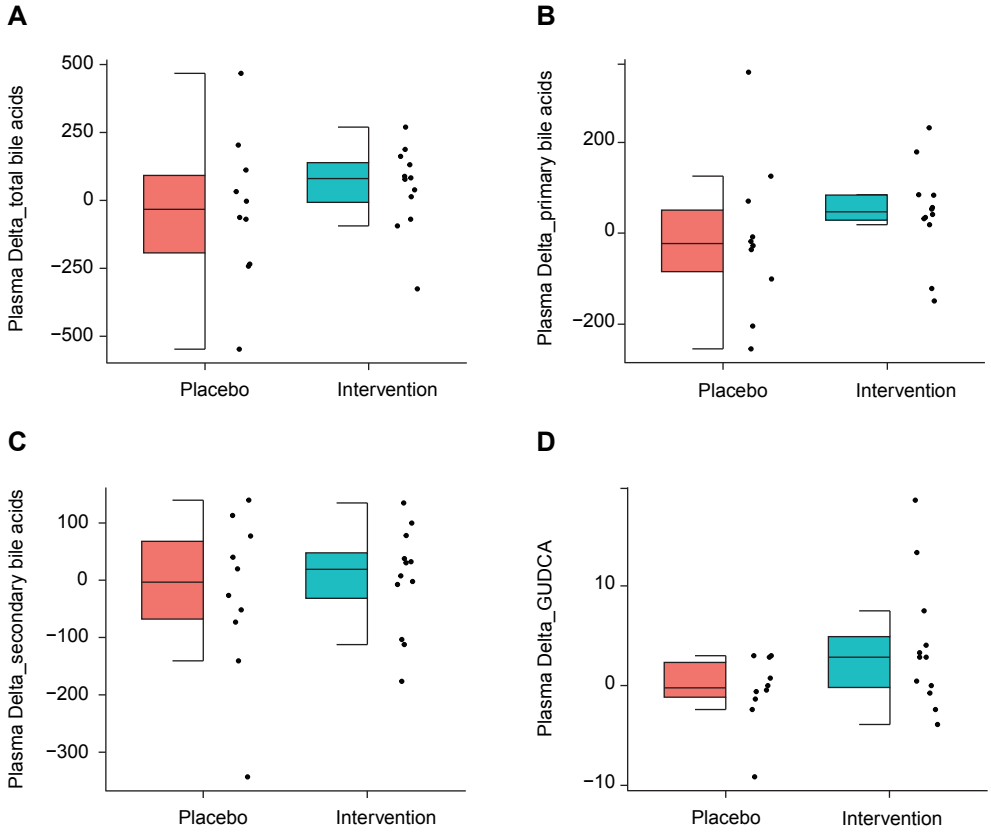

Figure 3. Effect of *A. soehngenii* supplementation on **(A)** Shannon index in the two different groups with the delta (mean). A p<0.05 was considered statistically significant. **(B)** Fecal microbiota composition at baseline and end of the intervention. The PCoA is created via genus-level Aitchison distance. The colors represent the placebo group (red) and the intervention group (green). The symbol represents the pre-intervention samples (circles) and post-intervention samples (triangles). The 80 % CI ellipses represent the baseline- (shaded ellipses) and post-intervention groups (dashed ellipses). The colored arrows represent the intervention effects with its length and direction corresponding to the shift in group centroid coordinates from baseline to endpoint for each treatment arm (re-scaled x4 and re-centered at baseline global centroid). **(C)** Relative abundances of *A. soehngenii* following placebo or *A. soehngenii* supplementation. **(D)** Replication activity of the *A. soehngenii* between the placebo- and intervention group over time with the delta values (mean). **(E)** Delta correlations within and between metabolites and clinical parameters. A blue circle indicates a significant positive correlation, whereas a red circle indicates a significant inverse correlation. p-values are not adjusted for multiple test companions.

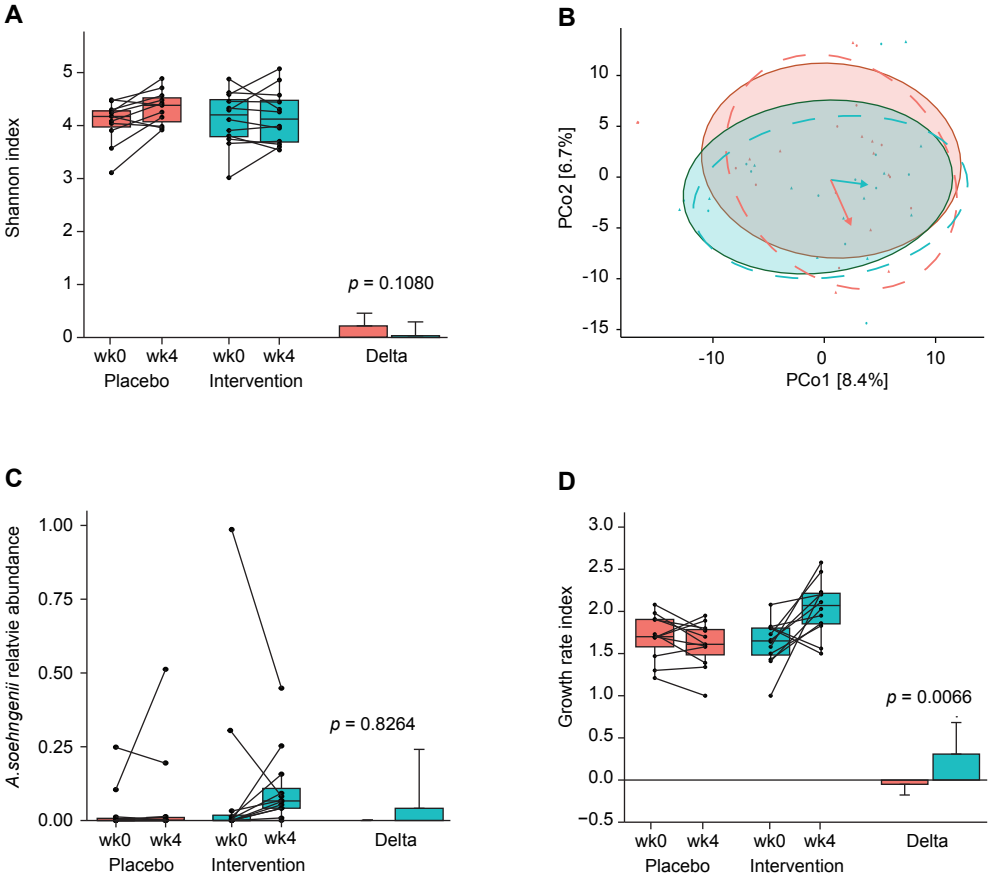
A
Shannon index
p = 0.1080
wk0 wk4 wk0 wk4 Delta
Placebo Intervention
B
PCo2 [6.7%]
PCo1 [8.4%]
C
A.soehngenii relatvie abundance
p = 0.8264
wk0 wk4 wk0 wk4 Delta
Placebo Intervention
D
Growth rate index
p = 0.0066
wk0 wk4 wk0 wk4 Delta
Placebo Intervention

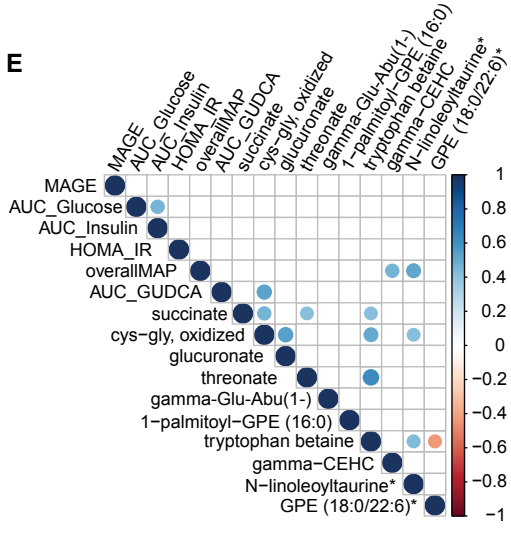
E
MAGE
AUC_Glucose
AUC_Insulin
HOMA_IR
overallMAP
AUC_GUDCA
succinate
cys−gly, oxidized
glucuronate
threonate
gamma-Glu-Abu(1-)
1−palmitoyl−GPE (16:0)
tryptophan betaine
gamma−CEHC
N−linoleoyltaurine*
GPE (18:0/22:6)*

during the allocation phase (**Suppl Figure 3**). Indeed, our intervention strain L2-7 completely replaced the native strain in one subject, resulting in a relative abundance comparable to that of other subjects receiving the intervention (**Figure 3C**). For the other subject, competition seemed evident, leading to a severe decrease in the relative abundance of the native strain (**Suppl Figure 3**). To circumvent the confusion of the relative abundance due to this potential competition for the niche in the GI tract, we assessed the growth rate index of the total *A. soehngenii*. This was significantly increased in individuals supplemented with *A soehngenii,* implying the presence of viable *A soehngenii* in the gut upon treatment ($p = 0.0066$, **Figure 3D**).

We then addressed whether the plasma metabolome of individuals that received two weeks of supplementation with *A. soehngenii* differed from the plasma metabolome of placebo-supplemented controls. We identified the top 10 plasma metabolites that were altered by the intervention, and performed correlation analyses with clinical markers (**Figure 3E)**. This study identified positive correlations between gamma-CEHC and N-linoleoyltaurine levels and MAP. No negative correlations were identified between the plasma metabolites and clinical markers.

DISCUSSION

In this randomized double-blind placebo-controlled trial, we showed that 14 days of oral treatment with *A. soehngenii L2-7* alters glucometabolic parameters in T2D subjects receiving stable metformin therapy. *A. soehngenii* supplementation significantly improved glycemic variability based on real-time measurements with continuous glucose monitoring. Moreover, we identified the changes in plasma metabolites and their correlation with several metabolic parameters.

Previous rodent and human studies have shown that *A. soehngenii* can positively influence glucose metabolism[16–18]. A study in obese mice showed that daily supplementation of *A. soehngenii,* through oral gavage for four weeks, improved insulin sensitivity and affected bile acid metabolism [16]. The positive effect of *A. soehngenii* supplementation on glucose metabolism was also confirmed in two human intervention studies, both focusing on treatment-naïve subjects with metabolic syndrome [17,18]. In a recent study, direct intestinal infusion of a single dose of *A. soehngenii* in the duodenum led to an improvement in glycemic variability, as measured via continuous glucose monitoring [18]. We speculate that this improvement may be modulated through changes in GLP-1 levels and/or secondary bile acids in individuals with metabolic syndrome. Here, we show that *A. soehngenii* supplementation lowers glycemic variability by lowering SD, MAGE, and MODD. These parameters are well-established glucose variability metrics that

correlate strongly with each other, poor metabolic health, and more cardiovascular events[25–28]. Despite being able to replicate the beneficial effects of *A. soehngenii* on glucose variability in our current study population, we were unable to find clinically relevant changes in GLP-1 or secondary bile acids.

It is important to note that previous human studies have focused on treatment-naïve metabolic syndrome subjects, whereas this study investigated the additional glucose-lowering effect of *A. soehngenii* supplementation in T2D subjects on metformin therapy, a well-known modulator of the gut microbiota [29]. GLP1 excursions were two-fold higher in T2D individuals on metformin than in individuals with metabolic syndrome. This is potentially due to metformin-mediated effects on GLP1 secretion [30] and might explain why we did not observe GLP1 effects of *A. soehngenii* in addition to metformin effects on GLP1, next to a more indirect way of treatment by ingestion instead of direct duodenal infusion.

Previous studies have shown that *A. soehngenii* supplementation can not only increase total plasma secondary bile acid levels after oral supplementation, but also following direct duodenal infusion[17,18]. These observations are important because bile acid metabolism, gut microbiota composition, and cardiometabolic health are closely associated[31]. However, the current study does not support previous findings of a significant increase in plasma secondary bile acid levels in individuals treated with *A. soehngenii*. However, we observed a trend (p=0.08) for an increased level of plasma GUDCA, a secondary bile acid that has been found to exert protective effects against diet-induced insulin resistance in preclinical models[32]. Of note, metformin treatment has been shown to affect the gut microbiota and increase the levels of GUDCA, which might abrogate further increases in GUDCA in the current study population [33].

A. soehngenii supplementation did not induce large-scale changes in alpha or beta diversity in this study, which is in accordance with previous studies[18]. Using advanced replication analysis, we confirmed that *A. soehngenii* engraftment was successful. Nevertheless, engraftment was not similar among all the participants in the treatment group. Two individuals in the treatment group had a similar *A soehngenii* strain present at baseline, which might have inhibited the L2-7 strain from engrafting in the intestine. This finding is in accordance with a recent study showing that the engraftment of exogenous strains is likely unsuccessful when (closely) related strains are already present in the gut[34]. However, in two other individuals, engraftment was inferior to that in other participants without prior presence of *A. soehngenii* strains at baseline. Although we monitored compliance and all participants returned the complete number of empty vials, we cannot exclude poor compliance in these individuals.

Gut microbiota-derived metabolites are thought to be key players and potential modifiable factors in the pathophysiology of T2D[2]. Therefore, this study investigated the effects of *A. soehngenii* supplementation on (gut-derived) plasma metabolites. Using untargeted semi-quantitative metabolomics, we identified several plasma metabolite changes that were altered by *A. soehngenii* treatment combined with metformin, which were subsequently correlated with clinical markers. Positive correlations were identified between plasma gamma-CEHC, N-linoleoyl taurine levels, and MAP. No negative correlations were identified between the plasma metabolites and clinical markers. The metabolites that correlate with MAP have been scarcely described in the literature and are linked to fatty acid metabolism (N-linoleoyl taurine [35]) and vitamin E metabolism (gamma-CEHC [36]). As such, the association of N-linoleoyl taurine and reduced blood pressure is a new finding of this study and it is tempting to speculate that this compound has a similar action as taurine that is known to reduce hypertension in human and animal models due to its structural similarity [37] Similarly gamma-CEHC has been shown to have anti-inflammatory properties rationalizing the observed correlation of this compound and blood pressure[38]. However, it is important to note that the identified metabolites are not well studied, and correlations found need to be interpreted with caution. Further research is needed on these plasma metabolites, with a specific emphasis on the clinical parameters with which we found correlations.

Limitations

Our study had several limitations. First, T2D participants were only treated for a relatively short period of time, and long-term studies will have to show if the observed effect of *A. soehngenii* on glucometabolic control is long-lasting. Second, this pilot study aimed to provide proof-of-concept insight into the potential synergy between next-generation probiotics and oral pharmacological treatment; thus, the size of our study was relatively small. Third, all participants received oral metformin therapy, which could have had a confounding effect as metformin also altered the gut microbiota composition [39]. However, metformin is among the first-choice therapies for type 2 diabetes; therefore, the selection of individuals included in this trial makes the results more generalizable to the patient population itself[40]. The fact that this study already provided significant findings following short-term *A. soehngenii* supplementation on glucometabolic control indicates the potential of *A. soehngenii* as an add-on therapy in the standard of care for T2D.

In conclusion, this is the first randomized, double-blind, placebo-controlled clinical trial to study the augmenting effects of two weeks of single bacterial strain *A. soehngenii* supplementation in type 2 diabetes subjects on stable metformin monotherapy. We found that *A. soehngenii* supplementation was well-tolerated and

improved glucose variability and mean arterial blood pressure. The results of this study indicate that *A. soehngenii* can act as a next-generation therapeutic microbe that can improve metabolic health following metformin therapy. Larger clinical trials are therefore warranted to investigate this augmenting effect in a more sex and ethnically diverse population and to determine if *A. soehngenii* supplementation for a longer duration has durable beneficial metabolic effects.

ACKNOWLEDGEMENTS

This study was supported by a Dutch Heart Foundation CVON IN CONTROL-2 Matching Grant (01-003-2021-0344 2021) to H.H, M.N., and A.K.G. H.H. was further supported by a Senior Fellowship of the Dutch Diabetes Research Foundation (2019.82.004). W. M. d. V. was supported by the SIAM Gravitation Grant 024.002.002 of The Netherlands Organization for Scientific Research. K.W., M.B., D.M.B., and E.R. were appointed to a CAMIT grant 2018 (to M.N.). The study reported here was additionally supported by Le Ducq consortium grant 17CVD01 and ZONMW VICI grant 2020 [09150182010020] to M.N. We are grateful to Dr. Sahin Gul of Caelus Pharmaceuticals for providing the cell counts based on flow cytometry. S.L.H. was supported in part by grants from the NIH and the Office of Dietary Supplements P01 HL147823 and R01 HL103866.

H.H. is the guarantor of this work and, as such, has full access to all the data in the study and takes responsibility for the integrity of the data and the accuracy of the data analysis.

COMPETING INTERESTS

M.N. and W.M.d.V. are founders and members of the Scientific Advisory Board of Caelus Pharmaceuticals in the Netherlands. W.M.d.V. is the founder and Chief Technology Officer of The Akkermansia Company, Belgium. S.L.H. reports are referred to as co-inventors on pending and issued patents held by the Cleveland Clinic relating to cardiovascular diagnostics and therapeutics, eligible to receive royalty payments for inventions or discoveries related to cardiovascular diagnostics or therapeutics from Cleveland HeartLab, a wholly owned subsidiary of Quest Diagnostics, Procter & Gamble, and Zehna therapeutics. S.L.H. also reports being a paid consultant formerly for Procter & Gamble and currently with Zehna Therapeutics and has received research funds from Procter & Gamble and Zehna Therapeutics.

REFERENCES

1. Boyle, J.P., Thompson, T.J., Gregg, E.W., Barker, L.E., and Williamson, D.F. (2010). Projection of the year 2050 burden of diabetes in the US adult population: dynamic modeling of incidence, mortality, and prediabetes prevalence. Popul Health Metr *8*, 29. 10.1186/1478-7954-8-29.
2. Herrema, H., and Niess, J.H. (2020). Intestinal microbial metabolites in human metabolism and type 2 diabetes. Diabetologia *63*, 2533–2547. 10.1007/s00125-020-05268-4.
3. Ridaura, V.K., Faith, J.J., Rey, F.E., Cheng, J., Duncan, A.E., Kau, A.L., Griffin, N.W., Lombard, V., Henrissat, B., Bain, J.R., et al. (2013). Gut Microbiota from Twins Discordant for Obesity Modulate Metabolism in Mice. Science (1979) *341*. 10.1126/science.1241214.
4. Pedersen, H.K., Gudmundsdottir, V., Nielsen, H.B., Hyotylainen, T., Nielsen, T., Jensen, B.A.H., Forslund, K., Hildebrand, F., Prifti, E., Falony, G., et al. (2016). Human gut microbes impact host serum metabolome and insulin sensitivity. Nature *535*, 376–381. 10.1038/nature18646.
5. Karlsson, F.H., Tremaroli, V., Nookaew, I., Bergström, G., Behre, C.J., Fagerberg, B., Nielsen, J., and Bäckhed, F. (2013). Gut metagenome in European women with normal, impaired and diabetic glucose control. Nature *498*, 99–103. 10.1038/nature12198.
6. Vallianou, N.G., Geladari, E., and Kounatidis, D. (2020). Microbiome and hypertension: where are we now? J Cardiovasc Med (Hagerstown) *21*, 83–88.
7. Barbara J.H. Verhaar, Didier Collard, Andrei Prodan, Johannes H.M. Levels, AeilkoH. Zwinderman, Fredrik Backhed, Liffert Vogt, Mike J.L. Peters, Majon Muller, Max Nieuwdorp, et al. (2020). Associations between gut microbiota, faecal short-chain fatty acids, and blood pressure across ethnic groups: the HELIUS study. Eur Heart J *41*, 4268–4270. 10.1093/eurheartj/ehaa760.
8. Flint, H.J., Duncan, S.H., Scott, K.P., and Louis, P. (2015). Links between diet, gut microbiota composition and gut metabolism. Proceedings of the Nutrition Society *74*, 13–22. 10.1017/S0029665114001463.
9. Kootte, R.S., Levin, E., Salojärvi, J., Smits, L.P., Hartstra, A. V., Udayappan, S.D., Hermes, G., Bouter, K.E., Koopen, A.M., Holst, J.J., et al. (2017). Improvement of Insulin Sensitivity after Lean Donor Feces in Metabolic Syndrome Is Driven by Baseline Intestinal Microbiota Composition. Cell Metab *26*, 611–619.e6. 10.1016/j.cmet.2017.09.008.
10. Shetty, S.A., Zuffa, S., Bui, T.P.N., Aalvink, S., Smidt, H., and De Vos, W.M. (2018). Reclassification of eubacterium hallii as Anaerobutyricum hallii gen. nov., comb. nov., and description of Anaerobutyricum soehngenii sp. nov., a butyrate and propionate-producing bacterium from infant faeces. Int J Syst Evol Microbiol *68*, 3741–3746. 10.1099/ijsem.0.003041.
11. Duncan, S.H., Louis, P., and Flint, H.J. (2004). Lactate-Utilizing Bacteria, Isolated from Human Feces, That Produce Butyrate as a Major Fermentation Product. Appl Environ Microbiol *70*, 5810–5817. 10.1128/AEM.70.10.5810-5817.2004.
12. Schwab, C., Ruscheweyh, H.-J., Bunesova, V., Pham, V.T., Beerenwinkel, N., and Lacroix, C. (2017). Trophic Interactions of Infant Bifidobacteria and Eubacterium hallii during L-Fucose and Fucosyllactose Degradation. Front Microbiol *8*. 10.3389/fmicb.2017.00095.
13. Wu, H., Esteve, E., Tremaroli, V., Khan, M.T., Caesar, R., Mannerås-Holm, L., Ståhlman, M., Olsson, L.M., Serino, M., Planas-Fèlix, M., et al. (2017). Metformin alters the gut microbiome of individuals with treatment-naive type 2 diabetes, contributing to the therapeutic effects of the drug. Nat Med *23*, 850–858. 10.1038/nm.4345.
14. Crawford, S.O., Ambrose, M.S., Hoogeveen, R.C., Brancati, F.L., Ballantyne, C.M., and Young, J.H. (2008). Association of lactate with blood pressure before and after rapid weight loss. Am J Hypertens *21*, 1337–1342. 10.1038/ajh.2008.282.
15. Cookson, T.A. (2021). Bacterial-Induced Blood Pressure Reduction: Mechanisms for the Treatment of Hypertension via the Gut. Front Cardiovasc Med *8*. 10.3389/fcvm.2021.721393.

16. Udayappan, S., Manneras-Holm, L., Chaplin-Scott, A., Belzer, C., Herrema, H., Dallinga-Thie, G.M., Duncan, S.H., Stroes, E.S.G., Groen, A.K., Flint, H.J., et al. (2016). Oral treatment with Eubacterium hallii improves insulin sensitivity in db/db mice. NPJ Biofilms Microbiomes *2*. 10.1038/npjbiofilms.2016.9.
17. Gilijamse, P.W., Hartstra, A. V., Levin, E., Wortelboer, K., Serlie, M.J., Ackermans, M.T., Herrema, H., Nederveen, A.J., Imangaliyev, S., Aalvink, S., et al. (2020). Treatment with Anaerobutyricum soehngenii: a pilot study of safety and dose–response effects on glucose metabolism in human subjects with metabolic syndrome. NPJ Biofilms Microbiomes *6*. 10.1038/s41522-020-0127-0.
18. Koopen, A., Witjes, J., Wortelboer, K., Majait, S., Prodan, A., Levin, E., Herrema, H., Winkelmeijer, M., Aalvink, S., Bergman, J.J.G.H.M., et al. (2021). Duodenal Anaerobutyricum soehngenii infusion stimulates GLP-1 production, ameliorates glycaemic control and beneficially shapes the duodenal transcriptome in metabolic syndrome subjects: a randomised double-blind placebo-controlled cross-over study. Gut. 10.1136/gutjnl-2020-323297.
19. Brown, M.D., Korytkowski, M.T., Zmuda, J.M., McCole, S.D., Moore, G.E., and Hagberg, J.M. (2000). Insulin sensitivity in postmenopausal women: independent and combined associations with hormone replacement, cardiovascular fitness, and body composition. Diabetes Care *23*, 1731–1736. 10.2337/diacare.23.12.1731.
20. Wortelboer, K., Koopen, A.M., Herrema, H., de Vos, W.M., Nieuwdorp, M., and Kemper, E.M. (2022). From fecal microbiota transplantation toward next-generation beneficial microbes: The case of Anaerobutyricum soehngenii. Front Med (Lausanne) *9*, 1077275. 10.3389/fmed.2022.1077275.
21. Milk and milk products — Starter cultures, probiotics and fermented products — Quantification of lactic acid bacteria by flow cytometry (2015). ISO 19344:2015 | IDF 232:2015 *12*, 1–25.
22. Dalla Man, C., Campioni, M., Polonsky, K.S., Basu, R., Rizza, R.A., Toffolo, G., and Cobelli, C. (2005). Two-hour seven-sample oral glucose tolerance test and meal protocol: minimal model assessment of beta-cell responsivity and insulin sensitivity in nondiabetic individuals. Diabetes *54*, 3265–3273. 10.1161/ATVBAHA.113.301765.
23. Attaye, I., van der Vossen, E.W.J., Mendes Bastos, D.N., Nieuwdorp, M., and Levin, E. (2022). Introducing the Continuous Glucose Data Analysis (CGDA) R Package: An Intuitive Package to Analyze Continuous Glucose Monitoring Data. J Diabetes Sci Technol *16*, 783–785. 10.1177/19322968211070293.
24. Danne, T., Nimri, R., Battelino, T., Bergenstal, R.M., Close, K.L., DeVries, J.H., Garg, S., Heinemann, L., Hirsch, I., Amiel, S.A., et al. (2017). International consensus on use of continuous glucose monitoring. Diabetes Care *40*, 1631–1640. 10.2337/dc17-1600.
25. Akasaka, T., Sueta, D., Tabata, N., Takashio, S., Yamamoto, E., Izumiya, Y., Tsujita, K., Kojima, S., Kaikita, K., Matsui, K., et al. (2017). Effects of the Mean Amplitude of Glycemic Excursions and Vascular Endothelial Dysfunction on Cardiovascular Events in Nondiabetic Patients With Coronary Artery Disease. J Am Heart Assoc *6*. 10.1161/JAHA.116.004841.
26. Zhou, Z., Sun, B., Huang, S., Zhu, C., and Bian, M. (2020). Glycemic variability: adverse clinical outcomes and how to improve it? Cardiovasc Diabetol *19*. 10.1186/s12933-020-01085-6.
27. Suh, S., and Kim, J.H. (2015). Glycemic Variability: How Do We Measure It and Why Is It Important? Diabetes Metab J *39*, 273. 10.4093/dmj.2015.39.4.273.
28. Tang, X., Li, S., Wang, Y., Wang, M., Yin, Q., Mu, P., Lin, S., Qian, X., Ye, X., and Chen, Y. (2016). Glycemic variability evaluated by continuous glucose monitoring system is associated with the 10-y cardiovascular risk of diabetic patients with well-controlled HbA1c. Clinica Chimica Acta *461*, 146–150. 10.1016/j.cca.2016.08.004.

29. Lee, H., Lee, Y., Kim, J., An, J., Lee, S., Kong, H., Song, Y., Lee, C.-K., and Kim, K. (2018). Modulation of the gut microbiota by metformin improves metabolic profiles in aged obese mice. Gut Microbes *9*, 155–165.
30. Bahne, E., Sun, E.W.L., Young, R.L., Hansen, M., Sonne, D.P., Hansen, J.S., Rohde, U., Liou, A.P., Jackson, M.L., de Fontgalland, D., et al. (2018). Metformin-induced glucagon-like peptide-1 secretion contributes to the actions of metformin in type 2 diabetes. JCI Insight *3*. 10.1172/jci.insight.93936.
31. Ridlon, J.M., Kang, D.J., Hylemon, P.B., and Bajaj, J.S. (2014). Bile acids and the gut microbiome. Curr Opin Gastroenterol *30*, 332–338. 10.1097/MOG.0000000000000057.
32. Cheng, L., Chen, T., Guo, M., Liu, P., Qiao, X., Wei, Y., She, J., Li, B., Xi, W., Zhou, J., et al. (2021). Glycoursodeoxycholic acid ameliorates diet-induced metabolic disorders with inhibiting endoplasmic reticulum stress. Clin Sci *135*, 1689–1706. 10.1042/CS20210198.
33. Sun, L., Xie, C., Wang, G., Wu, Y., Wu, Q., Wang, X., Liu, J., Deng, Y., Xia, J., Chen, B., et al. (2018). Gut microbiota and intestinal FXR mediate the clinical benefits of metformin. Nat Med *24*, 1919–1929. 10.1038/s41591-018-0222-4.
34. Schmidt, T.S.B., Li, S.S., Maistrenko, O.M., Akanni, W., Coelho, L.P., Dolai, S., Fullam, A., Glazek, A.M., Hercog, R., Herrema, H., et al. (2022). Drivers and determinants of strain dynamics following fecal microbiota transplantation. Nat Med *28*, 1902–1912. 10.1038/s41591-022-01913-0.
35. Ding, S., Jiang, H., Fang, J., and Liu, G. (2021). Regulatory Effect of Resveratrol on Inflammation Induced by Lipopolysaccharides via Reprograming Intestinal Microbes and Ameliorating Serum Metabolism Profiles. Front Immunol *12*. 10.3389/fimmu.2021.777159.
36. Cho, J.-Y., Kang, D.W., Ma, X., Ahn, S.-H., Krausz, K.W., Luecke, H., Idle, J.R., and Gonzalez, F.J. (2009). Metabolomics reveals a novel vitamin E metabolite and attenuated vitamin E metabolism upon PXR activation. J Lipid Res *50*, 924–937. 10.1194/jlr.M800647-JLR200.
37. Bae, M., Ahmed, K., and Yim, J.-E. (2022). Beneficial Effects of Taurine on Metabolic Parameters in Animals and Humans. J Obes Metab Syndr *31*, 134–146. 10.7570/jomes21088.
38. Devaraj, S., Leonard, S., Traber, M.G., and Jialal, I. (2008). Gamma-tocopherol supplementation alone and in combination with alpha-tocopherol alters biomarkers of oxidative stress and inflammation in subjects with metabolic syndrome. Free Radic Biol Med *44*, 1203–1208. 10.1016/j.freeradbiomed.2007.12.018.
39. Pascale, A., Marchesi, N., Govoni, S., Coppola, A., and Gazzaruso, C. (2019). The role of gut microbiota in obesity, diabetes mellitus, and effect of metformin: new insights into old diseases. Curr Opin Pharmacol *49*, 1–5.
40. 9. Pharmacologic approaches to glycemic treatment: Standards of medical care in diabetesd–2020 (2020). Diabetes Care *43*, S98–S110. 10.2337/dc20-S009.

SUPPLEMENTAL MATERIAL

Biochemical, Microbiome and Metabolome analyses

Plasma SCFA measurement

Plasma SCFAs were measured at Cleveland Clinic (OH, USA). Collected plasma heparin samples were directly frozen at -80°C and were used for gas chromatography coupled to tandem mass spectrometry (GC-MS/MS). For a brief, step-by-step description see Koopen et al.(1) .

Plasma incretin measurement

Two-hour mixed meal tests were performed in all individuals and plasma incretin levels were determined in the collected postprandial samples as described previously (2). Concentrations of total plasma GLP-1 were measured with the use of ELISA kits (cat no. 10-1258-01 and 10-1278-01, Mercodia, Sweden). The quality controls provided by the manufacturer were within the allowed limits and all samples of one individual were measured in the same assay run to reduce variability.

Plasma and fecal bile acid measurement

Ultra high-performance liquid chromatography-tandem mass spectrometry (UPLC-MS/MS) was used to measure the plasma concentrations of the primary, secondary, conjugated and unconjugated bile acids ursodeoxycholic acid (UDCA), cholic acid (CA), glycoursodeoxycholic acid (GUDCA), glycocholic acid (GCA), tauroursodeoxycholic acid (TUDCA), taurocholic acid (TCA), chenodeoxycholic acid (CDCA), deoxycholic acid (DCA), glycochenodeoxycholic acid (GCDCA), glycodeoxycholic acid (GDCA), taurochenodeoxycholic acid (TCDCA), taurodeoxycholic acid (TDCA), lithocholic acid (LCA), taurolithocholic acid (TLCA), glycolithocholic acid (GLCA) as described previously (3). For a brief, step- by step description please see elsewhere (4,5). Fecal samples (from 24hr fecal collection) were thawed and homogenized with distilled water (1:1; w/w). A total of 10 mL of fecal homogenate was dispensed into a 10 mL plastic tube. Bile salts were extracted and quantified as their methyl-trimethylsilyl derivatives (6). Bile salts were analyzed by gas chromatography (Agilent 6890) using a CPSil 19 capillary column (25 m × 0.25 mm × 0.2 μm; Chrompack).

Plasma metabolite profiling

Global untargeted targeted metabolite profiling was performed at both timepoints on the sampled blood by Metabolon (Morrisville, NC, USA) using ultra high-performance liquid chromatography coupled to tandem mass spectrometry, as

previously described (7). Metabolites that were either all zero or constant, were omitted. Next, the values of each metabolite across all samples were rescaled to 1, in which missing values were imputed with the lowest present value for its respective metabolite.

Fecal sample collection and analyses

Both fresh morning stool samples and 24-hour stool samples were directly frozen at -20°C after collection. Stool samples of all participants were taken at 0, 2 and 4 weeks after initiation of the study and transferred in frozen form to the study center, where the samples were stored at -80°C until use.

Fecal SCFA measurement

Short chain fatty acid (butyrate, acetate, propionate) levels were measured in fecal samples at Cleveland Clinic. Fresh morning stool samples were directly frozen at -20°C after collection and gas chromatography coupled to tandem mass spectrometry detection (GC-MS/MS) was used for the measurement of SCFA levels in these samples. To start, 20-100 mg of the sample was mixed with internal standards and freeze dried. Then HCl was added to the samples with the use of diethyl ether extraction SCFAs were extracted. The derivatization agent N-tert-butyldimethylsilyl-N- methyltrifluoroacetamide (Sigma-Aldrich, Stockholm, Sweden) was added to the collected organic supernatant and samples were incubated at room temperature overnight. Using a gas chromatograph (Agilent Technologies 7890A, Santa Clara, California, USA) coupled to a mass spectrometer (Agilent Technologies 5975C) SCFAs were quantified. SCFA standards were attained from Sigma-Aldrich (Stockholm, Sweden).

Gut microbiota profiling

Fecal samples were isolated as previously described (8) and analysed for microbiota composition using shotgun metagenomic sequencing (Novogene, Cambridge, UK). Raw reads were checked and quality- filtered using fastp (v.0.20.0). Here, the adapter was detected and removed, 5 bp in front for read1 was trimmed, and sliding window quality trimming was applied (with a window width of 4 bp and threshold Q-score of 15). After trimming and adapter removal, reads shorter than 70 bp were removed. Paired-end reads that passed the quality filtering were mapped against the human genome (hg19) using Bowtie 2 (v.2.4.1). SAMtools (v.1.9), sambamba (v.0.7.1) and BEDtools (v.2.27.1) were used to remove reads that were mapped to the human genome. Unmapped reads were subsampled to 20 milion reads. The remaining high-quality, non-human reads were fed to the MetaPhlAn pipeline (v.4.0.2) for taxonomic profiling (9).

Growth rates of A. soehngenii from metagenomic sequencing data

The growth of the A. soehngenii was determined using the growth rate index algorithm as previously described (10). In short, the principle is based on that most bacteria harbour a circular chromosome, in which bi-directional replication takes place from the origin of replication to the terminus. Hereby, in a fast-growing bacterium, the copy number of DNA will be larger at the origin of replication when compared to the terminus.

Differentiating the administered A. soehngenii strain from endogenous Anaerobutyricum spp.

The intervention strain A. soehngenii L2-7 was distinguished from endogenous A. soehngenii via single nucleotide variants (SNVs). For each subject, a unique subset of SNVs was used to discriminate between the administered A. soehngenii L2-7 and endogenous strains. Reads were first processed as described in "Gut microbiota profiling". After extracting A. soehngenii reads using the reference genome of the A. soehngenii L2-7, GATKs HaplotypeCaller was applied, with a ploidy assumption of 10. The pipeline consists of multiple filters. The first filters include a variant confidence standardized by depth (QD < 2.00), Fisher exact test for strand bias (FS > 60), strand odds ratio test for strand bias (SOR > 3.00), Mapping quality (MQ < 32.00), Rank sum test for mapping qualities of reference versus alternative reads (MQRankSum < -12.5) and rank sum test for relative positioning of reference versus alternative alleles within reads (ReadPosRankSum < -8.00). The second filter hereafter requires the SNV to have a depth of at least 6 reads per sample. The third filter is based on the removal of SNVs found in samples not containing A. soehngenii (e.g., spurious mapping locations such as mobile elements, 16s region).

Machine learning analyses

We applied an Extremely Randomized Trees machine learning classification algorithm to identify which parameters (relative changes at week 2 (allocation) and week 4 (end of study)) best distinguished between the intervention- and placebo group. Prior to applying the model, metabolites were filtered to reduce dimensionality. First, metabolites that were zero or constant for all subjects, were omitted. Hereafter, the Rosner's test for outliers was applied, omitting features that have one outlier. Features with the largest variance were included. Lastly, a univariate feature selection (SelectPercentile) was applied to include 50 metabolites in the model.

Within the machine learning simulation, all models were constructed with the same stability selection procedure to ensure robustness of the results and prevent overfitting. In total, the dataset is split up 20 times. Within these 20 random subsets, 85% of the subjects were included. Next, LeaveOneOut cross-validation was applied

where the training set included all samples except for one, in which this one sample left out was included in the test set. Within the training set, the hyperparameters of extremely randomized trees model were found by performing a randomised search with a three-fold cross-validation, based on 90% of the training set and validated on the remaining 10%. The parameter grid on which the randomised search was applied with the number of parameter settings tried was 10. Performance of the different models was estimated via an area under the curve (AUC) of the test dataset to distinguish the intervention group from the placebo group. The importance of each gut microbiota in the models was extracted and was based on the permutation importance. This machine learning pipeline was implemented in python (v3.7.7), using the scikit-learn (v0.23.1) package.

REFERENCES

1. Koopen A, Witjes J, Wortelboer K, Majait S, Prodan A, Levin E, et al. Duodenal Anaerobutyricum soehngenii infusion stimulates GLP-1 production, ameliorates glycaemic control and beneficially shapes the duodenal transcriptome in metabolic syndrome subjects: a randomised double-blind placebo-controlled cross-over study. Gut [Internet]. 2021 Oct 25; Available from: http://www.ncbi.nlm.nih.gov/pubmed/34697034
2. Kootte RS, Levin E, Salojärvi J, Smits LP, Hartstra A V., Udayappan SD, et al. Improvement of Insulin Sensitivity after Lean Donor Feces in Metabolic Syndrome Is Driven by Baseline Intestinal Microbiota Composition. Cell Metab. 2017;26(4):611–619.e6.
3. Hoogerland JA, Lei Y, Wolters JC, de Boer JF, Bos T, Bleeker A, et al. Glucose-6-Phosphate Regulates Hepatic Bile Acid Synthesis in Mice. Hepatology. 2019 Dec 24;70(6):2171–84.
4. Chen L, van den Munckhof ICL, Schraa K, ter Horst R, Koehorst M, van Faassen M, et al. Genetic and Microbial Associations to Plasma and Fecal Bile Acids in Obesity Relate to Plasma Lipids and Liver Fat Content. Cell Rep. 2020 Oct;33(1):108212.
5. Wang D, Doestzada M, Chen L, Andreu-Sánchez S, van den Munckhof ICL, Augustijn HE, et al. Characterization of gut microbial structural variations as determinants of human bile acid metabolism. Cell Host Microbe. 2021 Dec;29(12):1802–1814.e5.
6. Out C, Patankar J V, Doktorova M, Boesjes M, Bos T, de Boer S, et al. Gut microbiota inhibit Asbt-dependent intestinal bile acid reabsorption via Gata4. J Hepatol. 2015 Sep;63(3):697–704.
7. Koh A, Molinaro A, Ståhlman M, Khan MT, Schmidt C, Mannerås-Holm L, et al. Microbially Produced Imidazole Propionate Impairs Insulin Signaling through mTORC1. Cell [Internet]. 2018;175(4):947–961.e17. Available from: https://www.ncbi.nlm.nih.gov/pubmed/30401435
8. Koopen AM, de Clercq NC, Warmbrunn M V., Herrema H, Davids M, de Groot PF, et al. Plasma Metabolites Related to Peripheral and Hepatic Insulin Sensitivity Are Not Directly Linked to Gut Microbiota Composition. Nutrients. 2020 Jul 31;12(8):2308.
9. Blanco-Miguez A, Beghini F, Cumbo F, Mciver LJ, Thompson KN, Zolfo M, et al. Extending and improving metagenomic taxonomic profiling with uncharacterized species with MetaPhlAn 4. Available from: https://doi.org/10.1101/2022.08.22.504593
10. Emiola A, Oh J. High throughput in situ metagenomic measurement of bacterial replication at ultra-low sequencing coverage. Nat Commun. 2018 Dec 1;9(1).

SUPPLEMENTAL FIGURES

Suppl Figure 1. Study design EDM2 study.

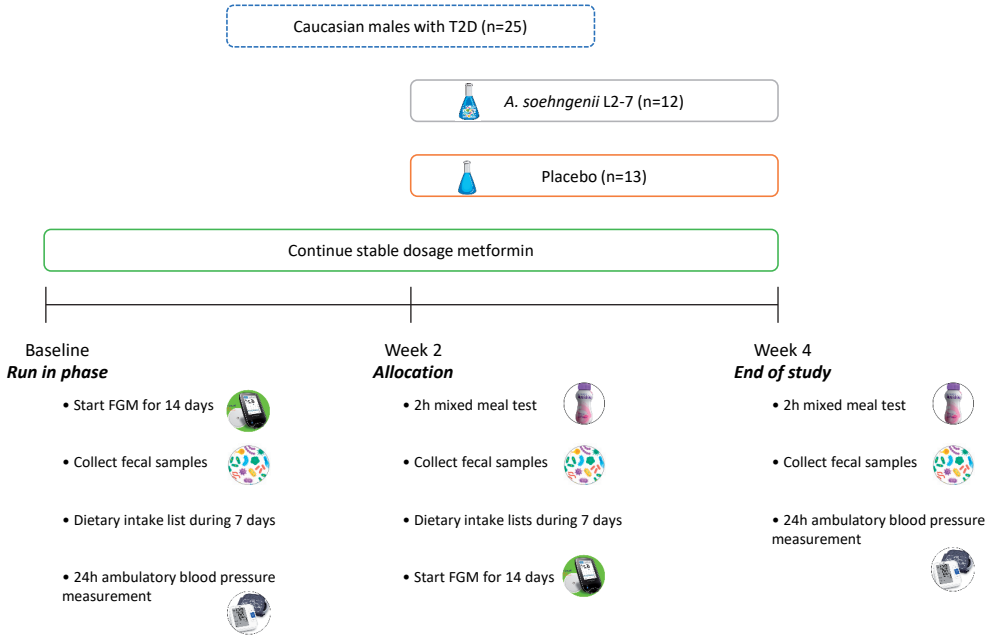

Suppl Figure 2.

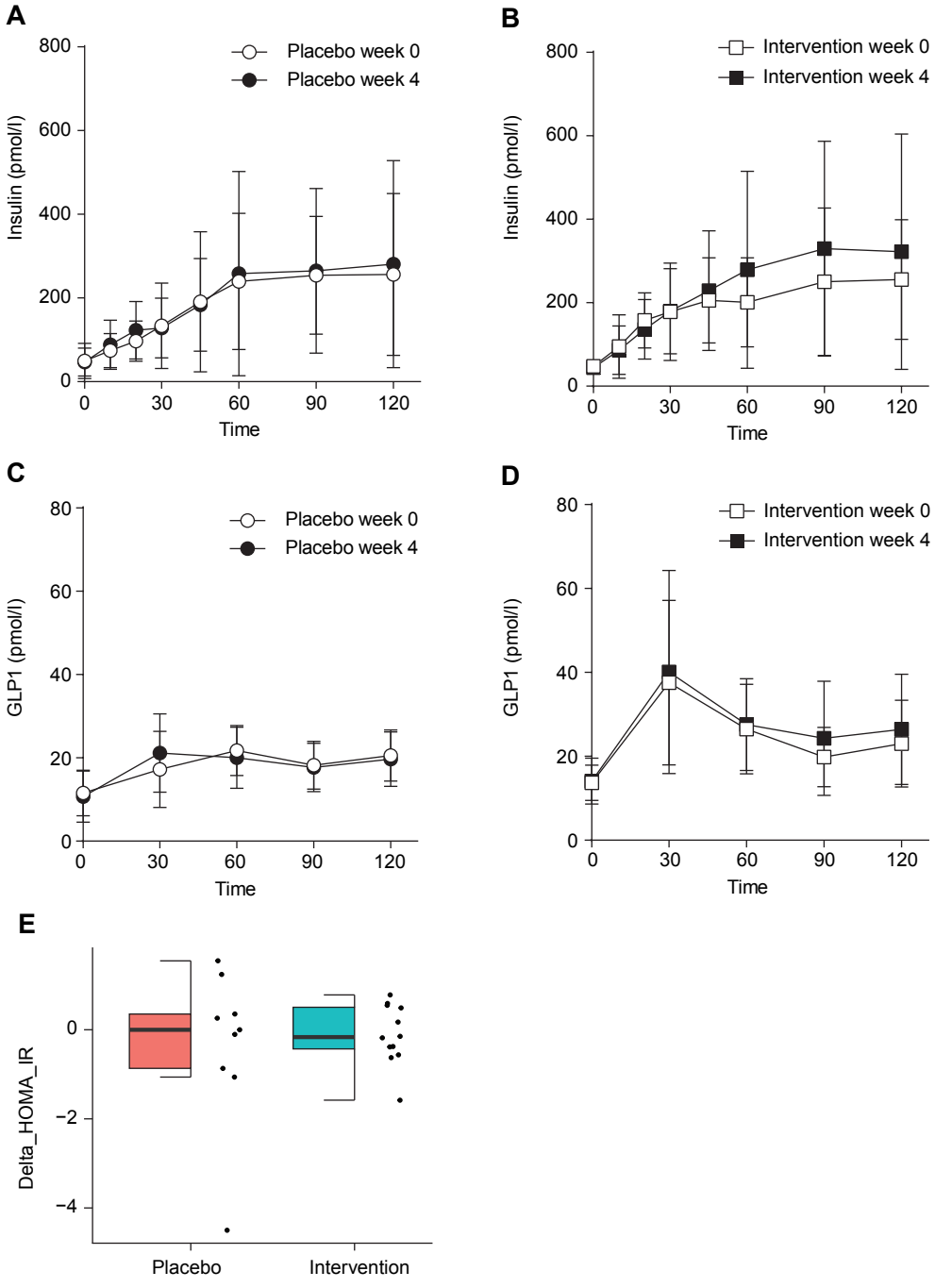

Effect of 14 days placebo (**A)** and *A. soehngenii* **(B)** supplementation on insulin levels following a 2-hour mixed-meal test (ns; data represented as mean± standard deviation). Effect of 14 days placebo (**C)** and *A. soehngenii* **(D)** supplementation on glucagon-like peptide 1 (GLP-1) levels following a 2-hour mixed-meal test (ns; data represented as mean± standard deviation). **(E)** Effect of placebo or *A. soehngenii* on –HOMA-IR following 14 days of supplementation (ns; data represented as median± interquartile range). Statistical significance was set at $p<0.05$.

Suppl Figure 3.

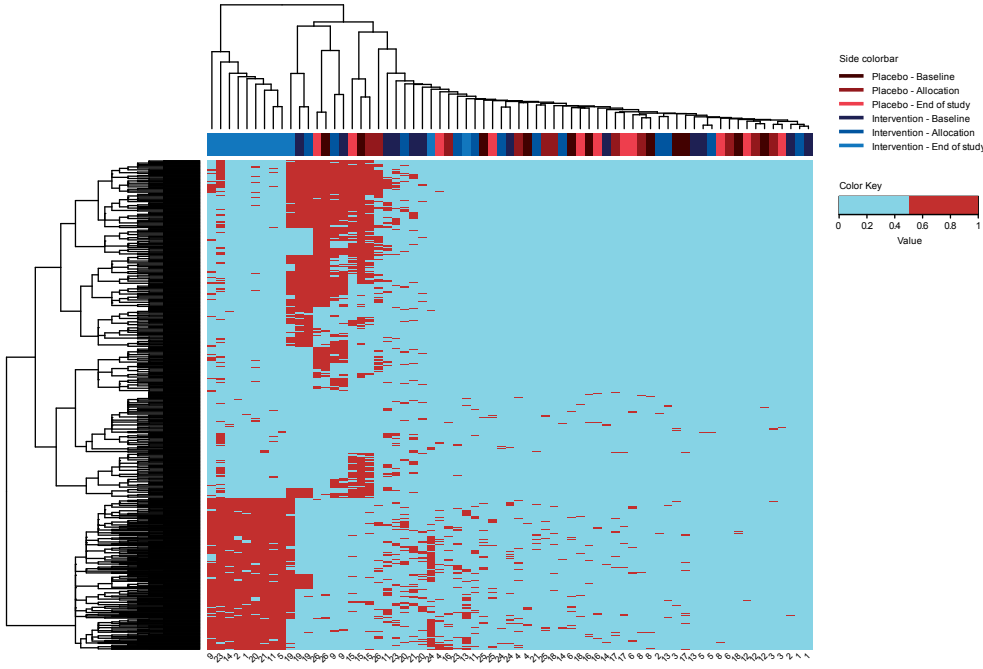

Filtered dichotomized clustered SNP profiles of different subjects at different time points. On the rows, different clusters of SNPs are visualized, and the columns with the side color bars represent the different subjects at different time points. The clustering of the subjects and time points was performed on a larger number of SNPs with the real values of the profile. Within the heatmap, blue represents the absence of a cluster of SNPs, and red represents their presence. On the side color bar, the different colors represent the group (e.g., placebo or intervention) and the time point (e.g., dark colors are time points before the intervention and bright colors represent post-intervention). Most of the subjects who received the intervention clustered together at the end of the study phase. Interestingly, subject 19 showed a combination of its own strain and our A. soehngenii L2-7 strain, with more emphasis on his own strain based on dendrogram clustering. Subjects 24 and 13 in the intervention group did not cluster together with the other intervention subjects at the end of the study phase based on the larger number of SNP clusters with real values, indicating poor engraftment.

SUPPLEMENTAL TABLES

Suppl Table 1. Baseline characteristics of the EDM2 study.

	Placebo (n = 12)	Intervention (n = 12)	p-value
Male sex (%)	100	100	
Age (y)	60.6 (5.7)	60.8 (6.2)	0.95
BMI (kg/m2)	27.2 (2.6)	27.7 (4.3)	0.73
Weight (kg)	86.41 (13.03)	91.35 (17.30)	0.44
Systolic blood pressure (mmHg)	133.50 (13.96)	141.00 (17.68)	0.26
Diastolic blood pressure	86.42 (5.11)	82.58 (8.45)	0.19
Fasting glucose (mmol/L)	8.47 (2.22)	7.83 (0.66)	0.35
Insulin (pmol/L)	45.00 (33.98)	45.75 (15.63)	0.95
HbA1c (%)	6.96 (1.01))	6.60 (0.49)	0.28
Total Cholesterol (mmol/L)	5.31 (0.65)	4.97 (0.85)	0.28
HDL (mmol/L)	1.32 (0.26)	1.30 (0.23)	0.86
LDL (mmol/L)	3.26 (0.59)	3.05 (0.63)	0.42
Triglycerides (mmol/L)	1.65 (1.06)	1.38 (0.54)	0.45
AST (U/L)	186.00 (379.80)	21.25 (3.44)	0.15
ALT (U/L)	29.50 (14.55)	23.50 (9.90)	0.25
AP (U/L)	71.17 (24.86)	66.33 (17.45)	0.59
yGT (U/L)	36.50 (29.86)	25.67 (20.03)	0.31
CRP (mg/mL)	1.98 (3.48)	1.10 (0.68)	0.396
Leucocytes (10^9/L)	5.97 (1.22)	5.86 (1.33)	0.84
Caloric intake (kcal/day)	1682.05 (351.67)	1727.95 (383.90)	0.78
Fat intake (g/day)	69.40 (21.98)	73.06 (21.22)	0.70
Carbohydrates intake (g/day)	153.46 (59.86)	150.22 (53.99)	0.90
Protein intake (g/day)	85.88 (39.95)	89.32 (21.55)	0.81
Fiber intake (g/day)	18.23 (5.03)	19.85 (6.75)	0.55

Data are expressed as mean ± standard deviation (SD) or %. BMI, body mass index; ALP, alkaline phosphatase; g-GT, gamma glutamyl transferase; ALT, alanine aminotransferase; AST, aspartate aminotransferase; HDLc, high-density lipoprotein cholesterol; LDL-C, low-density lipoprotein cholesterol; CRP, C-reactive protein.

Suppl Table 2. Plasma short-chain fatty acid AUC over 120 min (mean (SD)).

Baseline	Placebo (n=12)	Intervention (n=12)	**End of intervention**	Placebo (n=12)	Intervention (n=12)	**p-value**
SCFA_acetic_AUC	23494.82 (2462.42)	25057.38 (5631.50)	SCFA_acetic_AUC	23307.50 (4044.07)	25539.27 (3863.17)	0.754
SCFA_Butyric_AUC	1688.12 (107.43)	1855.53 (604.98)	SCFA_Butyric_AUC	1997.70 (313.63)	2089.82 (176.85)	0.716
SCFA_Proprionic_AUC	3181.20 (260.13)	3368.52 (895.78)	SCFA_Proprionic_AUC	3503.62 (577.02)	3625.95 (251.93)	0.846
SCFA_Isovaleric_AUC	225.28 (31.00)	251.88 (25.91)	SCFA_Isovaleric_AUC	204.83 (42.90)	228.43 (35.12)	0.819
SCFA_Lactic_AUC	216732.30 (94759.21)	185878.25 (78406.90)	SCFA_Lactic_AUC	201601.15 (91917.90)	176047.38 (39557.45)	0.854
SCFA_Succinic_AUC	2213.20 (997.30)	2241.75 (839.27)	SCFA_Succinic_AUC	2107.00 (594.24)	1844.55 (581.08)	0.466
SCFA_total_AUC	247534.92 (94962.18)	218653.30 (84026.25)	SCFA_total_AUC	232721.80 (92122.29)	209375.40 (39801.44)	0.859

P-value determined by the t-test for delta change.

Suppl Table 3. 24hr-fecal bile acids levels (mean (SD)). P-value determined by the t-test for delta change.

Baseline	Placebo (n=12)	Intervention(n=12)	End of Intervention	Placebo (n=12)	Intervention(n=12)	p-value
UDCA_AUC	5.70 (3.15)	4.90 (3.08)	UDCA_AUC	7.10 (4.53)	6.31 (3.27)	0.623
CA_AUC	20.51 (42.65)	5.42 (1.69)	CA_AUC	18.01 (22.33)	26.51 (57.92)	0.283
GUDCA_AUC	9.76 (6.35)	9.89 (5.40)	GUDCA_AUC	9.40 (4.81)	13.71 (8.63)	0.081
GCA_AUC	48.37 (31.74)	70.34 (61.63)	GCA_AUC	47.85 (38.29)	68.59 (45.07)	0.958
TUDCA_AUC	1.49 (0.57)	2.04 (1.03)	TUDCA_AUC	1.53 (0.58)	2.34 (1.15)	0.579
TCA_AUC	11.24 (7.83)	20.58 (18.01)	TCA_AUC	11.47 (9.06)	16.69 (9.20)	0.437
CDCA_AUC	35.15 (36.11)	16.34 (16.08)	CDCA_AUC	41.21 (45.79)	34.19 (34.82)	0.105
DCA_AUC	74.51 (36.37)	59.58 (32.74)	DCA_AUC	72.63 (37.67)	77.22 (48.58)	0.321
GCDCA_AUC	149.35 (81.93)	154.86 (95.86)	GCDCA_AUC	152.55 (105.88)	163.45 (84.77)	0.743
GDCA_AUC	94.27 (83.99)	131.75 (115.80)	GDCA_AUC	69.74 (47.02)	127.08 (116.28)	0.709
TCDCA_AUC	21.60 (15.28)	34.55 (23.74)	TCDCA_AUC	24.53 (21.39)	38.21 (27.71)	0.821
TDCA_AUC	18.65 (18.24)	29.70 (21.42)	TDCA_AUC	14.54 (8.91)	25.84 (12.82)	0.919
TLCA3S_AUC	14.36 (14.30)	19.94 (9.66)	TLCA3S_AUC	13.20 (9.08)	17.25 (7.41)	0.812
LCA_AUC	5.48 (1.32)	5.80 (2.97)	LCA_AUC	4.95 (1.23)	5.42 (2.63)	0.93
TLCA_AUC	2.59 (1.37)	4.09 (1.24)	TLCA_AUC	2.77 (1.10)	3.76 (1.22)	0.172
GLCA_AUC	9.59 (5.90)	12.64 (11.03)	GLCA_AUC	8.85 (4.80)	12.32 (10.18)	0.468
LCA3S_AUC	1.87 (1.02)	1.81 (1.02)	LCA3S_AUC	2.48 (1.38)	2.91 (1.52)	0.463
GLCA3S_AUC	55.72 (33.99)	67.88 (57.35)	GLCA3S_AUC	47.09 (22.93)	57.41 (38.57)	0.766
Total_AUC	580.43 (308.42)	651.72 (339.46)	Total_AUC	549.44 (269.00)	698.66 (299.71)	0.394
Prim_AUC	286.15 (182.76)	301.85 (177.51)	Prim_AUC	295.53 (215.63)	347.36 (170.35)	0.364
Secon_AUC	294.41 (173.49)	349.89 (195.83)	Secon_AUC	254.00 (91.01)	351.34 (187.95)	0.608

Suppl Table 4. Plasma bile acid AUC over 120 min (mean (SD)).

Baseline	Placebo (n=11)	Intervention (n=11)	**End of intervention**	Placebo (n=11)	Intervention (n=11)	**p-value**
UDCA	0.16 (0.28)	0.06 (0.11)	UDCA	0.08 (0.14)	0.09 (0.19)	0.148
CA	0.59 (1.19)	0.33 (0.84)	CA	0.15 (0.19)	0.23 (0.29)	0.404
GUDCA	0.01 (0.01)	0.01 (0.00)	GUDCA	0.01 (0.01)	0.01 (0.00)	0.685
GCA	0.07 (0.06)	0.03 (0.04)	GCA	0.10 (0.15)	0.05 (0.06)	0.877
TUDCA	0.00 (0.00)	0.00 (0.00)	TUDCA	0.00 (0.00)	0.00 (0.00)	0.493
TCA	0.02 (0.02)	0.03 (0.03)	TCA	0.03 (0.03)	0.04 (0.04)	0.513
CDCA	0.60 (0.89)	0.31 (0.43)	CDCA	0.24 (0.16)	0.27 (0.17)	0.258
DCA	10.23 (6.57)	7.47 (4.38)	DCA	11.03 (6.73)	7.25 (4.29)	0.445
GCDCA	0.09 (0.05)	0.05 (0.02)	GCDCA	0.10 (0.08)	0.06 (0.03)	0.939
GDCA	0.10 (0.07)	0.08 (0.05)	GDCA	0.09 (0.07)	0.08 (0.06)	0.639
TCDCA	0.03 (0.02)	0.03 (0.02)	TCDCA	0.04 (0.03)	0.04 (0.02)	0.429
TDCA	0.02 (0.02)	0.03 (0.02)	TDCA	0.03 (0.02)	0.03 (0.02)	0.915
LCA	4.27 (1.76)	3.50 (1.37)	LCA	5.51 (2.22)	3.27 (1.60)	**<0.001**
TLCA	0.01 (0.00)	0.01 (0.01)	TLCA	0.01 (0.01)	0.01 (0.01)	0.068
GLCA	0.01 (0.00)	0.02 (0.01)	GLCA	0.01 (0.00)	0.02 (0.01)	0.585
Total	16.21 (9.95)	11.96 (6.47)	Total	17.42 (9.25)	11.45 (5.95)	0.327
sum_ Coprostanol_ cholesterol	50.61 (21.08)	49.68 (22.54)	sum_ Coprostanol_ch olesterol	56.57 (19.89)	57.80 (22.51)	0.844

p-value determined by the t-test for delta change.

Part two

Development of microbiota-based therapeutics and noninvasive diagnostics in NAFLD

chapter 5

Gut microbiota and human NAFLD: disentangling microbial signatures from metabolic disorders

Judith Aron- Wisnewsky, Chloé Vigliotti, Julia J. Witjes, Phuong Le, Adriaan G. Holleboom, Joanne Verheij, Max Nieuwdorp, Karine Clément

Nature Reviews Gastroenterology & Hepatology,
volume 17, pages 279–297 (2020)

ABSTRACT

Gut microbiota dysbiosis has been repeatedly observed in obesity and type 2 diabetes mellitus (T2DM), two metabolic diseases strongly intertwined with nonalcoholic fatty liver disease (NAFLD). Animal studies have demonstrated a potential causal role of gut microbiota in NAFLD. Human studies have started to describe microbiota alterations in NAFLD and have found a few consistent microbiome signatures discriminating healthy individuals from NAFLD, nonalcoholic-steatohepatitis or cirrhosis. However, patients with NAFLD often present with obesity and/or insulin resistance and T2DM, and these metabolic confounding factors for dysbiosis have not always been taken into account. Patients with different NAFLD severity stages often present with heterogeneous lesions and variable demographic characteristics (including age, sex and ethnicity), which are known to affect the gut microbiome and have been overlooked in most studies. Finally, multiple gut microbiome sequencing tools and NAFLD diagnostic methods have been used across studies that could account for discrepant microbiome signatures. This Review provides a broad insight into microbiome signatures for human NAFLD and explores issues with disentangling these signatures from underlying metabolic disorders. More advanced metagenomics studies, as well as multi-omics studies using system biology approaches, are needed to improve microbiome biomarkers.

INTRODUCTION

The gut microbiota (that is the microbial community within the gastrointestal tract) has critical physiological roles in host digestion, immunity and metabolism[1,2]. Initially only studied by culture-based methods, the characterization of the gut microbiota[3] has deepened with the rapid development of high-throughput sequencing technology (shotgun sequencing or pyrosequencing). Constructed gut microbiota reference gene catalogues[4,5] have further enabled the determination of the composition of the gut microbiota and prediction of microbiome functions[6]. In addition to these technological advances, decreasing costs and reduced analytical turnaround due to bioinformatic pipeline development have enabled increasingly accessible and efficient microbiome studies. Thus, knowledge of microbiome characteristics in common diseases, especially metabolic diseases[7], has substantially increased in the past 15 years.

The need for microbiome characterization in metabolic diseases was initially stimulated by pioneering studies using germ-free mice and gut microbiota transfer, which reported the contribution of gut microbiota to weight gain and metabolic alterations[8,9]. Studies using conventional mice receiving lipopolysaccharide (LPS, a major component of the Gram-negative bacterial outer membrane) infusions also provided evidence of the role of gut microbiota in metabolic injuries and its influence on insulin resistance[10]. Since these initial studies, microbiome signatures linked to obesity[11–13] and type 2 diabetes mellitus (T2DM)[14,15] and associated complications were discovered, raising the concept of human gut microbiota dysbiosis (that is, alterations in microbiota composition and functional capacities with modification of microbiome signatures[16]) in metabolic diseases (reviewed elsewhere[17]). Currently, these findings are being pursued to develop microbiota-based therapeutics such as probiotics[18], prebiotics[19], synbiotics[20], and faecal microbiota transplantation (FMT)[21,22] to improve metabolic health and personalized patient care.

Nonalcoholic fatty liver disease (NAFLD), and the more advanced stage nonalcoholic steatohepatitis (NASH)[23], are common comorbidities of obesity and T2DM with an increasing burden for society[24]. NAFLD-related liver failure has become the second leading cause of liver transplantation in the Western world [25]. Liver biopsy is the diagnostic gold standard for NAFLD and NASH, yet it is an invasive, inconvenient and impractical tool in a public health setting[26], limiting the complete understanding of the complex pathophysiology of these diseases. Moreover, although mouse models of NAFLD and NASH are helpful, they are not optimal[27] and can limit the translation of results to clinical research[27]. As obesity, T2DM, and NAFLD–NASH are clinically and pathophysiologically linked, exploring the gut microbiome seems to be a relevant approach to gain a better understanding of NAFLD and NASH. Although

this level of characterization of NAFLD and NASH is markedly less than that for obesity and diabetes, there is a rapidly growing body of evidence exploring the contribution of the gut microbiome to NAFLD physiopathogenesis[28–30] using high-throughput sequencing in cohorts of individuals spanning the NAFLD–NASH disease spectrum. As there is a large overlap between NAFLD and metabolic disorders with respect to the disease spectrum and contributing factors, some metagenomic signatures of NAFLD might be shared with those already observed in obesity and T2DM. Thus, deciphering signatures specific to liver alterations would be most useful for future NAFLD diagnostic biomarkers. We herein review the gut microbial and gut microbially derived metabolite signatures associated with NAFLD development and progression focusing on their relationship with disease progression in humans. We specifically focus on which microbial signatures are specific to liver injury versus those common to other metabolic diseases and the putative methodological biases that could explain divergent results across the literature.

NAFLD AND RELATED LIVER FIBROSIS

NAFLD is defined as the pathological accumulation of lipid droplets in >5% of hepatocytes[23]. This disease can progress towards NASH, which is diagnosed by liver biopsy and the histological examination of the degree of steatosis, inflammation and hepatocyte ballooning[23,31]. NASH can also present with liver fibrosis[23,31,32], which is the main prognostic lesion for disease progression[33,34], eventually leading to cirrhosis[35] and/or hepatocellular carcinoma[36–38] and other liver-related complications, including ascites, hepatic encephalopathy and portal hypertension[39]. NAFLD is highly prevalent and has become the most common cause of chronic liver disease in the Western world, affecting up to 40% of the general population[40] and sometimes reaching 90%[41,42] in obese populations worldwide[43]. NAFLD is closely associated with overweight or obesity and metabolic disorders such as insulin resistance, hypertension and T2DM, and is even recognized as the hepatic component of metabolic syndrome[44,45] (**Box 1**). NAFLD and metabolic syndrome both increase the risk of cardiovascular diseases and T2DM[46]; and are therefore likely to have similar risk profiles[47].

For research purposes, several scores or algorithms based upon histological evaluation of liver biopsy samples have been developed to enable patient classifications in epidemiological studies. For example, the NALFD Activity Score (NAS) is a scoring system calculated from the semi-quantitative evaluation of steatosis, lobular inflammation and hepatocyte ballooning[48]. Although accurate in low (<3) or high (>5) values to respectively exclude or diagnose NASH, the NAS is often inaccurate within the intermediate values (scores 3–4)[31]. As a consequence,

Box 1. Definition of metabolic syndrome.

According to formal clinical guidelines[187], metabolic syndrome is defined as:
Android obesity with a waist circumference above the cut-off of 94cm and 80cm, respectively, for white men and women, plus any two of the following factors:

- Fasting plasma glucose ≥100mg/dl (5.55mmol/l) or with type 2 diabetes mellitus
- Systolic blood pressure level ≥130 mmHg or diastolic blood pressure level ≥85mmHg or patients taking any hypertension-lowering drugs
- Serum triglyceride levels ≥150mg/dl (1.69 mmol/l) or patients taking any kind of lipid-lowering treatment
- HDL cholesterol levels <40 mg/dl (1.04 mmol/l) in men or <50mg/dl (1.29 mmol/l) in women, or patients taking any kind of lipid-lowering treatment

European guidelines recommend the use of NAS only for disease severity evaluation once the diagnosis has been made[23]. A newer diagnostic algorithm, the Steatosis Activity and Fibrosis (SAF) score, which includes the semi-quantitative scoring of these factors, to enable the classification of patients as no NAFLD, NAFLD or NASH, has demonstrated improved performance compared with NAS, in particular within the intermediate values of the NAS (scores 3-4)[31]. Indeed, compared with NAS, the SAF score emphasizes the importance of activity, the main culprit of NASH, and therefore provides more accurate and comprehensive histological description. As such, it is now qualified as a true diagnostic score in the European guidelines[23]. Despite the utility of these scoring approaches, they rely on liver biopsy, which has drawbacks such as sampling error, inter-individual variations in pathologist reading and the risk of complications, of which the most worrisome is internal bleeding.

As performing liver biopsies[26] on all patients with NAFLD[49] is unfeasible for disease screening, diagnosis or examining progression in both routine care and research, noninvasive diagnostic methods using plasma samples[50], ultrasonography[51], MRI[52] or liver elastography (including both transient and magnetic resonance[53–55]) have been developed[56–58], and offer good diagnostic performance for liver fibrosis[53,54] (**Table 1**). These methods have been widely used for early disease detection (steatosis), disease severity assessment, identification of patients needing a liver biopsy for confirmatory diagnosis (patients with divergent results obtained upon two noninvasive tests[53,59,60]) and for assessment of disease progression (fibrosis). Despite their obvious benefit compared with liver biopsy, these noninvasive tools are also hampered by several limitations[58] (summarized in **Table 1)**. They are, in general, not sensitive enough to evaluate the complete spectrum of NAFLD histological lesions[45] and lack validity to be used for routine diagnosis (reviewed elsewhere[54,57,61]). However, transient elastography can be seen as an exception, however, as it was validated against liver biopsy with good area under the receiver operator characteristic (AUROC) values ranging from 0.70 to 0.89 for both steatosis and fibrosis in a large population composed of 450 patients with the complete spectrum of NAFLD fibrosis stages[62].

Table 1. Summary of usefulness of NAFLD diagnostic tools.

		Detection abilities				
Diagnostic tool	**Cost**	**Steatosis**	**NASH**	**Fibrosis**	**Cirrhosis**	**Key features**
Liver biopsy[56,57]	$$	Y	Y	Y	Y	Gold standard for diagnosis; poor patient tolerance as painful, inconvenient and potential for complications; possibility of false-negative results (liver injuries are not homogeneous, biopsy is only 1/50,000 of the liver mass). Scores or algorithms based on histology are available including the NAS score (score of 3 and 4 accurately diagnoses NAFLD or NASH) and SAF algorithm, which has improved diagnostic accuracy compared with NAS.
Serological markers[56a]						
AAR = AST/ ALT[57]	$	N	N	Y	Y	AUROC 0.83 for stage 3-4 ; this inexpensive tool has good negative predictive value, but positive predictive ability is limited; good accuracy.
FIB-4[57]	$	N	N	Y	N	AUROC 0.8 for stage 3-4) ; one of the best noninvasive tests in diagnosing advanced fibrosis in NAFLD; this tool is inexpensive; limitations for patients that have no advanced fibrosis.
NAFLD fibrosis score[57]	$	N	N	Y	N	AUROC 0.88 for stage 3-4; this inexpensive tool identifies advanced fibrosis well.
BARD score[×57]	$	N	N	Y	N	AUROC 0.81 for stage 3-4); good prediction for patients with no fibrosis (95–97%), but does not predict fibrosis well in patients with mild NAFLD (specifically in patients with obesity or T2DM), which limits its clinical use.
Procollagen III (PIINP)[57,58]	$	N	Y	Y	N	AUROC 0.77–0.82); could be a useful test to identify the highest risk patients before in depth-analysis, but it is less predictive than hyaluronic acid; needs further validation.
Cytoke-ratin-18[57]	$	N	Y	N	N	AUROC 0.83; needs to be validated.
Fibrotest[×57]	$	N	N	Y	N	AUROC 0.75–0.8 for stage 2–4; AUROC 0.81–0.92 for stage 3–4; not available in the UK.
Fibromax[188]	$	Y	N	Y	Y	High power for prediction with high predictive positive value (0.9); low negative predictive value (48.3%); difficulty to predict absence of steatosis.
Morphological phenotype						
Ultrasono-graphy[∞56,57]	$	Y	N	N	N	AUROC 0.97l good predictive tool for steatosis, but does not provide information regarding fibrosis.
Computed tomography[56]	$$	Y	N	N	N	high accuracy; cannot distinguish NASH from steatosis; exposure to radiation.

		Detection abilities				
Diagnostic tool	**Cost**	**Steatosis**	**NASH**	**Fibrosis**	**Cirrhosis**	**Key features**
Transient elastography[56]	**$**	Y	Y	Y	N	AUROC >0.8); less reliable those who are overweight or obese.
Acoustic radiation force impulse imaging[×56,57]	**$**	N	N	Y	N	AUROC 0.97l increasingly available on ultrasonography machines, but not available on every machine; still needs validation.
Real-time shear wave elastography[×]	**$**	N	N	Y	N	AUROC 0.85–0.88; results might be invalid in patients aged >52 years or with severe obesity or patients with T2DM; results might be different from liver biopsy; accurate if >30% of hepatocytes are steatotic.
Magnetic resonance imaging[56]	**$$**	Y	N	N	N	This accurate tool for steatosis diagnosis is less reliable for grading steatosis in patients with advanced fibrosis or cirrhosis;. It cannot be performed in patients with claustrophobia and the measurements are affected by hepatic iron deposition
Magnetic resonance spectroscopy[56]	**$$**	Y	N	N	N	Medium accuracy; results of this tool might be affected by respiration movements, claustrophobia and implanted devices;.it is not systematically available.
Magnetic resonance elastography[56]	**$$**	N	N	Y	N	AUROC >0.9; access to this tool is limited

$, low cost; $$, moderate cost; AAR , aspartate transaminase:alanine transaminase ratio; AUROC, area under the receiver operating characteristic; FIB-4, Fibrosis-4; N, no; NAFLD, non- alcoholic fatty liver disease; NAS, non-alcoholic fatty liver disease score; NASH, non- alcoholic steatohepatitis; PIINP, amino- terminal peptide of type III procollagen; SAF, Steatosis Activity and Fibrosis; T2DM, type 2 diabetes mellitus; Y, yes. [a]Mostly useful to diagnose one liver alteration (NAFLD or fibrosis) but not always accurate; some markers are expensive; several serological markers are available.

Despite these noninvasive tests, liver biopsy remains the gold standard for NAFLD and NASH diagnosis. Thus, new biology-based, inexpensive, easily accessible, highly sensitive and specific prognostic and diagnostic biomarkers are urgently needed. As the gut microbiota might have a pathophysiological role in NAFLD development, the use of noninvasive microbiota-related biomarkers from stool (microbiota signatures) and/or blood sampling (metabolic or microbiota-derived signatures) could be an interesting alternative to currently available noninvasive tests or could be considered as a complementary approach.

NAFLD AND GUT MICROBIOTA

Mouse studies and faecal transplant experiments have provided evidence of a causal role of gut microbiota in NAFLD development. First, cohousing experiments with mice prone to developing NASH due to genetic modifications in the inflammasome pathway and healthy wild-type mice demonstrate that microbiota sharing through coprophagia leads to wild-type mice developing liver steatosis and inflammation[63]. Additionally, direct FMT (from weight-matched obese mice with or without steatosis to germ-free recipients) replicates some NAFLD alterations[64]. These liver alterations include increased hepatic triglyceride content and augmented expression of hepatic genes involved in lipid uptake, lipogenesis, fatty acid catabolism and very low-density lipoprotein export[64]. These phenotypes were traced to gut microbiota composition differences between weight-matched mice with or without steatosis with steatotic mice displaying an increase in two bacterial species (Lachnospiraceae bacterium 609 and a relative of *Barnesiella intestinihominis*)[64]. Although mouse models might seem to be a solution to explore the microbiota and liver disease, mice experiments present many limitations to extrapolating information to humans. As reviewed at length[65], mouse models do not develop the complete spectrum of histological lesions observed in human NAFLD (that is, hepatocyte ballooning or cirrhosis), nor is the disease always associated with overweight and/or insulin resistance as in human NAFLD. Whereas some mouse models (choline-deficient mice) can ultimately develop the same final histological alterations as those observed in humans, the pathophysiology completely differs between mice and humans, since the former usually lose weight [65]. Additionally, the microbiota of mice and humans differs substantially[66]: in terms of composition (the vast majority of genera found in mice are absent in humans) and dominant genera as well as specific genus and species abundance. Finally, mice and humans display major digestive tract architecture differences, which also influences gut microbiota composition[66]. These limitations make the evaluation of the role of gut microbiota within NAFLD in mouse models a challenge. One solution to circumvent this hurdle is using FMT from diseased patients to germ-free mice in an attempt to reproduce the patients' hepatic phenotype. Indeed, FMT from humans with NASH to germ-free mice leads to the transmission of some NASH features including hepatic steatosis and inflammation, which are exacerbated during high-fat diet (HFD) feeding[67]. However, germ-free mice have an immature immune system[68] and immunity and/or inflammation balance is extremely important in metabolic disease development[10]. As conventional animals have a developed immune system and also allow engraftment of donor microbiota, use of conventional mouse models for FMT studies might be an alternative solution[68] for studying the role of the microbiota in rodent models. Notably, faecal transfer from obese women with hepatic steatosis to conventional mice fed a chow diet

induces increased hepatic triglyceride content within 14 days[69]. Despite some of these limitations, evidence from rodent studies collectively strengthen the idea that the gut microbiota contributes to NAFLD development.

Several hypotheses have provided mechanistic insights into the pathways of how the gut microbiota might contribute to NAFLD development and progression to NASH, reviewed in detail elsewhere[28,70]. In brief, they include increased intestinal permeability that leads to LPS release to the host, which can trigger tissue and systemic inflammation, and the action of microbially produced metabolites (including trimethylamine *N*-oxide (TMAO), choline or ethanol) and bile acid signaling, which can also affect immunity[28,70,71]. On the basis of these hypotheses, human studies have compared the gut microbiota composition between patients with NAFLD, NASH, NAFLD-cirrhosis, and healthy liver as controls to discover gut microbiota or microbiota-related metabolite signatures to be used as noninvasive diagnostic tools. We will hereafter focus on microbiota signatures observed in steatosis, NASH or NAFLD-cirrhosis in humans (mainly adults but also review some literature concerning paediatrics)[70,72]. Notably, gut dysbiosis occurs in obesity and T2DM[17]. We discuss signatures that are also seen during those metabolic diseases.

NAFLD GUT MICROBIOME SIGNATURES

Owing to heterogeneity in the literature, we have focused on concordant results across studies and describe bacterial signatures associated with the different stages of liver disease severity in humans. We summarize results according to taxonomic levels (bacterial phylum, family, genus and species) that are associated with different NAFLD progression stages (steatosis, NASH), NAFLD-fibrosis, and cirrhosis and show that some bacterial signatures overlap with those described in obesity or T2DM (**Figure 1 & 2**).

Simple steatosis to NASH signatures

Comparing patients with NAFLD to healthy individuals as controls[69,73], a consistent altered signature is observed at the level of phylum (increased Proteobacteria[69,74–76]), family (increased Enterobacteriaceae[74,77] and decreased Rikenellaceae[77,78] and Ruminoccaceae [73–75]), and genera (increased *Escherichia*[69,77], *Dorea*[75,78], *Peptoniphilus*[77,78] and decreased *Anaerosporobacter*[55,73], *Coprococcus*[69,73,77], *Eubacterium*[69,77], *Faecalibacterium*[55,77] and *Prevotella*[69,79]). Although these initial results suggest a measurable dichotomy in microbial signatures between individuals with hepatic steatosis and controls, large discrepancies are nevertheless found across studies with divergent results for phylum, family, genus and species[69,73–81], as described in detail in **Tables 2 and 3**.

Figure 1. Overlapping microbiota species and genera signatures in NAFLD, diabetes and obesity.

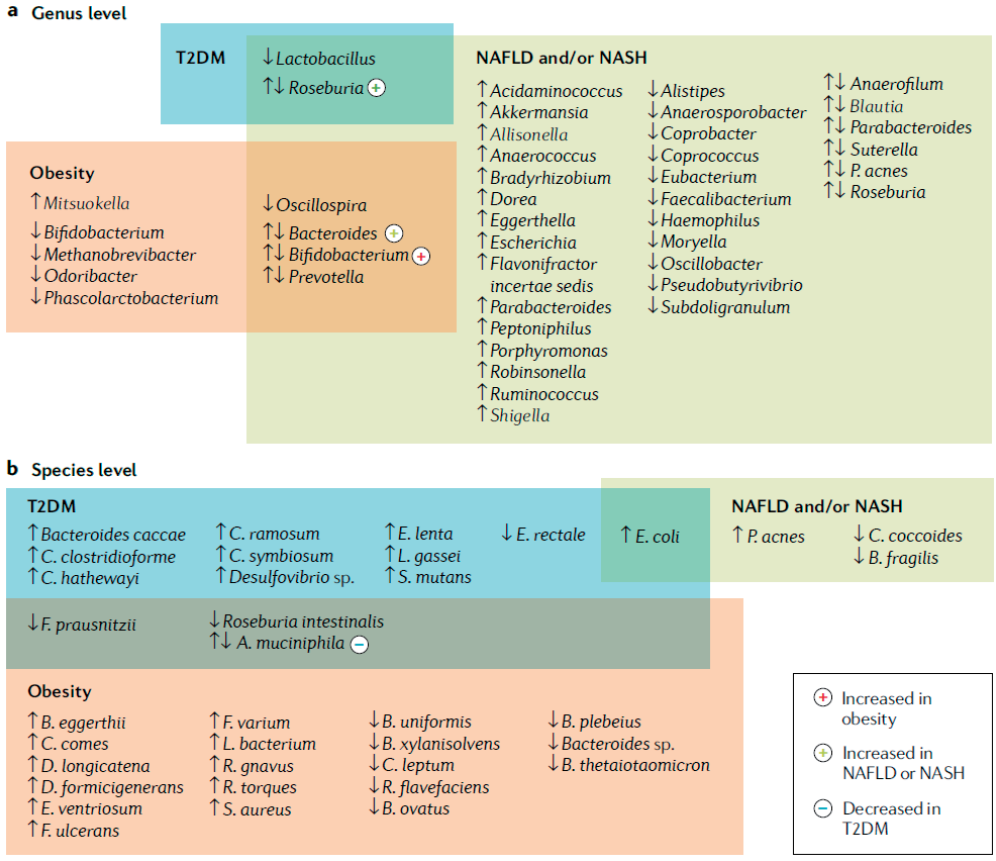

a | Specific genera signatures are observed during obesity , type 2 diabetes mellitus (T2DM) and non- alcoholic fatty liver disease (NAFLD, including non- alcoholic steatohepatitis (NASH)), and common genera signatures in these diseases are highlighted. **b** | Specific microbial species signatures are observed during obesity , T2DM and NAFLD, with common genera signatures in these diseases highlighted in the figure. For both panels, microorganisms with an up arrow are found to be more abundant in patients with these diseases than in healthy individuals as controls. Microorganisms noted with a down arrow are found to be less abundant in patients with these diseases than in healthy individuals. Microorganisms with both up and down black arrows have been reported with contradictory results showing them to be either more or less abundant in patients with these diseases depending on the study. Microorganisms with both up and down arrows are differentially abundant between diabetes, and/or obesity and/ or liver disease. If one disease is associated in all publications with a difference in abundance of a microorganism, a colour- coded + or – sign is added after the name to indicate the direction of change and in what disease (see key).

Similarly to NAFLD, when comparing patients with NASH with healthy individuals as controls, using either liver biopsy[42,69,74,76–81] or noninvasive biomarkers[73,75,78,81], some concordant microbial signatures are observed, which also overlap with NAFLD signatures: phylum (increased Proteobacteria[74–77]), family (increased Enterobacteriaceae[74,77] and decreased Ruminococcaceae[73–75,77,82] and Rikenellaceae[77,78]) and genera (increased *Dorea*[75,78] and decreased

Figure 2. Microbiota species and genera signatures in non-alcoholic steatohepatitis-related fibrosis, cirrhosis, diabetes and obesity.

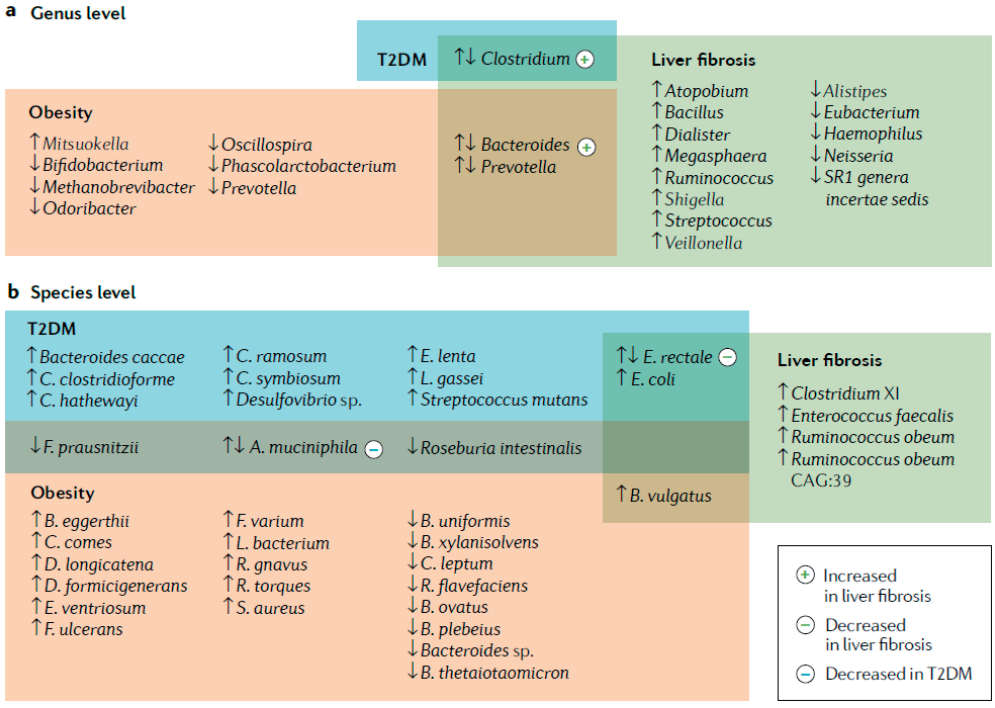

a | Specific genera signatures are observed during obesity , type 2 diabetes mellitus (T2DM) and liver fibrosis or cirrhosis; common genera signatures in two or three of these diseases are highlighted. **b** | Specific microbial species signatures observed during obesity , T2DM and liver fibrosis or cirrhosis; common genera signatures in two or three of these diseases are highlighted. For both panels, microorganisms with an up arrow are found to be more abundant in patients with these diseases than in healthy individuals as controls. Microorganisms with a down arrow are found to be less abundant in patients with these diseases than in healthy individuals as controls. Microorganisms with both up and down black arrows have been reported with contradictory results showing them to be either more or less abundant in patients with these diseases depending on the study. Microorganisms with both up and down arrows are differentially abundant between diabetes, and/or obesity and/or liver disease. If one disease is associated in all publications with a difference in abundance of a microorganism, a colour- coded + or – sign is added after the name to indicate the direction of change and in what disease (see key).

Faecalibacterium[77,82,83], *Coprococcus*[73,77,82], *Anaerosporobacter*[73,83]). However, similar to results observed for steatosis, the abundance of some bacteria[69,72–81,83] , display opposite trends across the literature as shown in **Tables 2 and 3.**

From NAFLD-fibrosis to NASH-cirrhosis

Few studies have focused specifically on microbiome signatures in NAFLD- fibrosis and even fewer have examined microbial composition as a function of fibrosis progression. Nevertheless, concordant signatures are observed and detailed in **Tables 2 and 3**. When compared with patients with advanced fibrosis, individuals with less severe liver alterations or healthy individuals as controls display a

Table 2. Taxonomic gut microbiota signatures of NAFLD and NAFLD fibrosis progression.

Characteristic	Microorganism	Status in NAFLD	Status in fibrosis
Taxonomic level			
Phylum	Verrucomicrobia	Increased[69]	Not assessed
Phylum	Fusobacteria	Increased[74]	Increased[87]
Phylum	Proteobacteria	Increased[69,74–77]	Discordant results[76,87,88]
Phylum	Firmicutes	Discordant results[69,73,75–78,83]	Discordant results[76,88]
Phylum	Bacteroidetes	Discordant results[73,74,78–80]	Discordant results[79,87]
Phylum	Actinobacteria	Discordant results[69,78,80]	Not assessed
Class	Gammaproteobacteria	Increased[81]	Increased74
Class	Bacteroidia	Increased[73]	Not assessed
Class	Epsilonproteobacteria	Increased[81]	Not assessed
Class	Clostridia	Decreased[73]	Not assessed
Family	Streptococcaceae	Increased[74]	Increased[87]
Family	Enterobacteriaceae	Increased[74,77]	Increased[74,77,89]
Family	Pasteurellaceae	Increased[75]	Increased[87]
Family	Veillonellaceae	Increased[75]	Increased[87]
Family	Erysipelotrichaceae	Increased[74]	Not assessed
Family	Kiloniellaceae	Increased[75]	Not assessed
Family	Succinivibrionaceae	Increased[83]	Not assessed
Family	Peptostreptococcaceae	Decreased[73]	Not assessed
Family	Ruminococcaceae	Decreased[73–75,77]	Decreased[89]
Family	Bifidobacteriaceae	Decreased[77]	Not assessed
Family	Rikenellaceae	Decreased[77,78]	Not assessed
Family	Lachnospiraceae	Discordant results[69,74,75,77]	Decreased[87,89]
Family	Prevotellaceae	Discordant results[74,77]	Decreased[79]
Family	Lactobacillaceae	Discordant results[73,75]	Not assessed
Family	Porphyromonadaceae	Discordant results[73,75]	Not assessed
Family	Fusobacteriaeae	Not assessed	Increased[87]
Family	Enterococcaeae	Not assessed	Increased[89]
Family	Staphylococcaceae	Not assessed	Increased[89]
Family	Bacteroidaceae	Not assessed	Decreased[87]
Family	Clostridiales XIV	Not assessed	Decreased[89]
Genus	*Shigella*	Increased[74]	Increased[74]
Genus	*Bacteroides*	Increased[79]	Increased[79]
Genus	*Ruminococcus*	Increased[79]	Increased[79]
Genus	*Acidaminococcus*	Increased[69]	Not assessed
Genus	*Akkermansia*	Increased[69]	Not assessed
Genus	*Eggerthella*	Increased[69]	Not assessed
Genus	*Flavonifractor*	Increased[69]	Not assessed
Genus	*Escherichia*	Increased[69,77]	Not assessed
Genus	*Lachnospiraceae_ incertae_sedis*	Increased[74]	Not assessed
Genus	*Robinsoniella*	Increased[75]	Not assessed
Genus	*Dorea*	Increased[75,78]	Not assessed
Genus	*Porphyromonas*	Increased[77]	Not assessed
Genus	*Anaerococcus*	Increased[78]	Not assessed

Characteristic	Microorganism	Status in NAFLD	Status in fibrosis
Genus	*Bradyrhizobium*	Increased[78]	Not assessed
Genus	*Peptoniphilus*	Increased[73,78]	Not assessed
Genus	*Allisonella*	Increased[83]	Not assessed
Genus	*Parabacteroides*	Increased[83]	Not assessed
Genus	*Haemophilus*	Decreased[69]	Decreased75
Genus	*Eubacterium*	Decreased[69,77]	Decreased76
Genus	*Coprobacter*	Decreased[69]	Not assessed
Genus	*Holdemania*	Decreased[69]	Not assessed
Genus	*Subdoligranulum*	Decreased[69]	Not assessed
Genus	*Coprococcus*	Decreased[69,73,77]	Not assessed
Genus	*Moryella*	Decreased[73]	Not assessed
Genus	*Pseudobutyrivibrio*	Decreased[73]	Not assessed
Genus	*Anaerosporobacter*	Decreased60,70	Not assessed
Genus	*Alistipes*	Decreased[77]	Not assessed
Genus	*Faecalibacterium*	Decreased[77,87]	Not assessed
Genus	*Oscillospira*	Decreased[78]	Not assessed
Genus	*Prevotella*	Discordant results[74,77,79,81]	Discordant results[77,87,89]
Genus	*Oscillibacter*	Discordant results[69,75]	Not assessed
Genus	*Bifidobacterium*	Discordant results[69,77]	Not assessed
Genus	*Blautia*	Discordant results[74,77–79]	Not assessed
Genus	*Lactobacillus*	Discordant results[73,75]	Not assessed
Genus	*Roseburia*	Discordant results[73,75,77]	Not assessed
Genus	*Bacilli*	Not assessed	Increased[87]
Genus	*Megasphaera*	Not assessed	Increased[87]
Genus	*Atopobium*	Not assessed	Increased[88]
Genus	*Dialister*	Not assessed	Increased[88]
Genus	*Clostridium*	Not assessed	Increased[90]
Genus	*Streptococcus*	Not assessed	Increased[90]
Genus	*Neisseria*	Not assessed	Decreased[87]
Genus	*SR1 genera incertae sedis*	Not assessed	Decreased[88]
Genus	*Alistipes*	Not assessed	Decreased[90]
Species	*Clostridium coccoides*	Increased[77]	Not assessed
Species	*Propionibacterium acnes*	Increased[79]	Not assessed
Species	*Bacteroides fragilis*	Decreased[79]	Increased[76]
Species	*Escherichia coli*	Increased[77]	Increased[76]
Species	*Eubacterium rectale*	Higher in moderate NAFLD[76]	Decrease[76]
Species	*Ruminococcus obeum CAG:39*	Not assessed	Increased[76]
General characteristics			
Gram stain	*Gram positive*	Decreased[73,76]	Decreased[76]
Gram stain	*Gram negative*	Increased[73,76]	Increased[76]

This table indicates the microorganisms found in different studies as microbial signature(s) of NAFLD or NAFLD-fibrosis at different taxonomic levels. The table displays whether the particular microorganism changes its abundance with the disease progression from normal state to nonalcoholic fatty liver disease (NAFLD, and nonalcoholic steatohepatitis) and also from normal to high fibrosis. Cases where previous studies found discordant results are also indicated.

decreased abundance of Gram-negative bacteria, decreased Fusobacteria phylum, increased Enterobacteriaceae family, (*Bacteroides, Ruminococcus, and Shigella* genera[74,79] and by contrast increased[76] Gram-positive bacteria, Firmicutes phylum, Prevotellaceae family and *Prevotella* genus.

One caution in interpreting the findings is that these studies used various experimental designs, each comparing different stages of fibrosis severity (that is, comparison of patients with mild to moderate fibrosis (F0-F2) versus advanced fibrosis (F3-F4), or cirrhosis)[76], whereas others compared patients with no to little fibrosis (F0–F1) to patients with moderate to advanced fibrosis (F≥2)[74]. Finally, another study compared patients with moderate to advanced fibrosis (F≥2) with patients having mild fibrosis (F0–F1) with or without NASH[79]. These differences in experimental design could explain discrepancies found in the proposed microbial signatures (**Tables 2 and 3).** For example, *Bacteroides vulgatus* and *Escherichia coli* are the most abundant species in advanced fibrosis (F3-F4)[76]. *B. vulgatus* abundance is also increased from mild–moderate fibrosis to advanced fibrosis[76]. Interestingly, the *B. vulgatus* signature is a common observation associated with metabolic alterations as it also increases with increasing BMI, specifically in severe obesity, which is characterized by decreased microbial gene richness[84]. Furthermore, *B. vulgatus* abundance increases with increasing haemoglobin A1c (Hba1c) levels[84]. *B. vulgatus* is also associated with insulin resistance[85] and is decreased in obese women receiving prebiotics (inulin-type fructans), a treatment that improves insulin sensitivity[19]. Likewise, *E. coli* has been shown to be increased in patients with T2DM[86]. These examples illustrate overlapping observations between bacterial signatures linked to NAFLD-fibrosis or NAFLD and those linked with metabolic disorders as obesity and diabetes (**Figures 1 and 2**). Although models have been proposed to use the microbiome as a reservoir for diagnostic signatures of NAFLD-fibrosis[76], further confirmation in independent cohorts and across geographical regions is necessary to assess their clinical relevance.

In patients with cirrhosis (some of whom had 'pure' NASH-related cirrhosis, whereas others were of different aetiology such as viral hepatitis, as detailed later), metagenomic signatures are relatively consistent across studies[76,87–90], confirming the importance of oral microbes invading the intestine in this disease. Taxa that are part of the oral cavity bacterial ecosystem, including *Prevotella*[88,90], *Veillonella*[73,90] and *Streptococcus*[87,90,91], seem to discriminate between patients with cirrhosis and healthy individuals. Likewise, whereas some signatures appear consistent when comparing patients with cirrhosis to healthy individuals as controls (decreased abundance of Lachnospiraceae[87,89], *Veillonella*[4,88], *Prevotella*[4,88] and increased abundance of Enterobacteriaceae[74,87,89,92]), others display contradictory trends across studies[76,87,88]. In general, microbial signatures of cirrhosis are related to a drastic shift

in taxa composition leading to an increase of pathogenic taxa and a decrease in taxa proposed to be metabolically beneficial[89] (**Tables 2 and 3**). A functional consequence of this taxa shift might be increased endotoxaemia. Indeed, it was demonstrated in mice that during HFD-induced NAFLD, there was a concomitant increase in LPS levels and changes in gut microbiota composition[93,94]. Furthermore, exacerbation of NAFLD into NASH was also associated with increased LPS levels[94]., and bacterial production of antibacterial peptides has been proposed to help maintain intestinal barrier integrity[89]. Thus, the combined effects of increased endotoxaemia, reduced butyrate production and reduced bile acid production (discussed further later) could worsen cirrhosis progression[89]. Another feature also associated with other common diseases is the reduction of levels of *Faecalibacterium prausnitzii*[95] in cirrhosis[90,91]. Indeed, *F. prausnitzii*, known to have anti-inflammatory properties and to be abundant in healthy conditions[11,12], is reduced in abundance in a number of diseases, including intestinal disorders (inflammatory bowel disease[96] or irritable bowel syndrome[97]), obesity[11,12] and diabetes[15,98].

However, the evaluation of gut microbiota contribution in liver disease progression (from steatosis to NASH, and NASH-cirrhosis) is limited and bacterial markers are frequently identified in one study, yet not confirmed in independent cohorts. As the origin of liver disease is heterogeneous by nature, most studies in cirrhosis have included patients with different aetiologies including hepatitis B[87,90], biliary disease-related cirhosis[88,90], alcohol-related cirrhosis[87,90], NASH or a combination of different diseases. Patients were also included at different stages of disease severity with compensated cirrhosis or decompensated cirrhosis[89,90]. These differences could collectively explain why associated metagenomic signatures of liver disease progression are not frequently replicated. Nevertheless, a study exploring well-characterized patients with non-NAFLD, NAFLD without advanced fibrosis or NAFLD-cirrhosis provides a potentially promising diagnostic signature, which includes 27 bacterial features and 3 demographic characteristics (BMI, age and gender). This signature is able to robustly identify NAFLD-cirrhosis and was further confirmed in an independent cohort with an AUROC of 0.92[91], which remained accurate after adjustment for T2DM. Although promising, this signature will need to be further confirmed in cohorts including various ethnicities and individuals from different geographical regions. Furthermore, to apply these microbial signatures in clinical practice, validated assays will have to be developed to enable easy and reproducible diagnosis.

Although the literature provides initial information regarding gut bacterial groups as promising signatures of different stages of liver disease progression, whether the microbiota is a causal factor, which interacts with the complex pathophysiological processes driving disease from mild fibrosis to severe fibrosis[74,76,79] and eventually cirrhosis still needs to be demonstrated.

Table 3. Study cohorts of gut microbiome in NAFLD research.

Reference	Sequencing method	T2DM Status	BMI status	NAFLD diagnostic method	Average age (years)	Sample size	Country
Hoyles et al.[69](2018)	Shotgun	No	Obese	Liver biopsy	43	63	Italy
Shen et al.[74] (2017)	16S rRNA	Yes	Overweight	Liver biopsy	48	47	China
Raman et al.[75] (2013)	Pyrosequencing	Yes	Obese	Ultrasonography, blood sample	50	66	Canada
Loomba et al.[76] (2017)	Shotgun	Yes	Obese	Liver biopsy	48	86	USA (white & hispanic)
Zhu et al.[77] (2013)	Pyrosequencing	ND	Obese	Liver biopsy	13	67	USA
Del Chierico et al.[78] (2016)	16S rRNA	No	Obese	liver biopsy, ultrasonography	11,5	115	Italy
Wang et al.[73] (2016)	Pyrosequencing	No	Lean	Ultrasonography	43	126	China
Boursier et al.[79] (2016)	16S rRNA	Yes	Obese	Liver biopsy	66	64	France
Mouzaki et al.[80](2013)	qRT-PCR	Yes	Obese	Liver biopsy	43,7	50	Canada
Michail et al.[81](2015)	16S rRNA & shotgun	No	Obese	47 Ultrasonography, 3 liver biopsy	13,4	50	USA
Wong et al.[83] (2013)	Pyrosequencing	Yes	Overweight	Liver biopsy	49	61	China
Chen et al.[87] (2011)	16S rRNA pyrosequencing	ND	NA	NA	47,5	66	China
Chen et al.[88](2016)	16S rRNA pyrosequencing	ND	NA	Ultrasonography or biopsy	50,5	48	China
Bajaj et al.[89] (2014)	Pyrosequencing	ND	Obese	Blood sample	63	244	USA
Qin et al.[90] (2014)	Shotgun	Yes	Obese	Liver biopsy	45	237	China[a]

NA, not applicable; NAFLD, nonalcoholic fatty liver disease; ND, not determined; qRT-PCR, quantitative RT-PCR; rRNA, ribosomal RNA; T2DM, type 2 diabetes mellitus. [a]Only the Chinese cohorts (discovery and validation) used for liver cirrhosis study is considered here.

GUT-DERIVED METABOLITES AND PATHWAYS

Studies have evaluated the metabolomic signatures associated with NAFLD or NAFLD-fibrosis and have been extensively reviewed elsewhere[99]. Among these signatures are molecules produced by bacterial communities (**Figure 3**) such as LPS[100], short-chain fatty acids such as butyrate, propionate and acetate (the balance of which mediates beneficial or detrimental effects on the liver)[71] and products derived from bile acid metabolism acting on FXR within the liver or the intestine[101–103] . Changes in these metabolites are suspected to have a role in the pathophysiology of liver injuries[99]. Herein, we choose to focus on novel studies exploring substrates of gut microbiota metabolism or circulating gut microbiota-derived metabolites. Importantly, all of these metabolites have also been demonstrated to be involved in obesity and metabolic alterations, including T2DM. For example, evidence from mice during obesity, LPS is increased and promotes the activation of insulin resistance pathways in tissues[93]. Although, SCFAs have beneficial effects on metabolic health, they are also involved in energy harvesting and, therefore, potentially contribute to increased weight gain[104]. Levels of SCFAs have been found to be increased in faecal samples from individuals who are obese as compared with healthy individuals[105]. Overall, understanding their specific role in NAFLD physiopathology is complex.

Choline, betaine and circulating methylamines

Mice fed a choline-deficient diet[106] are recognized as a representative model of NAFLD[107,108] and reducing dietary choline leads to both increased liver fat and gut bacteria modifications[108]. Choline is an essential nutrient and a component of phosphatidylcholine, which is a precursor of acetylcholine (a neurotransmitter) found in food. Choline is a substrate that can be oxidized to betaine. HFD-induced NAFLD mice fed a diet with standard levels of choline exhibit a decrease in systemic phosphatidylcholine with increasing severity of NAFLD[109]. This observation was translated to humans in which patients with an increasing severity of NAFLD display a decreased ratio of betaine to choline[110]. As demonstrated in mice and humans[111,112], dietary choline is metabolized by the gut microbiota into trimethylamine (TMA), which is further metabolized in the liver by the enzyme FMO3 and results in the production of TMAO[17]. Increased circulating TMAO is proposed as a biomarker of cardiovascular events and kidney dysfunction[17,112,113], and the increase of circulating levels TMAO positively correlates with the increase of *Deferribacteres* and *Tenericutes* in the gut in mice[113]. In humans, elevated levels of TMAO were seen in individuals with prevotella enterotype, and several OTUs were significantly increased in patients with higher concentrations of TMAO[113]. Mouse studies demonstrate that increased NAFLD severity is associated with increased urinary levels of both TMA and TMAO[109]. These

Figure 3. Gut-derived metabolites and factors that could drive progression of NAFLD.

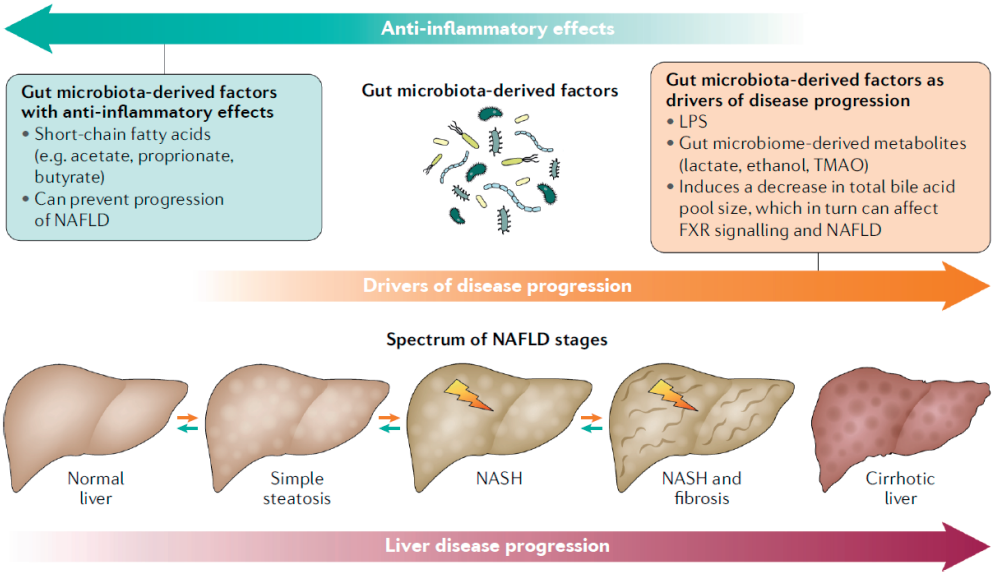

This figure illustrates how gut-derived metabolites are involved in the development and progression of non-alcoholic fatty liver disease (NAFLD), fibrosis and cirrhosis. Lactate, ethanol, trimethyl N- oxide (TMAO) can propel NAFLD progression (TMAO induces a decrease in the total bile acid pool size, which in turn can affect FXR signaling and NAFLD), as can lipopolysaccharide (LPS). On the other hand, short- chain fatty acids can have anti-inflammatory properties, which could prevent progression of NAFLD. NASH, non- alcoholic steatohepatitis.

observations can be seen as paradoxical as increased consumption of choline and phosphatidylcholine correlates with increased production of TMA and TMAO[111,112] . The pathophysiological explanation by which TMA and/or TMAO has a role in NAFLD development therefore needs further examination[114], but the proposed mechanisms include a reduction of host choline bioavailability due to a switch in microbiota metabolism to methylamine production as well as urinary excretion[114]. In human studies, TMAO is independently associated with increasing severity of NAFLD when comparing patients with NAFLD to healthy individuals[110].

TMAO and bile acids. Another major function of the gut microbiota is the deconjugation of primary bile acids into secondary bile acids. Overall, primary bile acids are involved in cholesterol metabolism, facilitate the absorption of dietary fat and fat-soluble molecules, and have a role in regulatory pathways[115]. Primary and secondary bile acids have endocrine functions and modulate numerous host metabolic pathways through different receptors[116]. Secondary bile acids are notably preferential ligands of the G protein-coupled bile acid receptor-1 (TGR5) a key actor of energy, glucose and lipid metabolism in the host[103]. The gut microbiota not only regulates secondary bile acid metabolism but also inhibits the liver synthesis of lipids

by alleviating FXR inhibition[117]. Differences in bile acid pool size and composition has been associated with metabolic diseases[118]. Thus, gut dysbiosis could influence bile acid pool, composition and homeostasis. Evidence from mice and humans suggests that bile acid bioconversion by the gut microbiota (deconjugation, dehydrogenation and dehydroxylation) is related to NAFLD and NASH progression[119], as previously reviewed[101]. Interestingly, a decrease in bile acids could be associated with NAFLD through TMAO production since TMAO induces a decrease in the total bile acid pool by inhibiting two key enzymes involved in bile acid metabolism: CYP7A1 and CYP27A1[110,113,120]. In agreement with this hypothesis, patients with advanced cirrhosis exhibit a decreased conversion of bile acids with concomitant modifications of their microbiota composition, including greater abundance of Enterobacteriaceae but lower abundance of Lachonospiraceae, Ruminococcaceae and *Blautia*[121,122].

3-(4-hydroxyphenyl) lactate. A study published in 2019 has shown that 3-(4-hydroxyphenyl) lactate is associated with increased severity of NAFLD-fibrosis both in a test and validation cohort, both comprising 156 individuals (one from the Twin and family study, the other from an independent prospective study)[123] (**Figure 3**). Interestingly, 3-(4-hydroxyphenyl) lactate is a gut microbiota-derived product of aromatic amino acid metabolism. These results are in line with another study performed in patients with different stages of steatosis, which showed decreased microbial gene richness and an alteration in aromatic amino acid and branched-chain amino acid metabolism in steatosis[69]. This metabolite could be used as non-invasive biomarker of NAFLD, but needs further confirmation.

Ethanol. Production of ethanol by the gut microbiota could also play a part in NAFLD physiopathology. In children, the gut microbiota of individuals with NAFLD exhibits increased abundance of ethanol-producing bacteria as compared with those who were obese or healthy children as controls[77]. In the absence of ethanol consumption, adults with NASH display increased breath ethanol concentrations[124], which could be attributed to those with NAFLD producing more gut microbiota-derived ethanol as compared with healthy controls. These results suggest that gut microbiota ethanol production might serve as a liver toxin contributing to the development of NAFLD and its progression towards NASH[125]. A study performed in mice and further validated in humans, indeed displayed that some bacteria (namely *Klebsiella pneumoniae*) were able to produce ethanol from glucose, in the absence of any alcohol consumption[126].

Short-chain fatty acids. Short-chain fatty acids (SCFAs), a group comprised of butyrate, acetate and propionate, are locally produced in the colon through microbial fermentation of normally non-digestible complex carbohydrates (dietary fiber)[99,127].

Their role and mechanism of action in NAFLD development has been extensively reviewed[127,128]. Microbially produced SCFAs are absorbed primarily through diffusion or co-transport in the colon whereas their intestinal signalling effects are mediated by activation of G-protein-coupled receptors (GPR41 and GPR43)[129]. SCFAs have been proposed as an important substrate to increase liver triglyceride levels and promote energy storage and weight gain[130] as SCFAs are involved in fatty acid synthesis and gluconeogenesis[131]. Human studies comparing NAFLD, NASH and healthy individuals as controls have observed an increased faecal concentration of SCFAs in patients with NAFLD and/or NASH [132] concomitantly with an increase in abundance of bacterial groups involved in their production. Furthermore, this increased faecal SCFA and microbial signature observed during NASH[132] are associated with reduced numbers of resting regulatory T-cells (CD4+CD45RA+CD25+) and higher T helper 17 cell to resting regulatory T cell ratio in peripheral blood, which are systemic immunological features previously observed in NASH[133] .

Nevertheless, SCFA action is quite complex, as they also can provide metabolic benefits. GRP43 activation by SCFAs reduces pro-inflammatory production and immune cell (T cells)[134] infiltration, whereas *GRP43*$^{-/-}$ mice or germ-free mice with lower levels of SCFA display increased inflammation both at the level of circulating immune cells as well as in the colon , a feature usually seen in NASH[135]. However, inflammation during NASH development was not assessed in these models and the effect of SCFAs on liver inflammation needs further investigation. Furthermore, although dietary fibres have been shown to be beneficial for metabolic health[10], some interventional studies using soluble fibres have, in contrast, led to increased liver disease in mice with genetically-induced or high fat diet-induced microbial dysbiosis[136,137]. Thus, although soluble fibres can induce positive metabolic effects, such as those observed on glucose metabolism, the effects of soluble fibre supplementation in NASH mouse models need further exploration before interventional studies in patients. Moreover, owing to interindividual variability in the gut microbiota, dietary supplementation of fibre might need to be personalized because of possible different effects in different individuals, which could also be further complicated by the variety of soluble fibre available. Most importantly, each SCFA exerts specific and somehow different metabolic effects. Thus, assessing their balance both at the fecal and systemic level in patients with NASH and after a dietary intervention would probably decipher more precisely their overall role in NAFLD development, exacerbation or improvement. Finally, it was reported that SCFAs could have a beneficial role in NAFLD through epigenetic modulation via histone deacetylase inhibition. Indeed, it was shown in rats that histone deacetylase inhibition decreased liver gene expression involved in NAFLD mostly lipogenic genes, such as acetyl-CoA carboxylase (Acc), fatty acid synthase (Fasn), and sterol

regulatory element binding protein 1c (Srebp1c)[138] . This finding provides important mechanistic insights, reviewed elsewhere[127,128].

New bacterial metabolites and derived factors will be identified as contributors to liver disease in the future. Thus, it will be essential to determine how these factors, together with changes in LPS, biliary acid metabolism and SCFAs, contribute to NAFLD development and progression. Investigations are now needed to determine the relevance of these molecules as biomarkers and/or predictors for diagnosis of NAFLD and NASH and its progression.

ISSUES IN NAFLD METAGENOMICS STUDIES

The number of clinical studies investigating gut microbiota signatures associated with NAFLD and/or NASH or fibrosis is increasing rapidly. However, careful interpretation is needed when reviewing the literature owing to the heterogeneous cohorts used across studies with differences in sex, ethnicity, liver disease severity stages, BMI, presence of T2DM, patient populations (paediatric or adult), corpulence, and other associated metabolic diseases. The gut microbiota sequencing technologies used vary among studies, and other critical factors influencing the gut microbiota, such as dietary consumption or drug intake are scarcely measured or under-reported.

Population variability in demographic characteristics. Although there is some consistency in the literature for microbiome signatures, there is a noticeable lack of reproduced findings or confirmation in independent cohorts. This heterogeneity might originate from different methodological approaches and from major inter-individual variability among recruited patients regarding particular demographic characteristics. While one study examined only women[69], most studies examined adults[69,73–76,79,80,83] and children[77,78,81] of both sexes. Yet some studies have controlled for sex[69,73–75,80,110] and most have also controlled for age[69,73–77,79,90,110]. Nevertheless, it is important to note that there are histological specificities for adolescent and adult NAFLD[139,140], as recalled in recent pediatric clinical guidelines[141]. For example, in paediatric NASH, the ballooning degeneration, classic zone 3 fibrosis, and parenchymal inflammation often seen in adult NASH are less common in children NASH[140,141]. Furthermore, several histological types are found in children: type 1 resembling the adult form, type 2 NASH is mainly characterized as NASH yet with no or minimal ballooning degeneration, and finally a third type with with overlapping features[139]. Studies were also performed in different geographical regions (North America, Canada[75,80] and USA[76,81]), Asia (China[73,83]), Europe (France[79], Italy and Spain[69]) probably with various ethnic backgrounds and cultural and food habits. Importantly,

ethnicity seems to strongly influence microbial composition even in individuals living in the same geographical area. For example, gut microbial diversity differed substantially in different ethnic groups all living in the Netherlands and ethnicity accounted for a major part of these differences [142]. Thus, whereas there are different liver disease risks across ethnicities[143], it might translate into differential microbiome-related signatures[142]. Notably, some studies controlled for dietary habits[73,74,77,80,81,110], which could relate, in part, to cultural differences.

Population variability in corpulence. Obesity, and particularly abdominal obesity, is a well-known risk factor for NAFLD[144], making these diseases strongly inter-dependent. In published reports, although some studies included lean individuals[73,74,83], others examined individuals who were overweight[74,83] or obese (mixing different classes of obesity)[69,75,76,78–81,87]. Several studies even further stratify by the severity of obesity classes (class I: BMI 30–35kg/m² [75,77,79]), one study in particular focused on severe or morbid obesity (BMI> 35 or BMI >40 [69]), and it has been demonstrated that gut microbiota dysbiosis is exacerbated with increasing obesity severity[11,84].

Metagenomic studies clearly demonstrate relationships between corpulence and gut microbiome changes. Microbial gene richness, for example, strongly decreases with increasing BMI[11,12,84]. Furthermore, although individuals with obesity generally share common bacterial signatures and modified functional properties, some signatures differ across the obesity spectrum[11], with peculiar signatures only found in populations with extreme BMIs (above 40kg/m²)[84]. On the basis of these findings, microbiome-related signatures in studies comparing patients with NASH with different degrees of obesity and lean or overweight patients with NAFLD as controls[80] or patients with different classes of obesity and NASH and healthy lean individual as controls[74] might be overestimated and mostly related to the degree of obesity[145]. The link between closely associated metabolic disorders, such as obesity and NAFLD is likely to be more complex than compositional shifts in bacterial composition alone. Thus, it remains difficult to conclude whether these signatures are solely related to liver alterations, BMI or both. In one study, Shen *et al.*[74] did not find any statistically significant shift in gut microbiota, when comparing patients with NAFLD stratified by BMI. Patient groups were, however, of small size (*n*=47) and the study had limited power to definitively conclude the absence of NAFLD–NASH specific microbial signatures according to corpulence. By contrast, Wang *et al.* focused their analytical comparisons between NAFLD and healthy individuals with normal and comparable BMI[73]. They demonstrate a microbiome signature of patients with NAFLD independently of corpulence differences. Finally, to limit bias owing to differences in corpulence, studies exploring NAFLD microbiome signature have adjusted their statistical analysis on BMI (for example, according to the studies, the

preformed partial Spearman's rank-based correlation (pSRC) coefficients adjusted on BMI, or linear regression adjusted for BMI, multivariate models, analysis of covariance (ANCOVA) or finally logistic regression analysis) [69,73,74,76,79,80,82,89,110].

Despite the described interactions between corpulence and liver disorders (from steatosis to cirrhosis considering individuals who are lean or obese), Enterobacteriaceae is consistently increased in both individuals with NAFLD and those who are obese in numerous studies[74,77,87,89,146,147]. Decreased microbial gene richness is found both in individuals with obesity[11,12] and patients with NAFLD in some studies[74,91], but also in lean individuals with NAFLD[73]. More importantly, BMI is a proxy of obesity and future studies should extend phenotyping to other measures related to body fat amount and distribution (for example, abdominal versus gynoid distribution) to examine the interplay between fat distribution, different stages of liver alterations and microbiome alterations. Indeed, microbial gene richness is negatively correlated with increasing visceral fat deposition[84].

Population variability in metabolic diseases and related treatments. Another major confounder lies in obesity-associated metabolic comorbidities, which are also involved in NAFLD physiopathology. Diabetes is a major risk factor involved in NAFLD development [148] and its presence strongly exacerbates NAFLD to overt NASH, including forms associated with mild and advanced fibrosis[149]. Metabolic syndrome[15] or T2DM[14,15,85] *per se* are known to be associated with microbial signatures. Thus, it might be tricky to disentangle microbial signatures from NAFLD and linked metabolic disorders, such as diabetes. Four NAFLD studies[74–76,79] included patients with T2DM and two other studies evaluated the signature and predicted function of the gut microbiome of patients with T2DM without known NAFLD[14,15]. Despite the difference in geographical demography (European women with diabetes[15] and Chinese adults with diabetes[14,15]), these studies showed one consensus finding: a statistically significant reduction in abundance of butyrate-producing bacteria in T2DM. However, they did not examine whether patients with T2DM had NAFLD; extrapolating from epidemiological evidence, most probably, those patients had both NAFLD and T2DM. Clostridia[73,150] and *Lactobaccillus*[15,75] are two common species signatures found in both T2DM and NAFLD (increased abundance of *Lactobacillus* and decreased abundances of Clostridia in both patients with NAFLD and those with T2DM compared with healthy groups). At a predicted functional level, both patients with T2DM and those with NAFLD display consistent decrease in butyrate-producing bacteria[15,73,77]. *E. coli* is consistently enriched in studies exploring either solely cirrhosis or solely diabetes [14,90]. By contrast, the *Roseburia* genus shows opposite trends across studies[15,73,75,77] (**Table 3**). However, one study included only six individuals with T2DM among their NAFLD cohort[75], potentially explaining these discrepant results

since *Roseburia* is also known to be decreased in T2DM[15]. Importantly, some studies looking for a NAFLD microbial signature actually controlled their analysis for the presence of T2DM[69,73,76,79,90] to limit this bias. For example, microorganisms signature remained associated with NAFLD after proper adjustments for T2DM but results were not always replicated in all studies (for example, *Propionibacterium acnes*[69], *Bacteroides fragilis*[69], *Anaerosporobacter*[73], Enterobacteriaceae[79]). In studies including patients without T2DM, only one controlled for insulin resistance[82].

Medication use is another critical feature influencing microbiome signature variability between individuals[151,152]. Studies exploring microbiome signatures of NAFLD[74–76,79,80] include patients with T2DM whereas others exclude them[73,77,78,81,83], but most do not clearly state the list of current medications that study participants are taking. Only three studies evaluating microbial signature during NAFLD have controlled for medication use[69,73,76]. Metformin is the first line of pharmaceutical therapy prescribed in T2DM and is commonly used in NAFLD since 50–75% of NAFLD patients have T2DM according to population and ethnicities[153,154].The effect of metformin on the gut microbiome is well-documented[86,155,156]. Metformin increases the abundance of *Akkermansia muciniphila*[155,156], a bacteria associated with improved insulin sensitivity in mice and humans[18,157,158]. Furthermore, treating mice on a HFD with metformin recapitulates the improvement in insulin sensitivity and switches the microbiota composition towards that of mice on chow diet[156]. Patients with T2DM taking metformin display a specific microbiome signature with an increase in *Escherichia* species[86], which could explain, in part, the increased *E. coli* found in patients with NAFLD-fibrosis[69,76,77] . Owing to increased risk of cardiovascular events, statins are frequently prescribed to patients with T2DM and NAFLD–NASH and could strongly influence the gut microbiome[159,160]. A study in mice observed a reduction in microbial diversity upon statin treatment, a modification in bile acid pools and a reduction of SCFA producing bacteria which was also confirmed in humans[160]. Nevertheless, those findings need further confirmation in larger-scaled studies. Proton pump inhibitors, which are frequently given to patients with cirrhosis, have been shown to switch microbiome composition towards an increased abundance of oral bacteria in the gut microbiota [161], thus the 'oral microbiome' signature observed in cirrhosis could well be related to drug intake rather than disease. It remains critical in microbiome studies examining patients with NAFLD or NASH to collect information on diabetes history and drug intake. Although some studies have controlled for medication, no study has yet controlled for each of the above potential biases when looking for a microbial signature of NAFLD.

Variability in liver injury diagnostic methods. Another source of variability in the reviewed studies is the different grades and stages and heterogeneity of liver

disease alterations (steatosis, NASH and fibrosis)[75,79,81]. Even if the use of the SAF score seems to improve inter-observer variability, the inter-individual pathologist variation when examining biopsy samples is acknowledged in NAFLD diagnosis[162,163]. As liver lesions are closely intertwined, deciphering the specific microbial signatures of each histological lesion is challenging. Studies have focused on different stages of disease progression. One study focused on the steatosis state[69], three on NASH[77,81,83], and seven investigated the NAFLD spectrum (from steatosis to NASH)[73–76,78–80]. Two reports focused on different fibrosis stage[74,79] and three on cirrhosis[87,89,90], whereas one study investigated a larger disease spectrum of fibrosis to cirrhosis[76]. However, in the latter study, patients with fibrosis probably displayed concomitant lesions of NASH and/or steatosis. As most studies do not focus on the same stages of disease progression, it is rather challenging to underline concordant microbial signatures.

The diagnostic method used to classify NAFLD lesions is also an important factor to consider when examining these studies. Liver biopsy, the most reliable diagnostic method and currently considered as the gold standard, was used in nine studies[69,74,76,77,79,80,83,88,90]. However, others used less reliable and noninvasive tools such as ultrasonography, MRI or blood tests[73,75,78,81] (such as liver enzymes (alanine aminotransferase, aspartate aminotransferase and γ-glutamyl transferase)[73,75,78,81], and also other metabolism-related biomarkers (levels of fasting serum glucose[73,78], insulin[78], triglyceride[78] or complete lipid profile[73]), or liver-related biomarkers (albumin and platelet count [73]) (**Table 1**). These noninvasive tools are designed to specifically characterize one histological aspect, it might well be that these patients displayed heterogeneous lesions (steatosis and some degree of fibrosis) that were not investigated. Furthermore, the degree of lesions severity is variably expressed. For example, some studies considered simple steatosis[78], whereas other took into account the steatosis score and discriminated steatosis severity from S0 to S3[69]. These aspects are critical and could partly explain disparities found in clinical studies exploring microbiome signatures of NAFLD and liver disease progression. In addition to placing a priority on using liver biopsy when possible, diagnostic tools and the interpretation of their results used to assess liver alterations should be taken into consideration when comparing across the literature.

Bias due to circadian rhythm. Another overlooked factor in the literature examining gut microbiota and NAFLD is the contribution of circadian rhythm. Circadian rhythm is a well-known and pivotal regulator of liver metabolic pathways, which are altered in NAFLD development[164]. For example, jetlag (seen as a perturbation of the circadian clock) is associated with the worsening of metabolic alterations (that is, the hallmarks of NAFLD), which show further perturbations during obesity[165]. Animal studies and experimental models have shown that feeding time also influences the

circadian rhythm and, subsequently, host physiology[166]. Some human population cohorts confirmed those findings[167]. Studies performed in different mouse models (genetic invalidation of clock genes, antibiotic treated or conventional mice with or without modification of the light–dark phases) have shown that the gut microbiota displays rhythmic oscillations in the colon during the day in terms of proliferation, composition, functions and metabolite production[168–170] and depend upon function of the host circadian clock. These oscillations (that is, existence of time-of-day-specific profiles of microbiota functionality) were demonstrated to be controlled by host feeding intake. Interestingly, modifying feeding times results in a shift of cycling bacteria. Moreover, timed feeding can restore the loss of fluctuations in circadian clock deficient mice[169]. Perturbations of the circadian rhythm are also associated with metabolic impairment and microbiota dysbiosis, both in experimental models as well as in humans[169]. On the other hand, the gut microbiota and its circadian oscillations also influence the rhythmic expression of host intestinal and liver genes that are not known to be involved in the circadian clock[168]. Additionally, these gene expression patterns are modified in the absence of gut microbiota as genes from several metabolic pathways lose their oscillatory patterns, whereas genes from other metabolic pathways gain rhythmicity with the lack of microbiota in animal models[168]. As such, germ-free mice submitted to light–dark cycle display impaired circadian hepatic gene expression[168], demonstrating the role of gut microbiota in the circadian clock effects. Thus, gut microbiota changes could influence the rhythmicity of several host metabolic pathways contributing to NAFLD physiopathology. This aspect could be due to microbiota functions rather than composition as gut microbiota-produced metabolites from the diet can also modulate liver clock gene expression, observed when treating hepatic organoids with different SCFA[170]. Furthermore, in clock gene knockout models, modulating feeding time can rescue abrogated host gene expression oscillation[170]. These observations highlight the combined contribution of both circadian clock and diet acting on gut microbiota and host physiology. Whether these results obtained in mice models are relevant in human needs further investigation. This aspect also raises the question if the methodology of studies examining gut microbiota signatures in NAFLD need to consider patients' circadian clock phenotype and food intake rhythm, which could help explain some discrepancies in gut microbial signatures observed across studies.

Sequencing methods. Another important point to be considered when comparing different results across the literature is the methods used to sequence and analyze the gut microbiota. Furthermore, sampling (for example, home faeces auto-collection use different devices that have not all been evaluated, one complete bowel movement stool or a sample of that material, mucosal or luminal microbiota in studies

including surgery sampling, faeces versus caecal or other parts of the intestine in mouse experiments) itself as well as the specific steps of analysis, including steps before sequencing (that is, sample concentration, lysis, purification and extraction), also need to be harmonized to enable comparisons between studies, as reviewed eslewhere[171]. Studies used a variety of methods, including quantitative PCR[80], 16S ribosomal RNA (rRNA) sequencing [74,78,79], or shotgun sequencing[69,76,90]. It has been previously shown that Sanger, Roche 454, or Illumina-based 16S rRNA or shotgun sequencing can lead to different results[172]. The results from 16S rRNA sequencing are less granular and accurate than those from whole shotgun sequencing, because the 16S approach sequences a single region of the bacterial genome whereas shotgun sequences the complete genome[173]. Species prediction is not optimal using 16S rRNA sequencing[171], and the results derived from pyrosequencing frequently lack numerous species because of the choice of tagged-primers[174]. Shotgun sequencing produces extended information regarding read sequences, since it can sequence and amplify the complete genome. Shotgun sequencing, therefore, produces more information as it also includes unknown metagenomic species, which potentially lead to increased discovery potential. Metagenomic sequencing enables the prediction of functional potential based on gene and species annotations.

In addition to the sequencing technology, the bioinformatic pipelines used to analyze sequencing data also contributes to the variability of results. Taxonomic analyses in 16S rRNA sequencing is easier owing to established standard pipelines such as QIIME[175] and Mothur[176] and functional profiling in 16S rRNA is predominantly done with PICRUST[177]. However, until now, few studies precisely describe the microbial species that could be used as indicators of liver disease status[76,90] and even fewer provide clues for the discovery of new species. Although microbiota catalogues are currently quite exhaustive, the variability of sequencing method and sequencing depth might influence findings. The use of whole metagenome sequencing can provide this information, but requires pipeline harmonization and dedicated bioinformatics expertise[178].

The lack of power in statistical analysis is another issue regarding the reliability of microbial biomarkers that can be used with confidence. Uncertainty about the absence or presence of certain aspects of NAFLD and unbalanced population distributions might affect statistical results. Obtaining a validated healthy and liver-biopsied group is difficult owing to obvious ethical reasons. Indeed, in other fields such as oncology, ethical concerns have already been raised about research biopsies and their potential risk to harm participants as well as the adequacy of voluntary informed consent [179,180].Thus, this aspect leads to a lack of statistical power and phenotypic uncertainty because of limitations in non-invasive testing. In addition to finding microbial abundance differences between groups, *P* values are often used

and interpreted as whether the abundance difference is statistically significant or not. However, *P* values alone do not provide reliable results. Some studies perform only *P* value tests without False Discovery Rate (FDR) correction[77,79,80,83,87,89]. By contrast, nine studies used FDR or Bonferroni corrections[69,73–76,78,81,88,90]. For example, in Mexican children with obesity, *B. plebeius* is negatively correlated with BMI percentile, but this finding is no longer statistically significant after FDR correction[181]. FDR should be mandatory when exploring metagenomics signatures. Importantly though, Falony *et al.* estimated that a sample size of approximately 1,700 individuals would be needed to adequately assess the relationship between obesity, NAFLD and microbiota composition in a cohort study when correcting for age, gender, ethnicity and other variables[151], which questions the feasibility of actually achieving such a trial.

Multi-omics approaches. As a complement to gut metagenomics, additional 'omics' data and systems biology approaches are a good method to further confirm microbial signature for a specific disease. By using both metagenomics and metabolomics[182] or lipidomics[183,184] , the gut microbiome compositional and functional signatures can be characterized and further linked with concentrations or production of gut-derived metabolites in blood, urine or faeces. An additional approach could also be to combine metagenomics to metatranscriptomics data, bringing some clarity to the gut microbiota genes specifically activated and providing further functional insights. Such approaches have already been used in other metabolic diseases (such as T2DM or obesity[84,185]) and are emerging in the field of NAFLD[69]. The use of approaches combing multi-omics techniques, coupled with computational science, will probably enable better insights regarding microbiota contribution in the pathophysiological pathways involved in these metabolic diseases and help stratify patients based on their multi-omics profiles. However, it does not preclude researchers from designing correct clinical trials in particular choosing carefully the best control groups.

CONCLUSIONS

Clinical studies have revealed gut microbiome signatures in NAFLD, NAFLD-fibrosis and cirrhosis, which could serve as future noninvasive diagnostic biomarkers for liver disease diagnosis or evolution prognosis. Nevertheless, the relevance of identified signatures needs to be further examined in longitudinal studies where physicians can prospectively examine the deterioration of liver status. This strategy was conducted for gut microbiota-derived factors in Crohn's disease[186] and in the cardiovascular field[111]. However, discrepancies are nevertheless observed across

Box 2. Proposal for new study investigations.

Study population
Inclusions of study groups should have similar ethnic origin, should include several groups of individuals (that is, obese with non- alcoholic fatty liver disease (NAFLD), obese with type 2 diabetes mellitus (T2DM) and NAFLD, with individuals with T2DM all treated at least with metformin). The diagnosis of NAFLD or non- alcoholic steatohepatitis should rely on liver biopsy.

Metagenomic data
Future studies should choose shotgun metagenomics sequencing data rather than 16S ribosomal RNA. This approach could enable the prediction of taxonomic composition as well as of functional composition. With this kind of data, metagenomic species, genes and gut microbial Kegg modules associated with NAFLD could be systematically predicted in each dataset.

Statistical analysis
Adjustments for diabetes, obesity, sex and age should be processed if there are variations on these parameters in the dataset (for example, analysis of covariance, logistic regression, P value trends by contrasts, linear regression adjusted). This approach would enable determination of whether the observed signatures originate from NAFLD per se or are due to underlying metabolic diseases. Sex disparity is also seen (with more prevalent obesity in women and more prevalent NAFLD in men); thus, results should be adjusted for sex and, eventually, ethnicity if patients from different ethnic groups have been included in the studies. More globally, considering patient clinical data in gut microbiome analyses should be good systematic practice.

Additionally, treatments (for example, for T2DM or with lipid- lowering drugs such as statins) should be considered. Indeed, treatment influences both clinical data (that is, normalizing systemic metabolic parameters) and the gut microbiome profiles. Moreover, although it represents an additional constraint, food intake should be monitored in these studies because of the major effect of diet on the gut microbiota.

Although most studies try to find disease- specific species or genes to be used as biomarker signatures, studying the whole microbial ecosystem using co- occurrence and co- abundance networks might also be interesting. The structure of the community might represent the signature of the disease. This approach could also enhance knowledge of disease pathophysiology and lead to further therapeutic development.

studies in NAFLD, which might originate from their large heterogeneity in terms of microbiome sequencing method, bioinformatic pipelines, liver diagnostic method and disease severity spectrum, as well as clinical and demographic characteristics. Obesity and T2DM are associated with strong microbiota dysbiosis and identified liver disease microbiome signatures are often biased by the additional presence of obesity and/or diabetes status, which are not always accounted for. There is, therefore, an urgent need for more investigations with strong study designs (**Box 2**). Studies should account for confounding metabolic disorders, such as T2DM and obesity, population background, medication and dietary intake. An option could also be to additionally examine identified-signatures in well-selected and clinically harmonized cohorts of patients with either T2DM or obesity. However, considering some potential confounding factors, such as circadian rhythm, might prove to be a complicated task for both researchers and patients. Future studies should also consider investigating gut microbiome signatures in a two-step manner; that is discovery and validation cohorts using varied and documented ethnic backgrounds

and include patients with a biopsy-proven NAFLD and/or NASH diagnosis. Where possible, repeated exploration with a second longitudinal study incorporating liver biopsy should also be considered to confirm clinical evolution. Overall, whether an optimal study design is feasible remains an open question and, in any case, should be considered in the context of large-scale research consortia. Moreover, the understandable reluctance from physicians and patients, as well as ethical committees, to repeat liver biopsy is also a limitation. Finally, advanced methods in predicting microbiome signature (such as deep learning combined with multi-omics approach) are needed in this field. Exploring the whole microbial ecosystem in which the interaction of microorganisms could be as important as the abundance of single or multiple family, genus or species is a priority. Similarly, the importance of microbiome-altering factors, such as phages or viruses and fungi, is worth examining. Combining microbiome signatures with systemic microbial-derived metabolites could help in the future to diagnose patients with liver alterations in routine care. The potential establishment of reliable biomarkers will determine how future NAFLD–NASH treatments modulate these signatures to develop biomarkers enabling follow-up for therapeutic response.

REFERENCES

1. Fouhy, F., Ross, R. P., Fitzgerald, G. F., Stanton, C. & Cotter, P. D. Composition of the early intestinal microbiota: knowledge, knowledge gaps and the use of high-throughput sequencing to address these gaps. *Gut Microbes* **3**, 203–220 (2012).
2. Prakash, S., Tomaro-Duchesneau, C., Saha, S. & Cantor, A. The gut microbiota and human health with an emphasis on the use of microencapsulated bacterial cells. *J. Biomed. Biotechnol.* **2011**, 981214 (2011).
3. Fraher, M. H., O'Toole, P. W. & Quigley, E. M. M. Techniques used to characterize the gut microbiota: a guide for the clinician. *Nat Rev Gastroenterol Hepatol* **9**, 312–322 (2012).
4. Qin, J. *et al.* A human gut microbial gene catalogue established by metagenomic sequencing. *Nature* **464**, 59–65 (2010).
5. Li, J. *et al.* An integrated catalog of reference genes in the human gut microbiome. *Nat. Biotechnol.* **32**, 834–841 (2014).
6. Karlsson, F., Tremaroli, V., Nielsen, J. & Bäckhed, F. Assessing the human gut microbiota in metabolic diseases. *Diabetes* **62**, 3341–3349 (2013).
7. Lynch, S. V. & Pedersen, O. The Human Intestinal Microbiome in Health and Disease. *N. Engl. J. Med.* **375**, 2369–2379 (2016).
8. Bäckhed, F. *et al.* The gut microbiota as an environmental factor that regulates fat storage. *Proc. Natl. Acad. Sci. U.S.A.* **101**, 15718–15723 (2004).
9. Ridaura, V. K. *et al.* Gut microbiota from twins discordant for obesity modulate metabolism in mice. *Science* **341**, 1241214 (2013).
10. Cani, P. D. *et al.* Changes in gut microbiota control metabolic endotoxemia-induced inflammation in high-fat diet-induced obesity and diabetes in mice. *Diabetes* **57**, 1470–1481 (2008).
11. Le Chatelier, E. *et al.* Richness of human gut microbiome correlates with metabolic markers. *Nature* **500**, 541 (2013).
12. Cotillard, A. *et al.* Dietary intervention impact on gut microbial gene richness. *Nature* **500**, 585–588 (2013).
13. Moreno-Indias, I., Cardona, F., Tinahones, F. J. & Queipo-Ortuño, M. I. Impact of the gut microbiota on the development of obesity and type 2 diabetes mellitus. *Frontiers in Microbiology* **5**, 190 (2014).
14. Qin, J. *et al.* A metagenome-wide association study of gut microbiota in type 2 diabetes. *Nature* **490**, 55–60 (2012).
15. Karlsson, F. H. *et al.* Gut metagenome in European women with normal, impaired and diabetic glucose control. *Nature* **498**, 99–103 (2013).
16. Tilg, H., Zmora, N., Adolph, T. E. & Elinav, E. The intestinal microbiota fuelling metabolic inflammation. *Nat. Rev. Immunol.* (2019) doi:10.1038/s41577-019-0198-4.
17. Aron-Wisnewsky, J. & Clément, K. The gut microbiome, diet, and links to cardiometabolic and chronic disorders. *Nat Rev Nephrol* (2015) doi:10.1038/nrneph.2015.191.
18. Plovier, H. *et al.* A purified membrane protein from Akkermansia muciniphila or the pasteurized bacterium improves metabolism in obese and diabetic mice. *Nat. Med.* **23**, 107–113 (2017).
19. Dewulf, E. M. *et al.* Insight into the prebiotic concept: lessons from an exploratory, double blind intervention study with inulin-type fructans in obese women. *Gut* **62**, 1112–1121 (2013).
20. Davis, C. D. The Gut Microbiome and Its Role in Obesity. *Nutrition today* **51**, 167—174 (2016).
21. Vrieze, A. *et al.* Transfer of intestinal microbiota from lean donors increases insulin sensitivity in individuals with metabolic syndrome. *Gastroenterology* **143**, 913-916.e7 (2012).
22. Kootte, R. S. *et al.* Improvement of Insulin Sensitivity after Lean Donor Feces in Metabolic Syndrome Is Driven by Baseline Intestinal Microbiota Composition. *Cell Metab.* **26**, 611-619.e6 (2017).

23. European Association for the Study of the Liver (EASL), European Association for the Study of Diabetes (EASD) & European Association for the Study of Obesity (EASO). EASL-EASD-EASO Clinical Practice Guidelines for the management of non-alcoholic fatty liver disease. *Diabetologia* **59**, 1121–1140 (2016).
24. Estes, C., Razavi, H., Loomba, R., Younossi, Z. & Sanyal, A. J. Modeling the epidemic of nonalcoholic fatty liver disease demonstrates an exponential increase in burden of disease. *Hepatology* **67**, 123–133 (2018).
25. Noureddin, M. *et al.* NASH Leading Cause of Liver Transplant in Women: Updated Analysis of Indications For Liver Transplant and Ethnic and Gender Variances. *Am. J. Gastroenterol.* **113**, 1649–1659 (2018).
26. Castera, L. Diagnosis of non-alcoholic fatty liver disease/non-alcoholic steatohepatitis: Non-invasive tests are enough. *Liver Int.* **38 Suppl 1**, 67–70 (2018).
27. Van Herck, M. A., Vonghia, L. & Francque, S. M. Animal Models of Nonalcoholic Fatty Liver Disease-A Starter's Guide. *Nutrients* **9**, (2017).
28. Aron-Wisnewsky, J., Gaborit, B., Dutour, A. & Clement, K. Gut microbiota and non-alcoholic fatty liver disease: new insights. *Clin. Microbiol. Infect.* **19**, 338–348 (2013).
29. Wieland, A., Frank, D. N., Harnke, B. & Bambha, K. Systematic review: microbial dysbiosis and nonalcoholic fatty liver disease. *Alimentary Pharmacology & Therapeutics* **42**, 1051–1063 (2015).
30. Roychowdhury, S., Selvakumar, P. C. & Cresci, G. A. The Role of the Gut Microbiome in Nonalcoholic Fatty Liver Disease. *Medical Sciences* **6**, 47 (2018).
31. Bedossa, P. *et al.* Histopathological algorithm and scoring system for evaluation of liver lesions in morbidly obese patients. *Hepatology* **56**, 1751–1759 (2012).
32. Brunt, E. M. *et al.* Nonalcoholic fatty liver disease (NAFLD) activity score and the histopathologic diagnosis in NAFLD: distinct clinicopathologic meanings. *Hepatology* **53**, 810–820 (2011).
33. Hagström, H. *et al.* SAF score and mortality in NAFLD after up to 41 years of follow-up. *Scandinavian Journal of Gastroenterology* **52**, 87–91 (2017).
34. Pais, R. *et al.* A systematic review of follow-up biopsies reveals disease progression in patients with non-alcoholic fatty liver. *J. Hepatol.* **59**, 550–556 (2013).
35. Liver cirrhosis. - PubMed - NCBI. https://www.ncbi.nlm.nih.gov/pubmed/18328931.
36. Fingas, C. D., Best, J., Sowa, J.-P. & Canbay, A. Epidemiology of nonalcoholic steatohepatitis and hepatocellular carcinoma. *Clinical Liver Disease* **8**, 119–122 (2016).
37. Ratziu, V., Bellentani, S., Cortez-Pinto, H., Day, C. & Marchesini, G. A position statement on NAFLD/NASH based on the EASL 2009 special conference. *J. Hepatol.* **53**, 372–384 (2010).
38. Karlas, T., Wiegand, J. & Berg, T. Gastrointestinal complications of obesity: non-alcoholic fatty liver disease (NAFLD) and its sequelae. *Best Pract. Res. Clin. Endocrinol. Metab.* **27**, 195–208 (2013).
39. Nusrat, S., Khan, M. S., Fazili, J. & Madhoun, M. F. Cirrhosis and its complications: evidence based treatment. *World J. Gastroenterol.* **20**, 5442–5460 (2014).
40. Lu, Z.-Y., Shao, Z., Li, Y.-L., Wulasihan, M. & Chen, X.-H. Prevalence of and risk factors for non-alcoholic fatty liver disease in a Chinese population: An 8-year follow-up study. *World Journal of Gastroenterology* **22**, 3663–3669 (2016).
41. Fazel, Y., Koenig, A. B., Sayiner, M., Goodman, Z. D. & Younossi, Z. M. Epidemiology and natural history of non-alcoholic fatty liver disease. *Metabolism* **65**, 1017–1025 (2016).
42. Wong, V. W.-S. *et al.* Beneficial effects of lifestyle intervention in non-obese patients with non-alcoholic fatty liver disease. *Journal of Hepatology* (2018) doi:10.1016/j.jhep.2018.08.011.
43. Ching-Yeung Yu, B., Kwok, D. & Wong, V. W.-S. Magnitude of Nonalcoholic Fatty Liver Disease: Eastern Perspective. *J Clin Exp Hepatol* **9**, 491–496 (2019).
44. Yki-Järvinen, H. Non-alcoholic fatty liver disease as a cause and a consequence of metabolic syndrome. *Lancet Diabetes Endocrinol* **2**, 901–910 (2014).

45. European Association for the Study of the Liver (EASL), European Association for the Study of Diabetes (EASD) & European Association for the Study of Obesity (EASO). EASL-EASD-EASO Clinical Practice Guidelines for the management of non-alcoholic fatty liver disease. *J. Hepatol.* **64**, 1388–1402 (2016).
46. Vanni, E. *et al.* From the metabolic syndrome to NAFLD or vice versa? *Digestive and Liver Disease* **42**, 320–330 (2010).
47. Yki-Järvinen, H. & Luukkonen, P. K. Diabetes, liver cancer and cirrhosis: What next? *Hepatology* **0**, (2018).
48. Younossi, Z. M. *et al.* Pathologic criteria for nonalcoholic steatohepatitis: Interprotocol agreement and ability to predict liver-related mortality. *Hepatology* **53**, 1874–1882 (2011).
49. Sumida, Y., Nakajima, A. & Itoh, Y. Limitations of liver biopsy and non-invasive diagnostic tests for the diagnosis of nonalcoholic fatty liver disease/nonalcoholic steatohepatitis. *World Journal of Gastroenterology : WJG* **20**, 475–485 (2014).
50. Shen, J. *et al.* Non-invasive diagnosis of non-alcoholic steatohepatitis by combined serum biomarkers. *J. Hepatol.* **56**, 1363–1370 (2012).
51. Dasarathy, S. *et al.* Validity of real time ultrasound in the diagnosis of hepatic steatosis: a prospective study. *J. Hepatol.* **51**, 1061–1067 (2009).
52. Wildman-Tobriner, B. *et al.* Association Between Magnetic Resonance Imaging-Proton Density Fat Fraction and Liver Histology Features in Patients With Nonalcoholic Fatty Liver Disease or Nonalcoholic Steatohepatitis. *Gastroenterology* (2018) doi:https://doi.org/10.1053/j.gastro.2018.07.018.
53. Friedrich-Rust, M., Poynard, T. & Castera, L. Critical comparison of elastography methods to assess chronic liver disease. *Nat Rev Gastroenterol Hepatol* **13**, 402–411 (2016).
54. Xiao, G. *et al.* Comparison of laboratory tests, ultrasound, or magnetic resonance elastography to detect fibrosis in patients with nonalcoholic fatty liver disease: A meta-analysis. *Hepatology* **66**, 1486–1501 (2017).
55. Wong, V. W.-S. *et al.* Diagnosis of fibrosis and cirrhosis using liver stiffness measurement in nonalcoholic fatty liver disease. *Hepatology* **51**, 454–462 (2010).
56. Papagianni, M., Sofogianni, A. & Tziomalos, K. Non-invasive methods for the diagnosis of nonalcoholic fatty liver disease. *World journal of hepatology* **7**, 638–648 (2015).
57. Dyson, J. K., Anstee, Q. M. & McPherson, S. Non-alcoholic fatty liver disease: a practical approach to diagnosis and staging. *Frontline Gastroenterol* **5**, 211 (2014).
58. Morra, R. *et al.* FibroMAX™: towards a new universal biomarker of liver disease? *Expert Review of Molecular Diagnostics* **7**, 481–490 (2007).
59. Alkhouri, N. *et al.* Evaluation of circulating markers of hepatic apoptosis and inflammation in obese children with and without obstructive sleep apnea. *Sleep Med.* **16**, 1031–1035 (2015).
60. Gunn, N. T. & Shiffman, M. L. The Use of Liver Biopsy in Nonalcoholic Fatty Liver Disease: When to Biopsy and in Whom. *Clin Liver Dis* **22**, 109–119 (2018).
61. Vilar-Gomez, E. & Chalasani, N. Non-invasive assessment of non-alcoholic fatty liver disease: Clinical prediction rules and blood-based biomarkers. *J. Hepatol.* **68**, 305–315 (2018).
62. Eddowes, P. J. *et al.* Accuracy of FibroScan Controlled Attenuation Parameter and Liver Stiffness Measurement in Assessing Steatosis and Fibrosis in Patients With Nonalcoholic Fatty Liver Disease. *Gastroenterology* (2019) doi:10.1053/j.gastro.2019.01.042.
63. Henao-Mejia, J. *et al.* Inflammasome-mediated dysbiosis regulates progression of NAFLD and obesity. *Nature* **482**, 179–185 (2012).
64. Le Roy, T. *et al.* Intestinal microbiota determines development of non-alcoholic fatty liver disease in mice. *Gut* **62**, 1787–1794 (2013).
65. Farrell, G. *et al.* Mouse models of nonalcoholic steatohepatitis Towards optimization of their relevance to human NASH. *Hepatology* (2018) doi:10.1002/hep.30333.

66. Nguyen, T. L. A., Vieira-Silva, S., Liston, A. & Raes, J. How informative is the mouse for human gut microbiota research? *Dis Model Mech* **8**, 1–16 (2015).
67. Chiu, C.-C. *et al.* Nonalcoholic Fatty Liver Disease Is Exacerbated in High-Fat Diet-Fed Gnotobiotic Mice by Colonization with the Gut Microbiota from Patients with Nonalcoholic Steatohepatitis. *Nutrients* **9**, 1220 (2017).
68. Le Roy, T. *et al.* Comparative Evaluation of Microbiota Engraftment Following Fecal Microbiota Transfer in Mice Models: Age, Kinetic and Microbial Status Matter. *Front Microbiol* **9**, 3289 (2018).
69. Hoyles, L. *et al.* Molecular phenomics and metagenomics of hepatic steatosis in non-diabetic obese women. *Nature Medicine* **24**, 1070–1080 (2018).
70. Brandl, K. & Schnabl, B. Intestinal microbiota and nonalcoholic steatohepatitis. *Curr. Opin. Gastroenterol.* **33**, 128–133 (2017).
71. Leung, C., Rivera, L., Furness, J. B. & Angus, P. W. The role of the gut microbiota in NAFLD. *Nat Rev Gastroenterol Hepatol* **13**, 412–425 (2016).
72. Loomba, R. Role of imaging-based biomarkers in NAFLD: Recent advances in clinical application and future research directions. *Journal of Hepatology* **68**, 296–304 (2018).
73. Wang, B. *et al.* Altered Fecal Microbiota Correlates with Liver Biochemistry in Nonobese Patients with Non-alcoholic Fatty Liver Disease. *Sci Rep* **6**, 32002 (2016).
74. Shen, F. *et al.* Gut microbiota dysbiosis in patients with non-alcoholic fatty liver disease. *HBPD INT* **16**, 375–381 (2017).
75. Raman, M. *et al.* Fecal microbiome and volatile organic compound metabolome in obese humans with nonalcoholic fatty liver disease. *Clin. Gastroenterol. Hepatol.* **11**, 868-875.e1–3 (2013).
76. Loomba, R. *et al.* Gut microbiome based metagenomic signature for non-invasive detection of advanced fibrosis in human nonalcoholic fatty liver disease. *Cell metabolism* **25**, 1054-1062.e5 (2017).
77. Zhu, L. *et al.* Characterization of gut microbiomes in nonalcoholic steatohepatitis (NASH) patients: A connection between endogenous alcohol and NASH. *Hepatology* **57**, 601–609 (2013).
78. Del Chierico, F. *et al.* Gut microbiota profiling of pediatric nonalcoholic fatty liver disease and obese patients unveiled by an integrated meta-omics-based approach. *Hepatology* **65**, 451–464 (2017).
79. Boursier, J. *et al.* The severity of NAFLD is associated with gut dysbiosis and shift in the metabolic function of the gut microbiota. *Hepatology (Baltimore, Md.)* **63**, 764–775 (2016).
80. Mouzaki, M. *et al.* Intestinal microbiota in patients with nonalcoholic fatty liver disease. *Hepatology* **58**, 120–127 (2013).
81. Michail, S. *et al.* Altered gut microbial energy and metabolism in children with non-alcoholic fatty liver disease. *FEMS Microbiol. Ecol.* **91**, 1–9 (2015).
82. Da Silva, H. E. *et al.* Nonalcoholic fatty liver disease is associated with dysbiosis independent of body mass index and insulin resistance. *Sci Rep* **8**, 1466 (2018).
83. Wong, V. W.-S. *et al.* Molecular characterization of the fecal microbiota in patients with nonalcoholic steatohepatitis--a longitudinal study. *PLoS ONE* **8**, e62885 (2013).
84. Aron-Wisnewsky, J. *et al.* Major microbiota dysbiosis in severe obesity: fate after bariatric surgery. *Gut* (2018) doi:10.1136/gutjnl-2018-316103.
85. Pedersen, H. K. *et al.* Human gut microbes impact host serum metabolome and insulin sensitivity. *Nature* **535**, 376–381 (2016).
86. Forslund, K. *et al.* Disentangling type 2 diabetes and metformin treatment signatures in the human gut microbiota. *Nature* **528**, 262–266 (2015).
87. Chen, Y. *et al.* Characterization of fecal microbial communities in patients with liver cirrhosis. *Hepatology* **54**, 562–572 (2011).

88. Chen, Y. *et al.* Dysbiosis of small intestinal microbiota in liver cirrhosis and its association with etiology. *Sci Rep* **6**, 34055 (2016).
89. Bajaj, J. S. *et al.* Altered profile of human gut microbiome is associated with cirrhosis and its complications. *J. Hepatol.* **60**, 940–947 (2014).
90. Qin, N. *et al.* Alterations of the human gut microbiome in liver cirrhosis. *Nature* **513**, 59–64 (2014).
91. Caussy, C. *et al.* A gut microbiome signature for cirrhosis due to nonalcoholic fatty liver disease. *Nat Commun* **10**, 1406 (2019).
92. Iebba, V. *et al.* Combining amplicon sequencing and metabolomics in cirrhotic patients highlights distinctive microbiota features involved in bacterial translocation, systemic inflammation and hepatic encephalopathy. *Sci Rep* **8**, 8210 (2018).
93. Cani, P. D. *et al.* Metabolic endotoxemia initiates obesity and insulin resistance. *Diabetes* **56**, 1761–1772 (2007).
94. Mao, J.-W. *et al.* Intestinal mucosal barrier dysfunction participates in the progress of nonalcoholic fatty liver disease. *Int J Clin Exp Pathol* **8**, 3648–3658 (2015).
95. Quévrain, E. *et al.* Identification of an anti-inflammatory protein from Faecalibacterium prausnitzii, a commensal bacterium deficient in Crohn's disease. *Gut* (2015) doi:10.1136/gutjnl-2014-307649.
96. Sokol, H. *et al.* Low counts of Faecalibacterium prausnitzii in colitis microbiota. *Inflamm. Bowel Dis.* **15**, 1183–1189 (2009).
97. Rajilić-Stojanović, M. *et al.* Global and deep molecular analysis of microbiota signatures in fecal samples from patients with irritable bowel syndrome. *Gastroenterology* **141**, 1792–1801 (2011).
98. Furet, J.-P. *et al.* Differential adaptation of human gut microbiota to bariatric surgery-induced weight loss: links with metabolic and low-grade inflammation markers. *Diabetes* **59**, 3049–3057 (2010).
99. Sharpton, S. R., Ajmera, V. & Loomba, R. Emerging Role of the Gut Microbiome in Nonalcoholic Fatty Liver Disease: From Composition to Function. *Clin. Gastroenterol. Hepatol.* (2018) doi:10.1016/j.cgh.2018.08.065.
100. Harte, A. L. *et al.* Elevated endotoxin levels in non-alcoholic fatty liver disease. *J Inflamm (Lond)* **7**, 15 (2010).
101. Arab, J. P., Karpen, S. J., Dawson, P. A., Arrese, M. & Trauner, M. Bile acids and nonalcoholic fatty liver disease: Molecular insights and therapeutic perspectives. *Hepatology* **65**, 350–362 (2017).
102. Cruz-Ramón, V., Chinchilla-López, P., Ramírez-Pérez, O. & Méndez-Sánchez, N. Bile Acids in Nonalcoholic Fatty Liver Disease: New Concepts and Therapeutic Advances. *Ann Hepatol* **16 Suppl 1**, S58–S67 (2017).
103. Chiang, J. Y. L. Bile acid metabolism and signaling in liver disease and therapy. *Liver Research* **1**, 3–9 (2017).
104. Canfora, E. E., Jocken, J. W. & Blaak, E. E. Short-chain fatty acids in control of body weight and insulin sensitivity. *Nat Rev Endocrinol* **11**, 577–591 (2015).
105. Schwiertz, A. *et al.* Microbiota and SCFA in lean and overweight healthy subjects. *Obesity (Silver Spring)* **18**, 190–195 (2010).
106. Raubenheimer, P. J., Nyirenda, M. J. & Walker, B. R. A Choline-Deficient Diet Exacerbates Fatty Liver but Attenuates Insulin Resistance and Glucose Intolerance in Mice Fed a High-Fat Diet. *Diabetes* **55**, 2015 (2006).
107. Yu, D. *et al.* Higher Dietary Choline Intake Is Associated with Lower Risk of Nonalcoholic Fatty Liver in Normal-Weight Chinese Women. *The Journal of Nutrition* **144**, 2034–2040 (2014).
108. Spencer, M. D. *et al.* Association between composition of the human gastrointestinal microbiome and development of fatty liver with choline deficiency. *Gastroenterology* **140**, 976–986 (2011).

109. Dumas, M.-E. *et al.* Metabolic profiling reveals a contribution of gut microbiota to fatty liver phenotype in insulin-resistant mice. *Proc. Natl. Acad. Sci. U.S.A.* **103**, 12511–12516 (2006).
110. Chen, Y. *et al.* Associations of gut-flora-dependent metabolite trimethylamine-N-oxide, betaine and choline with non-alcoholic fatty liver disease in adults. *Sci Rep* **6**, 19076 (2016).
111. Wang, Z. *et al.* Gut flora metabolism of phosphatidylcholine promotes cardiovascular disease. *Nature* **472**, 57–63 (2011).
112. Tang, W. H. W. *et al.* Intestinal microbial metabolism of phosphatidylcholine and cardiovascular risk. *N. Engl. J. Med.* **368**, 1575–1584 (2013).
113. Koeth, R. A. *et al.* Intestinal microbiota metabolism of L-carnitine, a nutrient in red meat, promotes atherosclerosis. *Nature medicine* **19**, 576–585 (2013).
114. Dumas, M.-E., Kinross, J. & Nicholson, J. K. Metabolic phenotyping and systems biology approaches to understanding metabolic syndrome and fatty liver disease. *Gastroenterology* **146**, 46–62 (2014).
115. Di Ciaula, A. *et al.* Bile Acid Physiology. *Ann Hepatol* **16 Suppl 1**, S4–S14 (2017).
116. Wahlström, A., Sayin, S. I., Marschall, H.-U. & Bäckhed, F. Intestinal Crosstalk between Bile Acids and Microbiota and Its Impact on Host Metabolism. *Cell Metab.* **24**, 41–50 (2016).
117. Sayin, S. I. *et al.* Gut microbiota regulates bile acid metabolism by reducing the levels of tauro-beta-muricholic acid, a naturally occurring FXR antagonist. *Cell Metab.* **17**, 225–235 (2013).
118. Staley, C., Weingarden, A. R., Khoruts, A. & Sadowsky, M. J. Interaction of Gut Microbiota with Bile Acid Metabolism and its Influence on Disease States. *Appl Microbiol Biotechnol* **101**, 47–64 (2017).
119. Ridlon, J. M., Kang, D. J., Hylemon, P. B. & Bajaj, J. S. Bile Acids and the Gut Microbiome. *Current opinion in gastroenterology* **30**, 332–338 (2014).
120. Liu, H., Hu, C., Zhang, X. & Jia, W. Role of gut microbiota, bile acids and their cross-talk in the effects of bariatric surgery on obesity and type 2 diabetes. *Journal of Diabetes Investigation* **9**, 13–20 (2018).
121. Kakiyama, G. *et al.* Modulation of the Fecal Bile Acid Profile by Gut Microbiota in Cirrhosis. *Journal of hepatology* **58**, 949–955 (2013).
122. Chávez-Talavera, O., Tailleux, A., Lefebvre, P. & Staels, B. Bile Acid Control of Metabolism and Inflammation in Obesity, Type 2 Diabetes, Dyslipidemia, and Nonalcoholic Fatty Liver Disease. *Gastroenterology* **152**, 1679-1694.e3 (2017).
123. Caussy, C. *et al.* Link between gut-microbiome derived metabolite and shared gene-effects with hepatic steatosis and fibrosis in NAFLD. *Hepatology* (2018) doi:10.1002/hep.29892.
124. Volynets, V. *et al.* Nutrition, Intestinal Permeability, and Blood Ethanol Levels Are Altered in Patients with Nonalcoholic Fatty Liver Disease (NAFLD). *Digestive Diseases and Sciences* **57**, 1932–1941 (2012).
125. Bashiardes, S., Shapiro, H., Rozin, S., Shibolet, O. & Elinav, E. Non-alcoholic fatty liver and the gut microbiota. *Molecular Metabolism* **5**, 782–794 (2016).
126. Yuan, J. *et al.* Fatty Liver Disease Caused by High-Alcohol-Producing Klebsiella pneumoniae. *Cell Metab.* **30**, 675-688.e7 (2019).
127. Kolodziejczyk, A. A., Zheng, D., Shibolet, O. & Elinav, E. The role of the microbiome in NAFLD and NASH. *EMBO molecular medicine* **11**, e9302 (2019).
128. Chu, H., Duan, Y., Yang, L. & Schnabl, B. Small metabolites, possible big changes: a microbiota-centered view of non-alcoholic fatty liver disease. *Gut* **68**, 359–370 (2019).
129. Brown, A. J. *et al.* The Orphan G protein-coupled receptors GPR41 and GPR43 are activated by propionate and other short chain carboxylic acids. *J. Biol. Chem.* **278**, 11312–11319 (2003).
130. Samuel, B. S. *et al.* Effects of the gut microbiota on host adiposity are modulated by the short-chain fatty-acid binding G protein-coupled receptor, Gpr41. *Proc. Natl. Acad. Sci. U.S.A.* **105**, 16767–16772 (2008).

131. den Besten, G. *et al.* Gut-derived short-chain fatty acids are vividly assimilated into host carbohydrates and lipids. *Am. J. Physiol. Gastrointest. Liver Physiol.* **305**, G900–910 (2013).
132. Rau, M. *et al.* Fecal SCFAs and SCFA-producing bacteria in gut microbiome of human NAFLD as a putative link to systemic T-cell activation and advanced disease. *United European gastroenterology journal* **6**, 1496–1507 (2018).
133. Rau, M. *et al.* Progression from Nonalcoholic Fatty Liver to Nonalcoholic Steatohepatitis Is Marked by a Higher Frequency of Th17 Cells in the Liver and an Increased Th17/Resting Regulatory T Cell Ratio in Peripheral Blood and in the Liver. *J. Immunol.* **196**, 97–105 (2016).
134. Sun, M., Wu, W., Liu, Z. & Cong, Y. Microbiota metabolite short chain fatty acids, GPCR, and inflammatory bowel diseases. *Journal of gastroenterology* **52**, 1–8 (2017).
135. Maslowski, K. M. *et al.* Regulation of inflammatory responses by gut microbiota and chemoattractant receptor GPR43. *Nature* **461**, 1282–1286 (2009).
136. Wen, W. & Schwabe, R. F. Soluble fibers improve metabolic syndrome but may cause liver disease and hepatocellular carcinoma. *Hepatology* (2019) doi:10.1002/hep.30565.
137. Singh, V. *et al.* Dysregulated Microbial Fermentation of Soluble Fiber Induces Cholestatic Liver Cancer. *Cell* **175**, 679-694.e22 (2018).
138. Kim, M. *et al.* Histone deacetylase inhibition attenuates hepatic steatosis in rats with experimental Cushing's syndrome. *Korean J Physiol Pharmacol* **22**, 23–33 (2018).
139. Loomba, R., Sirlin, C. B., Schwimmer, J. B. & Lavine, J. E. Advances in pediatric nonalcoholic fatty liver disease. *Hepatology* **50**, 1282–1293 (2009).
140. Nobili, V. *et al.* NAFLD in children: new genes, new diagnostic modalities and new drugs. *Nat Rev Gastroenterol Hepatol* **16**, 517–530 (2019).
141. Vos, M. B. *et al.* NASPGHAN Clinical Practice Guideline for the Diagnosis and Treatment of Nonalcoholic Fatty Liver Disease in Children: Recommendations from the Expert Committee on NAFLD (ECON) and the North American Society of Pediatric Gastroenterology, Hepatology and Nutrition (NASPGHAN). *J. Pediatr. Gastroenterol. Nutr.* **64**, 319–334 (2017).
142. Deschasaux, M. *et al.* Depicting the composition of gut microbiota in a population with varied ethnic origins but shared geography. *Nat. Med.* **24**, 1526–1531 (2018).
143. Bambha, K. *et al.* Ethnicity and nonalcoholic fatty liver disease. *Hepatology* **55**, 769–780 (2012).
144. Gangarapu, V., Yildiz, K., Ince, A. T. & Baysal, B. Role of gut microbiota: obesity and NAFLD. *Turk J Gastroenterol* **25**, 133–140 (2014).
145. Ley, R. E., Turnbaugh, P. J., Klein, S. & Gordon, J. I. Microbial ecology: human gut microbes associated with obesity. *Nature* **444**, 1022–1023 (2006).
146. Jie, Z. *et al.* The gut microbiome in atherosclerotic cardiovascular disease. *Nature Communications* **8**, 845 (2017).
147. Karlsson, C. L. J. *et al.* The Microbiota of the Gut in Preschool Children With Normal and Excessive Body Weight. *Obesity* **20**, 2257–2261 (2012).
148. Tilg, H., Moschen, A. R. & Roden, M. NAFLD and diabetes mellitus. *Nat Rev Gastroenterol Hepatol* **14**, 32–42 (2017).
149. Loomba, R. *et al.* Association between diabetes, family history of diabetes, and risk of nonalcoholic steatohepatitis and fibrosis. *Hepatology* **56**, 943–951 (2012).
150. Larsen, N. *et al.* Gut microbiota in human adults with type 2 diabetes differs from non-diabetic adults. *PLoS ONE* **5**, e9085 (2010).
151. Falony, G. *et al.* Population-level analysis of gut microbiome variation. *Science* **352**, 560–564 (2016).
152. Maier, L. *et al.* Extensive impact of non-antibiotic drugs on human gut bacteria. *Nature* **555**, 623–628 (2018).
153. Rhee, E. J. Nonalcoholic Fatty Liver Disease and Diabetes: An Epidemiological Perspective. *Endocrinol Metab (Seoul)* **34**, 226–233 (2019).

154. Lonardo, A., Ballestri, S., Marchesini, G., Angulo, P. & Loria, P. Nonalcoholic fatty liver disease: a precursor of the metabolic syndrome. *Dig Liver Dis* **47**, 181–190 (2015).
155. Wu, H. *et al.* Metformin alters the gut microbiome of individuals with treatment-naive type 2 diabetes, contributing to the therapeutic effects of the drug. *Nat. Med.* **23**, 850–858 (2017).
156. Shin, N.-R. *et al.* An increase in the Akkermansia spp. population induced by metformin treatment improves glucose homeostasis in diet-induced obese mice. *Gut* **63**, 727–735 (2014).
157. Depommier, C. *et al.* Supplementation with Akkermansia muciniphila in overweight and obese human volunteers: a proof-of-concept exploratory study. *Nat. Med.* **25**, 1096–1103 (2019).
158. Dao, M. C. *et al.* Akkermansia muciniphila and improved metabolic health during a dietary intervention in obesity: relationship with gut microbiome richness and ecology. *Gut* (2015) doi:10.1136/gutjnl-2014-308778.
159. Pastori, D. *et al.* The efficacy and safety of statins for the treatment of non-alcoholic fatty liver disease. *Dig Liver Dis* **47**, 4–11 (2015).
160. Caparrós-Martín, J. A. *et al.* Statin therapy causes gut dysbiosis in mice through a PXR-dependent mechanism. *Microbiome* **5**, 95 (2017).
161. Imhann, F. *et al.* Proton pump inhibitors affect the gut microbiome. *Gut* **65**, 740–748 (2016).
162. Yeh, M. M. & Brunt, E. M. Pathology of nonalcoholic fatty liver disease. *Am. J. Clin. Pathol.* **128**, 837–847 (2007).
163. Koch, L. K. & Yeh, M. M. Nonalcoholic fatty liver disease (NAFLD): Diagnosis, pitfalls, and staging. *Ann Diagn Pathol* **37**, 83–90 (2018).
164. Reinke, H. & Asher, G. Circadian Clock Control of Liver Metabolic Functions. *Gastroenterology* **150**, 574–580 (2016).
165. Parsons, M. J. *et al.* Social jetlag, obesity and metabolic disorder: investigation in a cohort study. *Int J Obes (Lond)* **39**, 842–848 (2015).
166. Asher, G. & Sassone-Corsi, P. Time for food: the intimate interplay between nutrition, metabolism, and the circadian clock. *Cell* **161**, 84–92 (2015).
167. Archer, S. N. *et al.* Mistimed sleep disrupts circadian regulation of the human transcriptome. *Proc. Natl. Acad. Sci. U.S.A.* **111**, E682-691 (2014).
168. Thaiss, C. A. *et al.* Microbiota Diurnal Rhythmicity Programs Host Transcriptome Oscillations. *Cell* **167**, 1495-1510.e12 (2016).
169. Thaiss, C. A. *et al.* Transkingdom control of microbiota diurnal oscillations promotes metabolic homeostasis. *Cell* **159**, 514–529 (2014).
170. Leone, V. *et al.* Effects of diurnal variation of gut microbes and high-fat feeding on host circadian clock function and metabolism. *Cell Host Microbe* **17**, 681–689 (2015).
171. Thomas, V., Clark, J. & Doré, J. Fecal microbiota analysis: an overview of sample collection methods and sequencing strategies. *Future Microbiol* (2015) doi:10.2217/fmb.15.87.
172. Poretsky, R., Rodriguez-R, L. M., Luo, C., Tsementzi, D. & Konstantinidis, K. T. Strengths and limitations of 16S rRNA gene amplicon sequencing in revealing temporal microbial community dynamics. *PLoS ONE* **9**, e93827 (2014).
173. Ranjan, R., Rani, A., Metwally, A., McGee, H. S. & Perkins, D. L. Analysis of the microbiome: Advantages of whole genome shotgun versus 16S amplicon sequencing. *Biochem. Biophys. Res. Commun.* **469**, 967–977 (2016).
174. Youssef, N. *et al.* Comparison of species richness estimates obtained using nearly complete fragments and simulated pyrosequencing-generated fragments in 16S rRNA gene-based environmental surveys. *Appl. Environ. Microbiol.* **75**, 5227–5236 (2009).
175. Caporaso, J. G. *et al.* QIIME allows analysis of high-throughput community sequencing data. *Nature methods* **7**, 335–336 (2010).
176. Schloss, P. D. *et al.* Introducing mothur: Open-Source, Platform-Independent, Community-Supported Software for Describing and Comparing Microbial Communities. *Appl. Environ. Microbiol.* **75**, 7537 (2009).

177. Langille, M. G. I. *et al.* Predictive functional profiling of microbial communities using 16S rRNA marker gene sequences. *Nature Biotechnology* **31**, 814 (2013).
178. Ten Hoopen, P. *et al.* The metagenomic data life-cycle: standards and best practices. *Gigascience* **6**, 1–11 (2017).
179. Olson, E. M., Lin, N. U., Krop, I. E. & Winer, E. P. The ethical use of mandatory research biopsies. *Nat Rev Clin Oncol* **8**, 620–625 (2011).
180. Peppercorn, J. *et al.* Ethics of mandatory research biopsy for correlative end points within clinical trials in oncology. *J. Clin. Oncol.* **28**, 2635–2640 (2010).
181. López-Contreras, B. E. *et al.* Composition of gut microbiota in obese and normal-weight Mexican school-age children and its association with metabolic traits. *Pediatric Obesity* **13**, 381–388 (2017).
182. Dao, M. C. *et al.* A Data Integration Multi-Omics Approach to Study Calorie Restriction-Induced Changes in Insulin Sensitivity. *Front Physiol* **9**, 1958 (2018).
183. Kayser, B. D. *et al.* Serum lipidomics reveals early differential effects of gastric bypass compared to banding on phospholipids and sphingolipids independent of differences in weight loss. *Int J Obes (Lond)* (2017) doi:10.1038/ijo.2017.63.
184. Kayser, B. D. *et al.* Phosphatidylglycerols are induced by gut dysbiosis and inflammation, and favorably modulate adipose tissue remodeling in obesity. *FASEB J.* **33**, 4741–4754 (2019).
185. A Data Integration Multi-Omics Approach to Study Calorie Restriction-Induced Changes in Insulin Sensitivity. - PubMed - NCBI. https://www-ncbi-nlm-nih-gov.gate2.inist.fr/pubmed/30804813.
186. Wright, E. K. *et al.* Microbial Factors Associated with Postoperative Crohn's Disease Recurrence. *J Crohns Colitis* **11**, 191–203 (2017).
187. Alberti, K. G. M. M. *et al.* Harmonizing the Metabolic Syndrome: A Joint Interim Statement of the International Diabetes Federation Task Force on Epidemiology and Prevention; National Heart, Lung, and Blood Institute; American Heart Association; World Heart Federation; International Atherosclerosis Society; and International Association for the Study of Obesity. *Circulation* **120**, 1640–1645 (2009).
188. Grattagliano, I. *et al.* Utility of noninvasive methods for the characterization of nonalcoholic liver steatosis in the family practice. The "VARES" Italian multicenter study. 8.

chapter

Donor Fecal Microbiota Transplantation Alters Gut Microbiota and Metabolites in Obese Individuals With Steatohepatitis

Julia J. Witjes,* Loek P. Smits,* Ceyda T. Pekmez, Andrei Prodan, Abraham S. Meijnikman, Marian A. Troelstra, Kristien E.C. Bouter, Hilde Herrema, Evgeni Levin, Adriaan G. Holleboom, Maaike Winkelmeijer, Ulrich H. Beuers, Krijn van Lienden, Judith Aron-Wisnewky, Ville Mannisto, Jacques J. Bergman, Jurgen H. Runge, Aart J. Nederveen, Lars O. Dragsted, Prokopis Konstanti, Erwin G. Zoetendal, Willem de Vos, Joanne Verheij, Albert K. Groen, Max Nieuwdorp

*Both authors contributed equally

Hepatology Communications,
VOL. 4, NO. 11, P 1578–1590, 2020

ABSTRACT

Introduction The intestinal microbiota has been linked to development and prevalence of steatohepatitis. Interestingly, steatohepatitis is significantly lower in individuals taking a plant-based, low animal protein diet which is thought to be mediated by gut microbiota. However, data on causality between these observations in humans is scarce. In this regard, fecal microbiota transplantation (FMT) using healthy donors is safe and is capable of changing microbial composition in human disease.

Design and Results We thus performed a double-blind randomized controlled proof-of-principle study in which individuals with hepatic steatosis on ultrasound were randomized to two study arms; lean vegan donor (allogenic n=10) or own (autologous n=11) FMT, which were performed three times at eight-week intervals. A liver biopsy was performed at baseline and after 24 weeks in every subject to determine histopathology (NASH-CRN) classification and changes in hepatic gene expression based on RNA sequencing. Secondary outcome parameters were changes in intestinal microbiota composition and fasting plasma metabolomics. We observed a trend towards improved necro-inflammatory histology, and found significant changes in expression of hepatic genes involved in inflammation and lipid metabolism upon allogenic FMT. Intestinal microbial community structure changed upon allogenic FMT, which was associated with changes in plasma metabolites as well as markers of .

Conclusions Allogenic FMT using lean vegan donors in individuals with hepatic steatosis shows an effect on intestinal microbiota composition, which associated with beneficial changes in plasma metabolites and markers of steatohepatitis.

INTRODUCTION

As a consequence of the pandemic spread of obesity and type 2 diabetes (T2DM), non-alcoholic fatty liver disease (NAFLD) is now recognized as the most prevalent chronic liver disease worldwide [1]. NAFLD represents a spectrum of liver disease, with clinical and histological abnormalities ranging from simple steatosis (NAFL) to steatohepatitis (NASH), with the latter being diagnosed when the liver biopsy shows hepatocyte ballooning and inflammation, in addition to steatosis. The current estimated global prevalence of NAFLD is 25 – 30% and reaching staggering numbers up to 80% in individuals with metabolic syndrome and T2DM[1]. Although it has been showed that individuals with NAFLD can progress towards NASH[2,3], the presence of steatosis has little prognostic value for disease development [4]. Increasing evidence suggest that disease activity also known as the necro-inflammation score (i.e. inflammation and hepatocyte ballooning) independent of steatosis is clinically the most relevant parameter of NAFLD[5] [6]. This relatively new concept in steatohepatitis describes and measures inflammation and liver cell injury and builds on the evidence that disease activity is highly associated with fibrosis progression [5] [6]. In line, individuals with a high necro-inflammation score, thus high active inflammation, have a considerably higher risk of developing hepatic (cirrhosis, hepatocellular carcinoma, liver transplantation) and extrahepatic (mainly atherosclerotic cardiovascular) complication. As annual medical costs directly attributable to NAFLD keep increasing per year, this underscores the need of interventions to alleviate or even prevent an adverse disease course [1].

In search of potential new and effective treatment options, the gut microbiome has gained a lot of interest, mainly based on human observational studies and animal experiments. Indeed, alterations in gut microbial composition have frequently been observed in individuals with NAFLD [8–10]. Accordingly, alterations in plasma metabolites derived from gut microbiota as well as from diet have been linked to NAFLD development[9]. Compared to omnivorous diets, plant-based low animal protein diets, as practiced by vegans, are associated with reduced NAFLD incidence[11]. Compared to omnivores, vegans have an altered gut microbiota composition [12] with concomitant alterations in plasma metabolites such as carnitine derivatives[13]. This has previously been linked to a lower incidence of NAFLD in Chinese[14] and Western subjects[11]. Although causality of these gut microbiota alterations on liver disease has been suggested in mice, in humans this remains to be elucidated. To find cause-and-effect relations between the gut microbiome and human disease in general, feces from affected individuals have been transplanted into rodents[15]. Interestingly, in a recent systematic review, it was shown that 95% of published studies described the successful transfer of the pathological phenotype of human NAFLD into rodents,

indicative of substantial publication bias as many studies were underpowered[16]. Combined with the complexity of causal relations, these findings suggest that this high success rate of inter-species transferable pathologies overestimates the role of the gut microbiome in human disease[16]. Lessons from studies performing fecal microbiota transplantation (FMT) in humans have shown that FMT is relatively safe when performed in a clinical setting and capable of changing gut microbial composition with concomitant (modest) effects on human metabolism. For example, transfer of healthy donor feces was found to improve insulin sensitivity, alter short chain fatty acid (SCFA) production and affect plasma metabolite levels in individuals with metabolic syndrome[17]. Nevertheless, not all FMT change metabolic traits or microbiota composition in treated individuals[17] and the effect seems to be modulated by donor's metabolic status as well as by the recipient's microbiota composition[18]. This underscores the complexity of the relation between human diet, metabolism, composition and function of the gut microbiome in relation to cardiometabolic diseases and NAFLD. It also suggests that (diet specific) personal characteristics of both donor and acceptor determine the individual's response upon donor FMT[19]. To date, dissecting causality of intestinal microbiota in NAFLD using FMT from donors on a plant-based, low animal-protein diet has not been performed. Therefore, the aim of our pilot randomized controlled trial study was to investigate a potential causal role of intestinal microbiota on NAFLD in humans.

METHODS

Design

This study was a single-center, double-blind, randomized controlled proof-of-principle pilot study comparing the effect of three eight-weekly lean vegan donor FMT versus autologous FMT on the severity of NAFLD, using liver biopsies in individuals with hepatic steatosis on ultrasound (**Supplemental figure 1**). The study was conducted in the Amsterdam University Medical Centers, location Academic Medical Center (AMC METC 2013_207), in compliance with the principles of the declaration of Helsinki and CONSORT guidelines. The protocol was reviewed and approved by the institutional review board of the AMC, and was registered in the Dutch Trial Register (registration number NTR4339). All participants provided written informed consent.

Participants and donors

Caucasian, overweight, treatment-naïve, omnivorous individuals with hepatic steatosis on ultrasound were included. The main inclusion criteria were age 21-69

years, male or postmenopausal female, BMI > 25 kg/m2 with hepatic steatosis on previous ultrasound with suspicion of NAFLD (based on elevated liver enzymes, impaired glucose tolerance, severity of steatosis on ultrasound). Exclusion criteria were any medication use, history of cardiovascular disease, T2DM, renal disease, cholecystectomy; compromised immunity; use of proton-pump inhibitors, antibiotics or anticoagulants in the past three months, any current use of medication, a history of moderate to heavy alcohol use (>12 grams per day), or other causes of liver disease besides NAFLD (*e.g.* hemochromatosis, auto-immune hepatitis, cirrhosis, hepatitis B or C, hemochromatosis, alpha-1 antitrypsin deficiency and alcoholic liver disease). None of the participants underwent bariatric surgery. Fecal donors were healthy, lean (BMI < 25 kg/m^2), treatment naïve, male or female Caucasian individuals on a stable (>3 months) plant-based low animal-protein (vegan) diet. They completed questionnaires on dietary and bowel habits, travel history, comorbidity including family history of diabetes mellitus and medication use. Donors were screened for the presence of infectious diseases as recommended[18,19].

Study visits

All participants were advised to retain their usual dietary habits during the study and were asked to fill out an online nutritional diary for the duration of one week before the baseline visit and the 24 weeks visit to monitor caloric intake including total calories, dietary carbohydrates, fat, proteins and fibers. Blood pressure, body weight and changes in health status were documented.

Intervention

All visits took place after an overnight fast with plasma samples taken and partly stored at -80°C for later analyses. Participants were randomized to treatments with either lean donor or autologous FMT performed according to the previously described procedure[19] at eight-week intervals (baseline gastroduodenoscopy whereas at 8 and 16 weeks a duodenal tube was placed by means of CORTRAK enteral access). This as we have previously observed that gut microbiota composition in the recipient is affected up to 8-12 weeks after donor FMT[18,19], we chose this time-window to ensure a stable donor gut microbiota composition over this 24 weeks period. The fecal samples received from the donors were collected approximately 6 hours before infusion into the recipients. Donors were not specifically matched with recipients based on histological or clinical characteristics. We preferred to use duodenal infusion for FMT administration over infusion via colonoscopy, because of the potential role of the duodenum in metabolism, combined with our established experience with, and the low complication rate of this method at our institution[18–20].

Randomization and blinding

Subjects were randomized using computerized block randomization, using blocks of four individuals. At the day of FMT, the independent physician provided the trial physician with the fecal material with the intended treatment from either the assigned donor or NAFLD individual. The study participants (*e.g.* vegan donors and NAFLD individuals) and all trial physicians (including all authors) were blinded for the treatment until completion of the trial.

Liver biopsy

Percutaneous liver biopsies were performed in the recruiting center on the basis of clinical indications according to local standard procedure. All histologic specimens were scored by a liver pathologist (J.V.) who was blinded to any other results. The NASH-CRN classification[20] was assessed with use of hematoxylin-eosin stained slides for steatosis, inflammation and ballooning and with a Sirius red stained slide for evaluation of fibrosis. The NAFLD activity score (NAS) is the unweighted sum of steatosis (0-3), lobular inflammation (0-3) and hepatocellular ballooning (0-2). RNA for RNA sequencing analysis was isolated using an RNA isolation protocol optimized for (very small) percutaneous liver biopsies directly frozen in liquid nitrogen after biopsy and stored at -80˚C (see supplemental data). RNA sequencing raw data (raw reads) were processed using Kallisto (v0.43.1) [21] to obtain gene counts. The R package tximport [22] was used to import gene counts into R (v3.4), where differential gene expression analysis was performed using DESeq2 (v1.16)[23]. Differential gene expression was aimed at finding genes that showed a statistically significant interaction between the change in gene expression in time (between baseline and 24 weeks) and treatment allocation (autologous FMT versus allogenic vegan donor FMT). P-values for the interaction effects were adjusted using the Benjamin-Hochberg correction. Genes with adjusted p-values < 0.1 were considered significant (*i.e.* their expression levels changed differently in subjects that received autologous FMT compared to subjects that received allogenic vegan donor FMT).

Biochemistry

Glucose and C-reactive protein (CRP, Roche, Switzerland) were determined in fasted plasma samples. Also, alkaline phosphatase, gamma-GT, AST, ALT, total cholesterol, high density (HDLc) and low density (LDLc) cholesterol and triglycerides (TG) were determined in EDTA-containing fasted plasma samples using commercially available assays (Randox, Antrim, UK and DiaSys, Germany). All lipid analyses were performed using a Selectra autoanalyzer (Sopachem, The Netherlands). Low-density lipoprotein cholesterol (LDLC) was calculated using the Friedewald formula.

Plasma metabolites

Fasting plasma metabolites were measured at the University of Copenhagen. Plasma samples were centrifuged at 2000 x g for 15 min at 4°C from full blood mixed with EDTA, then stored at -80°C. The order of the samples was randomized within the analytical batch. Sample processing was performed at 4°C using an ice bath. The plasma samples were thawed on ice and subjected to protein precipitation using a 96-well Sirocco™ plate. 180 µl of solvent B (acetonitrile : methanol (50:50, v/v)) was added to plasma samples (40 µl) and spiked with an internal standard mixture of 7 compounds (10 µl) after which analyses were performed as previously described [24] (also see supplemental methods and Supplemental Table 1).

Fecal microbiota profiling

Fecal samples of donors and participants were taken at 0 and 24 weeks after initiation of study and analyzed for microbiota composition using 16S rRNA amplicon sequencing[25]. DNA extraction from fecal samples was performed using the repeated bead beating protocol as previously described [26]. At baseline and 24 weeks, NAFLD individuals underwent gastro-duodenoscopy and uodenal biopsies were immediately collected in sterile tubes, snap-frozen in liquid nitrogen and stored at -80°C. DNA was isolated from duodenal biopsies using a slightly modified protocol and 16S sequencing was performed for small intestinal microbiota profiling as described previously[27] (also see supplemental methods)

Power and study endpoints

Based on previous intervention studies in NAFLD, for instance the study of Belfort et al.[28] in which treatment with pioglitazone in individuals with NASH led to a 54% reduction of steatosis compared to placebo, we performed a power analysis to calculate the number of participants necessary to detect a 25% reduction in our primary outcome parameter, reversal of steatosis and necro-inflammation upon donor FMT. For a desired alpha of 0.05 and a desired power of 0.8, a sample size of 27 per arm was needed. Hence, 54 individuals were needed in total. A data safety and monitoring board (DSMB) was appointed for safety monitoring. The primary endpoint parameters of this study were histological change in NAFLD parameters including steatosis and hepatic necro-inflammatory activity (ballooning and lobular inflammation following NASH-CRN classification), without worsening of fibrosis in lean vegan donor versus autologous FMT treatment. To assess these outcome parameters, histopathological evaluation of a percutaneously obtained liver biopsy sample was performed at baseline and after 24 weeks (8 weeks after the third FMT) in combination with changes in hepatic gene expression (using RNA sequencing in the

liver biopsy taken at baseline and after 24 weeks). Secondary outcome parameters comprised the change in intestinal microbiota composition between baseline and after 24 weeks. Other secondary outcome parameters included change in fasting plasma targeted metabolites, , plasma markers of fatty liver disease (ALT/AST) and inflammation (monocytes) at these time points.

Machine learning and follow-up statistical analyses

For baseline differences between groups, unpaired Student's t-test or the Mann-Whitney U tests were used dependent on the distribution of the data. Accordingly, data are expressed as mean ± the standard deviation or the median with interquartile range. The change in hepatic steatosis and hepatic necro-inflammatory activity (lobular inflammation and ballooning) following lean vegan donor FMT versus autologous FMT was tested using a Mann-Whitney U-test. Changes in plasma biochemistry derived outcome parameters between both treatment groups were tested using a student T-test or Mann-Whitney U-test, respectively for normal and non- parametrically distributed data. For correlation analyses, Spearman's rank test was used (as all parameters were non-parametric). A p-value < 0.05 was considered statistically significant. An Elastic Net machine learning classification algorithm in combination with a stability selection procedure [29] was used to identify biological features that changed differently between the two treatment groups as previously published[19] (also see supplemental data).

RESULTS

Between 2014 and 2017, 26 treatment-naïve obese individuals with metabolic syndrome and hepatic steatosis on ultrasound were included. In total, four of the included NAFLD individuals were excluded before randomization due to the diagnosis of new onset T2DM (n=3) or loss-of follow-up (n=1). After randomization, one individual had to be excluded due to the diagnosis new onset T2DM. Due to slow recruitment, after 21 subjects were enrolled and completed the study, the trial was prematurely stopped. Baseline characteristics of the participants are shown in **Table 1**. Daily dietary intake, divided in four macronutrients and caloric content, did not significantly differ between the allogenic and autologous FMT recipients and remained stable over the course of the study (data not shown). Feces from four healthy lean vegan donors (two donated three times and five times respectively, the other two donated only once) were used for allogenic gut microbiota transfer to NAFLD individuals. The same donor was used for the three consecutive FMT's in each participant. There were no (serious) adverse events or adverse changes in

Table 1. Baseline characteristics of 21 individuals with biopsy-proven NAFLD.

	Autologous FMT (n=11)	**Allogenic FMT (n=10)**
Age, y	48.5 ± 10.2	51.2 ± 6.6
Male gender, %	96	86
BMI, kg/m2	31.5 ± 4.8	31.7 ± 3.5
Glucose, mmol/L	5.7 ± 0.5	5.8 ± 0.7
AST, IU/L	29.0 [26.5-33.0]	39.5 [37.0-49.5]
ALT, IU/L	48.1 ± 16.5	70.8 ± 23.4
ALP, IU/L	83.0 [54.0-120.5]	71.0 [58.8-76.8]
g-GT, IU/L	41.1 ± 21.4	45.1 ± 19.3
Cholesterol, mmol/L	5.8 ± 1.6	6.0 ± 0.8
HDL-C, mmol/L	1.2 [1.0-1.4]	1.2 [1.0-1.4]
LDL-C, mmol/L	4.0 ± 1.3	4.2 ± 0.7
Triglycerides, mmol/L	1.2 ± 0.6	1.4 ± 0.5
CRP, mg/mL	2.2 [0.8-4.3]	1.5 [0.9-3.2]
Leucocytes, 10^9/L	6.8 ± 1.8	5.8 ± 1.3
Monocytes, 10^9/L	0.56 ± 0.18	0.54 ± 0.18
Calories, kcal/day	1811.2 ± 376.3	2024.7 ± 499.3
Fat, g/day	68.6 ± 19.0	80.1 ± 19.6
Carbohydrates, g/day	191.8 ± 53.9	203.7 ± 64.3
Protein, g/day	82.9 ± 19.0	91.2 ± 27.1
Fiber, g/day	22.5 ± 6.2	18.4 ± 8.2
Steatosis, %	35.0 ± 20.7	34.1 ± 20.4
NAS score	2.45 ± 0.82	3.0 ± 0.94
Necroinflam. score	0.91 ± 0.30	1.4 ± 0.52
Fibrosis score	0.91 ± 0.70	1.2 ± 0.92

Data is expressed as mean ± standard deviation or median [interquartile range], depending on the distribution of the data. BMI: body mass index, ALP: alkaline phosphatase, g-GT: gamma glutamyl transferase, ALT: alanine aminotransferase, AST aspartate aminotransferase, HDLc: high-density lipoprotein cholesterol, LDLc: low-density lipoprotein cholesterol, CRP: C-reactive protein, NAS score: NAFLD activity score.

plasma biochemistry and none of the study subjects used any medication (including no antibiotics) during the study.

Primary outcomes

Liver histology and gene expression alterations after FMT

Analyzing paired liver biopsies for histology (**Supplemental Table 3**), we found no statistically significant change in the overall NAFLD activity score (NAS) (**Figure 1A**), and steatosis grade (**Figure 1D**). We however did observe a trend towards improvement of the necro-inflammation score (comprising both lobular inflammation and hepatocellular ballooning) (**Figure 1B**) upon allogenic FMT approaching significance. Finally, fibrosis scores (**Figure 1C**) did not change over the period of 24 weeks in both groups.

Figure 1. Changes in liver histology and gene expression.

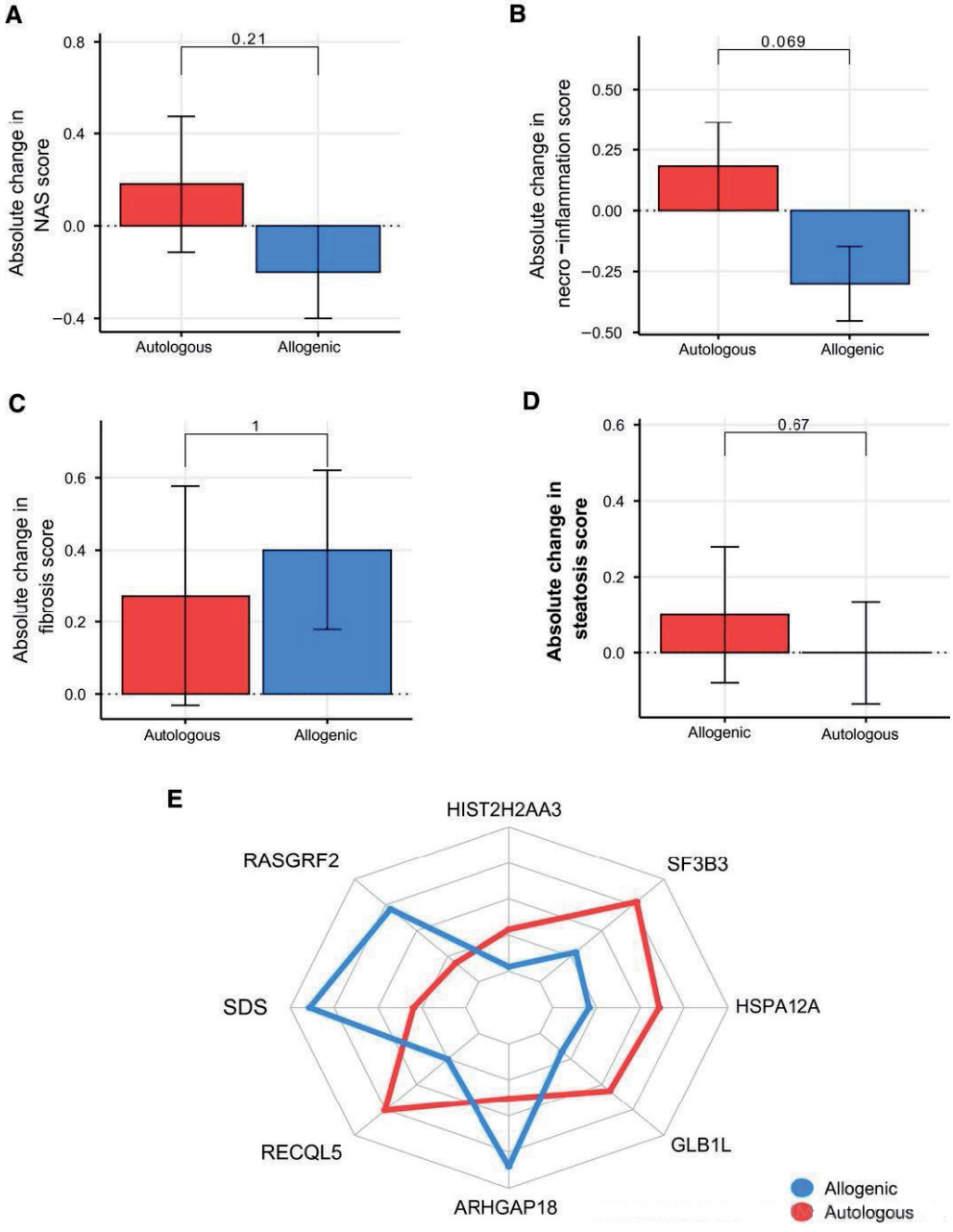

Error bars show standard errors of the means. **a**) NAFLD activity score (NAS-score); **b**) Necro-inflammation score; **c**) Fibrosis score; **d**) Steatosis score; **e**) Liver gene expression.

In line, there were significant changes in gene expression in liver biopsies in the allogenic FMT group, compared to the autologous FMT (**Figure 1E**). For example, *ARHGAP18* expression, a protective gene that maintains endothelial cell alignment, increased upon allogenic FMT (p = 0.002). Furthermore, *serine dehydratase (SDS)* expression was significantly increased upon allogenic FMT (p = 0.049). SDS catalyzes the conversion of serine into pyruvate and ammonia and is found to be decreased during liver damage [30]. In contrast, hepatic expression of *RECQL5* (p = 0.014), a gene that is implicated in DNA double strand break (DSB) repair [31] and is thus linked to the DNA damage response signaling pathway [32] and *SF3B3* (splicing factor 3b subunit 3) (p = 0.004), a gene promoting cell proliferation and known to be an early stage driver in the development of liver cancer [33,34] both increased upon autologous FMT.

Secondary outcomes

Biochemistry results 24 weeks after FMT

Upon FMT, the gamma-GT levels in the allogenic FMT group decreased (mean delta -6.4 ± 8.3, p = 0.038), while it remained unchanged in the autologous treated individuals (mean delta 0.7 ± 15.4, p = 0.883) (**Table 2**). Furthermore, ALT levels tended to decrease more in the allogenic treated group (mean delta -14.3 ± 24.6, p = 0.099) compared to the autologous treated group (mean delta -3.1 ± 20.2, p = 0.639).

FMT alters gut microbial composition

There was no difference in fecal microbiota alpha diversity (Shannon index) at baseline between NAFLD individuals and allogenic FMT donors (Shannon index: NAFLD 4.7 ± 0.4 vs donor 4.8 ± 0.1, ns.). Redundancy analysis showed a trend towards distinction in fecal microbiota composition between donors and NAFLD subjects (**Supplemental Figure 2**) together with a significant difference of fiber intake in vegan donors (**Supplemental Table 4**). Amongst others, bacteria related to *Prevotella* were associated with a plant-based diet, whereas several groups belonging to the *Lachnospiraceae* were related to the NAFLD individuals. Upon FMT, no significant changes in fecal microbiota diversity (Shannon index p = 0.84 for the allogenic FMT; p = 0.32 for the autologous FMT) were observed between baseline and week 24, however a change in gut microbiota composition, although not significant, was found upon allogenic FMT (**Supplemental Figure 2**). Compared to autologous FMT, increases in fecal microbiota abundance upon allogenic FMT were seen in bacteria related to *Ruminococcus, Eubacterium hallii, Faecalibacterium* and *Prevotella copri* (**Figure 2A**). In contrast, autologous FMT resulted in minor shifts in microbiota composition, and was primarily associated with changes in the abundance of bacteria related to *Lachnospiraceae*. There was no difference in duodenal microbiota diversity and composition before and after 24 weeks in either FMT group (data not shown).

Table 2. Metabolic and histologic parameters after FMT treatment.

	Autol. FMT – 24 weeks	p-value	Allogenic FMT – 24 weeks	p-value
Glucose, mmol/L	5.6 ± 0.8	0.241	5.8 ± 0.6	0.945
AST, IU/L	31.5 [18.8-41.3]	0.553	36.0 [29.0-42]	0.116
ALT, IU/L	46.6 ± 23.3	0.639	56.5 ± 19.2	0.099
ALP, IU/L	86.0 [66.8-112]	0.611	70.0 [57.3-83]	0.358
g-GT, IU/L	40.7 ± 28.5	0.883	38.7 ± 21.2	***0.038***
Cholesterol, mmol/L	5.5 ± 1.5	0.055	5.8 ± 0.8	0.139
HDL-C, mmol/L	1.2 [0.9-1.3]	0.280	1.1 [1.0-1.2]	0.308
LDL-C, mmol/L	3.7 ± 1.2	0.099	4.0 ± 0.8	0.378
Triglycerides, mmol/L	1.2 ± 0.6	0.796	1.4 ± 0.4	0.603
CRP, mg/mL	3.5 [0.6-6.3]	0.721	1.5 [0.7-4.4]	0.678
Leucocytes, 10^9/L	6.6 ± 1.7	0.643	6.0 ± 1.2	0.643
Monocytes, 10^9/L	0.53 ± 0.18	0.425	0.59 ± 0.25	0.460
Steatosis, %	30.5 ± 25.5	0.316	36.5 ± 25.3	0.527
NAS score	2.64 ± 1.36	0.553	2.8 ± 1.23	0.343
Necroinflam. Score	1.09 ± 0.54	0.341	1.10 ± 0.57	0.081
Fibrosis score	1.18 ± 0.75	0.391	1.60 ± 0.70	0.104

Data is expressed as mean ± standard deviation or median [interquartile range], depending on the distribution of the data. BMI: body mass index, ALP: alkaline phosphatase, g-GT: gamma glutamyl transferase, ALT: alanine aminotransferase, AST aspartate aminotransferase, HDLc: high density lipoprotein cholesterol, LDLc: low density lipoprotein cholesterol, CRP: C-reactive protein, NAS score: NAFLD activity score.

Figure 2. Radar plots of significantly altered biological features.

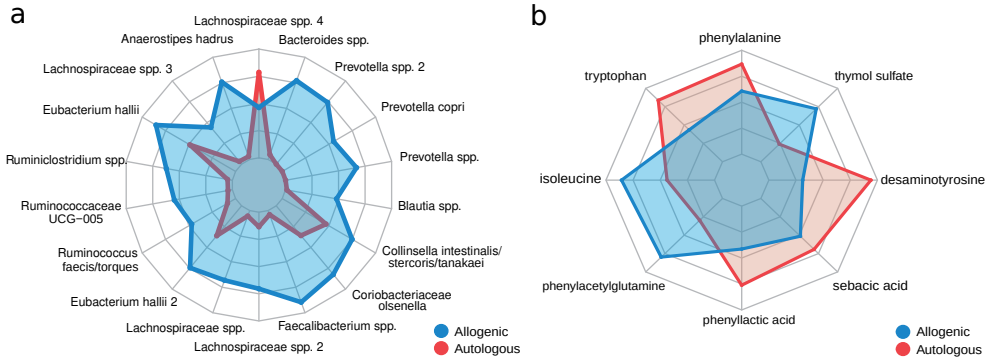

Radar plots of significantly altered biological features upon either autologous (red) or allogenic (blue) FMT; **a**) Fecal microbial strains; **b**) Plasma metabolites.

FMT alters plasma metabolite composition

Fasting plasma metabolites of both the autologous and the allogenic treated group significantly changed between baseline and 24 weeks after FMT (Figure 2b). Both plasma levels of the amino acids isoleucine (p = 0.039) and phenylacetylglutamine (p = 0.027) increased in plasma upon allogenic FMT (**Supplemental Table 2**). In contrast, plasma phenyllactic acid, which is an adverse microbial product of

Figure 3. Correlation plot.

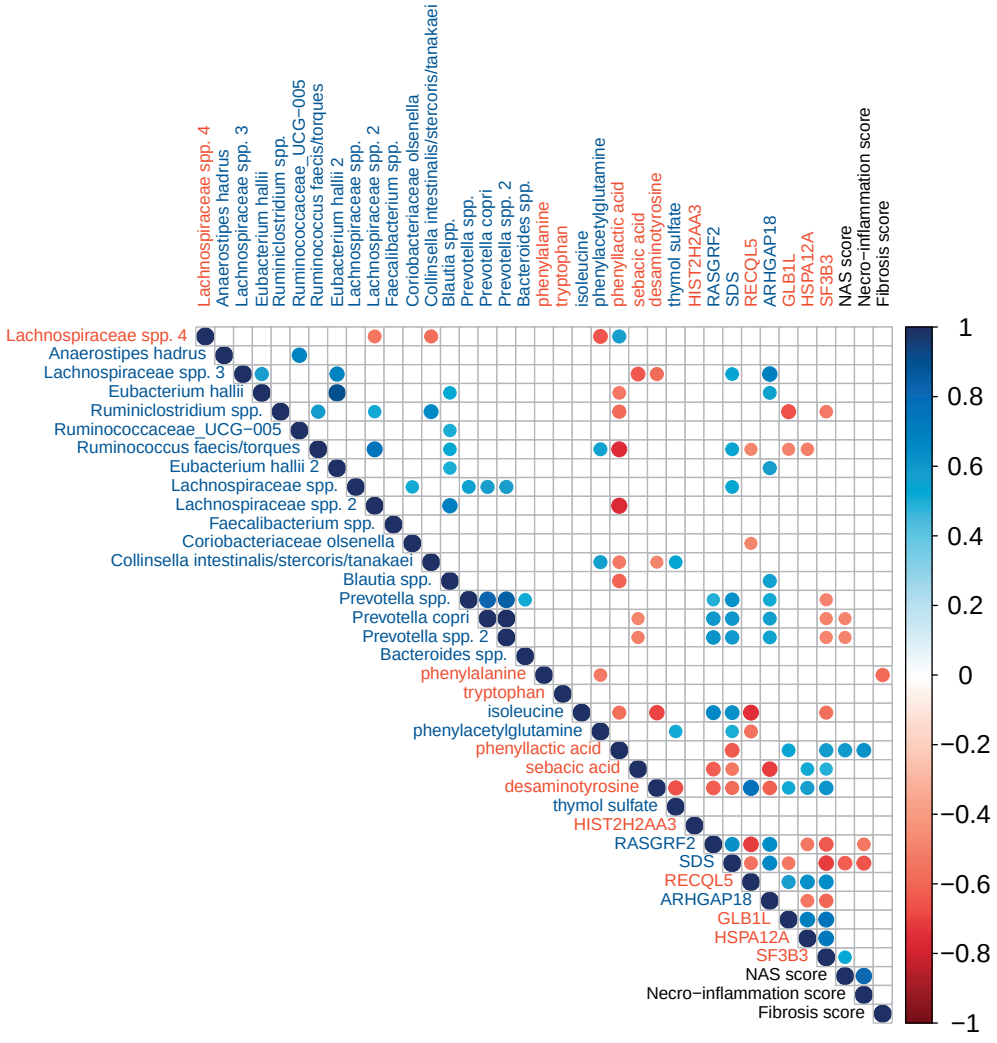

Correlation plot showing significant correlations between liver genes, fecal bacteria and plasma metabolite levels (Spearman's rho). Blue: increased in allogenic FMT/decreased in autologous FMT; red: increased in autologous FMT/decreased in allogenic FMT. Liver histology scores are included in black font.

aromatic amino acid metabolism, was increased upon autologous FMT (p = 0.008). Also, plasma levels of desaminotyrosine, a microbial metabolite known to trigger type I interferon signaling (IFN1) were increased upon autologous FMT (p = 0.008). Finally, we found correlations between liver gene expression, fecal gut microbiota composition and plasma metabolite levels upon either autologous or allogenic FMT, as given in **Figure 3** and further described in the discussion.

DISCUSSION

We here show the effect of lean vegan donor (allogenic) versus own (autologous) fecal microbiota transplantation (FMT) on obese treatment naïve individuals with metabolic syndrome and biopsy-proven NAFLD, which are the subjects in whom one typically observes NAFLD. Although the present study was underpowered, allogenic FMT from vegan donors on a plant-based, low animal protein diet decreased the necro-inflammation score in paired liver biopsies. In addition, allogenic FMT showed an effect on intestinal microbiota composition, which was associated with both beneficial changes in plasma metabolites and the expression of liver genes involved in inflammation and lipid metabolism after donor FMT. Using differences in histology data in both treatment groups between baseline and 24 weeks after treatment, we calculated that 21 participants per treatment arm would have been needed to detect a significant beneficial effect of allogenic FMT in the necro-inflammation score, whereas 120 participants per group are needed to detect a significant difference on overall NAFLD activity score. Therefore, our study could serve as a blueprint for sample sizes and specific FMT donor selection of future microbiota-based intervention trials in liver biopsy-proven NAFLD individuals.

Interactions between changes in microbiota and liver genes/ histology upon FMT

As donor metabolic characteristics can be transferred by FMT[18] in this study we opted for FMT donors on a plant-based low animal protein diet, known to have less NAFLD[11]. In line with a recent paper, assessing the effect of donor FMT on MR-spectroscopy-derived proton density fat fraction signal in NAFLD, we did not find changes in steatosis grade upon allogenic FMT as determined by liver biopsy[35], however we did find that liver necro-inflammation score improved, which was aligned by significant changes in several hepatic genes (**Figure 1**). In this regard, the *ARHGAP18* gene is a protective gene that maintains endothelial cell alignment and loss of *ARHGAP18* may predispose to atherosclerosis development[36]. Liver endothelial cells play a pivotal role in maintaining liver homeostasis and endothelial cell dysfunction (i.e. loss of fenestrations) occurs early in the pathogenesis of NAFLD, promoting steatosis, inflammation and liver fibrosis[37]. Moreover, a mutual relation between gut microbiota composition and liver endothelial cell fenestration has been described[38], with a positive relation between the abundance of *Firmicutes* and endothelial integrity. Upon allogenic FMT, ARHGAP18 was positively correlated with *E. hallii*, suggesting a protective role of this bacterial species in maintaining liver endothelial cell function. Moreover, *ARHGAP18* was inversely correlated with plasma desaminotyrosine levels, a microbial metabolite that is known to trigger type I interferon signaling (IFN1)[39]. Recently it was shown that a high-fat diet induces an IFN1 response, which via metabolically activated intrahepatic T cell pathogenicity, results in NAFLD progression[40].

Finally, we observed that after allogenic FMT, hepatic *serine dehydratase (SDS)* expression was significantly increased and showed an inverse relation with necro-inflammation and steatosis in liver histology (**Figure 3**). In human liver biopsies, *SDS* resides predominantly in the perivenous region of the hepatocyte[41] and expression decreased during liver damage[30]. *SDS* catalyzes the conversion of serine into pyruvate and ammonia and previous studies have linked these metabolites to specific microbiota composition, like *P. copri* abundance[42]. With regard to the latter, in our study NAS scores were inversely related with *P. copri,* which is in line with data reported by Boursier *et al*[10], but conflict with other publications that have linked an increased abundance of this species to NAFLD[43]. Hepatocyte injury and inflammatory cell infiltration in the perivenous (efferent) areas of the liver are a hallmark of NASH and this area is involved in glycolysis, lipogenesis, ureagenesis from ammonia, and biotransformation of plasma compounds, including metabolites[44]. In line, plasma phenyllactic acid levels, which is a microbial product of aromatic amino acid metabolism and already linked to NAFLD in humans[45], were inversely related to hepatic *SDS* expression upon allogenic FMT. As phenyllactic acid is produced by lactic acid bacteria, the observed inverse relation between phenyllactic acid and *E. hallii* is interesting to note, as this bacterial species can use lactic acid for butyrate production and has beneficial metabolic effects in humans[46]. Taken together, our data point towards a beneficial role of vegan donor FMT on prevention of NAFLD by reducing specific gut microbiota derived plasma metabolites that are toxic to the liver.

Interactions between changes in plasma metabolites and liver genes/ histology upon FMT

The linear correlation of the SDS gene with isoleucine and phenylacetylglutamine (both increased in plasma upon allogenic FMT) is of interest, as a recent paper using genome-scale models indicated that individuals with NAFLD have altered metabolism of these amino acids[47]. Alterations in circulating amino acids and branched chain amino acids are often explained to be the result of impaired amino acid metabolism linked to insulin resistance, especially in the muscle[48]. Only recently it has been revealed that the gut microbiome is associated with plasma metabolite alterations of amino acids and branched chain amino acids[42]. Our results strengthen the observation that the gut microbiome contributes to plasma amino acids and branched chain amino acid composition. The inverse relation between plasma phenylalanine with the fibrosis score corroborates with older literature that phenylalanine metabolism is decreased in individuals with hepatopathy, with plasma phenylalanine values decreasing with relatively early liver fibrosis[49].

However, only recently it was shown that metabolic pathways involved in the biosynthesis of phenylalanine are increased in the gut microbiome of individuals

with NAFLD[9]. Despite the enhanced capacity of the gut microbiome to produce phenylalanine, plasma levels are dependent on the liver to catabolize this metabolite. Under normal circumstances and homeostasis, phenylalanine is converted in the liver to tyrosine and when the liver is not capable of metabolizing phenylalanine, phenyllactic acid and/or phenylacetylglutamine is produced, products that are negatively (phenylacetylglutamine)[9] or positively (phenyllactic acid)[45] associated with NAFLD according to recent findings. Although phenylalanine and downstream metabolites are highlighted in this study, it is most likely part of a much broader multifactorial process, only partly orchestrated by the gut microbiome. Thus, further research to prove causality of the gut microbiome in the development of NAFLD and NASH is warranted.

Study limitations

First, due to slow recruitment, our study was underpowered as we prematurely had to terminate our trial. Second, although we observed no significant differences in baseline liver histology (NAFL-NASH classifications) between autologous and allogenic FMT groups (**Table 2**), differences in baseline AST and ALT levels were observed. As participants were randomized this difference occurred by chance, but could have influenced the outcome of our study. However, if this would be the case, this baseline difference would have led to an underestimation of the allogenic donor effect as all parameters were increased in that group. A third limitation is the use of untargeted analysis of hepatic gene expression, since the genes found to be differentially expressed are not classical markers of hepatic inflammation in NAFLD. Another limitation is our choice of FMT donors, as donor metabolic characteristics can be transferred by FMT[18]. We therefore chose FMT donors consuming a plant-based low animal protein diet who are known to have less NAFLD[11]. Yet, we did not compare the effect of lean FMT from donors on either an omnivorous or plant-based diet. Finally, our population is relatively healthy and does not fully reflect the typical NAFLD individual who is often affected by multiple diseases besides NAFLD and thus treated with multiple medications. This is reflected by the relatively low necro-inflammation score found. However, numerous medications, not limited to proton pump inhibitors and antibiotics, dramatically alter gut microbial composition, even with inter-individual differences [50,51]. In order to demonstrate causality between the gut microbiome and the development of NAFLD, the use of medication was an exclusion criterion for participation in this study. Bearing these limitations in mind, the question to what extent the gut microbiome plays a significant role in the development of NAFLD and especially in individuals with a more progressive form (i.e. higher necro-inflammation score) remains to be answered.

In conclusion, our study shows that repetitive allogenic donor FMT in individuals with NAFLD affects hepatic gene expression and plasma metabolites involved in inflammation and lipid metabolism, highlighting the crosstalk between gut microbiota composition and NAFLD. Therefore, our work does not only further validate previous associative studies on the relation between NAFLD and gut microbiota, but also provides future sample sizes for microbiota-based intervention trials aimed at treating NAFLD in humans.

REFERENCES

1. Younossi Z, Tacke F, Arrese M, Chander Sharma B, Mostafa I, Bugianesi E, et al. Global Perspectives on Nonalcoholic Fatty Liver Disease and Nonalcoholic Steatohepatitis. Hepatology [Internet]. 2019 Jun;69(6):2672–82. Available from: http://doi.wiley.com/10.1002/hep.30251
2. Pais R, Charlotte F, Fedchuk L, Bedossa P, Lebray P, Poynard T, et al. A systematic review of follow-up biopsies reveals disease progression in patients with non-alcoholic fatty liver. J Hepatol [Internet]. 2013;59(3):550–6. Available from: http://dx.doi.org/10.1016/j.jhep.2013.04.027
3. McPherson S, Hardy T, Henderson E, Burt AD, Day CP, Anstee QM. Evidence of NAFLD progression from steatosis to fibrosing-steatohepatitis using paired biopsies: Implications for prognosis and clinical management. J Hepatol [Internet]. 2015 May;62(5):1148–55. Available from: https://linkinghub.elsevier.com/retrieve/pii/S0168827814008836
4. Ekstedt M, Hagström H, Nasr P, Fredrikson M, Stål P, Kechagias S, et al. Fibrosis stage is the strongest predictor for disease-specific mortality in NAFLD after up to 33 years of follow-up. Hepatology [Internet]. 2015 May;61(5):1547–54. Available from: http://doi.wiley.com/10.1002/hep.27368
5. Ratziu V. Back to Byzance: Querelles byzantines over NASH and fibrosis. Journal of Hepatology. 2017.
6. Kleiner DE, Brunt EM, Wilson LA, Behling C, Guy C, Contos M, et al. Association of Histologic Disease Activity With Progression of Nonalcoholic Fatty Liver Disease. JAMA Netw open. 2019 Oct;2(10):e1912565.
7. Fazel Y, Koenig AB, Sayiner M, Goodman ZD, Younossi ZM. Epidemiology and natural history of non-alcoholic fatty liver disease. Metabolism [Internet]. 2016;65(8):1017–25. Available from: http://dx.doi.org/10.1016/j.metabol.2016.01.012
8. Loomba R, Seguritan V, Li W, Long T, Klitgord N, Bhatt A, et al. Gut Microbiome-Based Metagenomic Signature for Non-invasive Detection of Advanced Fibrosis in Human Nonalcoholic Fatty Liver Disease. Cell Metab [Internet]. 2019 Sep;30(3):607. Available from: https://linkinghub.elsevier.com/retrieve/pii/S1550413119304310
9. Hoyles L, Fernández-Real JM, Federici M, Serino M, Abbott J, Charpentier J, et al. Molecular phenomics and metagenomics of hepatic steatosis in non-diabetic obese women. Nat Med. 2018;24(7):1070–80.
10. Boursier J, Mueller O, Barret M, Machado M, Fizanne L, Araujo-Perez F, et al. The severity of nonalcoholic fatty liver disease is associated with gut dysbiosis and shift in the metabolic function of the gut microbiota. Hepatology [Internet]. 2016 Mar;63(3):764–75. Available from: http://doi.wiley.com/10.1002/hep.28356
11. Mazidi M, Kengne AP. Higher adherence to plant-based diets are associated with lower likelihood of fatty liver. Clin Nutr. 2019 Aug;38(4):1672–7.
12. Wu GD, Compher C, Chen EZ, Smith SA, Shah RD, Bittinger K, et al. Comparative metabolomics in vegans and omnivores reveal constraints on diet-dependent gut microbiota metabolite production. Gut. 2016 Jan;65(1):63–72.
13. Koeth RA, Lam-Galvez BR, Kirsop J, Wang Z, Levison BS, Gu X, et al. l-Carnitine in omnivorous diets induces an atherogenic gut microbial pathway in humans. J Clin Invest. 2018 Dec;129(1):373–87.
14. Chen Y, Liu Y, Zhou R, Chen X, Wang C, Tan X, et al. Associations of gut-flora-dependent metabolite trimethylamine-N-oxide, betaine and choline with non-alcoholic fatty liver disease in adults. Sci Rep. 2016 May;6(1):19076.
15. Meijnikman AS, Gerdes VE, Nieuwdorp M, Herrema H. Evaluating Causality of Gut Microbiota in Obesity and Diabetes in Humans. Endocr Rev [Internet]. 2018 Apr 1;39(2):133–53. Available from: https://academic.oup.com/edrv/article/39/2/133/4772276

16. Walter J, Armet AM, Finlay BB, Shanahan F. Establishing or Exaggerating Causality for the Gut Microbiome: Lessons from Human Microbiota-Associated Rodents. Cell [Internet]. 2020 Jan;180(2):221–32. Available from: https://linkinghub.elsevier.com/retrieve/pii/S009286741931387X
17. Vrieze A, Van Nood E, Holleman F, Salojärvi J, Kootte RS, Bartelsman JFWMWM, et al. No Title. Gastroenterology. 2012 Oct;143(4):913–916.e7.
18. de Groot P, Scheithauer T, Bakker GJ, Prodan A, Levin E, Khan MT, et al. Donor metabolic characteristics drive effects of faecal microbiota transplantation on recipient insulin sensitivity, energy expenditure and intestinal transit time. Gut [Internet]. 2020 Mar;69(3):502–12. Available from: http://gut.bmj.com/lookup/doi/10.1136/gutjnl-2019-318320
19. Smits LP, Kootte RS, Levin E, Prodan A, Fuentes S, Zoetendal EG, et al. Effect of vegan fecal microbiota transplantation on carnitine- and choline-derived trimethylamine-N-oxide production and vascular inflammation in patients with metabolic syndrome. J Am Heart Assoc. 2018;7(7).
20. Kleiner DE, Brunt EM, Van Natta M, Behling C, Contos MJ, Cummings OW, et al. Design and validation of a histological scoring system for nonalcoholic fatty liver disease. Hepatology [Internet]. 2005 Jun;41(6):1313–21. Available from: http://doi.wiley.com/10.1002/hep.20701
21. Bray NL, Pimentel H, Melsted P, Pachter L. Near-optimal probabilistic RNA-seq quantification. Nat Biotechnol [Internet]. 2016 May 4;34(5):525–7. Available from: http://www.nature.com/articles/nbt.3519
22. Soneson C, Love MI, Robinson MD. Differential analyses for RNA-seq: transcript-level estimates improve gene-level inferences. F1000Research [Internet]. 2015 Dec 30;4:1521. Available from: https://f1000research.com/articles/4-1521/v1
23. Love MI, Huber W, Anders S. Moderated estimation of fold change and dispersion for RNA-seq data with DESeq2. Genome Biol [Internet]. 2014 Dec 5;15(12):550. Available from: http://genomebiology.biomedcentral.com/articles/10.1186/s13059-014-0550-8
24. Barri T, Holmer-Jensen J, Hermansen K, Dragsted LO. Metabolic fingerprinting of high-fat plasma samples processed by centrifugation- and filtration-based protein precipitation delineates significant differences in metabolite information coverage. Anal Chim Acta [Internet]. 2012 Mar;718:47–57. Available from: https://linkinghub.elsevier.com/retrieve/pii/S0003267012000062
25. Taylor M, Wood HM, Halloran SP, Quirke P. Examining the potential use and long-term stability of guaiac faecal occult blood test cards for microbial DNA 16S rRNA sequencing. J Clin Pathol [Internet]. 2017 Jul;70(7):600–6. Available from: http://jcp.bmj.com/lookup/doi/10.1136/jclinpath-2016-204165
26. Salonen A, Nikkilä J, Jalanka-Tuovinen J, Immonen O, Rajilić-Stojanović M, Kekkonen RA, et al. Comparative analysis of fecal DNA extraction methods with phylogenetic microarray: Effective recovery of bacterial and archaeal DNA using mechanical cell lysis. J Microbiol Methods. 2010;81(2):127–34.
27. Zoetendal, E., Heilig, H., Klaassens E. Isolation of DNA from bacterial samples of the human gastrointestinal tract. Nat Protoc. 2006;1(2):870–873.
28. Belfort R, Harrison SA, Brown K, Darland C, Finch J, Hardies J, et al. A Placebo-Controlled Trial of Pioglitazone in Subjects with Nonalcoholic Steatohepatitis. N Engl J Med [Internet]. 2006 Nov 30;355(22):2297–307. Available from: http://www.nejm.org/doi/abs/10.1056/NEJMoa060326
29. Meinshausen N, Bühlmann P. Stability selection. J R Stat Soc Ser B (Statistical Methodol [Internet]. 2010 Jul 5;72(4):417–73. Available from: http://doi.wiley.com/10.1111/j.1467-9868.2010.00740.x

30. López-Flores I, Barroso JB, Valderrama R, Esteban FJ, Martínez-Lara E, Luque F, et al. Serine dehydratase expression decreases in rat livers injured by chronic thioacetamide ingestion. Mol Cell Biochem. 2005;268(1–2):33–43.
31. Liao W-Q. Recql5 protects against lipopolysaccharide/D-galactosamine-induced liver injury in mice. World J Gastroenterol [Internet]. 2015;21(36):10375. Available from: http://www.wjgnet.com/1007-9327/full/v21/i36/10375.htm
32. Ciccia A, Elledge SJ. The DNA Damage Response: Making It Safe to Play with Knives. Mol Cell [Internet]. 2010 Oct;40(2):179–204. Available from: https://linkinghub.elsevier.com/retrieve/pii/S1097276510007471
33. Shen Q, Nam SW. SF3B4 as an early-stage diagnostic marker and driver of hepatocellular carcinoma. BMB Rep [Internet]. 2018 Feb 28;51(2):57–8. Available from: http://www.bmbreports.org/journal/view.html?doi=10.5483/BMBRep.2018.51.2.021
34. Mas VR, Fisher RA, Archer KJ, Maluf DG. Proteomics and liver fibrosis: identifying markers of fibrogenesis. Expert Rev Proteomics [Internet]. 2009 Aug 9;6(4):421–31. Available from: http://www.tandfonline.com/doi/full/10.1586/epr.09.59
35. Craven L, Rahman A, Nair Parvathy S, Beaton M, Silverman J, Qumosani K, et al. Allogenic Fecal Microbiota Transplantation in Patients With Nonalcoholic Fatty Liver Disease Improves Abnormal Small Intestinal Permeability. Am J Gastroenterol [Internet]. 2020 May 15;Publish Ah. Available from: https://journals.lww.com/10.14309/ajg.0000000000000661
36. Lay AJ, Coleman PR, Formaz-Preston A, Ting KK, Roediger B, Weninger W, et al. ARHGAP18: A Flow-Responsive Gene That Regulates Endothelial Cell Alignment and Protects Against Atherosclerosis. J Am Heart Assoc [Internet]. 2019 Jan 22;8(2). Available from: https://www.ahajournals.org/doi/10.1161/JAHA.118.010057
37. Hammoutene A, Rautou P-E. Role of liver sinusoidal endothelial cells in non-alcoholic fatty liver disease. J Hepatol [Internet]. 2019 Jun;70(6):1278–91. Available from: https://linkinghub.elsevier.com/retrieve/pii/S0168827819301278
38. Cogger VC, Mohamad M, Solon-Biet SM, Senior AM, Warren A, O'Reilly JN, et al. Dietary macronutrients and the aging liver sinusoidal endothelial cell. Am J Physiol Circ Physiol [Internet]. 2016 May 1;310(9):H1064–70. Available from: https://www.physiology.org/doi/10.1152/ajpheart.00949.2015
39. Steed AL, Christophi GP, Kaiko GE, Sun L, Goodwin VM, Jain U, et al. The microbial metabolite desaminotyrosine protects from influenza through type I interferon. Science (80-) [Internet]. 2017 Aug 4;357(6350):498–502. Available from: https://www.sciencemag.org/lookup/doi/10.1126/science.aam5336
40. Ghazarian M, Revelo XS, Nøhr MK, Luck H, Zeng K, Lei H, et al. Type I interferon responses drive intrahepatic T cells to promote metabolic syndrome. Sci Immunol [Internet]. 2017 Apr 21;2(10):eaai7616. Available from: https://immunology.sciencemag.org/lookup/doi/10.1126/sciimmunol.aai7616
41. Kashii T, Gomi T, Oya T, Ishii Y, Oda H, Maruyama M, et al. Some biochemical and histochemical properties of human liver serine dehydratase. Int J Biochem Cell Biol [Internet]. 2005 Mar;37(3):574–89. Available from: https://linkinghub.elsevier.com/retrieve/pii/S1357272504003152
42. Pedersen HK, Gudmundsdottir V, Nielsen HB, Hyotylainen T, Nielsen T, Jensen BAH, et al. Human gut microbes impact host serum metabolome and insulin sensitivity. Nature [Internet]. 2016 Jul 13;535(7612):376–81. Available from: http://www.nature.com/articles/nature18646
43. Schwimmer JB, Johnson JS, Angeles JE, Behling C, Belt PH, Borecki I, et al. Microbiome Signatures Associated With Steatohepatitis and Moderate to Severe Fibrosis in Children With Nonalcoholic Fatty Liver Disease. Gastroenterology [Internet]. 2019 Oct;157(4):1109–22. Available from: https://linkinghub.elsevier.com/retrieve/pii/S0016508519410378

44. Abdelmalek MF, Diehl AM. Nonalcoholic Fatty Liver Disease as a Complication of Insulin Resistance. Med Clin North Am [Internet]. 2007 Nov;91(6):1125–49. Available from: https://linkinghub.elsevier.com/retrieve/pii/S0025712507000740
45. Caussy C, Hsu C, Lo M-T, Liu A, Bettencourt R, Ajmera VH, et al. Link between gut-microbiome derived metabolite and shared gene-effects with hepatic steatosis and fibrosis in NAFLD. Hepatology [Internet]. 2018 Sep;68(3):918–32. Available from: http://doi.wiley.com/10.1002/hep.29892
46. Gilijamse PW, Hartstra A V., Levin E, Wortelboer K, Serlie MJ, Ackermans MT, et al. Treatment with Anaerobutyricum soehngenii: a pilot study of safety and dose–response effects on glucose metabolism in human subjects with metabolic syndrome. npj Biofilms Microbiomes [Internet]. 2020 Dec 27;6(1):16. Available from: http://www.nature.com/articles/s41522-020-0127-0
47. Mardinoglu A, Agren R, Kampf C, Asplund A, Uhlen M, Nielsen J. Genome-scale metabolic modelling of hepatocytes reveals serine deficiency in patients with non-alcoholic fatty liver disease. Nat Commun [Internet]. 2014 May 14;5(1):3083. Available from: http://www.nature.com/articles/ncomms4083
48. Newgard CB, An J, Bain JR, Muehlbauer MJ, Stevens RD, Lien LF, et al. A Branched-Chain Amino Acid-Related Metabolic Signature that Differentiates Obese and Lean Humans and Contributes to Insulin Resistance. Cell Metab [Internet]. 2009 Apr;9(4):311–26. Available from: https://linkinghub.elsevier.com/retrieve/pii/S1550413109000400
49. Ishii Y, Suzuki S, Kohno T, Aoki M, Kohno T, Ito A, et al. L-[1- 13 C] phenylalanine breath test reflects histological changes in the liver. J Surg Res [Internet]. 2003 Oct;114(2):120–5. Available from: https://linkinghub.elsevier.com/retrieve/pii/S0022480403002786
50. Maier L, Pruteanu M, Kuhn M, Zeller G, Telzerow A, Anderson EE, et al. Extensive impact of non-antibiotic drugs on human gut bacteria. Nature [Internet]. 2018 Mar 19;555(7698):623–8. Available from: https://www.nature.com/articles/nature25979
51. Zaneveld JR, McMinds R, Vega Thurber R. Stress and stability: applying the Anna Karenina principle to animal microbiomes. Nat Microbiol [Internet]. 2017 Sep 24;2(9):17121. Available from: http://www.nature.com/articles/nmicrobiol201712

SUPPLEMENTAL METHODS

Liver samples for RNA sequencing

In short, biopsies were mixed with 300 μl TriPure (Roche, Basel, Switzerland) and homogenized on ice using a sterile, RNAse free pestle. After short centrifugation, 60 μl of chloroform was added. Samples were then added to a Heavy Phase Lock gel tube (Quanta Bio, Beverly, USA) and centrifuged (15 min, 12.000 x g, 4˚C). The aqueous phase was transferred and mixed with 1 volume of 70% ethanol. The mixture was added to a RNeasy MinElute spin column (QIAgen, Tegelen, the Netherlands). RNA was washed according to manufacturer's protocol and eluted in 14 μl RNAse free water. RNA concentration was measured using the NanoDrop 1000 (Thermo Scientific, Landsmeer, the Netherlands). RIN scores were assessed on a Bioanalyzer 2100 using Eukaryote Total RNA Nano chips (Agilent Technologies, Santa Clara, USA). RNA was depleted from rRNA and sequenced on a HiSeq4000 (paired-end, 150 bp) by Genomescan BV, Amsterdam, The Netherlands.

Plasma metabolites

The plate was vortexed for 5 min and kept in the refrigerator at 4°C for 10 min to enhance protein precipitation. Solvent B was eliminated using a vacuum centrifuge. Dry plasma samples were dissolved in 200 μl of Solvent A (Milli-Q water:formic acid (1000:1, v/v)) before the analysis. A blank sample (Solvent A) treated similarly to the plasma samples, an external standard containing 44 biologically relevant metabolites (metabolomics standard) [1] and a pooled sample containing equal amounts of each sample were added to spare wells and analyzed repeatedly (every fifteen samples) throughout the run for quality control. Quality control samples were used to evaluate possible contamination, and for monitoring drifts in mass accuracy, retention time and instrumental sensitivity. Samples were analyzed by Ultra Performance Liquid Chromatography (UPLC) coupled with a quadrupole-Time of Flight Mass Spectrometer (q-TOF-MS) equipped with electrospray ionization (ESI) (SYNAPT, Waters, Manchester, UK). A rerversed phase HSS T3 C18 column (2.1x100 mm, 1.8 μm) coupled with a pre-column (VanGuard HSS T3 C18 column, 2.1x5 mm, 1.8 μm) was used for chromatographic separation, as earlier described [1].

The raw data were converted to netCDF format using DataBridge Software and imported into MZmine version 2.28 [2]. A subset of samples was used to optimize the preprocessing parameters for the positive and negative mode data separately. Optimized preprocessing parameters are given in **Supplemental table 1**. Each detected peak was represented by a feature defined with a retention time (RT) and a mass to charge ratio (m/z). The data matrix was imported into MATLAB R2015b (The Mathworks, Inc., MA, USA). Features that were present in the blanks, early and

late eluting (RT<0.3 and RT>6.4) features, potential isotopes as well as features with implausible masses were removed from the dataset with an in-house algorithm. Features not present in at least 70% of the samples in each intervention group were removed to reduce noise[3]. Features within 0.01 min RT tolerance and having correlation coefficients >0.7 were grouped together to ease the feature identification step. Pooled samples were used for linear correction of signal drift throughout the analysis [4].

We carried out a search within an in-house standards database for potential matches with identified compounds, including their parent ions, adducts and fragments. For the unidentified features, MS/MS experiments were performed with collision dissociation energies (CDE) of 10, 20 and 30 eV on a Waters ACQUITY UPLC H–Class System (Waters, Manchester, UK) coupled with a Vion ion mobility q-TOF-MS equipped with ESI (Waters Corporation, Manchester, UK). Experimental conditions for the full scan MS mode on the new platform are described elsewhere [5]. Fragmentation patterns were compared with available databases, such as HMDB (http://www.hmdb.ca), LIPID MAPS (http://www.lipidmaps.org), MetFrag (https://msbi.ipb-halle.de/MetFragBeta), Metlin (https://metlin.scripps.edu), SIRIUS-version.3.5.1 (https://bio.informatik.uni-jena.de/software/sirius) and similar. The standards were run together with the samples with highest intensity on the same batch and platform. The identification level of compounds used categories from level I (identity confirmed with m/z and RT) to level IV (unknown), according to criteria published by Sumner et al. [6] (**Supplemental table 2**).

Fecal microbiota profiling

DNA was eluted in 50 µl of DNAse- RNAse-free water and its concentration and quality were evaluated using NanoDrop 2000 spectrophotometry. Subsequently, DNA was diluted to reach a concentration of 20 ng/µl which served as template for PCR. The V5-V6 region of 16S ribosomal RNA (rRNA) gene was amplified in duplicate PCR reactions for each sample in a total reaction volume of 50 µl [7] using a master mix containing 1 µl of a unique barcoded primer, 784F-n and 1064R-n (10 µM each per reaction), 1 µl dNTPs mixture, 0.5 µl Phusion Green Hot Start II High-Fidelity DNA Polymerase (2 U/µl; Thermo Scientific, Landsmeer, The Netherlands), 10 µl 5× Phusion Green HF Buffer, and 36.5 µl DNAse- RNAse-free water. The amplification program included 30 s of initial denaturation step at 98°C, followed by 25 cycles of denaturation at 98 °C for 10 s, annealing at 42 °C for 10 s, elongation at 72 °C for 10 s, and a final extension step at 72 °C for 7 min. The PCR product was visualised on 1% agarose gel (~280 bp) and purified with CleanPCR kit (CleanNA, Alphen aan den Rijn, The Netherlands). The concentration of the purified PCR product was measured with Qubit dsDNA BR Assay Kit (Invitrogen, California, USA) and 200 ng of microbial

DNA from each sample were pooled for the creation of the final amplicon library which was sequenced (150 bp, paired-end) on the Illumina HiSeq 2500 platform (GATC Biotech, Constance, Germany)[8].

Raw reads were demultiplexed using the Je software suite (v2.0.) allowing no mismatches in the barcodes. After removing the barcodes, linkers and primers, reads were mapped against the human genome using bowtie2 in order to remove human reads. Surviving microbial forward and reverse reads were pipelined separately using DADA2 [8] (v1.12.1). Amplicon Sequence Variants (ASVs) inferred from the reverse reads were reverse-complemented and matched against ASVs inferred from the forwards reads. Only non-chimeric forward reads ASVs that matched reverse-complemented reverse reads ASVs were kept. ASV sample counts were inferred from the forward reads. ASV taxonomy was assigned using DADA2 and the SILVA (v132) database. The resulting ASV table and taxonomy assignments were integrated using the phyloseq R package (v1.28.0) and rarefied to 150000 counts per sample. The raw amplicon sequencing microbiome data from this study will be deposited in the European Nucleotide Archive repository.

Duodenal microbiota profiling

DNA was isolated from duodenal biopsies using a slightly modified protocol as described previously [9]. In short, duodenal biopsies were added to a bead-beating tube with 300 µl Stool Transport and Recovery (STAR) buffer, 0.25 g of sterilized zirconia beads (0.1 mm). Six µl of Proteinase K (20mg/ml; QIAGEN, Venlo, The Netherlands) was added and the mixture was incubated for 1 h at 55 °C. The biopsies were then homogenized by bead-beating three times (60 s × 5.5 ms) followed by incubation for 15 min at 95 °C at 1000 rpm. Samples were then centrifuged for 5 min at 4 °C and 14,000 g and supernatants transferred to sterile tubes. Pellets were re-processed using 200 µl STAR buffer and both supernatants were pooled. DNA purification was performed with a customized kit (XAS1220; Promega) using 250 µl of the final supernatant pool. A first PCR using the 27F and the 1369R primer was used for primary enrichment in a master mix containing 1µl of 10uM primer, 1µl dNTPs mixture, 0.5 µl Phusion Green Hot Start II High-Fidelity DNA Polymerase (2 U/µl; Thermo Scientific, Landsmeer, The Netherlands), 10 µl 5× Phusion Green HF Buffer, and 36.5 µl DNAse- RNAse-free water. The amplification program included 30 s of initial denaturation step at 98°C, followed by 25 cycles of denaturation at 98 °C for 30 s, annealing at 52 °C for 40 s, elongation at 72 °C for 90 s, and a final extension step at 72 °C for 7 min. Subsequently, a nested-PCR was performed to amplify he V5-V6 region of 16S rRNA gene as described above. Microbiota analysis of 16S rRNA amplicons was done similarly as described for fecal microbiota profiling.

Machine learning approach

All data were scaled to zero mean and unit variance. To train each model, the two hyper-parameters (alpha – the size of the regularization penalty; and L1 ratio – the ratio of L1-norm/L2-norm in the model penalty) were optimized using a 5-fold cross-validation procedure on a training subset comprising 80% of the data. The resulting model was then tested on the remaining 20% of the data. This procedure was repeated 100 times per analysis using different random splitting of the data into training and test subsets. The stability of each feature was calculated as the proportion of runs in which the feature had a non-zero regression coefficient. This technique was used on duodenal microbial composition, on fecal microbiota composition, and on fasting plasma metabolite levels. We used the relative change (delta) of each feature between 0 and 24 weeks. We selected the top parameters from each analysis that accurately (*i.e.,* ROC AUC ≥ 0.8) or moderately (ROC AUC > 0.7) predicted group allocation for closer study, using an arbitrary cutoff. This cutoff was generally a relative importance of around 30% or higher. Then, we visualized the change in time of the selected parameters (Wilcoxon's signed rank tests), studied between-group differences at each time point and finally, using Spearman's rank test, we correlated these parameters with our primary endpoint and with other key parameters that were identified in this way.

REFERENCES

1. Barri, T., Holmer-Jensen, J., Hermansen, K. & Dragsted, L. O. Metabolic fingerprinting of high-fat plasma samples processed by centrifugation- and filtration-based protein precipitation delineates significant differences in metabolite information coverage. *Anal. Chim. Acta* **718**, 47–57 (2012).
2. Pluskal, T., Castillo, S., Villar-Briones, A. & Orešič, M. MZmine 2: Modular framework for processing, visualizing, and analyzing mass spectrometry-based molecular profile data. *BMC Bioinformatics* **11**, 395 (2010).
3. Bijlsma, S. *et al.* Large-Scale Human Metabolomics Studies: A Strategy for Data (Pre-) Processing and Validation. *Anal. Chem.* **78**, 567–574 (2006).
4. van der Kloet, F. M., Bobeldijk, I., Verheij, E. R. & Jellema, R. H. Analytical Error Reduction Using Single Point Calibration for Accurate and Precise Metabolomic Phenotyping. *J. Proteome Res.* **8**, 5132–5141 (2009).
5. Pekmez, C. T., Bjørnshave, A., Pratico, G., Hermansen, K. & Dragsted, L. O. Pre-meal protein intake alters postprandial plasma metabolome in subjects with metabolic syndrome. *Eur. J. Nutr.* (2019). doi:10.1007/s00394-019-02039-9
6. Sumner, L. W. *et al.* Proposed minimum reporting standards for chemical analysis. *Metabolomics* **3**, 211–221 (2007).
7. Ramiro-Garcia, J. *et al.* NG-Tax, a highly accurate and validated pipeline for analysis of 16S rRNA amplicons from complex biomes [version 2; referees: 2 approved, 1 approved with reservations, 1 not approved]. *F1000Research* **5**, (2018).
8. Callahan, B. J. *et al.* DADA2: High-resolution sample inference from Illumina amplicon data. *Nat. Methods* **13**, 581–583 (2016).
9. Zoetendal, E., Heilig, H., Klaassens, E. Isolation of DNA from bacterial samples of the human gastrointestinal tract. *Nat. Protoc.* **1**, 870–873 (2006).

SUPPLEMENTAL FIGURES

Supplemental Figure 1. *Graphical summary of the study design of the trial.*

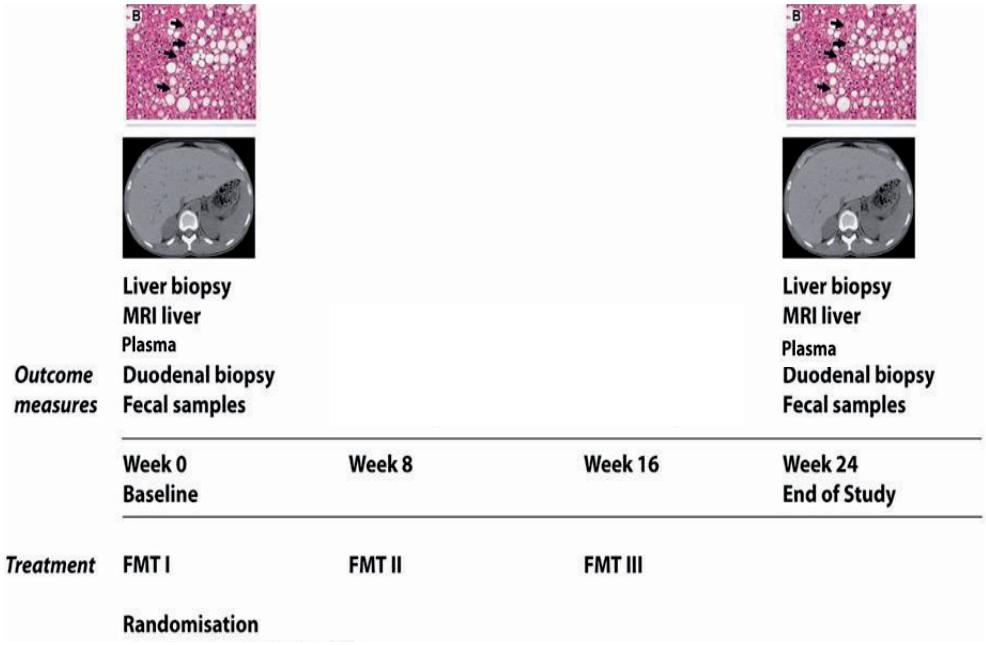

Supplemental Figure 2. *Redundancy analysis (RDA) of changes in fecal microbiota upon allogenic and autologous FMT.*

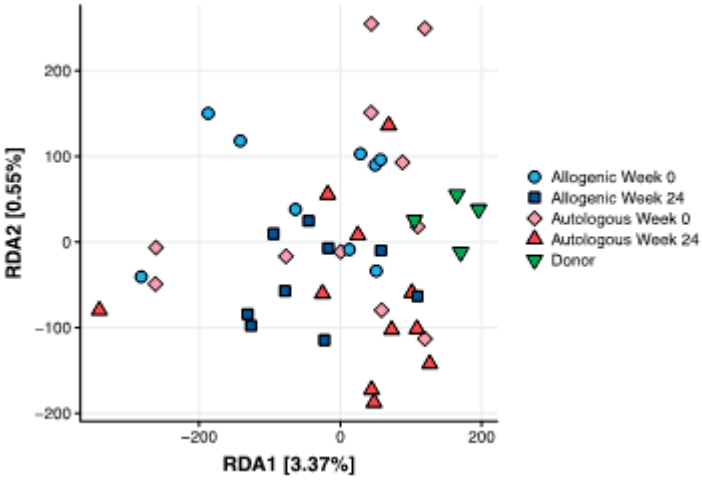

SUPPLEMENTAL TABLES

Supplemental Table 1. Optimized parameters used for pre-processing the data in mzMine2.28.

	Batch step	Parameters
Positive mode	Raw data import	
	Mass detection	Noise level: 9.0E1
	Chromatogram builder	Min time span (min): 0.02 Min height:2.0E2 ; m/z tolerance: 0.03 mz or 20 ppm
	Smoothing	Filter width: 7
	Chromatogram deconvolution	Chromatographic threshold: 95%; Search minimum in RT range (min): 0.01; Minimum relative height: 5%; Minimum absolute height: 2.5E2; Min ratio of peak/top edge: 1.5; Peak duration range (min): 0.01-0.3
	Isotopic pattern	m/z tolerance: 0.06 or 30 ppm; Retention time tolerance: 0.02; Monotonic shape; maximum charge: 1
	Join aligner	m/z tolerance: 0.03 or 20 ppm; Absolute retention time tolerance: 0.05; Weight for both m/z tolerance and retention time tolerance: 10
	Peak list rows filter	Min peaks in a row: 4 and 0 (for samples and blanks respectively) Minimum peaks in an isotope pattern: 1; m/z range: 0-1500; RT range: 0-10; peak duration range: 0.01-0.3
	Peak finder (gap filling)	Intensity tolerance: 50%; m/z tolerance: 0.02 or 15 ppm; Absolute retention time tolerance: 0.05
Negative mode	Raw data import	
	Mass detection	Noise level: 8.0E1
	Chromatogram builder	Min time span (min): 0.02; Min height: 1.8 E2 ; m/z tolerance: 0.03 mz or 20 ppm
	Smoothing	Filter width: 7
	Chromatogram deconvolution	Chromatographic threshold: 95%; Search minimum in RT range (min): 0.01; Minimum relative height: 5%; Minimum absolute height: 2.3 E2 ; Min ratio of peak/top edge: 1.5; Peak duration range (min): 0.01-0.3
	Isotopic pattern	m/z tolerance: 0.06 or 30 ppm; Retention time tolerance: 0.02; Monotonic shape; maximum charge: 1
	Join aligner	m/z tolerance: 0.03 or 20 ppm; Absolute retention time tolerance: 0.05; Weight for both m/z tolerance and retention time tolerance: 10
	Peak list rows filter	Min peaks in a row: samples: 4 blanks: 0 Minimum peaks in an isotope pattern: 1; m/z range: 0-1500; RT range: 0-10; peak duration range: 0.01-0.4
	Peak finder (gap filling)	Intensity tolerance: 50.0%; m/z tolerance: 0.02 or 15 ppm; Absolute retention time tolerance: 0.05

Supplemental Table 2. Top 10 plasma metabolites related to fecal microbiota transplantation.

Annotation/Level of Identificationx	Measured Mass (m/z)	RT (min)	Molecular Formula	Suggested ion	Fragments (m/z)	KEGG or HMDB ID
4-amino-deoxychorismate[2]	224.0607	3.83	$C_{10}H_{11}NO_5$	$[M-H]^-$	96.9587 79.9559	C11355
Desaminotyrosine[1]	165.0549	3.47	$C_9H_{10}O_3$	$[M-H]^-$	147.0432 121.0634 119.0489 106.0421	HMDB0002199
Phenlyacetylglutamine[1]	145.0606	3.15	$C_{13}H_{16}N_2O_4$	$[C_5H_9N_2O_3]^-$	263.1025[y]	HMDB0006344
Sebacic acid[1]	201.1063	3.78	$C_{10}H_{18}O_4$	$[M-H]^-$	183.1004 139.1113 111.0798	HMDB0000792
Isoleucine[1]	130.0859	0.97	$C_6H_{13}NO_2$	$[M-H]^-$		HMDB0000172
Thymol sulfate[1]	229.0530	3.88	$C_{10}H_{14}O_4S$	$[M-H]^-$	149.0962 79.9571	HMDB0062720
Phenylalanine[1]	72.0074	1.68	$C_9H_{11}NO_2$	$[C_2H_4NO_2\text{-}H]\text{-}H^-$	164.0712[y] 147.0448 103.0547	HMDB0000159
Tryptophan[1]	74.0233	2.46	$C_{11}H_{12}N_2O_2$	$[C_2H_4NO_2]^-$	203.0811[y] 142.0660 116.0494	HMDB0000929
Unknown[4]	189.0953	0.84		N	172.0683 127.0762 99.0531 74.0144	
Unknown[4]	180.9710	0.48		N		

Abbreviations: RT, retention time; min, minutes; N, negative ionization mode; Superscript letters: [x]confidence of identity: 1: confidently identified compounds 2: putatively annotated compounds 3: putatively annotated compound classes, 4: unknown compounds; y, the pseudomolecular ion.

Supplemental Table 3. Absolute fibrosis scores in biopsies according to the NASH CRN criteria.

		0 - None	1 – Mild/ Moderate	2 - Portal	3 - Bridging
Autologous FMT	Baseline	3	6	2	0
	24 weeks	2	5	4	0
Allogenic FMT	Baseline	2	5	2	1
	24 weeks	0	5	4	1

Supplemental Table 4. Daily nutritional intake in NAFLD individuals and lean vegan FMT donors

	NAFLD individuals (n=21)	Vegan donors (n=4)	P-value
Calories, kcal/day	1925.0 ± 444.4	2009.2 ± 289.8	0.760
Fat, g/day	74.7 ± 19.5	65.8 ± 13.1	0.463
Carbohydrates, g/day	198.1 ± 57.9	250.0 ± 55.6	0.174
Protein, g/day	87.3 ± 23.2	69.1 ± 6.7	0.206
Fiber, g/day	20.3 ± 7.4	46.2 ± 22.5	**0.001**

Shown is daily dietary intake, divided in four macronutrients and caloric content as calculated from a 7-day dietary record. Data are depicted as means ± standard deviation. A p-value < 0.05 was considered significant.

chapter 7

Assessment of Imaging Modalities Against Liver Biopsy in Nonalcoholic Fatty Liver Disease: The Amsterdam NAFLD- NASH Cohort

Julia J. Witjes,* Marian A. Troelstra,* Anne-Marieke van Dijk, Anne L. Mak, Oliver Gurney-Champion, Jurgen H. Runge, Diona Zwirs, Daniela Stols-Gonçalves, Aelko H. Zwinderman, Marije ten Wolde, Houshang Monajemi, Sandjai Ramsoekh, Ralph Sinkus, Otto M. van Delden, Ulrich H. Beuers, Joanne Verheij, Max Nieuwdorp, Aart J. Nederveen, Adriaan G. Holleboom

*Both authors contributed equally

Journal of Magnetic Resonance Imaging 2021,
VOLUME 54: PAGES 1937–1949

ABSTRACT

Background: Non-invasive diagnostic methods are urgently required in disease stratification and monitoring in non-alcoholic fatty liver disease (NAFLD). Multiparametric MRI is a promising technique to assess hepatic steatosis, inflammation and fibrosis, potentially enabling non-invasive identification of individuals with active and advanced stages of NAFLD.

Purpose: To examine the diagnostic performance of multiparametric MRI for the assessment of disease severity along the NAFLD disease spectrum with comparison to histological scores.

Study type: prospective, cohort.

Population: 37 patients with NAFLD.

Fieldstrength/sequence: Multiparametric MRI at 3.0T consisted of MR spectroscopy (MRS) with multi-echo stimulated-echo acquisition mode, magnitude-based and three-point-Dixon using a two-dimensional multi-echo gradient echo, MR elastography (MRE) using a generalized multi-shot gradient-recalled echo sequence and intravoxel incoherent motion (IVIM) using a multi-slice diffusion weighted single-shot echo-planar sequence.

Assesment: Histological steatosis grades were compared to proton density fat fraction measured by MRS ($PDFF_{MRS}$), magnitude-based MRI ($PDFF_{MRI-M}$) and 3-point-Dixon ($PDFF_{Dixon}$), as well as FibroScan® controlled attenuation parameter (CAP). Fibrosis and disease activity were compared to IVIM and MRE. FibroScan® liver stiffness measurements (LSM) were compared to fibrosis levels. Diagnostic performance of all imaging parameters was determined for distinction between simple steatosis and non-alcoholic steatohepatitis (NASH).

Statistical tests: Spearman's rank test, Kruskal-Wallis test, Dunn's post-hoc test with Holm-Bonferroni p-value adjustment, Receiver operating characteristic curve analysis. A p-value < 0.05 was considered statistically significant.

Results: Histological steatosis grade correlated significantly with $PDFF_{MRS}$ (r_s=0.66, p<0.001), $PDFF_{MRI-M}$ (r_s=0.68, p<0.001) and $PDFF_{Dixon}$ (r_s =0.67, p<0.001), whereas no correlation was found with CAP. MRE and IVIM diffusion and perfusion significantly correlated with disease activity (r_s=0.55, p<0.001, r_s=−0.40, p=0.016, r_s=−0.37, p=0.027

respectively) and fibrosis (r_s=0.55, p<0.001, r_s=−0.46, p=0.0051; r_s=−0.53, p<0.001 respectively). MRE and IVIM diffusion had the highest area-under-the-curve for distinction between simple steatosis and NASH (0.79 and 0.73 respectively).

Data conclusion: Multiparametric MRI is a promising method for non-invasive, accurate and sensitive distinction between simple hepatic steatosis and NASH, as well as for the assessment of steatosis and fibrosis severity.

INTRODUCTION

Along with the global increase in obesity and type 2 diabetes mellitus (T2DM), the prevalence of non-alcoholic fatty liver disease (NAFLD) is rising; in fact, NAFLD is currently the most common cause of liver dysfunction worldwide[1]. It represents a spectrum of liver disease ranging from simple hepatic steatosis, through non-alcoholic steatohepatitis (NASH) to advanced fibrosis and cirrhosis. Advanced stages may ultimately be complicated by hepatocellular carcinoma[2].

The overall global prevalence of NAFLD is estimated to be around 25% in the general population, while 60% of individuals with T2DM have NAFLD. Approximately 25% of individuals with simple steatosis are found to progress to NASH[1]. The transition from simple steatosis to NASH and especially the subsequent development of fibrosis is associated with an increased risk of cardiovascular disease and mortality from liver-related disease[3,4]. Given the potential clinical consequences, it is of crucial importance to differentiate simple steatosis from the active form of the disease (NASH) in order to identify and closely follow-up progressors along the NAFLD disease spectrum[5].

Currently, liver biopsy remains the diagnostic reference standard for NAFLD, as it is the most reliable test to distinguish simple steatosis from NASH and to assess the degree of inflammation and fibrosis[6]. However, a liver biopsy has apparent disadvantages: it is invasive with a small risk of complications (most notably bleeding) and potentially painful and labor-intensive, thus hampering its application in large scale studies. In addition, it is prone to sampling error as biopsies consist of only a focal assessment of the liver[7,8]. These drawbacks render liver biopsy a suboptimal diagnostic method for screening and monitoring of NAFLD in clinical practice.

Therefore, non-invasive methods that accurately assess hepatic fat content and even hepatic inflammation and fibrosis are in development for risk stratification of disease severity in NAFLD. Recently, Eddowes and colleagues demonstrated in a biopsy-controlled study that controlled attenuation parameter (CAP) and liver stiffness measurement (LSM) determined with vibration-controlled transient elastography on the FibroScan® device accurately assesses steatosis and fibrosis respectively in individuals with NAFLD[9]. However, this method is unable to capture the active form of the disease, i.e. steatohepatitis[10]. Therefore, MRI has been proposed as a tool to assess the full spectrum of NAFLD[11]. While many studies have compared a single MRI sequence to a histopathological outcome, few studies have assessed the full NAFLD disease spectrum.

Multiparametric MRI is a promising technique to assess hepatic steatosis as well as inflammation and fibrosis, potentially enabling non-invasive identification of individuals with active and advanced stages of NAFLD. Thus the aim of our current

proof-of-principle study is to assess the use of multiparametric MRI and determine the best performing imaging parameters for identifying the full NAFLD disease spectrum in a subgroup of the Amsterdam NAFLD-NASH cohort.

MATERIAL AND METHODS

Design

The study protocol was reviewed and approved by the institutional review board of the Amsterdam University Medical Centres, location Academic Medical Centre (AMC) and was registered in the Dutch Trial Register (registration number NTR7191). All participants in this study provided written informed consent. The Amsterdam NAFLD-NASH cohort (ANCHOR) study is an observational prospective study that aims to identify and validate non-invasive diagnostic methods, both imaging and molecular markers, for the assessment of the entire NAFLD disease spectrum. To this end, participants undergo multiparametric MRI of the liver, hepatic FibroScan®, ultrasound guided liver biopsy and urine, faeces and blood sampling both at baseline and during follow-up after five years. The study was begun at the end of 2018 and is still ongoing. It is conducted at the AMC, in compliance with the principles in the declaration of Helsinki and according to Good Clinical Practice guidelines.

Participants

The first 37 individuals from the ANCHOR study were included in this proof-of-principle analysis. Individuals from Amsterdam UMC outpatient clinics with hepatic steatosis on abdominal ultrasound performed for other clinical reasons were included. The other main inclusion criteria were age above 18 years, levels above the upper limit of normal for either ASAT and/or ALAT and a BMI above 25kg/m^2. Exclusion criteria were contraindications for undergoing MRI, excessive alcohol use (women > 14 units/week, men > 21 units/week), known bleeding disorders, the use of anticoagulant therapy and platelet aggregation inhibitors, diagnosis of decompensated liver cirrhosis and/or hepatocellular carcinoma, the use of drugs with a potential role in aggravation of pre-existing NAFLD and other known causes of liver steatosis other than NAFLD (auto-immune hepatitis, hemochromatosis, hepatitis B and/or C, Wilsons disease, alpha-1-antitrypsin deficiency).

MRI Acquisition

All individuals underwent multiparametric MRI of the liver using a clinical 3.0 Tesla MRI Unit (Ingenia; Philips, Best, the Netherlands) using a 16-channel phased-array anterior coil and a 10-channel phase-arrayed posterior coil. All data were acquired in

a single ~45-minute session. Participants were required to fast for a minimum of four hours before scanning. Images were analyzed by a single observer (M.T.) with three years of experience in hepatic MRI, who was blinded to the histopathology results.

To quantify the grade of hepatic steatosis, magnetic resonance spectroscopy (MRS), magnitude-based MRI (MRI-M) proton density fat fraction (PDFF) and 3-point Dixon were performed. MRS data acquisition was performed using a multi-echo stimulated-echo acquisition mode (STEAM), according to our previously described protocol[12]. MRI-M and 3-point Dixon consisted of a two-dimensional multi-echo gradient echo sequence with respectively six and three echo times (TE). 3-point Dixon sequence acquired both magnitude and phase data, while MRI-M only acquired magnitude data.

Disease activity and fibrosis were quantified using intravoxel incoherent motion (IVIM) imaging and magnetic resonance elastography (MRE). The IVIM sequence consisted of a free-breathing multi-slice diffusion weighted single shot echo-planar imaging sequence with 18 unique b-values. MRE was performed using a gravitational transducer at 50Hz and a generalized multi-shot gradient-recalled echo (Ristretto MRE)[13]. All imaging sequences were assessed for performance in distinguishing simple steatosis from NASH. MRI acquisition parameters and sequence details for all included sequences are listed in Table 1 and in the supplementary material, respectively.

MRI Analysis

MRS PDFF ($PDFF_{MRS}$)

MRS data analysis was performed using our previously described protocol[12]. Spectral data were fitted using the AMARES algorithm[14] in jMRUI version 4.0 (http://www.jmrui.eu/)[15]. $PDFF_{MRS}$ values for each subject were calculated using the T2-corrected water and combined fat peak amplitudes, after correcting for the amplitudes of fat peaks overlapping the water peak[16].

MRI-M PDFF ($PDFF_{MRI-M}$)

Three regions of interest (ROI) in the magnitude images of the right hepatic lobe were selected in three different slices, avoiding large vessels, bile ducts and liver edges. Mean signal intensity per TE was determined and the PDFF calculated in Matlab R2018a (Mathworks, Natick, MA, USA) using a multi-echo and multi-frequency fat signal model to correct for T2* effects[17]. The mean $PDFF_{MRI-M}$ of all three ROIs was used to establish an average fat percentage of the liver.

Table 1. Overview of MRI acquisition for each imaging sequence included.

PARAMETER	MRS	MRI-M	3-POINT DIXON	MRE	IVIM
MRS VOXEL SIZE (MM^3)	20x20x20	-	-	-	-
FIELD OF VIEW (MM^2)	-	448x320	420x300	448x448	450x295
RESOLUTION (MM^2)	-	4.0x4.0	2.4x2.4	4.0x4.0	3.0x3.0
SLICE THICKNESS (MM)	-	5	10	4	6
SLICE GAP (MM)	-	0	11.4	0	1
SLICES	-	36	5	9	27
PARALLEL IMAGING SENSE FACTOR	-	2	-	3	1.3
PARTIAL AVERAGING FACTOR	-	-	-	-	0.6
REPETITION TIME (MS)	3500	150	50	75	7000
ECHO TIME (MS)	10, 15, 20, 25, 30	1.15, 2.33, 3.51, 4.69, 5.87, 7.05	3.1, 3.88, 4.66	6.91	45.5
FLIP ANGLE (°)	-	10	5	20	90
BANDWIDTH	2000 Hz	1666 Hz	436 Hz	2146 Hz	20.8 Hz/pixel
ACQUISITION DURATION	21 second breath-hold	18 second breath-hold	19 second breath-hold	4x15 second breath-hold	8.01 min free-breathing
OTHER	- 1024 datapoints; - pencil beam volume B0 shimming	-	-	- 4 wave-phase offsets; - MEG frequency 165Hz; - Hadamard encoding; - Ristretto sequence; - Gravitational transducer 50Hz	- b-values: 0, 1, 2, 5, 10, 20, 30, 40, 50, 75, 100, 150, 200, 300, 400, 500, 600, 700 s/mm2; - SPAIR fat suppression

MRS: magnetic resonance spectroscopy, MRI-M: magnitude-based MRI, MRE: magnetic resonance elastography, IVIM: intravoxel incoherent motion; MEG: motion encoding gradient.

Three-point DIXON PDFF ($PDFF_{Dixon}$)

Magnitude images were used to draw ROIs of the liver in all slices, avoiding major blood vessels, bile ducts and liver edges. Image analysis was performed in Matlab, using a toolbox with multi-point fat-water separation using a hierarchical field map estimation[18] from the ISMRM Fat-Water Toolbox 2012 (https://github.com/maxdiefenbach/MRI_field_contributions/tree/master/fwtoolbox_v1_code). Both

phase and magnitude images were used for the reconstruction. The ROI was overlaid on the reconstructed fat image to determine an average fat $PDFF_{Dixon}$ of the entire liver in all five slices.

MRE

Images were analyzed using ROOT software[19] as described previously by Sinkus et al.[20]. Phase images were locally unwrapped and filtered using a Gaussian filter (width σ 0.5). Viscoelastic parameter maps were reconstructed using a finite element-based inversion algorithm[21]. Mean stiffness based on the shear modulus (*G'*)) and loss modulus (*G''*) was determined from an ROI drawn in the middle three slices, proximal to the transducer, avoiding large vessels and liver edges[13].

IVIM imaging

ROIs were drawn in all slices containing liver tissue in the reconstructed combined b-value images, avoiding large vessels, bile ducts and liver edges. Slices or areas with artefacts were excluded from the mask. Diffusion (D), pseudo-diffusion (D*) and perfusion fraction (F) parameter maps of the masked regions were compiled in MATLAB using a Bayesian-probability based fit[22]. Mean values across the masked liver area were reported for D, D* and F.

FibroScan® CAP and LSM

FibroScan® examinations were performed by a physician (J.W., A.v.D. or A.M.) who performed over 50 examinations and was blinded to the participants' histological evaluation. The device used was a FibroScan® 530 Compact (Echosens, France) equipped with both the M- and XL-probe. The type of probe used depended on the real-time assessment of the skin-to-liver capsule distance for each participant. The measurement was obtained in fasting condition of at least 2 hours with the participant in a supine position with their right arm fully abducted. Measurements were performed in the right liver lobe through a midaxillary intercostal space. FibroScan® was performed either at the moment of screening, within a month of the MRI and liver biopsy, or on the day of MRI. By using transducer-induced vibrations, the FibroScan® captures simultaneous recordings of CAP to quantify hepatic steatosis, and transient elastography to obtain LSM as an indicator of the presence of liver fibrosis[23].

Liver biopsy

Percutaneous ultrasound-guided liver biopsies were performed by either an interventional radiologist or a hepatologist according to local standard procedure. All histologic specimens were scored by a liver pathologist (J.V., fifteen years of

experience), who was blinded to all other data. Biopsy samples were stained using a hematoxylin and eosin (H&E) stain and a Sirius Red (SR) stain. The histological parameters were defined with the use of the steatosis, activity and fibrosis (SAF) score[24], classifying either non-NAFLD, simple steatosis or NASH. The SAF-score graded the degree of steatosis by the percentage of hepatocytes containing large and medium-sized intracytoplasmic lipid droplets, on a scale of 0–3 (0: <5%; 1: 5–33%; 2: 34–66%; 3: >67%); hepatocellular ballooning was graded from 0 to 2 (0: normal hepatocytes; 1: clusters of hepatocytes with rounded shape and pale cytoplasm, but normal size; 2: as for grade 1, but with at least one enlarged/ballooned hepatocyte); and lobular inflammation was defined as a focus of 2 or more inflammatory cells within the lobule organized either as microgranulomas or located within the sinusoids (grade 0: none; 1:<–2 foci per lobule; 2:>2 foci per lobule). NAFLD was defined by the presence of steatosis in at least 5% of the hepatocytes. NASH was diagnosed in cases with steatosis where hepatocellular ballooning grade was ≥1 and where lobular inflammation grade ≥1 was present. Activity grade (A0-4) was the unweighted addition of hepatocyte ballooning and lobular inflammation. Fibrosis was scored according to the NASH Clinical Research Network (CRN)[25] as follows: stage 0 (F0) no fibrosis; stage 1 (F1): 1a or 1b perisinusoidal zone 3 or 1c periportal fibrosis; stage 2 (F2): perisinusoidal and periportal fibrosis without bridging; stage 3 (F3): bridging fibrosis; and stage 4 (F4): cirrhosis.

Statistical analysis

Was performed using R version 3.6.3[26]. For baseline differences between two groups, unpaired Student t-test or the Mann-Whitney U test was used depending on the distribution of the data. Normality was tested according to the Shapiro-Wilk method. Differences in median or means between the simple steatosis and NASH groups were determined for all imaging parameters, expressed as mean ± standard deviation or median with interquartile range. Spearman's rank test was used for correlation analysis, as all parameters were non-parametric. A p-value < 0.05 was considered statistically significant. Comparison of medians for analysis of multiple groups was performed using the Kruskal-Wallis test, followed by Dunn's post-hoc test with Holm-Bonferroni p-value adjustment when appropriate. Correlations and comparison of medians were assessed for steatosis grade compared to $PDFF_{MRS,\ MRI-M,\ Dixon}$ and FibroScan® CAP; activity grade compared to IVIM and MRE; and fibrosis grade compared to IVIM, MRE and FibroScan® LSM. Receiver operating characteristic (ROC) curve analysis was used to determine the diagnostic performance of imaging parameters, reporting the area under the receiver operating characteristic (AUROC) and optimal cut-off values with sensitivity and specificity. ROC analysis was used to assess the performance of $PDFF_{MRS,\ MRI-M,\ Dixon}$ and FibroScan® CAP for distinguishing

between steatosis S1 and S2-3; MRE and IVIM for distinguishing between no/mild fibrosis (F0-F2) and advanced fibrosis (F3-F4). Finally, ROC analysis was reported for determining the performance of all imaging parameters for stratifying individuals in simple steatosis and NASH groups. In case of missing data, the analysis was performed for all available parameters.

RESULTS

Inclusion

Between September 2018 and October 2020, a total of 37 individuals (23 men, 14 women) with hepatic steatosis on ultrasound were included. Mean age of the participants was 49.0 years (SD±13.2) and mean BMI was 33.2 kg/m^2 (SD±3.8). No adverse events were recorded during the MRI or liver biopsy. Liver biopsy was performed within one week of the MRI, with the exception of one participant whose biopsy was performed 2 months after the MRI. MRE data were not available for two individuals due to technical issues with the MRE hardware, one IVIM scan was not included in the analysis due to a low signal-to-noise ratio and data was missing for one $PDFF_{Dixon}$. Clinical characteristics of the participants are shown in **Table 2**.

Liver histology results

All biopsies were included in the final analysis. The mean biopsy length was 18mm (SD±5.5). Twenty participants fell in the S1 grade, thirteen S2 and four S3. Disease activity according to the SAF-score showed three individuals with no activity (A0), twelve A1, sixteen A2, five A3 and one A4. According to the SAF-score, NASH was present in 22 of the 37 participants. According to the NASH-CRN criteria for fibrosis, two individuals exhibited no fibrosis (F0), seven F1, twenty F2, seven F3 and one cirrhosis (F4). Of the two individuals with missing MRE data, one had F2 and one F4. IVIM data was missing for an individual with F2.

Steatosis grade did not correlate with either disease activity grade (rs=0.26, p=0.12) or fibrosis stage (rs=-0.04, p=0.81). Fibrosis grade did correlate significantly with disease activity score (rs=0.65, p<0.001).

Assessment of steatosis

Histological steatosis grade correlated significantly with $PDFF_{MRS}$ (r_s=0.66, p<0.001), $PDFF_{MRI-M}$ (r_s=0.68, p<0.001) and $PDFF_{Dixon}$ (r_s =0.67, p<0.001). Differences in hepatic fat fraction between grades of steatosis indicated a significant difference in the percentage of hepatic fat and steatosis grade ($PDFF_{MRS}$: χ^2=15.75, p<0.001, df=2; $PDFF_{MRI-M}$: χ^2=16.54, p<0.001, df=2; $PDFF_{Dixon}$: χ^2=15.99, p<0.001, df=2). All three

Table 2. Clinical characteristics of 37 individuals with biopsy-proven NAFLD.

	Reference range	Study participants, N = 37
Age, y		49.0 ± 13.2
Male gender, %		62
BMI, kg/m^2		33.2 ± 3.8
T2DM, %		43
Glucose, mmol/L	3.5 – 6.1	5.9 [5.4-8.2]
ASAT, IU/L	0 – 40	41.5 [37.0-51.0]
ALAT, IU/L	0 – 40	59 [46.5-79.0]
ALP, IU/L	40 – 120	88.0 ± 29.0
g-GT, IU/L	6 – 50	62.0 [42.0-88.0]
Cholesterol, mmol/L	3 – 5.5	5.2 ± 1.0
HDL-C, mmol/L	0.9 – 1.7	1.2 ± 0.3
LDL-C, mmol/L	1.6 – 4.8	3.0 ± 1.0
Triglycerides, mmol/L	0.7 – 2.1	2.2 [1.3-2.5]
CRP, mg/mL	0 – 5	2.9 [1.7-4.3]
Steatosis, %		30.0 [20.0-50.0]
Fibrosis score		2.0 [1.5-2.0]

Data are expressed as mean ± standard deviation or median [interquartile range], depending on the distribution of the data. BMI: body mass index, ALP: alkaline phosphatase, g-GT: gamma glutamyl transferase, ALAT: alanine aminotransferase, ASAT aspartate aminotransferase, HDL: high density lipoprotein, LDL: low density lipoprotein, CRP: C-reactive protein.

methods showed a significant difference in medians between steatosis grade 1 and grade 2, and grade 1 and grade 3 **(Figure 1)**. In contrast, we found no correlation between histological steatosis grade and CAP measured by FibroScan® (r_s =0.04, p=0.82) **(Supplemental Figure 1)**.

ROC analysis for differentiating S1 from S2-S3 showed similar values for all three MRI methods. $PDFF_{MRS}$ had an AUROC of 0.86 (95% CI 0.74-0.98) with a sensitivity of 70.6% and specificity 100% at a cut-off value of 21.98%. $PDFF_{MRI-M}$ showed an AUROC of 0.87 (95% CI 0.75-0.99) with a sensitivity of 70.6% and specificity of 95.0% at a cut-off of 22.93%. $PDFF_{Dixon}$ had an AUROC of 0.86 (95% CI 0.74-0.99), with a sensitivity of 68.8% and specificity 95.0% at a cut-off of 20.53%.

$PDFF_{MRS}$, $PDFF_{MRI-M}$ and $PDFF_{Dixon}$ strongly correlated amongst themselves ($PDFF_{MRS}$ versus $PDFF_{MRI-M}$: r(35)=0.99, p<0.001; $PDFF_{MRS}$ versus $PDFF_{Dixon}$: r(34)=0.98, p<0.001; $PDFF_{MRI-M}$ versus $PDFF_{Dixon}$: r(34)=0.99, p<0.001).

Assessment of disease activity: lobular inflammation and hepatocyte ballooning

MRE

G' showed a significantly positive correlation with activity grade (r_s=0.55, p<0.001), and comparison of stiffness results for individual activity grades showed a significant difference in medians between the groups (χ^2=11.02, df=4, p=0.026) **(Figure 2)**. *G''* did

Figure 1. MRS and MRI based PDFF values versus histological steatosis grade as seen in H&E stain.

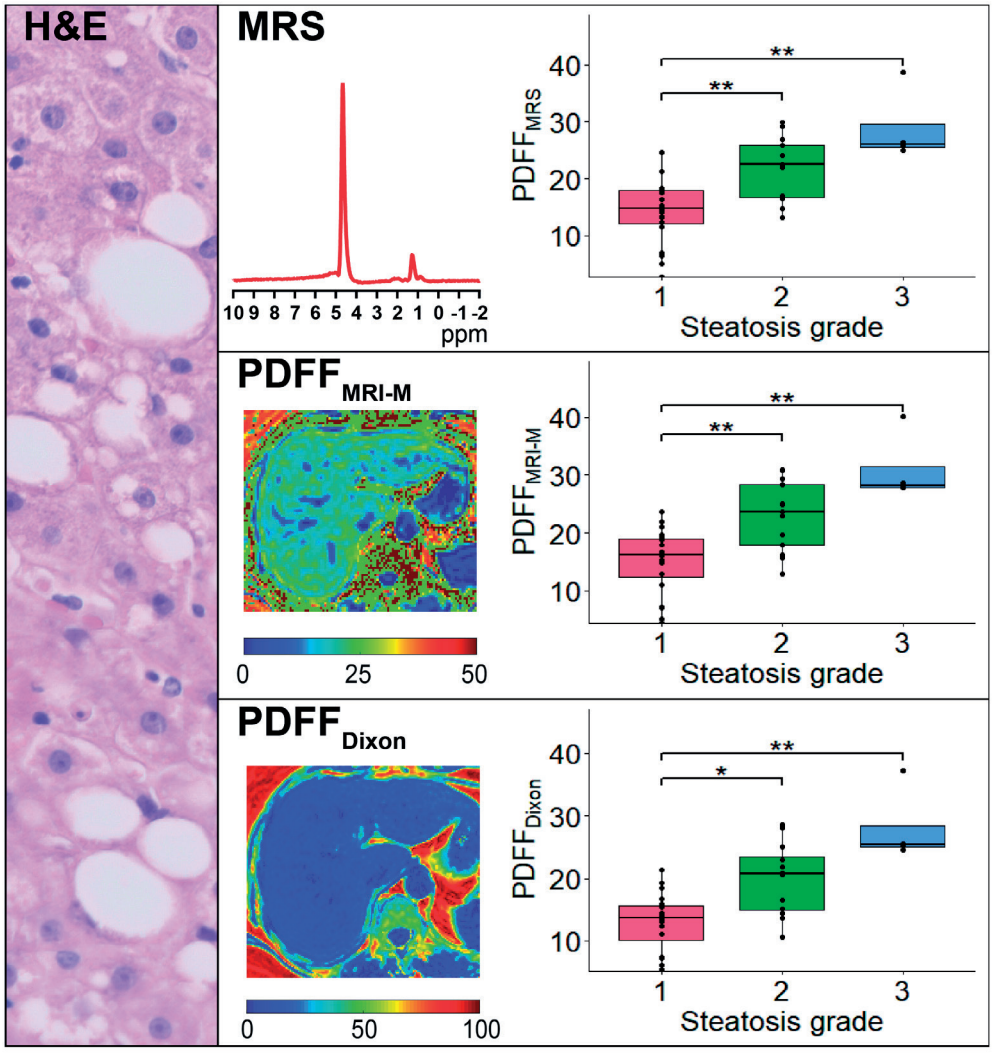

Median PDFF values for grade 1, 2 and 3 were 14.8%, 22.5% and 26.1% respectively, for PDFFMRS; 16.2%, 23.7% and 28.2% respectively, for PDFFMRI-M; and 13.6%, 20.7% and 25.4% respectively, for PDFFDixon. All three parameters showed a significant difference in medians between grades 1-2 and grades 1-3.

not show a correlation with activity grade (r_s=0.28) or difference in medians between groups (χ^2=7.44, df=4, p=0.11).

IVIM

For both D (r_s=-0.40, p=0.016) and F (r_s=-0.37, p=0.027), we found a significant negative correlation with histological activity grade. D* had no significant correlation with activity grade. Kruskal-Wallis tests did not show a significant difference in

medians between activity grades for any IVIM parameter (D: χ^2=8.00, df=4, p=0.11; D*: χ^2=4.05, df=4, p=0.40; F: χ^2=6.73, df=4, p=0.15) **(Figure 2)**.

FibroScan® LSM

Liver stiffness measured by FibroScan® showed a significant correlation with histological activity grade (r_s=0.43, p=0.0077). However, comparison of medians did not show significant differences between activity grades (χ^2=7.58, df=4, p=0.11) **(Supplemental Figure 2)**.

Assessment of the individual components of the activity score revealed that MRE (r_s=0.55, p<0.001), IVIM D (r_s=−0.37, p=0.025), IVIM F (r_s=−0.35, p=0.037) and FibroScan® LSM (r_s=0.45, p=0.0087) correlated significantly with ballooning. In contrast, none of the available imaging modalities correlated with histopathological inflammation grade. Comparison of medians revealed a significant difference between ballooning grades for MRE (χ^2=10.46, df=2) and FibroScan® LSM (χ^2=7.69, df=2, p=0.021). Inflammation grade did not show significant differences in medians for any imaging modality.

Assessment of fibrosis

MRE

We noted a significant positive association between MRE shear stiffness and the histological fibrosis score (r_s=0.55, p<0.001). Furthermore, we observed a significant difference between liver stiffness and fibrosis stage (χ^2=14.45, p=0.0024, df=3). Post-hoc analysis showed a significant difference in liver stiffness between fibrosis stage F0-F3, F1-F3 and F2-F3 **(Figure 3)**. *G''* did not provide a significant correlation with fibrosis grade (rs=0.27, p=0.11) or show significant differences between the various grades (χ^2=4.09, df=3, p=0.25).

For distinguishing individuals with no/mild (F0-F2) versus advanced (F3, due to lack of F4 data in MRE cohort) fibrosis grade, the AUROC for MRE was 0.92 (95% CI 0.83-1), with a sensitivity of 100% and a specificity of 78.6% at an optimal cut-off of 2.30 kPa. *G''* showed an AUROC of 0.74 (95% CI 0.48-1), with a sensitivity of 71.4% and specificity of 92.9% at an optimal cut-off of 0.94 kPa.

IVIM

Significant correlations between IVIM parameters and fibrosis grade were found for two of the three parameters: D (r_s=−0.46, p=0.0051) and F (r_s=−0.53, p<0.001). D* did not show a significant correlation (r_s=−0.26, p=0.13). Differences in medians for IVIM parameters between fibrosis stages only indicated a significant difference for F (χ^2=13.39, df=4), and not for D (χ^2=7.78, p=0.10, df=4) or D* (χ^2=3.03, p=0.55, df=4). Post-hoc analysis only showed a significant difference between the median F values of the F0 and F3 stages **(Figure 3)**.

Figure 2. MRE and IVIM parameters versus histological disease activity grade as seen in H&E stain.

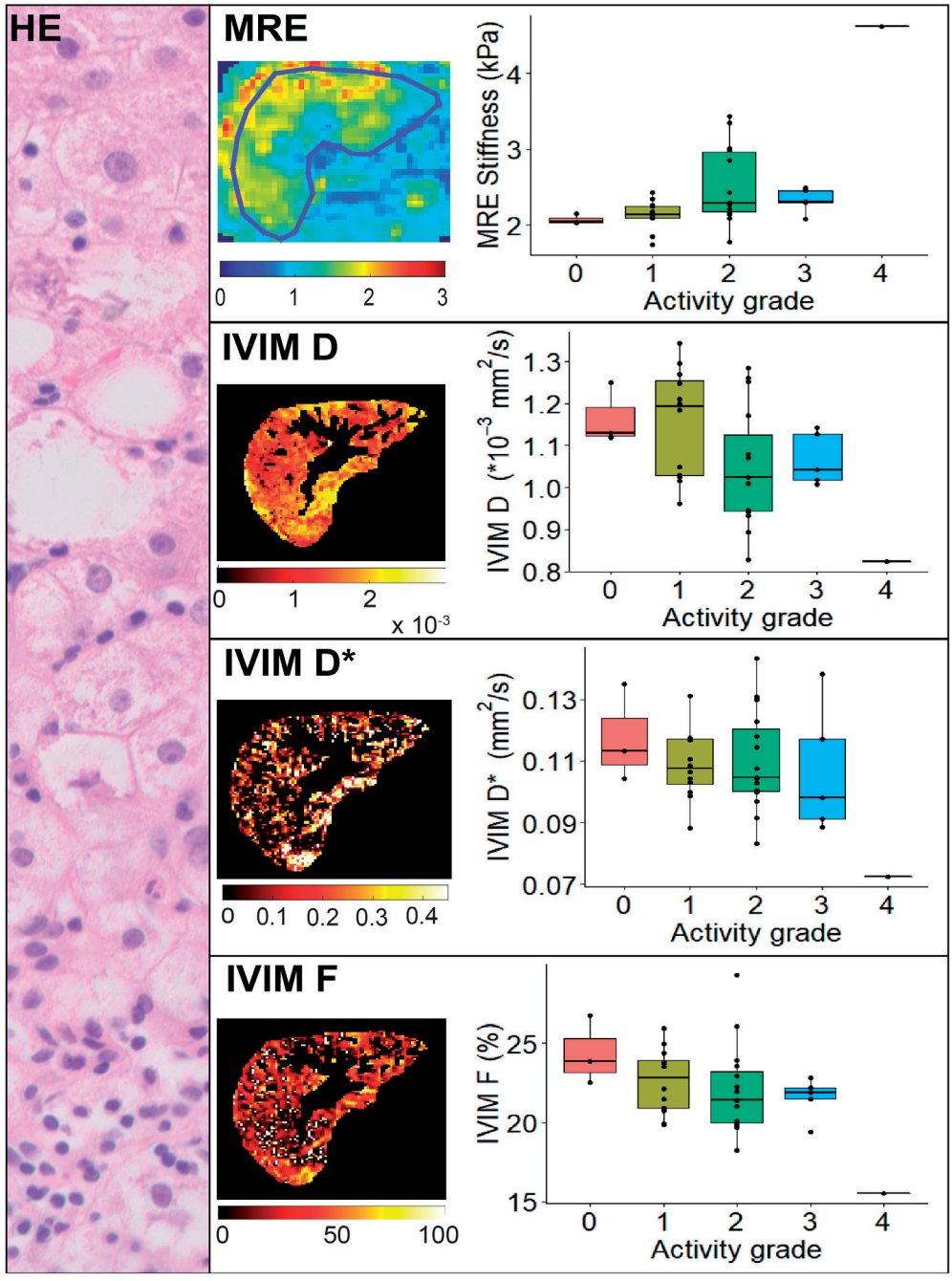

MRE showed median stiffness values of: 2.04 kPa for grade 0, 2.14 kPa for grade 1, 2.29 kPa for grade 2, 2.31 kPa for grade 3 and a single value of 4.62 kPa for grade 4. Kruskal–Wallis tests indicated a significant difference in medians between activity grades, however, post-hoc analysis did not provide a significant difference between individual grades. Median IVIM values for grade 0, 1, 2, 3 and 4 were 1.13, 1.19, 1.03, 1.04, 0.83 ×10−3 mm2/s respectively, for D; 0.11, 0.11, 0.10, 0.10, 0.07 mm2/s respectively, for D*; and 23.8, 22.8, 21.4, 21.9, 15.5% for F. No IVIM parameters showed a significant difference in medians between activity grades.

Distinction between no/mild (F0-F2) and advanced (F3-F4) fibrosis for D resulted in an AUROC of 0.79 (95% CI 0.63-0.95), with a sensitivity of 75.0% and specificity of 78.6% at an optimal cut-off value of 0.00102 mm^2/s. D* had an AUROC of 0.70 (95% CI 0.47-0.93), with a sensitivity of 62.5% and specificity of 75.0% at a cut-off of 0.10 mm^2/s. F performed best out of the IVIM parameters for distinguishing between mild and advanced fibrosis with an AUROC of 0.88 (95% CI 0.72-1), sensitivity of 75.0% and specificity of 100% at an optimal cut-off at 19.85%.

FibroScan® LSM

There was a significant correlation between LSM by FibroScan® and histological fibrosis grade (r_s=0.47, p=0.0034), however, differences in liver stiffness between stages of fibrosis indicated no significant difference between liver stiffness and fibrosis stage (χ^2=8.27, p=0.082, df=4) **(Supplemental Figure 3)**.

Distinction between no/mild (F0-F2) and advanced (F3-F4) fibrosis using FibroScan® LSM resulted in an AUROC of 0.77 (95% CI 0.58-0.96), with a sensitivity of 87.5% and specificity of 69.0% at an optimal cut-off value of 9.9kPa.

Distinction simple steatosis - NASH

As reported under "Liver histology results", NASH was histopathologically identified in 22 of the 37 participants using the SAF-score. For MRE *G'* (W=62, p=0.0027), IVIM D (t=2.66, df=31.97, p=0.012) and FibroScan® LSM (W=89, p=0.019) medians of the NASH group were all significantly different compared to the simple steatosis group **(Figure 4)**. IVIM F, D* and steatosis imaging parameters did not correlate with the presence of NASH.

To determine the performance of each imaging modality for distinguishing individuals with NASH from those with simple steatosis, ROC analysis was performed. AUROC, sensitivity and specificity values for each imaging modality are reported in **Table 3**. MRE G' showed the highest AUROC of 0.79, followed by FibroScan LSM and IVIM D (both 0.73). Of these, specificity was highest for both MRE and Fibroscan LSM at 86.7%, while IVIM D showed the highest sensitivity at 85.7%.

Figure 3. MRE and IVIM parameters versus histological fibrosis grade as seen in SR stain.

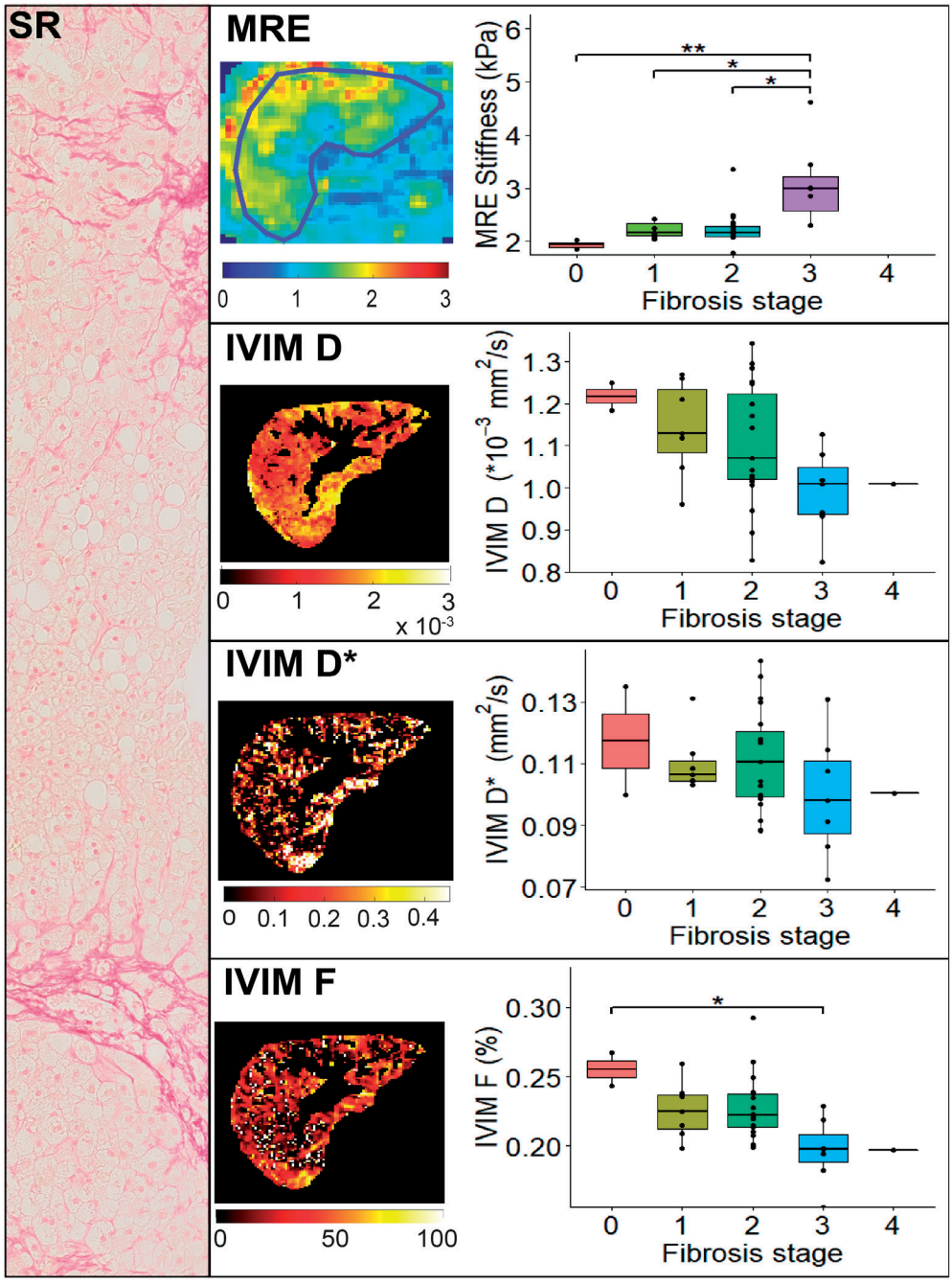

Median MRE stiffness values were: 1.93 kPa for grade 0, 2.16 kPa for grade 1, 2.17 kPa for grade 2 and 2.99 kPa for grade 3. There was a significant difference in medians between fibrosis grades 0–3, grades 1–3 and grades 2–3. Median IVIM values for grades 0, 1, 2, 3 and 4 were 1.22, 1.14, 1.10, 0.99, 1.01 ×10−3 mm2/s respectively, for D; 0.12, 0.11, 0.11, 0.10, 0.10 mm2/s respectively, for D*; and 25.5, 22.5, 22.2, 19.7, 19.7% respectively, for F. Only IVIM F showed a significant difference in medians between fibrosis grades 1–3.

Figure 4. MRE G', FibroScan LSM and IVIM D parameters for simple steatosis versus NASH individuals.

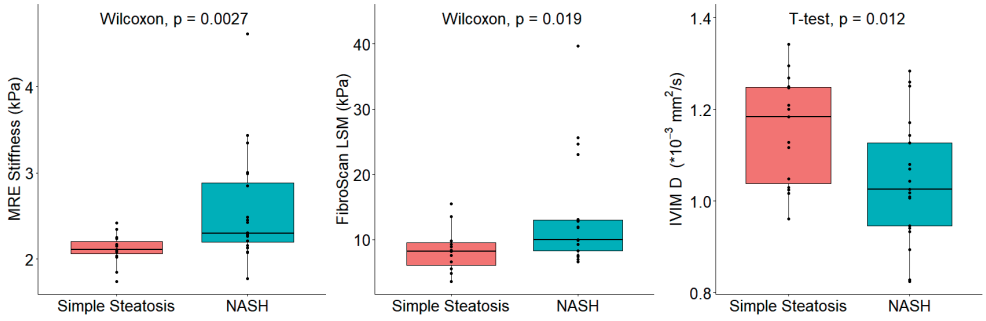

Median MRE G' values were 2.11 kPa for simple steatosis and 2.30 kPa for NASH. Median FibroScan LSM values were 8.35 kPa for simple steatosis and 13.1 kPa for NASH. Median D values were 1.15 ×10-3 mm2/s for simple steatosis and 1.04 ×10-3 for NASH. All three parameters showed a significant difference in median/mean between the simple steatosis and NASH group, in contrast to other imaging parameters.

Table 3. Diagnostic performance of imaging parameters in distinguishing between simple steatosis and NASH.

	AUROC	CUT-OFF VALUES	SENSITIVITY (%)	SPECIFICITY (%)
MRE G'	0.79	2.27 kPa	70	86.7
FIBROSCAN® LSM	0.73	9.9 kPa	63.6	86.7
IVIM D	0.73	0.0012 mm2/s	85.7	53.3
MRE G''	0.69	0.88 kPa	45	100
IVIM F	0.68	22.90%	81	53.3
FIBROSCAN® CAP	0.65	336 m/s	77.3	53.3
IVIM D*	0.58	0.10 mm2/s	47.6	80
$PDFF_{MRI-M}$	0.57	23.72%	40.9	86.7
$PDFF_{MRS}$	0.56	21.19%	45.5	73.3
$PDFF_{DIXON}$	0.52	21.84%	33.3	86.7

MRE: magnetic resonance elastography, LSM: liver stiffness measurement, IVIM D: intravoxel incoherent motion diffusion imaging, IVIM F: intravoxel incoherent motion perfusion fraction imaging, CAP: controlled attenuation parameter, IVIM D*: intravoxel incoherent motion pseudodiffusion imaging, $PDFF_{MRI-M}$: magnitude-based MRI proton density fat fraction, $PDFF_{MRS}$: magnetic resonance spectroscopy proton density fat fraction, $PDFF_{Dixon}$: three-point DIXON proton density fat fraction.

DISCUSSION

The present proof-of-principle analysis shows that with the use of multiparametric MRI, NAFLD severity - particularly steatosis and fibrosis, and to a lesser extent disease activity - can be assessed. To evaluate the risk of progression towards advanced NASH and fibrosis and to determine treatment and monitoring plans, distinction between simple steatosis and NASH, and detection and staging of fibrosis are essential, yet challenging, components in the workup of an individual

with NAFLD. This study presents the initial results from the Amsterdam NAFLD-NASH cohort (ANCHOR) study, aimed at improving the non-invasive diagnosis and follow-up of individuals with various grades and stages of NAFLD. Inclusion in the Amsterdam NAFLD cohort is still ongoing and future studies in this cohort will have to determine whether a combination of these MRI parameters can be used to predict histopathological outcomes. The current population captures the complete spectrum of NAFLD disease severity.

The non-invasive assessment of hepatic steatosis has been extensively studied for all of the imaging techniques used in this study: CAP, $PDFF_{MRS}$, $PDFF_{MRI-M}$ and $PDFF_{Dixon}$ [9,16,17,27]. Our findings are consistent with previous reports, showing strong correlations between steatosis grade and PDFF found with the MRI techniques. The strong correlation amongst the three MRI techniques would suggest that a single imaging technique for determining steatosis should be sufficient when performing multiparametric MRI.

Interestingly, FibroScan® CAP measurements did not correlate with histological steatosis grade, in contrast with previous studies[9,12]. At S1 steatosis grade, the CAP values showed a large spread in the, and medians of CAP did not differ between the three histological steatosis grades (S1-S3). This could potentially be due to our sample size and the relatively sizeable percentage of patients with S1 steatosis. In a recent cohort study, Eddowes and colleagues found no difference in CAP between histological steatosis grades 2 and 3 [9], indicating the small difference in CAP values between these groups, which may only be observable in large cohorts. Another explanation could be the nonlinear relationship of CAP values with the number of hepatocytes affected and grade of steatosis at biopsy[12], complicating the use of CAP as a tool to stage hepatic steatosis.

MRE *G'*, IVIM D and IVIM F significantly correlated with the disease activity score, despite substantial overlap between values of the various levels. We also performed an analysis of the individual components of the activity score, comprised of inflammation and ballooning. MRE *G'*, IVIM F, IVIM D and FibroScan® LSM showed significant correlations with ballooning, while only IVIM D correlated with inflammation. Previous studies have shown correlations between MRE *G'* measurements and inflammation and/or ballooning stages[28,29], yet also with substantial overlap between severity grades. Loss modulus measured via MRE has shown promising results for evaluating inflammation levels[30,31], but this correlation was not present in our cohort. Murphy and colleagues showed a correlation between IVIM F and both inflammation and ballooning, however, those correlations did not uphold in a multivariable regression analysis[32]. Poor correlations between imaging parameters and inflammation grade were likely caused by a relatively small spread in our cohort, with the majority exhibiting lobular inflammation grade 1 (n = 32). The

imaging correlations with activity score were thus chiefly driven by the contrast in ballooning grade.

Staging individuals with NAFLD by fibrosis severity has clear prognostic consequences: progression into the fibrotic stages of NAFLD is strongly associated with liver-related and overall mortality[3,4], thus timely detection of NAFLD fibrosis is necessary. Here we show the capability of multiparametric MRI in differentiating between no/mild (F0-F2) and advanced (F3-F4) fibrosis.

Differences in MRE hardware, MRE scan acquisition techniques, vibrational frequencies and post-processing techniques make it difficult to directly compare stiffness values found with MRE between studies[33]. No previous studies with MRE wave generation of 50 Hz in individuals with NAFLD are available, however, a larger retrospective study scanned at 60 Hz showed a similar diagnostic accuracy for distinguishing F0-F2 from F3-F4 (AUROC 0.954, sensitivity 0.85, specificity 0.929 at a cut-off of 4.15 kPa)[34].

Diagnostic accuracy of LSM by FibroScan® for distinguishing no/mild fibrosis from advanced fibrosis was found to be inferior to MRE, as reported in previous studies[35]. LSM accuracy in this study was slightly inferior to the diagnostic performance found in a recent study by Eddowes and colleagues, reporting an AUROC of 0.80 (95% CI, 0.75-0.84)[9].

A recent review assessing correlations between IVIM and fibrosis grade showed substantial heterogeneity in found results[36]. In the present study, IVIM F showed a strong correlation with fibrosis stage and showed good performance for distinguishing between no/mild and advanced fibrosis, yet issues with reproducibility shown in previous studies[37] require further investigation.

Differentiating NASH from simple steatosis enables early detection of typically asymptomatic active disease. Currently available serum biomarkers for non-invasively differentiating simple steatosis from NASH such as ALT-levels and cytokeratin-18 fragments are suboptimal, exhibiting poor reproducibility and low accuracy[38]. The FAST score however, a score that identifies patients with progressive NASH and has been validated in multiple large global cohorts, showed good performance with an AUROC ranging from 0.74 to 0.95[10]. Previous MRI-based studies have shown promising results for the distinction of simple steatosis from NASH using various techniques. T1-based liver inflammation score showed an AUROC of 0.80, however, while the sensitivity was high at 91%, specificity proved to be limited at 52%[39]. Ultrasmall superparamagnetic iron oxide particle (USPIO)–enhanced MRI found an AUROC of 0.87 in a group of 24 participants[40], yet concerns raised about the safety of USPIO administration[41] make it less desirable as a diagnostic method. A previous MRE study showed an AUROC of up to 0.93 for distinguishing between NASH and simple steatosis using MRE shear stiffness, yet these findings suggest that this could

be explained by the increase in liver stiffness caused by fibrosis[28]. More recent work assessing MRE for identifying cases with NASH and fibrosis ≥2 suggest other results, with an AUROC of only 0.66[42]. Hence, disease stratification in NAFLD is currently still reliant on liver biopsy, which comes with several disadvantages, as described in the introduction.

The current proof-of-concept study shows that the MRI parameters MRE *G'* and IVIM D have the potential to non-invasively differentiate simple steatosis from NASH. Of these methods, sensitivity was highest for IVIM D and specificity highest for MRE *G'*. Non-invasive methods with a high specificity such as MRE are particularly interesting as they have the potential to reduce the amount of liver biopsies in individuals with an early disease stage.

Development of models using a combination of imaging parameters, with or without ultrasonic parameters and plasma biomarkers to distinguish between simple steatosis, are of increasing interest. In recent work an AUROC of 0.87 was found combining MRE with PDFF for distinguishing between simple steatosis and NASH[43], while the combination of cT1, AST and fasting glucose levels had an AUROC of 0.90 for identifying NASH with fibrosis ≥ 2[44]. Finding the ideal combination of biomarkers will be the focus of further studies from the ANCHOR cohort.

Limitations

We report the initial results from the ANCHOR cohort study with promising diagnostic performance of multiparametric MRI in NAFLD, however, while the current population captures the complete spectrum of NAFLD disease severity, not all groups were evenly represented, and the cohort size is modest. Multiple imaging modalities correlated with histopathology, however, the median values found with MRI often did not significantly differ between the histopathologically determined disease severity grades due to the limited number of subjects in some groups. Furthermore, combination of outcomes in a multivariate regression analysis will only be possible when the ANCHOR cohort has advanced in size in the upcoming years. This would be of additional value as single imaging parameters have often provided promising results, but either show overlapping values between the target groups or lack sensitivity and/or specificity for providing a definite diagnosis. While power analysis for distinction between simple steatosis and NASH shows that a sample size starting from 23 participants for the best performing imaging parameter should be sufficient, theory suggests that introduction of a logistical regression model would require a minimum of 100 participants[45], making this the minimum sample size for ensuing MRI studies from this cohort. Furthermore, MRE data for two individuals were unavailable, leaving no individuals with F4 fibrosis and limiting the assessment of its diagnostic accuracy in fibrosis severity. Finally, the use of a liver biopsy as a

reference standard has the chance of sampling error and inter-observer variability. This emphasizes the advantage of MRI, capturing the entire liver with quantitative measurements.

CONCLUSION

Overall, our results indicate that multiparametric MRI is a promising non-invasive method for the accurate assessment of steatosis and fibrosis severity, as well as ballooning, with the potential to distinguish between simple hepatic steatosis and NASH.

REFERENCES

1. Younossi, Z. *et al.* Global Perspectives on Nonalcoholic Fatty Liver Disease and Nonalcoholic Steatohepatitis. *Hepatology* **69**, 2672–2682 (2019).
2. Hardy, T., Oakley, F., Anstee, Q. M. & Day, C. P. Nonalcoholic Fatty Liver Disease: Pathogenesis and Disease Spectrum. *Annu. Rev. Pathol. Mech. Dis.* (2016). doi:10.1146/annurev-pathol-012615-044224
3. Dulai, P. S. *et al.* Increased risk of mortality by fibrosis stage in nonalcoholic fatty liver disease: Systematic review and meta-analysis. *Hepatology* **65**, 1557–1565 (2017).
4. Taylor, R. S. *et al.* Association Between Fibrosis Stage and Outcomes of Patients With Nonalcoholic Fatty Liver Disease: A Systematic Review and Meta-Analysis. *Gastroenterology* **158**, 1611–1625.e12 (2020).
5. Diehl, A. M. & Day, C. Cause, Pathogenesis, and Treatment of Nonalcoholic Steatohepatitis. *N. Engl. J. Med.* **377**, 2063–2072 (2017).
6. Marchesini, G. *et al.* EASL–EASD–EASO Clinical Practice Guidelines for the management of non-alcoholic fatty liver disease. *J. Hepatol.* **64**, 1388–1402 (2016).
7. Gilmore, I. T. *et al.* Indications, methods, and outcomes of percutaneous liver biopsy in England and Wales: an audit by the British Society of Gastroenterology and the Royal College of Physicians of London. *Gut* **36**, 437–441 (1995).
8. Seeff, L. B. *et al.* Complication Rate of Percutaneous Liver Biopsies Among Persons With Advanced Chronic Liver Disease in the HALT-C Trial. *Clin. Gastroenterol. Hepatol.* **8**, 877–883 (2010).
9. Eddowes, P. J. *et al.* Accuracy of FibroScan Controlled Attenuation Parameter and Liver Stiffness Measurement in Assessing Steatosis and Fibrosis in Patients With Nonalcoholic Fatty Liver Disease. *Gastroenterology* **156**, 1717–1730 (2019).
10. Newsome, P. N. *et al.* FibroScan-AST (FAST) score for the non-invasive identification of patients with non-alcoholic steatohepatitis with significant activity and fibrosis: a prospective derivation and global validation study. *Lancet Gastroenterol. Hepatol.* **5**, 362–373 (2020).
11. Dulai, P. S., Sirlin, C. B. & Loomba, R. MRI and MRE for non-invasive quantitative assessment of hepatic steatosis and fibrosis in NAFLD and NASH: Clinical trials to clinical practice HHS Public Access. *J Hepatol* **65**, 1006–1016 (2016).
12. Runge, J. H. *et al.* MR Spectroscopy–derived Proton Density Fat Fraction Is Superior to Controlled Attenuation Parameter for Detecting and Grading Hepatic Steatosis. *Radiology* **286**, 547–556 (2018).
13. Runge, J. H. *et al.* A novel magnetic resonance elastography transducer concept based on a rotational eccentric mass: preliminary experiences with the gravitational transducer. *Phys. Med. Biol.* **64**, 045007 (2019).
14. Vanhamme, L., van den Boogaart, A. & Van Huffel, S. Improved Method for Accurate and Efficient Quantification of MRS Data with Use of Prior Knowledge. *J. Magn. Reson.* **129**, 35–43 (1997).
15. Stefan, D. *et al.* Quantitation of magnetic resonance spectroscopy signals: the jMRUI software package. *Meas. Sci. Technol.* **20**, 104035 (2009).
16. Hamilton, G. *et al.* In vivo characterization of the liver fat 1H MR spectrum. *NMR Biomed.* **24**, 784–790 (2011).
17. Yokoo, T. *et al.* Estimation of Hepatic Proton-Density Fat Fraction by Using MR Imaging at 3.0 T. *Radiology* **258**, 749–759 (2011).
18. Tsao, J. & Jiang, Y. Hierarchical IDEAL: Fast, robust, and multiresolution separation of multiple chemical species from multiple echo times. *Magn. Reson. Med.* **70**, 155–159 (2013).
19. Brun, R. & Rademakers, F. ROOT — An object oriented data analysis framework. *Nucl. Instruments Methods Phys. Res. Sect. A Accel. Spectrometers, Detect. Assoc. Equip.* **389**, 81–86 (1997).

20. Green, M. A., Bilston, L. E. & Sinkus, R. In vivo brain viscoelastic properties measured by magnetic resonance elastography. *NMR Biomed.* **21**, 755–764 (2008).
21. Fovargue, D., Kozerke, S., Sinkus, R. & Nordsletten, D. Robust MR elastography stiffness quantification using a localized divergence free finite element reconstruction. *Med. Image Anal.* **44**, 126–142 (2018).
22. Barbieri, S., Donati, O. F., Froehlich, J. M. & Thoeny, H. C. Impact of the calculation algorithm on biexponential fitting of diffusion-weighted MRI in upper abdominal organs. *Magn. Reson. Med.* **75**, 2175–2184 (2016).
23. Sasso, M. *et al.* Liver Steatosis Assessed by Controlled Attenuation Parameter (CAP) Measured with the XL Probe of the FibroScan: A Pilot Study Assessing Diagnostic Accuracy. *Ultrasound Med. Biol.* **42**, 92–103 (2016).
24. Bedossa, P. Utility and appropriateness of the fatty liver inhibition of progression (FLIP) algorithm and steatosis, activity, and fibrosis (SAF) score in the evaluation of biopsies of nonalcoholic fatty liver disease. *Hepatology* **60**, 565–575 (2014).
25. Kleiner, D. E. *et al.* Design and validation of a histological scoring system for nonalcoholic fatty liver disease. *Hepatology* **41**, 1313–1321 (2005).
26. R Core Team. R: A Language and Environment for Statistical Computing. (2020).
27. Heba, E. R. *et al.* Accuracy and the effect of possible subject-based confounders of magnitude-based MRI for estimating hepatic proton density fat fraction in adults, using MR spectroscopy as reference. *J. Magn. Reson. Imaging* **43**, 398–406 (2016).
28. Chen, J. *et al.* Early Detection of Nonalcoholic Steatohepatitis in Patients with Nonalcoholic Fatty Liver Disease by Using MR Elastography. *Radiology* **259**, 749–756 (2011).
29. Imajo, K. *et al.* Magnetic Resonance Imaging More Accurately Classifies Steatosis and Fibrosis in Patients With Nonalcoholic Fatty Liver Disease Than Transient Elastography. *Gastroenterology* **150**, 626–637.e7 (2016).
30. Sinkus, R. *et al.* Rheological determinants for simultaneous staging of hepatic fibrosis and inflammation in patients with chronic liver disease. *NMR Biomed.* **31**, e3956 (2018).
31. Yin, M. *et al.* Distinguishing between Hepatic Inflammation and Fibrosis with MR Elastography. *Radiology* **284**, 694–705 (2017).
32. Murphy, P. *et al.* Associations between histologic features of nonalcoholic fatty liver disease (NAFLD) and quantitative diffusion-weighted MRI measurements in adults. *J. Magn. Reson. Imaging* **41**, 1629–1638 (2015).
33. Trout, A. T. *et al.* Liver Stiffness Measurements with MR Elastography: Agreement and Repeatability across Imaging Systems, Field Strengths, and Pulse Sequences. *Radiology* **281**, 793–804 (2016).
34. Kim, D., Kim, W. R., Talwalkar, J. A., Kim, H. J. & Ehman, R. L. Advanced fibrosis in nonalcoholic fatty liver disease : Noninvasive assessment with MR elastography. *Radiology* **268**, 411–419 (2013).
35. Xiao, G. *et al.* Comparison of laboratory tests, ultrasound, or magnetic resonance elastography to detect fibrosis in patients with nonalcoholic fatty liver disease: A meta-analysis. *Hepatology* **66**, 1486–1501 (2017).
36. Li, Y. T. *et al.* Liver intravoxel incoherent motion (IVIM) magnetic resonance imaging: a comprehensive review of published data on normal values and applications for fibrosis and tumor evaluation. *Quant. Imaging Med. Surg.* **7**, 59–78 (2017).
37. Klaassen, R. *et al.* Evaluation of Six Diffusion-weighted MRI Models for Assessing Effects of Neoadjuvant Chemoradiation in Pancreatic Cancer Patients. *Int. J. Radiat. Oncol.* **102**, 1052–1062 (2018).
38. Younossi, Z. M. *et al.* Diagnostic modalities for nonalcoholic fatty liver disease, nonalcoholic steatohepatitis, and associated fibrosis. *Hepatology* **68**, 349–360 (2018).

39. Pavlides, M. *et al.* Multiparametric magnetic resonance imaging for the assessment of non-alcoholic fatty liver disease severity. *Liver Int.* **37**, 1065–1073 (2017).
40. Smits, L. P. *et al.* Noninvasive Differentiation between Hepatic Steatosis and Steatohepatitis with MR Imaging Enhanced with USPIOs in Patients with Nonalcoholic Fatty Liver Disease: A Proof-of-Concept Study. *Radiology* **278**, 782–791 (2016).
41. Vasanawala, S. S. *et al.* Safety and technique of ferumoxytol administration for MRI. *Magn. Reson. Med.* **75**, 2107–2111 (2016).
42. Imajo, K. *et al.* Quantitative multiparametric magnetic resonance imaging can aid non-alcoholic steatohepatitis diagnosis in a Japanese cohort. *World J. Gastroenterol.* **27**, 609–623 (2021).
43. Dzyubak, B. *et al.* Automated Analysis of Multiparametric Magnetic Resonance Imaging/ Magnetic Resonance Elastography Exams for Prediction of Nonalcoholic Steatohepatitis. *J. Magn. Reson. Imaging* jmri.27549 (2021). doi:10.1002/jmri.27549
44. Dennis, A. *et al.* A composite biomarker using multiparametric magnetic resonance imaging and blood analytes accurately identifies patients with non-alcoholic steatohepatitis and significant fibrosis. *Sci. Rep.* **10**, 15308 (2020).
45. Long, J. S. *Regression models for categorical and limited dependent variables.* (Thousand Oaks, CA: Sage Publications, Inc., 1997).

SUPPLEMENTAL METHODS

MRI Acquisition

Magnetic resonance spectroscopy

MRS data acquisition and analysis was performed using our previously described protocol1. Briefly, data were acquired using a multi-echo stimulated-echo acquisition mode (STEAM) in a single breath-hold of 21 seconds. A single voxel of 20×20×20mm3 was positioned in the right hepatic lobe, avoiding major blood vessels, bile ducts and liver margins. First order pencil beam volume B0 shimming was used. 1024 datapoints were acquired at a bandwidth of 2000Hz at five seperate echo times (TE) of 10, 15, 20, 25 and 30ms and a repetition time (TR) of 3500ms.

Magnitude-based MRI PDFF

MRI-M for determination of PDFF was performed using a two-dimensional multi-echo gradient echo sequence. Six echo times were used, with an initial TE of 1.15ms, and ΔTE of 1.18ms. A flip angle of 10° and a repetition time of 150ms was used for all scans. The field-of-view (FOV) was kept the same throughout all individuals, set at 448×320mm2, 4.0×4.0mm2 acquisition resolution, 36 slices and 5mm slice thickness. Parallel imaging (SENSE) was used to accelerate data acquisition using a SENSE factor of 2, resulting in full liver coverage in a single 18-second breath-hold.

Three-point DIXON

Three-point Dixon scans were performed using a two-dimensional multi-slice gradient echo sequence. Images were acquired at three echo times, with an initial TE of 3.1ms and ΔTE 0.78ms. The flip angle was 5°, and TR was 50ms. The acquisition was obtained in a single breath-hold of 19 seconds. The FOV was 420×300mm2, 2.4×2.4mm2 acquisition resolution, slice thickness 10mm, slice gap 11.4mm, and five slices were acquired.

MRE

Magnetic resonance elastography was performed using a gravitational transducer2, with single frequency mechanical wave generation set at 50Hz. The transducer was positioned in the mid-axillary line adjacent to the liver and held in position using an elastic strap. Image acquisition was performed using a two-dimensional Ristretto MRE sequence, a generalised multi-shot gradient-recalled echo MRE sequence proposed by Guenthner and colleagues3. MRE settings were as follows: four wave-phase offsets, motion-encoding gradient frequency 165Hz, Hadamard encoding, Ristretto sequence timing Nw/Nd 5/3. Nine slices were acquired with a FOV of 448 x 448 mm, 4.0x4.0 mm2 acquisition resolution and 4.0 mm slice thickness. The flip

angle was 20°, TE was 6.91 ms and TR 75 ms. Parallel imaging acceleration factor 3.0 resulted in an acquisition time of four 15 second breath holds.

Intravoxel incoherent motion (IVIM) imaging

IVIM imaging was performed using a free-breathing multi-slice diffusion weighted single-shot echo-planar imaging sequence. Eighteen unique b-values were used: 0, 1, 2, 5, 10, 20, 30, 40, 50, 75, 100, 150, 200, 300, 400, 500, 600, and 700 s/mm2. The TR was set at 7000 ms, TE 45.5 ms and bandwidth 20.8Hz/pixel. The FOV was 450×295 mm2 with a 3.0x3.0 mm2 acquisition resolution. 27 slices were imaged with a slice thickness of 6.0 mm and a 1.0 mm slice gap. Scans were accelerated using a parallel imaging factor of 1.3 and partial averaging factor of 0.6. Fat suppression was implemented using spectral attenuated inversion recovery (SPAIR). Three saturation slabs were positioned to suppress signal arising from the anterior abdominal wall. Image acquisition time was 8.1 minutes.

REFERENCES

1. Runge JH, Smits LP, Verheij J, et al. MR spectroscopy-derived proton density fat fraction is superior to controlled attenuation parameter for detecting and grading hepatic steatosis. Radiology. 2018;286(2):547-556. doi:10.1148/radiol.2017162931
2. Runge JH, Hoelzl SH, Sudakova J, et al. A novel magnetic resonance elastography transducer concept based on a rotational eccentric mass: preliminary experiences with the gravitational transducer. Phys Med Biol. 2019;64(4):045007. doi:10.1088/1361-6560/aaf9f8
3. Guenthner C, Sethi S, Troelstra M, Dokumaci AS, Sinkus R, Kozerke S. Ristretto MRE: A generalized multi-shot GRE-MRE sequence. NMR Biomed. 2019;32(5):e4049. doi:10.1002/nbm.4049

SUPPLEMENTAL FIGURES

Supplemental Figure 1. FibroScan® CAP values versus histological steatosis grade.

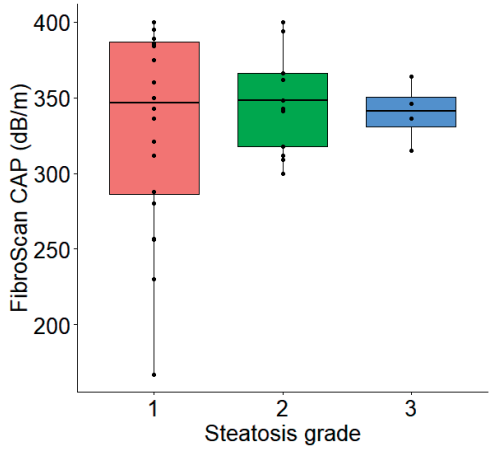

Median values for grade 1, 2 and 3 were 324, 348 and 336 dB/m resp. There were no significant difference in medians between steatosis grades.

Supplemental Figure 2. FibroScan® LSM versus histological activity grade.

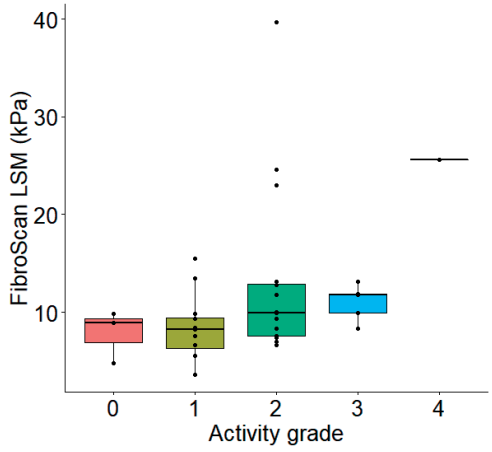

Median stiffness values were: 6.85 kPa for grade 0, 6.93 kPa for grade 1, 10.50 kPa for grade 2 and 11.1 kPa for grade 3. There was no significant difference in medians between activity grades.

Supplemental Figure 3. FibroScan® LSM versus histological fibrosis grade.

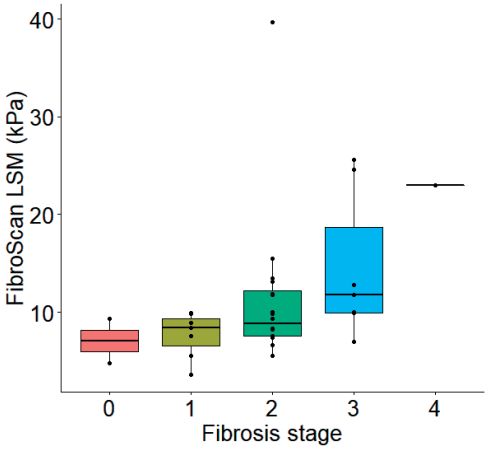

Median stiffness values were: 7.05 kPa for grade 0; 7.26 kPa for grade 1; 8.48 kPa for grade 2; 10.40 kPa for grade 3; and 23.00 kPa for grade 4. There were no significant differences in medians between fibrosis grades.

chapter 8

Summary

SUMMARY

In this thesis we targeted the human gut microbiome for the development of therapeutic strategies in metabolic disorders, specifically by studying the effect of probiotic treatment in metabolic syndrome and T2D individuals on insulin resistance as well as the effect of multiple FMTs on liver histology in individuals diagnosed with MASLD. Moreover, we aimed to identify and validate noninvasive diagnostic methods in disease progression in MASLD.

PART I - THE GUT MICROBIOME AS A THERAPEUTIC TARGET IN CARDIOMETABOLIC DISORDERS

This part of the thesis focused on the potential role of the gut microbiome in treating metabolic diseases. First, we provided an overview of the interplay between the gut microbiota composition and the development of insulin resistance and cardiovascular disease (CVD) as well as how these findings are being pursued to develop novel diagnostic and therapeutic targeting options for metabolic disorders (**chapter 2**). By supplying missing bacterial strains or their produced metabolites, intestinal microbiota composition might be beneficially altered and thus prevent the development of cardiometabolic disorders. Previous studies have shown that transplantation of lean healthy microbiota in individuals with insulin resistance significantly increased insulin sensitivity[1] and found an increased abundance of butyrate-producing bacteria in the gut[2], specifically in the butyrate-producing specie *Anaerobutyricum soehngenii* (previously known as *Eubacterium hallii)*. In **chapter 3** we performed a randomized placebo-controlled cross-over study in individuals with the metabolic syndrome in which we showed that a single duodenal infusion of *A. soehngenii* improved peripheral glycemic control, specifically by stimulating postprandial intestinal GLP-1 production. Moreover, administration of *A. soehngenii* L2-L7 resulted in an altered small intestinal gene expression signature and, most prominently, in the upregulation of the expression of regenerating islet-protein 1B (REG1B)-encoding gene.

As *A. soehngenii* has the capacity to produce butyrate from lactate and acetate in an acid environment as found in the small intestine[3], it is interesting to note that individuals with T2D treated with metformin have increased levels of lactate in their feces[4]. Since *A. soehngenii* uses intestinally produced lactate to produce the SCFA butyrate, which is known to exert beneficial effects on glucose metabolism, these findings prompted us to study the effect of a 2 weeks oral *A. soehngenii* treatment in individuals with T2D treated with metformin on their glycemic control (**chapter 4**).

Here we showed that *A. soehngenii* supplementation on top of metformin treatment significantly improved glycemic variability and decreased mean arterial 24h blood pressure (MAP) compared to placebo-treated controls. These findings suggest that *A. soehngenii* can aid in improving glycemic control in metformin-treated individuals with T2D.

PART II - DEVELOPMENT OF MICROBIOTA-BASED THERAPEUTICS AND NONINVASIVE DIAGNOSTICS IN MASLD

The second part of the thesis focused on MASLD, currently the most common cause of chronic liver dysfunction worldwide[5]. As mentioned, it is emerging that the gut microbiome has a profound influence on human health and disease. Over the last decades, the development of culture-independent approaches, using high-throughput metagenomic sequencing, has drastically increased the knowledge of the gut microbiome, now linking any disturbances in it, both in human and animal models, to the pathophysiology of metabolic diseases. In **chapter 5** we reviewed the gut microbial and gut microbial-derived metabolite signatures associated with the development and disease progression of MASLD, focusing on which microbial signatures are specific to liver injury versus those common to other metabolic diseases. We found Proteobacteria to be consistently enriched in individuals with steatosis and steatohepatitis. However, we found discrepant microbiome signatures across studies owing to the heterogeneous cohorts used across studies, with differences in sex, ethnicity, liver disease severity stage, BMI, presence of T2DM, patient population (pediatric or adult), adiposity and other associated metabolic diseases.

To dissect causality of intestinal microbiota in MASLD, in **chapter 6** we performed a single-center, double-blind, randomized controlled proof-of-principle pilot study comparing the effect of three 8-weekly lean vegan donor FMT versus autologous FMT on the severity of MASLD, using liver biopsies in individuals with hepatic steatosis on ultrasound. In order to determine the severity of MASLD, the liver biopsies were scored according to the NAFLD activity (NAS) score, which is the unweighted sum of steatosis (0-3), lobular inflammation (0-3), and hepatocellular ballooning (0-2)[6]. We found no significant change in the overall NAS score and steatosis grade following FMT. However, we did observe a trend towards improvement in the necro-inflammation score upon allogenic FMT. The necro-inflammation score is a surrogate marker for disease activity and comprises lobular inflammation and hepatocyte ballooning. A major drawback of these histological scoring approaches is their dependence on a liver biopsy, which has apparent disadvantages like sampling error,

interindividual variations in pathologist reading and the risk of complications[7]. Non-invasive methods that measure liver stiffness or use magnetic resonance imaging (MRI) have been proposed as alternatives to liver biopsy for assessing the severity of fibrosis and steatohepatitis in patients with MASLD. Hence, in **chapter 7** we examined the diagnostic performance of multiparametric MRI for the assessment of disease severity along the MASLD disease spectrum with comparison to histological scores. In this study, a total of 37 individuals with hepatic steatosis on ultrasound were included. According to the Steatosis Activity and Fibrosis (SAF) score[8], MASH was present in 22 of the 37 participants. We showed that MASLD severity can be assessed with the use of multiparametric MRI. In particular steatosis and fibrosis can be graded well, and multiparametric MRI modalities have the potential to distinguish between simple hepatic steatosis and MASH. Both the distinction between simple steatosis and MASH as the detection and staging of fibrosis are essential yet challenging elements of the workup of an individual with MASLD, as they enable the evaluation of the risk of progression toward advanced MASH fibrosis and cirrhosis and to determine treatment and monitoring plans.

REFERENCES

1. Vrieze, A. *et al.* Transfer of Intestinal Microbiota From Lean Donors Increases Insulin Sensitivity in Individuals With Metabolic Syndrome. *Gastroenterology* **143**, 913-916.e7 (2012).
2. Kootte, R. S. *et al.* Improvement of Insulin Sensitivity after Lean Donor Feces in Metabolic Syndrome Is Driven by Baseline Intestinal Microbiota Composition. *Cell Metab.* **26**, 611-619.e6 (2017).
3. Duncan, S. H., Louis, P. & Flint, H. J. Lactate-Utilizing Bacteria, Isolated from Human Feces, That Produce Butyrate as a Major Fermentation Product. *Appl. Environ. Microbiol.* **70**, 5810–5817 (2004).
4. Wu, H. *et al.* Metformin alters the gut microbiome of individuals with treatment-naive type 2 diabetes, contributing to the therapeutic effects of the drug. *Nat. Med.* **23**, 850–858 (2017).
5. Younossi, Z. *et al.* Global Perspectives on Nonalcoholic Fatty Liver Disease and Nonalcoholic Steatohepatitis. *Hepatology* **69**, 2672–2682 (2019).
6. Kleiner, D. E. *et al.* Design and validation of a histological scoring system for nonalcoholic fatty liver disease. *Hepatology* **41**, 1313–1321 (2005).
7. Sumida, Y. Limitations of liver biopsy and non-invasive diagnostic tests for the diagnosis of nonalcoholic fatty liver disease/nonalcoholic steatohepatitis. *World J. Gastroenterol.* **20**, 475 (2014).
8. Bedossa, P. Utility and appropriateness of the fatty liver inhibition of progression (FLIP) algorithm and steatosis, activity, and fibrosis (SAF) score in the evaluation of biopsies of nonalcoholic fatty liver disease. *Hepatology* **60**, 565–575 (2014).

chapter 9

General discussion and future perspectives

GENERAL DISCUSSION AND FUTURE PERSPECTIVES

Due to the global increase in obesity and subsequent insulin resistance, type 2 diabetes mellitus and MASLD are increasing problems for global health. The currently available therapeutic strategies for MASLD are insufficient to prevent the long-term complications of MASLD, marking the urgent need for novel therapies. The human gut microbiome is increasingly recognized to have critical physiological roles in host digestion, immunity and metabolism[1,2]. Disturbances in the gut microbiome have repeatedly been observed in metabolic disorders, such as obesity and T2D[3,4]. Currently, these findings are being pursued to develop gut microbiota-based therapeutics in order to improve metabolic health and prevent metabolic disease.

PART I - THE GUT MICROBIOME AS A THERAPEUTIC TARGET IN CARDIOMETABOLIC DISORDERS

This part of the thesis focused on the potential role of the gut microbiome in treating metabolic diseases. We showed that administration of A. soehngenii can aid in improving glycemic control by altering metabolic parameters in both individuals with the metabolic syndrome as metformin-treated individuals with T2D, indicating that *A. soehngenii* can act as a next generation therapeutic microbe. However, the isolation, cultivation and storage of these oxygen-sensitive bacteria is a time consuming and challenging process. Future studies have to prove this effect in a larger and more diverse population and have to determine if long term *A. soehngenii* supplementation has durable beneficial metabolic effects.

PART II - NONINVASIVE DIAGNOSTICS IN MASLD

The second part of the thesis focused on MASLD, currently the most common cause of chronic liver dysfunction worldwide[5]. Chapter 6 describes a proof-of-principle pilot study comparing the effect of vegan donor FMT versus autologous FMT on the severity of MASLD, using liver biopsies in individuals with hepatic steatosis on ultrasound. We found no significant change in steatosis or MASH histology grade following FMT. Previous studies showed a beneficial effect of autologous FMT on glucose metabolism in individuals with type 1 diabetes[6], suggesting that the extent to which the donor's microbiota can colonize the recipient microbiome is more important than using donors with a highly diverse microbiome. Future studies matching donor-recipient microbiomes could increase colonization of the recipient and hence clinical benefit and are therefore warranted.

In this study, we used the MASLD activity (NAS) score, which is the unweighted sum of steatosis (0-3), lobular inflammation (0-3), and hepatocellular ballooning (0-2)[7] in order to determine the severity of MASLD. As the NAS-score often is inaccurate, the European guidelines recommend the use of this score only for disease severity evaluation within the MASLD disease spectrum once the diagnosis has been made[8]. A newer diagnostic algorithm, the Steatosis Activity and Fibrosis (SAF) score, which emphasizes the importance of disease activity (i.e. lobular inflammation and hepatocyte ballooning), has demonstrated improved performance compared with the NAS-score, as it provides a more accurate and comprehensive histological evaluation[9]. Therefore, the SAF-score is qualified as the diagnostic score for MASLD in the European guidelines. However, a major drawback of these scoring approaches is their dependence on a liver biopsy, which has apparent disadvantages like sampling error, interindividual variations in pathologist reading and the risk of complications[10]. As these drawbacks render a liver biopsy a suboptimal diagnostic method for MASLD in both routine care and research, noninvasive diagnostic methods are urgently required in disease stratification and monitoring in MASLD. A large biopsy-controlled study showed that FibroScan® controlled attenuation parameter (CAP) and liver stiffness measurement (LSM) determined with vibration-controlled transient elastography (VCTE) accurately assesses steatosis and fibrosis respectively in individuals with MASLD[11]. Moreover, the latest MASLD care path recommends a noninvasive FIB-4 measurement followed by VCTE or ELF-test to screen for MASLD fibrosis in primary care[12]. If both tests indicate an increased risk of MASLD fibrosis, a third, noninvasive, test should be done to estimate the risk of advanced fibrosis. If this third test also shows an elevated test result, there is a high risk of advanced fibrosis and no liver biopsy is required to confirm diagnosis and stage, a promising step towards preventing many liver biopsies, with all associated disadvantages. However, this care path still needs to be validated in cohorts with diverse patient populations, in primary care practices and diabetology clinics instead of hepatology clinics, with lower prevalence of advanced MASLD, various ethnic backgrounds, large age ranges and a myriad of comorbidities.

Moreover, in this thesis we showed the ability of multiparametric MRI in assessing MASLD severity, in particular steatosis and fibrosis, with the potential to distinguish between simple hepatic steatosis and MASH. Although costly and time-consuming, MRI is a noninvasive method and represents the whole liver, hereby excluding the risk of bleeding and sampling error. Future research should focus on the ability of the MRI scan to replace the liver biopsy in diagnosing MASLD.

To conclude, al lot of research is being done to replace the invasive liver biopsy by noninvasive diagnostic tests, with promising results. To date, the most effective treatment and prevention for MASH and metabolic disorders like the metabolic

syndrome and T2D is significant weight reduction, either by combined lifestyle intervention or bariatric surgery. In my opinion more attention, time and money should be spent on preventing MASLD and related metabolic lifestyle diseases such as T2DM by combatting obesity. Pharmacological treatment should be reserved for those with progressive MASLD stages despite lifestyle interventions.

REFERENCES

1. Fouhy, F., Ross, R. P., Fitzgerald, G. F., Stanton, C. & Cotter, P. D. Composition of the early intestinal microbiota. *Gut Microbes* **3**, 203–220 (2012).
2. Prakash, S., Tomaro-Duchesneau, C., Saha, S. & Cantor, A. The Gut Microbiota and Human Health with an Emphasis on the Use of Microencapsulated Bacterial Cells. *J. Biomed. Biotechnol.* **2011**, 1–12 (2011).
3. Ridaura, V. K. *et al.* Gut microbiota from twins discordant for obesity modulate metabolism in mice. *Science* **341**, 1241214 (2013).
4. Pedersen, H. K. *et al.* Human gut microbes impact host serum metabolome and insulin sensitivity. *Nature* **535**, 376–381 (2016).
5. Younossi, Z. *et al.* Global Perspectives on Nonalcoholic Fatty Liver Disease and Nonalcoholic Steatohepatitis. *Hepatology* **69**, 2672–2682 (2019).
6. Kootte, R. S. *et al.* Improvement of Insulin Sensitivity after Lean Donor Feces in Metabolic Syndrome Is Driven by Baseline Intestinal Microbiota Composition. *Cell Metab.* **26**, 611-619. e6 (2017).
7. Kleiner, D. E. *et al.* Design and validation of a histological scoring system for nonalcoholic fatty liver disease. *Hepatology* **41**, 1313–1321 (2005).
8. Association, E., Association, E., Easd, D., Association, E. & Easo, O. EASL–EASD–EASO Clinical Practice Guidelines for the management of non-alcoholic fatty liver disease. *J. Hepatol.* **64**, 1388–1402 (2016).
9. Bedossa, P. Utility and appropriateness of the fatty liver inhibition of progression (FLIP) algorithm and steatosis, activity, and fibrosis (SAF) score in the evaluation of biopsies of nonalcoholic fatty liver disease. *Hepatology* **60**, 565–575 (2014).
10. Sumida, Y. Limitations of liver biopsy and non-invasive diagnostic tests for the diagnosis of nonalcoholic fatty liver disease/nonalcoholic steatohepatitis. *World J. Gastroenterol.* **20**, 475 (2014).
11. Eddowes, P. J. *et al.* Accuracy of FibroScan Controlled Attenuation Parameter and Liver Stiffness Measurement in Assessing Steatosis and Fibrosis in Patients With Nonalcoholic Fatty Liver Disease. *Gastroenterology* **156**, 1717–1730 (2019).
12. Cusi, K. *et al.* American Association of Clinical Endocrinology Clinical Practice Guideline for the Diagnosis and Management of Nonalcoholic Fatty Liver Disease in Primary Care and Endocrinology Clinical Settings: Co-Sponsored by the American Association for the Study of Liver Diseases (AASLD). *Endocr. Pract.* **28**, 528–562 (2022).

Appendices

Nederlandse samenvatting

In dit proefschrift onderzochten we de potentie van het menselijke darmmicrobioom voor de behandeling van verschillende metabole ziekten. Zo hebben we het effect van een probiotische behandeling op insulineresistentie in mensen met het metabool syndroom en diabetes mellitus type 2 (DM2) bestudeerd, alsook gekeken naar het effect van meerdere fecale microbioom transplantaties (ook wel poeptransplantaties) op de mate van leververvetting en leverontsteking bij mensen met de diagnose metabool geassocieerde steatose van de lever (MASLD). Bovendien wilden we niet-invasieve diagnostische methoden voor het vaststellen van ziekteprogressie van deze leverziekte identificeren en valideren.

DEEL I - HET DARMMICROBIOOM ALS THERAPEUTISCH AANGRIJPINGSPUNT IN CARDIOMETABOLE STOORNISSEN

Dit deel van het proefschrift richtte zich op de mogelijke rol van het darmmicrobioom bij de behandeling van metabole ziekten. Ten eerste hebben we een overzicht gegeven van de wisselwerking tussen de samenstelling van de darmmicrobiota en de ontwikkeling van insulineresistentie en hart- en vaatziekten (HVZ), evenals hoe deze wisselwerking kan worden gebruikt om nieuwe diagnostische en therapeutische aangrijpingspunten voor metabole stoornissen te ontwikkelen (**hoofdstuk 2**). Door ontbrekende bacteriestammen of hun geproduceerde metabolieten toe te dienen, kan de samenstelling van de darmmicrobiota gunstig worden veranderd en zo de ontwikkeling van cardiometabole stoornissen worden voorkomen. Eerdere studies hebben aangetoond dat transplantatie van ontlasting (en zodoende het darmmicrobioom) van magere, gezonde personen naar personen met insulineresistentie de insulinegevoeligheid significant verbeterde. Ook werd er na transplantatie een verhoogd aantal butyraatproducerende bacteriën in de darm gevonden, met name de butyraat producerende soort Anaerobutyricum soehngenii (voorheen bekend als Eubacterium hallii). In **hoofdstuk 3** hebben we een gerandomiseerde, placebogecontroleerde cross-over studie uitgevoerd bij personen met het metabool syndroom, waarin we hebben aangetoond dat een enkele duodenale infusie van A. soehngenii de perifere glucose controle verbeterde, met name door het stimuleren van de postprandiale intestinale GLP-1-productie. Bovendien resulteerde de toediening van A. soehngenii in een veranderde genexpressie in de dunne darm en, het meest opvallend, in de opwaartse regulatie van de expressie van het regenererende eilandje-eiwit 1B (REG1B) -coderende gen.

A. soehngenii heeft het vermogen om butyraat te produceren uit lactaat en acetaat in een zure omgeving zoals in de dunne darm. Uit onderzoek is gebleken dat personen met DM2 die met metformine worden behandeld, verhoogde niveaus van lactaat in hun ontlasting hebben. A. soehngenii gebruikt dit in de darm geproduceerde lactaat om het korte keten vetzuur butyraat te produceren, waarvan bekend is dat het gunstige effecten heeft op het glucosemetabolisme. Deze bevindingen hebben ons geïnspireerd om het effect van een 2 weken durende orale A. soehngenii-behandeling in mensen met DM2 die met metformine worden behandeld te bestuderen (**hoofdstuk 4**). In dit hoofdstuk toonden we aan dat A. soehngenii-suppletie bovenop metforminebehandeling de glucose variabiliteit aanzienlijk verbeterde en de gemiddelde arteriële 24-uurs bloeddruk (MAP) verlaagde in vergelijking met placebo behandelde controles. Deze bevindingen suggereren dat A. soehngenii kan helpen bij het verbeteren van de glucose controle in personen met DM2 die behandeld worden met metformine.

DEEL II - ONTWIKKELING VAN OP MICROBIOTA GEBASEERDE THERAPIEËN EN NIET-INVASIEVE DIAGNOSTIEK IN MASLD

Het tweede deel van dit proefschrift richtte zich op MASLD, momenteel de meest voorkomende oorzaak van chronische leverziekte wereldwijd. Zoals eerder vermeld, wordt het steeds meer duidelijk dat het darmmicrobioom een grote invloed heeft op de gezondheid en ziekte van de mens. In de afgelopen decennia heeft de ontwikkeling van cultuuronafhankelijke benaderingen de kennis van het darmmicrobioom drastisch vergroot. Verstoringen in de samenstelling van het darmmicrobioom, aangetoond in zowel menselijke als dierlijke modellen, worden nu gekoppeld aan de pathofysiologie van metabole ziekten. In **hoofdstuk 5** hebben we de darmmicrobiota en de door de darmbacteriën geproduceerde metabolieten bekeken die geassocieerd zijn met de ontwikkeling en ziekteprogressie van MASLD. We hebben ons gefocust op welke microbiota specifiek zijn voor leverbeschadiging versus welke darmbacteriën veel voorkomen bij andere metabole ziekten. Zo ontdekten we dat Proteobacteriën consequent verhoogd aanwezig waren bij personen met steatose en steatohepatitis. We vonden echter discrepante microbioomsamenstellingen in de verschillende onderzoeken vanwege de heterogene cohorten die werden gebruikt, met verschillen in geslacht, etniciteit, het stadium van de ernst van de leverziekte, BMI, aanwezigheid van DM2, patiëntenpopulatie (pediatrisch of volwassen) en de aanwezigheid van andere geassocieerde metabole ziekten.

Om causaliteit van darmmicrobiota bij het ontstaan van MASLD te onderzoeken, hebben we in **hoofdstuk 6** een single-center, dubbelblinde, gerandomiseerde

placebo-gecontroleerde pilotstudie uitgevoerd. In deze studie keken we naar het effect van drie fecale microbioom transplantaties (FMT), van magere veganistische donoren naar mensen met leververvetting op echografie, op de ontwikkeling van MASLD. In de controlearm ontvingen de deelnemers een autologe (een van henzelf afkomstige) FMT. Om de ernst van MASLD te bepalen ondergingen de deelnemers een leverbiopt, deze werden gescoord volgens de NAFLD-activiteit score (NAS). We vonden geen significante verandering in de algehele NAS-score en mate van steatose na FMT. Wel zagen we een trend naar verbetering van de mate va ontsteking na donor FMT in vergelijking met autologe transplantaties.

List of publications

Included in this thesis:

Witjes JJ, van Raalte DH, Nieuwdorp M. About the gut microbiome as a pharmacological target in atherosclerosis. *Eur J Pharmacol*, 2015 Sep;763:75–8.

Koopen A, **Witjes J**, Wortelboer K, Majait S, Prodan A, Levin E, Herrema H, Winkelmeijer M, Aalvink S, Bergman JJGHM, Havik S, Hartmann B, Levels H, Bergh PO, van Son J, Balvers M, Bastos DM, Stroes E, Groen AK, Henricsson M, Kemper EM, Holst J, Strauch CM, Hazen SL, Bäckhed F, De Vos WM, Nieuwdorp M, Rampanelli E. Duodenal Anaerobutyricum soehngenii infusion stimulates GLP-1 production, ameliorates glycaemic control and beneficially shapes the duodenal transcriptome in metabolic syndrome subjects: a randomised double-blind placebo-controlled cross-over study. *Gut*, 2021; 1–11.

Aron-Wisnewsky J, Vigliotti C, **Witjes J**, Le P, Holleboom AG, Verheij J, Nieuwdorp M, Clément K. Gut microbiota and human NAFLD: disentangling microbial signatures from metabolic disorders. *Nat Rev Gastroenterol Hepatol*., 2020 May 9;17(5):279–97.

Witjes JJ*, Smits LP*, Pekmez CT, Prodan A, Meijnikman AS, Troelstra MA, Bouter KEC, Herrema H, Levin E, Holleboom AG, Winkelmeijer M, Beuers UH, van Lienden K, Aron-Wisnewky J, Mannisto V, Bergman JJ, Runge JH, Nederveen AJ, Dragsted LO, Konstanti P, Zoetendal EG, de Vos W, Verheij J, Groen AK, Nieuwdorp M. Donor Fecal Microbiota Transplantation Alters Gut Microbiota and Metabolites in Obese Individuals With Steatohepatitis. *Hepatol Commun*, 2020 Nov 7;4(11):1578–90.

Witjes JJ*, Troelstra* MA, Dijk A, Mak AL, Gurney-Champion O, Runge JH, Zwirs D, Stols-Gonçalves D, Zwinderman AH, Wolde M, Monajemi H, Ramsoekh S, Sinkus R, Delden OM, Beuers UH, Verheij J, Nieuwdorp M, Nederveen AJ, Holleboom AG. Assessment of Imaging Modalities Against Liver Biopsy in Nonalcoholic Fatty Liver Disease: The Amsterdam NAFLD-NASH Cohort. *J Magn Reson Imaging*, 2021 Dec 15;54(6):1937–49.

Other:

Baldewpersad Tewarie NMS, Burgers IAV, Dawood Y, den Boon HC, den Brok MGHE, Klunder JH, Koopmans KB, Rademaker E, van den Broek HB, van den Bersselaar SM, **Witjes JJ**, Van Noorden CJF, Atai NA. NADP+-dependent IDH1R132 mutation and its relevance for glioma patient survival. *Med Hypotheses,* 2013 Jun;80(6):728–31.

Bernelot Moens SJ, Mooij HL, Hassing H. C, Kruit JK, **Witjes JJ**, van de Sande MAJ, Nederveen AJ, Xu D, Dallinga-Thie GM, Esko JD, Stroes ESG, Nieuwdorp M. Carriers of Loss-of-Function Mutations in EXT Display Impaired Pancreatic Beta-Cell Reserve Due to Smaller Pancreas Volume. PLoS One, 2014 Dec 26; 9(12): e115662.

Mooij HL, Bernelot Moens SJ, Gordts PSM, Stanford K, Foley E, van den Boogert MW, **Witjes J**, Hassing HC, Tanck M, van de Sande MJ, Levels JH, Kastelein JP, Stroes EG, Dallinga-Thie G, Esko J, Nieuwdorp M. Ext1 heterozygosity causes a modest effect on postprandial lipid clearance in humans. J Lipid Res, 2015 Mar;56(3):665–73.

Pérez-Medina C, Binderup T, Lobatto ME, Tang J, Calcagno C, Giesen L, Wessel CH, **Witjes J**, Ishino S, Baxter S, Zhao Y, Ramachandran S, Eldib M, Sánchez-Gaytán BL, Robson PM, Bini J, Granada JF, Fish KM, Stroes ESG, Duivenvoorden R, Tsimikas S, Lewis JS, Reiner T, Fuster V, Kjær A, Fisher EA, Fayad ZA, Mulder WJM. In Vivo PET Imaging of HDL in Multiple Atherosclerosis Models. JACC Cardiovasc Imaging, 2016 Aug;9(8):950–61.

Udayappan SD, Kovatcheva-Datchary P, Bakker GJ, Havik SR, Herrema H, Cani PD, Bouter KE, Belzer C, **Witjes JJ**, Vrieze A, de Sonnaville N, Chaplin A, van Raalte DH, Aalvink S, Dallinga-Thie GM, Heilig HGHJ, Bergström G, van der Meij S, van Wagensveld BA, Hoekstra JBL, Holleman F, Stroes ESG, Groen AK, Bäckhed F, de Vos WM, Nieuwdorp M. Intestinal Ralstonia pickettii augments glucose intolerance in obesity. Chavakis T. PLoS One, 2017 Nov 22;12(11):e0181693.

Lobatto ME, Binderup T, Robson PM, Giesen LFP, Calcagno C, **Witjes J**, Fay F, Baxter S, Wessel CH, Eldib M, Bini J, Carlin SD, Stroes ESG, Storm G, Kjaer A, Lewis JS, Reiner T, Fayad ZA, Mulder WJM, Pérez-Medina C. Multimodal Positron Emission Tomography Imaging to Quantify Uptake of 89 Zr-Labeled Liposomes in the Atherosclerotic Vessel Wall. Bioconjug Chem, 2020 Feb 19;31(2):360–8.

Koopen AM, Almeida EL, Attaye I, **Witjes JJ**, Rampanelli E, Majait S, Kemper M, Levels JHM, Schimmel AWM, Herrema H, Scheithauer TPM, Frei W, Dragsted L, Hartmann B, Holst JJ, O'Toole PW, Groen AK, Nieuwdorp M. Effect of Fecal Microbiota Transplantation Combined With Mediterranean Diet on Insulin Sensitivity in Subjects With Metabolic Syndrome. Front Microbiol, 2021 Jun 10;12.

Troelstra MA, Van Dijk AM, **Witjes JJ**, Mak AL, Zwirs D, Runge JH, Verheij J, Beuers UH, Nieuwdorp M, Holleboom AG, Nederveen AJ, Gurney-Champion OJ. Self-supervised neural network improves tri-exponential intravoxel incoherent motion model fitting compared to least-squares fitting in non-alcoholic fatty liver disease. Front Physiol, 2022 Sep 6;13.

Stols-Gonçalves D, Mak AL, Madsen MS, van der Vossen EWJ, Bruinstroop E, Henneman P, Mol F, Scheithauer TPM, Smits L, **Witjes J**, Meijnikman AS, Verheij J, Nieuwdorp M, Holleboom AG, Levin E. Faecal Microbiota transplantation affects liver DNA methylation in Non-alcoholic fatty liver disease: a multi-omics approach. *Gut Microbes*, 2023 Dec 31;15(1).

*equally contributed

Portfolio

Name PhD student: J.J. Witjes
PhD period: September 2017 – April 2022 (minus June 2021 – December 2021)
Name PhD supervisors: Prof. dr. M. Nieuwdorp, prof. dr. U.H.W. Beuers, dr. A.G. Holleboom, prof. dr. ir. A.J. Nederveen

Courses, seminars and masterclasses	**Year**	**ECTS**
Basiscursus Regelgeving Klinisch Onderzoek (BROK)	2017	1.5
Good Clinical Practice (GCP)	2017	0.2
Crash course: 'Chemistry, biochemistry and molecular biology for MD's (re) entering scientific research'	2018	0.5
Practical biostatistics	2018	1.4
MRI: Basic Understanding for (Bio)Medical Research	2019	1.0
Data analysis in Matlab	2019	0.4
Weekly Journal club, dept Vascular Medicine, AMC	2017-2021	4.0
Weekly Clinical Education in Vascular Medicine, dept Vascular Medicine, AMC	2017-2021	4.0
Two-weekly Diabetes AMC/VUMC meeting	2017-2021	2.0
Monthly Microbiota Journal club	2017-2021	1.0
Monthly NAFLD Journal club	2018-2021	1.0

Oral & Poster presentations		
Steatohepatitis bij obesitas en DM2, Prevents Diabetes Overleg	2018	0.5
Assessment of imaging modalities against liver biopsy in non-alcoholic fatty liver disease: the Amsterdam NAFL-NASH cohort, the International Liver Congress	2021	0.5

(Inter)national conferences		
Radboud New Frontiers in the Microbiome, Nijmegen, The Netherlands	2017	0.5
AG&M symposium Gut inflammation and metabolism, Amsterdam, The Netherlands	2017	0.5
Annual Dutch Diabetes Research Meeting, Oosterbeek, The Netherlands	2017	0.5
European Fatty Liver Congress, Vaalsbroek, The Netherlands	2018	1.0
EASL Gut-Lives Axis, Leuven, Belgium	2018	1.0
Amsterdam symposium on vascular & metabolic disease, Amsterdam, The Netherlands	2018	0.5
EMBO | EMBL Symposium: The Human Microbiome, Heidelberg, Germany	2018	1.0
Vascular Medicine Symposium Amsterdam, the Netherlands	2018	0.5
Symposium Gut Day, Amsterdam UMC, loc. AMC, the Netherlands	2019	0.5

Teaching		
Bachelor thesis Nina Frerichs	2017	1.0
Bachelor thesis Tessa Siertsema	2018	1.0
Supervising first and second degree medical school students during their vascular medicine internship	2018-2019	1.0

Organization skills		
WIT festival ('Wetenschap Inspiratie Talent') AMC Foundation	2018	1.0
Representative PhD students Department of Vascular Medicine	2019-2020	0.5

Dankwoord

Dit dankwoord wil ik graag kort houden en gebruiken om de mensen die direct betrokken zijn geweest bij mijn promotie te bedanken.

Allereerst dank aan alle patienten en deelnemers van de studies, zonder jullie was dit proefschrift er nooit geweest.

Prof. Nieuwdorp, beste Max, wij kenden elkaar al langere tijd voor ik bij jou kwam promoveren. Ik heb altijd met veel plezier op Hannah, Matthias en Leah gepast. Wellicht was het vanwege die sociale relatie in de eerste periode even zoeken naar een professionele omgang, maar ik denk dat we daar allebei een goede vorm in gevonden hebben! Open voor eigen invulling, vertrouwen en mogelijkheid tot verblijf in het buitenland. Veel dank!

Prof. Beuers, beste Ulrich, hoewel we elkaar niet veel zagen, vond ik de momenten bij de leverpathologie bespreking en het verrichten van de leverbiopten voor de ANCHOR-studie erg leerzaam, dank hiervoor.

Beste Onno, wij begonnen samen aan het opzetten van een nieuw onderzoeksveld binnen de vasculaire geneeskunde. Jij als jonge klare en ik als promovenda. Hoewel we een andere manier van werken en ook een andere werkethos hebben (werk jij niet van 7 u 's ochtends tot 8 u's avonds?! Lees jij je werkmail niet na werktijd en ook niet in het weekend?!), vond ik ons een erg goed team en fijn om met je samen te werken. Nu, 4 jaar later, heb je een waar NAFLD-onderzoeksteam met meerdere promovendi en laboranten, missie geslaagd lijkt me! Heel veel dank voor je betrokken en intensieve begeleiding.

Prof. Nederveen, beste Aart, dank je wel voor je begeleiding en fijne gesprekken. Bedankt ook dat je mij aan Marian hebt voorgesteld!

Geachte leden van de promotiecommissie, dank voor het kritisch beoordelen van de inhoud van dit proefschrift.

Collega's van het trialbureau, van het lab en van de MRI, veel dank voor jullie hulp, ondersteuning en fijne samenwerking.

En dan het belangrijkst, de collega's van F4, het thuiswerken tijdens de COVID-pandemie heeft me des te meer doen beseffen dat promoveren niet half zo leuk

is zonder collega's. Nicolien en Annefleur, jullie hebben me leren poeproeren en ik kon me geen fijnere collega's wensen binnen de Max groep. Annefleur, de werkdag was niet begonnen als wij niet eerst samen koffie hadden gedronken. En samen clampen en maaltijdtesten doen is zoveel leuker dan alleen. Fritsie, we begonnen op dezelfde dag en zaten de eerste paar jaar naast elkaar op F4. Jij druk met de zoveelste meta-analyse en het in elkaar draaien van een chemokuurfiguur en ik nog steeds in gevecht met de METC. Samen met Baffie waren we het beste en leukste lunchteam! Rens, hoewel je vaak eerst even zuchtte als ik je voor de zoveelste keer vroeg om me te helpen met het maken van een figuur, een analyse in SPSS of een instelling te veranderen in Word, hielp je me altijd en gaf je niet op voordat het klaar was. Dank ook voor het stiekem veranderen van mijn digitale handtekening en dit vervolgens vergeten te vertellen! Floris, dank voor je humor, je positivisme en natuurlijk de gezamenlijke worstenbroodjescursus.

Ilias, hoewel we de uitvoering van onze studiedagen totaal anders invulden (jij nam het niet zo nauw met de in- en exclusiecriteria voor deelnemers of het exact uitvoeren van het protocol voor poep mengen) hebben we altijd goed kunnen samenwerken. Dank voor al je hulp tijdens mijn studiedagen en bij het schrijven van het manuscript. De vieze memes is iets dat ik niet mis! Stijn, ook jij bedankt voor je hulp bij het schrijven en voor onze fijne gesprekken over werk, toekomst en natuurlijk onze kinderen.

Diona, dank je wel voor al je hulp tijdens de onderzoeksdagen en het volledig overnemen van mijn studies als ik weer eens met zwangerschapsverlof ging. Ik vond het super fijn samenwerken!

Hank, ik leerde je pas in het tweede deel van mijn promotie kennen, maar het was meteen dikke mik. Ik waardeer je eerlijkheid en oprechtheid en ben blij met onze vriendschap. Dank voor je al je hulp bij het afronden van dit proefschrift én dat je mijn paranimf wil zijn! (Dit laatste geldt natuurlijk ook voor jou Fritzl ☺).

(Studio) Sander, dank voor je gave ontwerp voor de lay-out van dit proefschrift!

Lieve pap en mam en lieve Hetty, dank jullie wel voor de wekelijkse oppasdagen. Of we nou in Amsterdam, Utrecht of zelfs Kaapstad verbleven, jullie stonden (en staan) altijd voor ons klaar.

Lieve Bram, zo vaak vertelde jij me dat ik het anders moest doen: "Maak nou eens een weekplanning met wat je dag voor dag gaat doen!" "Begin gewoon met het schrijven

van de koppen van de alinea's, dan komt de rest echt vanzelf!" Maar ik ben net zo eigenwijs als jij, dus ik deed het toch op mijn eigen manier, en zie hier het resultaat. Ons verblijf in Kaapstad waren de 4 mooiste maanden van mijn promotie. Of het ook de meest productieve maanden waren laat ik maar even in het midden.

En dan tot slot Janne en Bente, verreweg de twee beste én mooiste resultaten van mijn promotietijd!

Julia Witjes

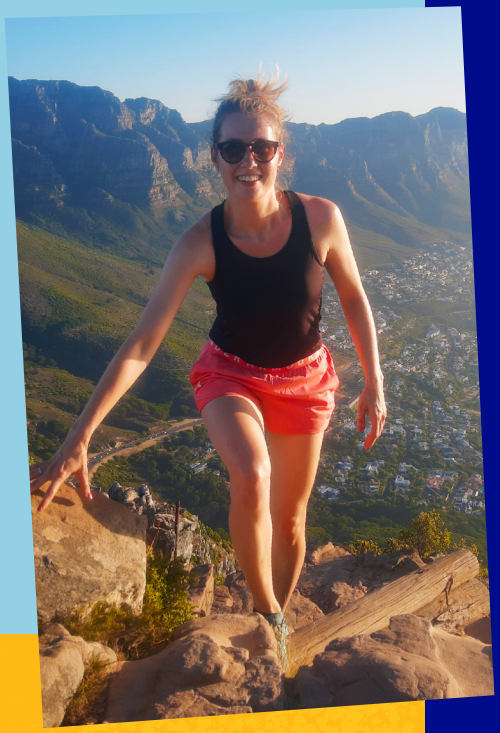

is op 10 december 1990 geboren als oudste dochter van Peter en Jacqueline en groeide samen met haar broer Daniël en zus Vivian op in Amsterdam.

Na het afronden van de middelbare school aan het Sint Nicolaas Lyceum is zij na een jaar te hebben gereisd begonnen aan de opleiding geneeskunde aan de Universiteit van Amsterdam. Tijdens de opleiding heeft zij haar wetenschappelijke stage uitgevoerd in het Mount Sinai Hospital te New York en rondde ze haar coschappen af met een schakeltraject van 6 maanden binnen de interne geneeskunde in het OLVG Oost te Amsterdam.

Na haar afstuderen startte zij eind 2017 met een promotieonderzoek gericht op het darmmicrobioom en leververvetting binnen de Vasculaire Geneeskunde in het AMC onder leiding van Max Nieuwdorp en Onno Holleboom. Tijdens het afronden van de dataverwerking heeft zij gedurende zes maanden gewerkt als ANIOS ouderengeneeskunde in Nieuwegein. De laatste periode van haar promotieonderzoek verbleef zij met haar gezin in Kaapstad, alwaar zij het schrijven van haar thesis afrondde.

Nadien heeft zij gedurende zes maanden als ANIOS interne geneeskunde in het Tergooi Ziekenhuis in Hilversum gewerkt, waarna zij de beslissing nam huisarts te willen worden. Inmiddels is Julia in opleiding tot huisarts aan de Radboud Universiteit Nijmegen en woont zij samen met haar man Bram en hun twee dochters Janne en Bente in het mooie Zutphen.